

**STUDIES ON PHOTOCATALYTIC TiO<sub>2</sub>-MWCNTs  
NANOCOMPOSITES FOR ANTIBACTERIAL APPLICATION**

A THESIS SUBMITTED TO  
**D. Y. PATIL UNIVERSITY**  
**D. Y. PATIL EDUCATION SOCIETY, KOLHAPUR**  
(Declared u/s 3 of the UGC Act 1956)  
FOR THE DEGREE OF  
**DOCTOR OF PHILOSOPHY**  
**IN CHEMISTRY**  
**UNDER THE FACULTY OF INTERDISCIPLINARY STUDIES**

BY  
**Mr. VALMIKI BALU KOLI**  
M.Sc.

UNDER THE GUIDANCE OF  
**PROF. (Dr.) S. D. DELEKAR**  
M.Sc., Ph.D. NET, SET, Raman Fellow USA  
**DEPARTMENT OF CHEMISTRY**  
**SHIVAJI UNIVERSITY, KOLHAPUR– 16 004 (MS) INDIA**  
AND

**PROF. (Dr.) S. H. PAWAR**  
M.Sc., Ph.D., F.I.C.C., F.M.A.Sc.  
**EMERITUS SCIENTIST (CSIR), DISTINGUISHED PROFESSOR**  
**AND VICE-CHANCELLOR (Emeritus),**  
**D. Y. PATIL UNIVERSITY, KOLHAPUR–416 006 (MS) INDIA**  
**AND DIRECTOR,**  
**CRTD, SINHGAD INSTITUTES, SOLAPUR–413 255 (MS) INDIA**

**CENTRE FOR INTERDISCIPLINARY RESEARCH**  
**D.Y. PATIL UNIVERSITY**  
**KOLHAPUR– 416 006 (MS) INDIA**

**JULY 2017**



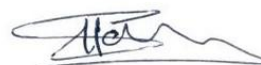
## CERTIFICATE

This is to certify that the thesis entitled "**Studies on Photocatalytic TiO<sub>2</sub>-MWCNTs Nanocomposites for Antibacterial Application**" which is submitted herewith for the degree of Doctor of Philosophy in Chemistry of D. Y. Patil University, Kolhapur by **Mr. Valmiki Balu Koli** is absolutely based upon his own work under our supervision and that neither this thesis nor any part of it has been submitted for any degree/diploma or any other academic award anywhere before.

Date:

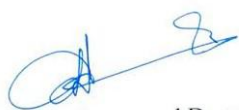


Research Guides



Prof. (Dr.) S. D. Delekar  
Professor, Inorganic Chemistry  
Department of Chemistry  
Shivaji University,  
Kolhapur - 416 004

Prof. (Dr.) S. H. Pawar  
Emeritus Scientist (CSIR) &  
Distinguished Professor &  
Vice- Chancellor (Emeritus),  
D. Y. Patil University,  
Kolhapur - 416 006 (India) &  
Director, CRTD,  
Sinhgad Institutes,  
Solapur- 413 225 (India)



Research Director and Dean  
Center for Interdisciplinary Research,  
D. Y. Patil University, Kolhapur - 416 006





## DECLARATION

I hereby declare that the work presented in this thesis entitled "**Studies on Photocatalytic TiO<sub>2</sub>-MWCNTs Nanocomposites for Antibacterial Application**" is entirely original and was carried out by me independently in the D. Y. Patil University, Kolhapur under the supervision of Prof. (Dr.) S. D. Delekar, Professor in Inorganic Chemistry, Department of Chemistry, Shivaji University, Kolhapur and Prof. (Dr.) S. H. Pawar, Emeritus scientist (CSIR) and Distinguished Professor and Vice-chancellor (emeritus), D. Y. Patil University, Kolhapur. I further declare that it has not formed the basis for the award of any degree, diploma, fellowship or associateship or similar title of any University or Institution. The extent of information derived from the existing literature has been indicated in the body of the thesis at appropriate places giving the references.

Place: Kolhapur

Date:



**Research Student**

Mr. Valmiki Balu Koli

Center for Interdisciplinary Research

D. Y. Patil University,

Kolhapur-416 006, (MS) India



## Acknowledgments

*I wish to express my deep sense of gratitude and profound thanks to my supervisor Prof. (Dr.) Sagar D. Delekar, Department of Chemistry, Shivaji University, Kolhapur and Prof. Dr. Shivaji. H. Pawar, Emeritus scientist (CSIR) and Distinguished Professor and Vice-chancellor (emeritus), D. Y. Patil University, Kolhapur, for their invaluable guidance, constant encouragement, inspiring and thought provoking discussions throughout my Ph. D. program. I have been able to learn a great deal from them and consider my association with them as a rewarding experience. I greatly appreciate the freedom my supervisor gave me and the opportunity to pursue my research in my own way.*

*I would like to acknowledge to Dr. V. V. Bhosale, Registrar and Mr. S. P. Kole, Finance Officer of D. Y. Patil University, Kolhapur and other staff members who have helped me directly or indirectly during my research work.*

*I also express my gratitude to Prof. C. D. Lokhande, Research Director and Dean, D Y Patil University, Kolhapur for his guidance, constant encouragement, inspiring and thought provoking discussions throughout my Ph. D. program and I would like to acknowledge to Prof. S. J. Ghosh, Head, Department of Microbiology, D. Y. Patil University, Kolhapur for her help and support.*

*I take this opportunity to convey my hearty admiration to all my teachers from my school days to post graduation level.*

*Special thanks to all the group members without their unconditional help and support, this study would not have been successful. To my other co-workers in the Shivaji University, Kolhapur. I thank all of you for your help, time and input. I am lucky to have had the opportunity to meet all of you. I wish to thank to all my friends for being there for me always*

*I am indebted to my parents, other family members whose dedication, love, encouragement, and persistent confidence in me has taken the load off my shoulders.*

*Finally, I acknowledge the financial assistance from the Department of Science and Technology, New Delhi in the form of junior research fellowships and also financial support under ITS to participate in international conference in south Korea.*

*I sincerely apologize for any omissions and sincerely thanks all concert.*

*Mr. Valmiki B. Koli*

## **CONTENTS**

	<b>Page No.</b>
<b>Chapter 1 Introduction</b>	
<b>1.1 Introduction</b>	1
<b>1.2 Nanocomposites</b>	3
1.2.1 Classification of nanocomposites	4
1.2.2 Non-polymer based nanocomposites	5
1.2.2.1 Metal/metal nanocomposite	5
1.2.2.2 Metal/ceramic nanocomposites	6
1.2.2.3 Ceramic/ceramic nanocomposites	7
1.2.3 Polymer based nanocomposites	7
1.2.3.1 Polymer/ceramic nanocomposite	8
1.2.3.2 Inorganic/organic polymer nanocomposites	8
1.2.3.3 Inorganic/organic hybrid nanocomposite	9
1.2.3.4 Polymer/layered silicate nanocomposites	10
<b>1.3 Photoactive nanocomposites</b>	11
1.3.1 Metal oxide-metal oxide based nanocomposites	11
1.3.2 Carbon nanotube based nanocomposites	12
1.3.3 Noble metal based nanocomposites	12
1.3.4 TiO <sub>2</sub> based nanocomposites	13
1.3.4.1 Structure of TiO <sub>2</sub> nanoparticles	14
1.3.4.2 TiO <sub>2</sub> -metal oxide nanocomposites	16
1.3.4.3 TiO <sub>2</sub> -metal nanocomposites	16
<b>1.4 TiO<sub>2</sub>-MWCNTs nanocomposites</b>	17
1.4.1 Plausible photocatalytic mechanism for TiO <sub>2</sub> -MWCNTs nanocomposites	18
1.4.2 Effect of MWCNTs on photocatalytic properties of TiO <sub>2</sub> nanoparticles	21
<b>1.5 Statement of the problem</b>	23
<b>1.6 Objectives of the proposed research work</b>	24

<b>1.7 Plan of work</b>	<b>24</b>
References	27

## **Chapter 2 Photocatalytic nanocomposites for antibacterial agent : Theoretical Background**

<b>2.1 Introduction</b>	<b>33</b>
<b>2.2 Infectious diseases and antibacterial surfaces</b>	<b>37</b>
<b>2.3 Photocatalytic inactivation of bacteria by using nanocomposites</b>	<b>38</b>
<b>2.4 Controlling of infectious diseases with photo-inactivation</b>	<b>40</b>
2.4.1 Mechanism for photo inactivation of bacteria	40
2.4.2 Extracellular target sites	41
2.4.3 Intracellular target sites	44
<b>2.5 Photoactive nanomaterials</b>	<b>46</b>
2.5.1 Zinc Oxide (ZnO)	47
2.5.2 Carbon nanotubes (CNTs)	47
2.5.3 TiO <sub>2</sub> Nanoparticles	48
<b>2.6 Strategies for improving photocatalytic properties of TiO<sub>2</sub> NPs</b>	<b>50</b>
2.6.1 Transition metal doping	51
2.6.2 Nobel metal loading	51
2.6.3 Non-metal doping	51
2.6.4 Hybrid nanocomposites	52
<b>2.7 Future prospect of photo-induced nanomaterials in antibacterial activity</b>	<b>54</b>
References	56

## **Chapter 3 Characterization Techniques**

<b>3.1 Introduction</b>	<b>62</b>
<b>3.2 Structural and Surface Techniques</b>	<b>62</b>

3.2.1 X-ray diffraction	62
3.2.2 Transmission electron microscopy	66
3.2.3 X-ray photoelectron spectroscopy	68
<b>3.3 Spectroscopic and Thermal analysis Techniques</b>	<b>71</b>
3.3.1 UV-Visible diffuse reflectance spectroscopy	71
3.3.2 Fourier transform infrared spectroscopy	74
3.3.3 Raman spectroscopy	76
3.3.4 Photoluminescence spectroscopy	79
3.3.5 Thermogravimetric analysis	82
<b>3.4 Cytotoxicity studies</b>	<b>84</b>
References	86

## **Chapter 4 Synthesis and characterization of photocatalytic TiO<sub>2</sub>-MWCNTs nanocomposites**

<b>4.1 Introduction</b>	<b>89</b>
<b>4.2 Synthesis methods</b>	<b>89</b>
4.2.1 Hydrothermal method	89
4.2.2 Solvothermal method	90
4.2.3 Electrochemical method	90
4.2.4 Sonochemical method	91
4.2.5 Microwave method	91
4.2.6 Microemulsion method	92
<b>4.3 Sol-gel method</b>	<b>92</b>
<b>4.4 Synthesis of TiO<sub>2</sub> nanoparticles with sol-gel method</b>	<b>97</b>
<b>4.5 Functionalization of MWCNTs</b>	<b>98</b>
<b>4.6 Synthesis of TiO<sub>2</sub>-MWCNTs nanocomposites</b>	<b>99</b>
<b>4.7 Characterization of TiO<sub>2</sub> nanoparticles and TiO<sub>2</sub>-MWCNTs nanocomposites</b>	<b>99</b>

<b>4.7.1 Characterization of TiO<sub>2</sub> nanoparticles</b>	99
4.7.1.1 Thermal analysis	100
4.7.1.2 X-ray diffraction studies	101
4.7.1.3 Transmission electron microscopy	102
<b>4.7.2 Characterization of TiO<sub>2</sub>-MWCNTs nanocomposites</b>	103
4.7.2.1 Thermal analysis	103
4.7.2.2 X-ray diffraction studies	104
4.7.2.3 Transmission electron microscopy	107
<b>4.8 Conclusions</b>	109
References	110

## **Chapter 5 Effect of MWCNTs content on photocatalytic properties of TiO<sub>2</sub> nanoparticles**

<b>5.1 Introduction</b>	113
<b>5.2 Spectroscopic properties of TiO<sub>2</sub> nanoparticles</b>	114
5.2.1 UV-Visible diffuse reflectance spectroscopy studies	114
5.2.2 Fourier transform infrared spectroscopy studies	115
5.2.3 Raman spectroscopy	116
5.2.4 Photoluminescence spectroscopy	117
5.2.5 X-ray photoelectron spectroscopy	118
<b>5.3 Cytotoxicity study of TiO<sub>2</sub> nanoparticles</b>	121
<b>5.4 Spectroscopic properties of TiO<sub>2</sub>-MWCNTs nanocomposites</b>	122
5.4.1 UV-Visible diffuse reflectance spectroscopy studies	122
5.4.2 Fourier transform infrared spectroscopy studies	124
5.4.3 Raman spectroscopy	126
5.4.4 Photoluminescence spectroscopy	128
5.4.5 X-ray photoelectron spectroscopy	129
<b>5.5 Cytotoxicity study of TiO<sub>2</sub>-MWCNTs nanocomposites</b>	132



<b>5.6</b>	<b>Conclusions</b>	133
	Reference	134

## **Chapter 6 Photocatalytic inactivation of bacteria**

<b>6.1</b>	<b>Introduction</b>	137
<b>6.2</b>	<b>Experimental details</b>	139
	6.2.1 Material	139
	6.2.2 Photocatalytic bactericidal activity	139
<b>6.3</b>	<b>Effect of TiO<sub>2</sub> nanoparticles on photo-inactivation of bacteria</b>	140
	6.3.1 Under dark condition	140
	6.3.2 Under irradiation of UV light	143
<b>6.4</b>	<b>Effect of TiO<sub>2</sub> nanoparticles and TiO<sub>2</sub>-MWCNTs nanocomposites on photo-inactivation of bacteria</b>	146
	6.4.1 Under dark condition	146
	6.4.2 Under irradiation visible light	149
<b>6.5</b>	<b>Conclusions</b>	154
	References	155

## **Chapter 7 Fe-doped TiO<sub>2</sub>-MWCNTs nanocomposites as an antibacterial agent**

<b>7.1</b>	<b>Introduction</b>	158
<b>7.2</b>	<b>Experimental</b>	160
	7.2.1 Material	160
	7.2.2 Synthesis of Fe-TiO <sub>2</sub> -MWCNTs nanocomposites	160
	7.2.3 Photocatalytic inactivation of bacteria	161
	7.2.4 Characterization	162
<b>7.3</b>	<b>Structural characterization of Fe-TiO<sub>2</sub> nanoparticles and Fe-TiO<sub>2</sub>-MWCNTs nanocomposites</b>	162
	7.3.1 X-ray diffraction studies	162

7.3.2	Transmission electron microscopy	164
7.3.3	X-ray photoelectron spectroscopy	167
7.4	<b>Spectroscopic Characterization</b>	170
7.4.1	UV-Visible diffuse reflectance spectroscopy	170
7.5	<b>Photo inactivation of bacteria</b>	172
7.6	<b>Reactive Oxygen species measurement</b>	174
7.7	<b>Overall discussion</b>	175
7.8	<b>Conclusions</b>	177
	References	178

## **Chapter 8 Visible Light Assisted Antibacterial paint (VLAAP)**

8.1	<b>Introduction</b>	182
8.2	<b>Preparation of light activated antibacterial paint</b>	185
8.3	<b>Experiential setup for testing antibacterial activity of VLAAP</b>	185
8.4	<b>Characterization of VLAAP</b>	186
8.4.1	UV-Visible diffuse reflectance spectroscopy	186
8.4.2	X-ray diffraction studies	188
8.4.3	water contact angle measurement	189
8.5	<b>Leaching test</b>	191
8.6	<b>Photo-inactivation of bacteria</b>	192
8.7	<b>Photocatalytic stability of VLAAP</b>	196
8.8	<b>Conclusion</b>	197
	References	199

## **Chapter 9 Summary and Conclusions**

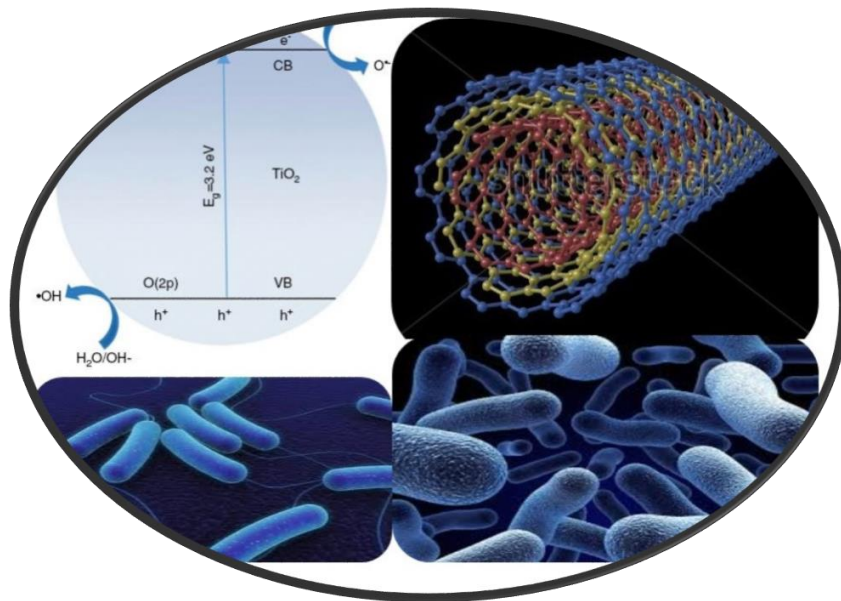
9.1	<b>Competent Components of the Thesis</b>	202
9.2	<b>Major breakthroughs</b>	207

<b>9.3</b>	<b>Future scope of the thesis</b>	207
	<b>Curriculum Vitae</b>	208



# Chapter 1

## Introduction





---

### 1.1 Introduction

Nanotechnology is the branch of technology that deals with dimensions and tolerances of less than 100 nanometers, especially the manipulation of individual atoms and molecules. Nanotechnology can create many new materials and devices. 1 nm is equal to  $1 \times 10^{-9}$  meter. Typical carbon-carbon bond lengths are in the range 0.12–0.15 nm and DNA double-helix is around 2 nm wide [1]. Interestingly, the smallest cellular life-forms (the bacterial genus *Mycoplasma*) are of length around 200 nm [2]. Now days, nanotechnology is widely used in various applications from air and water purifications to surface disinfection incorporating antibacterial effects, and also environmental remediation, energy fields, including pollutant degradation, hydrogen evolution, photo-electrochemical conversion, sterilization, biomedicine, and biotechnology etc. [3]. Different physicochemical properties of nanomaterials have made them interesting candidates for their use in various fields in recent years. These properties differ from those in bulk and are strongly influenced by size and shape of the material.

Nowadays, nanotechnology attracting great attention in the field of hospital acquired infection (HAIs) for controlling microbial infections by nanoparticles. Antibacterial agents are paramount to fight infectious diseases. However, with their extensive use and exploitation, the emergence of bacterial resistance to antibacterial material has become a common phenomenon, which is a major problem [4]. The common pathogenic bacteria such as *Staphylococcus aureus* is mainly responsible for post-operative wound infections, toxic shock syndrome, endocarditis, osteomyelitis and food poisoning [5]. Similarly, *Escherichia coli* is present in the human intestine and causes lower urinary tract infection, coleocystis or septicemia [6]. Early chemical based disinfectants which have been applied for centuries in environmental cleaning include chlorine, phenols, iodine, alcohols, and aldehydes [7]. Even though these chemical based disinfectants are effective against pathogenic microorganisms; however

they have disadvantages. Many of these form environmental toxic byproduct in disinfection process. To overcome these limitations use of nanotechnology is an emerging technology for safe environmental disinfection.

The metal nanoparticles like silver, copper and gold are effective against a wide range of microorganism. While the synthesis of these nanoparticles (NPs) involves complicating steps, as well these NPs suffering with instability. These NPs easily convert from pure metal nanoparticles to metal oxide NPs, also overall production cost is very high, and it may be reduce its applicability. Currently, photocatalytic bactericidal activity holds great promise as an alternative approach to the disinfection of bacteria [8]. Also individual NPs are showing less efficiency against bacterial infection may be due to aggregation. To solve this problem formation of nanocomposite is the best way. To this end titanium dioxide based nanocomposites are the one of the best photoactive bactericidal material and widely used due to its ability of killing a wide range of Gram-negative and Gram-positive bacteria, filamentous and unicellular fungi, algae, protozoa, mammalian viruses, bacteriophage and cancer cells [9].

Although, with advantages, bare  $\text{TiO}_2$  nanoparticles also suffering with few limitations like, high band gap (3.2 eV), it is active under the Ultraviolet (UV) electromagnetic spectrum. Additionally, the high rate of recombination of photo-generated electron-hole pairs in  $\text{TiO}_2$  lower its photocatalytic bactericidal activity [10]. Therefore to overcome these limitation, there is need to modify  $\text{TiO}_2$  with low optical band gap which will be decreasing the recombination rate of electron-hole pairs. Various strategies including doping with metal/non-metal ions, formation of nanocomposites (NCs), and noble metal loading with optimized parameters. The photocatalytic performance of anatase  $\text{TiO}_2$  nanoparticles (NPs) is desired to increase, an attempt to use it in a weak intensity visible light. The anatase phase type is expected to be suitable for such applications because of high photo-activity. Therefore, aims of this study are to tune the band gap of  $\text{TiO}_2$  in the visible region of light and examine the



effect of carbon nanotube on photo-catalytic antibacterial activity under visible light illumination.

### 1.2 Nanocomposites

The composite material is defined as it is a mixture of two or more materials constantly ones that have different properties. The two materials work together to give the unique composite properties. However, within the composite you can easily tell the different materials apart as they do not dissolve or blend into each other [11]. Making composites are well known from thousands of years. One early example is mud bricks. Mud can be dried out into a brick shape to give a building material with this composites material have application in various fields. Generally composite material involves of one or more discontinuous phases of dispersed in one continuous phase. Hybrid components are that which are with several discontinuous phases of different natures. Discontinuous phase is usually harder with superior mechanical properties than the continuous phase. The continuous phase is called “matrix”. The discontinuous phase is called “reinforcement, or reinforcing material” [12].

The term “nanocomposite” represents a new and exciting field in material science and technology. The definition of nanocomposite material has over the years broadened significantly to encompass a large variety of systems such as one-dimensional, two-dimensional, three-dimensional and amorphous materials, made of distinctly dissimilar components and mixed at the nanometer scale [13]. Nanocomposites are the materials with a nanoscale structure that improve the macroscopic properties of products. Nanocomposites that have been developed and that have proved technological importance have been composed of two phases, and can be microstructurally classified into three principal types as showed in Fig. 1.1.

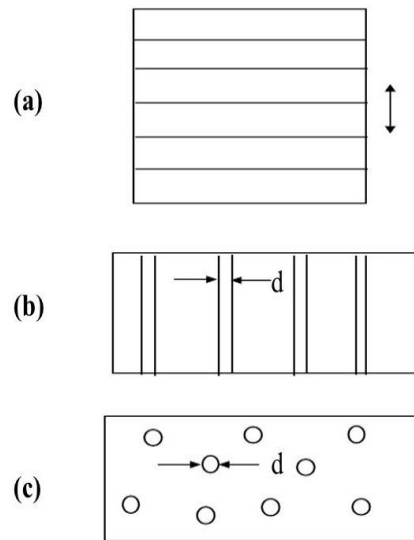


**Fig. 1.1 Schematic representation of types of different composites**

- (a) Nanolayered composite composed of alternating layers of nanoscale dimension;
- (b) The nanofilamentary composites made up of a matrix with surrounded (and generally aligned) nanoscale diameter filaments;
- (c) Nanoparticulates composites composed of a matrix with embedded nanoscale particles.

As with conventional composites, the properties of nanocomposites can display synergistic improvements over those of the component phases individually.

### 1.2.1 Classification of Nanocomposites

On the bases of their engineering applications, nanocomposites can be classified as shown in Fig.1.2.

- (1) Functional materials i.e. based on electrical, magnetic, and/or optical behavior, example is nanolayered semiconductor (semiconductor super lattice) composed of alternating layer of single crystal GaAs and  $\text{GaAl}_{1-x}\text{As}_x$ .
- (2) Structural materials i.e. based on their mechanical properties.

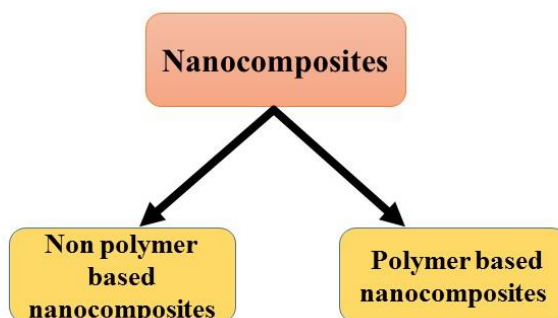


**Fig. 1.2 Types of nanocomposites**

### 1.2.2 Non polymer based nanocomposites

The nanocomposites rather than polymer or copolymer known as Non-polymer nanocomposites and these nanocomposites are classified as showed in Fig. 1.3

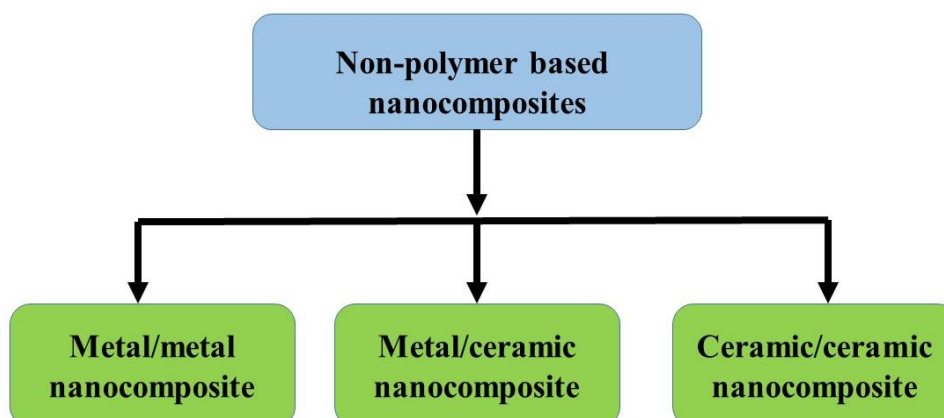


**Fig. 1.3 Classification of Non polymer based nanocomposites**

#### 1.2.2.1 Metal/metal Nanocomposites

Metal/metal nanocomposites result from non miscible metals and give access to attractive alternatives to traditional metal alloys with superior mecha-

nical [14], magnetic [15], tribological [16] properties. The beneficial effects are the result of combining metals of completely different physical properties at the nanometer scale. such metal mixtures have been challenging to prepare when using traditional metallurgy which has motivated the development of mechanical alloying, severe plastic deformation, or rapid solidification [17]. These top-down approaches have yielded interesting developments in metallurgy, but they require vast amounts of energy and long processing time. It is postulated their interesting physico-chemical properties, result from the combination of two kinds of metals and their fine structures. These type nanocomposite have application in various field such photocatalytic, biomedical application as well as attractive for the development of lead-free bearings in energy efficient engines [18].

### 1.2.2.2 Metal/ceramic nanocomposites

Metal/ceramic composites with at least one dimension of the metal phase or ceramic phase smaller than 100 nm. There are several types of metal/ceramic nanocomposites: nanometer sized ceramic particles dispersed in metal matrix, nanometer sized metal or semiconductor in ceramic matrix, nano-meter scaled multilayered metal/ceramic composites etc. Metal/ceramic nanocomposites combine the dramatically different nature of metals, semiconductors and ceramics and may offers enhancement in electric, magnetic, chemical, optical and mechanical properties of both phases, which will help for the increase in performance, durability, reliability, hardness, high mechanical strength at high temperature, stiffness, low density, optical conductivity, electrical insulation and conductivity, thermal insulation and conductivity, radiation resistance, and so on. Ceramic technologies have been widely used in aircraft and aerospace applications, wear-resistant parts, bio-ceramics, cutting tools, advanced optics, superconductivity, nuclear reactor [19, 20].

### 1.2.2.3 Ceramic/ceramic nanocomposites

Ceramic/ceramic nanocomposites is a subgroup of non-polymer based nanocomposites. They consist of ceramic fibres embedded in a ceramic matrix, thus forming a ceramic fibres reinforced ceramic material within nanometer scale. The matrix and fibers can consist of any ceramic material, whereby carbon and carbon fibres can also be considered a ceramic material. These nanocomposites could solve the problem of fracture failures in artificial joint implants; these would extend patient's mobility and eliminate the high cost of surgery [21]. The use of Zirconia-toughened alumina nanocomposite to form ceramic/ceramic implants with potential life spans of more than 30 years.

### 1.2.3 Polymer based nanocomposites

Polymer nanocomposites are composites with a polymer matrix and filler with at least one dimension less than 100 nm [22]. Fillers can be (clay), high aspect ratio, nanotubes and lower aspect ratio or nanoparticles. The detailed classification shown in Fig. 1.4.

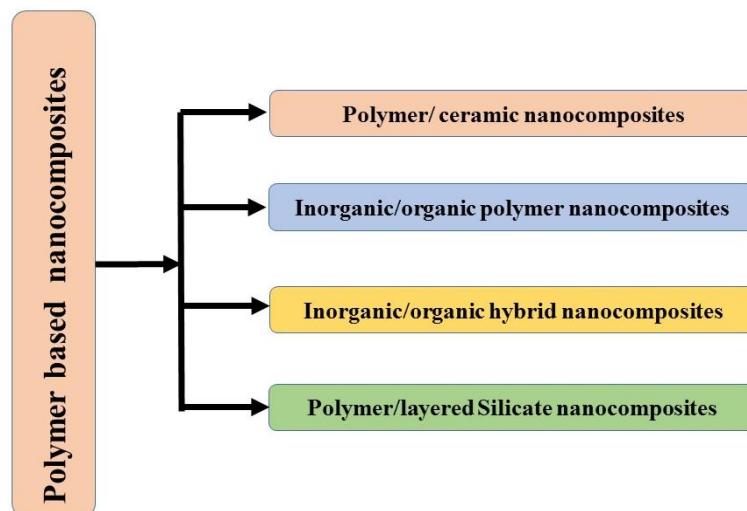


**Fig. 1.4 Classification of polymer based nanocomposites**

---

### 1.2.3.1 Polymer/ceramic nanocomposites

Polymer/ceramic nanocomposites as an inorganic-organic composites consisting of ceramic fillers and a matrix of organic polymers particularly polysiloxanes [23]. The formation of polymer/ceramics nanocomposites is based on thermal curing of functionalized resins being able to form ceramic like structures in the result of heat treatment above 200 °C. Polymer/ceramics nanocomposites can be processed by a broad variety of plastic forming techniques like high pressure injection molding or extrusion. Polymer/ceramic nanocomposites have advantages like cost efficient, easy processing of the material including plastic forming techniques in order to realize complex shaped parts are required and the thermal stability of standard materials like plastics does not suffice [24]. Various electro-technical components subjected to heavy thermal load could be developed based on polymer/ceramic nanocomposites. The diversity of application of polymer-ceramics could also be demonstrated by the development of joining materials and foamed materials exhibiting high thermal stability and good thermal isolation capability [25]. The prepared polymer ceramic nanocomposite also used for direct joining of bones [26]. Natural bone is a nanocomposite-bone consisting of approximately 30% matrix (collagen) material and 70 % nanosized minerals (hydroxyapatite).

### 1.2.3.2 Inorganic/organic polymer nanocomposites

Inorganic/organic polymer nanocomposites attract attention because of unique properties of inorganic materials which are dispersed in polymer matrix. The typical size of such inorganic material is approximately 1-100 nm. The properties of nanocomposites such as band gap, spectral properties, the transport of electrons are very different from individual inorganic and organic polymer materials [27]. Inorganic/organic polymer nanocomposites based on combinations of polymers, with metals, ceramics, or both, have been prepared by a variety of synthetic methods and have been exploited in different applications.

The use of an appropriate polymer coating provides solubility and high colloidal stability of the inorganic nanomaterials in organic or aqueous solvents, thus facilitating their low-temperature, low-cost processing [28]. Whereas it enables their applicability in certain areas requiring the use of nanoparticles with long-term colloidal stability in solution (e.g., magnetic nanoparticles destined for use as contrast enhancement agents in magnetic resonance imaging (MRI) or ceramic-based nanocontainers employed as drug delivery systems). A targeted polymer-based nanocomposites was synthesized with various method considering the unique properties like flexibility in materials' as well as other properties. System enables the development of novel multifunctional materials with new characteristics and functions that derive from the combination of the properties of the organic and the inorganic components, as well as from additional synergistic effects that allow the tailoring and fine-tuning of the materials properties.

### **1.2.3.3 Inorganic/organic hybrid nanocomposites**

Recently, Inorganic/organic hybrid nanocomposites have shown attention for their surprising properties and wide spread applications in diverse fields such as cell imaging, drug delivery, photo-thermal therapy, bio-sensing, catalysis, energy storage and conversion, gas sensing, etc. [29, 30]. Inorganic /organic hybrid nanocomposite, the term 'hybrid' refers to the combination of inorganic and organic components that form a single material called nanocomposite with improved/unique properties than the individual components [31]. Origin of the properties of an Inorganic/organic hybrid nanocomposite can found dependent upon its particle morphology in addition to the extent of interfacial/chemical interactions existed between the components [32].

An Inorganic /organic hybrid nanocomposite, can be more advantageous than the ordinary mixture of components for several advanced applications, among the varieties of organic component for Inorganic/Organic hybrid nanoc-

omposite, Graphene is mostly recognized as one of the potential biocompatible materials because living cells can adhere and proliferate well on graphene sheets [33]. Among the inorganic component, silica from silane chemistry is a popular material for drug or gene delivery due to its low cytotoxicity and existence of well-established bio-conjugation mechanism [34]. The hollow porous silica nanoparticles have been employed as a carrier to control the release behavior of a model drug [34].

### **1.2.3.4 Polymer/ layered silicate nanocomposites:**

Last few decades are Polymer/layered silicate nanocomposites have shown great interest, in industry as well as academia, because they often exhibit remarkable improvement in materials properties when compared with virgin polymer or conventional micro and macro-composites. These improvements can include high moduli [35], increased strength and heat resistance [36], decreased gas permeability and flammability [37, 38], and increased biodegradability of biodegradable polymers [39]. On the other hand, there has been considerable interest in theory and simulations addressing the preparation and properties of these materials [40], and they are also considered to be unique model systems to study the structure and dynamics of polymers in confined environments [41]. Although, intercalation chemistry of polymers when mixed with appropriately modified layered silicate and synthetic layered silicates has long been known [42], the field of polymer/layered silicate nanocomposites has gained momentum recently. Two major findings have stimulated the revival of interest in these materials: first, the report from the Toyota research group of a Nylon-6 (N6)/montmorillonite (MMT) nanocomposite. To improve the thermal and mechanical properties nanocomposites a very small amounts of layered silicate loaded. Vaia et al. [43] that it is possible to melt-mix polymers with layered silicates, without the use of organic solvents.



---

### 1.3 Photoactive nanocomposites

#### 1.3.1 Metal oxide -metal oxide based nanocomposites

Nanocomposites can be based on a metal oxide matrix in which the filler is also metal oxide nanoparticles, nanowires, etc. It is well known that, metal oxides are important semiconductors which can be used as photoactive nanomaterials in photocatalytic application [44]. Due to the wide band gap semiconductor oxides offered advantages in their stability in air, relative inexpensiveness, and easy preparation. As well as the porous metal oxides have attractive properties such as simplicity of preparation, tunable porosity, good chemical stability, low-temperature encapsulation, mechanical and biodegradable stability. The metal oxide based nanocomposites can be prepared by various methods. There are some methods like mechanical and chemical, which can be used, by using mechanical method which can grind the metal and give very small grain size and also give a homogeneous mixture (ball milling) [45]. The process can prepare highly metastable structures such as amorphous alloys and nanocomposite structures with high flexibility. Materials prepared by this method were used in various application such photo-inactivation of bacteria, photocatalytic degradation and gas sensing. For example, it was found that photocatalytic activity of on  $\text{TiO}_2$  with  $\text{ZnO}/\text{NiO}/\text{CuO}$  nanocomposites prepared this way showed improved photocatalytic activity [46]. Scaling up of synthesized materials to industrial quantities is easily achieved for this mechanical alloying process, but purity and homogeneity of structures produced remains a challenge.

Metal oxides based nanocomposites can also be prepared by sol-gel processes. Aerogels, because of their high-porosity structure, are an ideal starting material for use in nanocomposites. Aerogel nanocomposites can be fabricated in various ways, depending on when the second phase is introduced into the aerogel material. The second component can be added during the sol-gel processing of metal oxides (before supercritical drying) [47]. It can also be

added into the vapor phase (after supercritical drying) or chemical modification of the aerogel particles may be effected through reactive gas treatments. These general approaches can produce many varieties of nanocomposites.

### 1.3.2 Carbon nanotube based nanocomposites

Among all carbon products, carbon nanotubes have been of great interest, both from a fundamental point of view and for potential applications [48]. Their mechanical and unique electronic properties open up a broad range of applications, including nanoelectronic devices, composites, photocatalytic application. They also provide tremendous opportunities in the design of multifunctional materials systems [49]. In particular, they promise to provide solutions to many vexing problems encountered during the application of traditional composite materials. For example, they are electrically conductive and therefore are suitable for applications that require the ability to discharge electrostatic potentials. Carbon nanotubes (CNTs) can be classified as single-walled Carbon nanotubes (SWCNTs) and multi walled Carbon Nanotubes (MWCNTs). SWNTs consist of a cylindrical single sheet with a diameter between 1 and 3 nm and a length of several micrometers. They possess a cylindrical nanostructure formed by rolling up a single graphite sheet into a tube [50] MWCNTs consist of a coaxial arrangement of concentric single nanotubes like rings of a tree trunk separated from one another by 0.34 nm. They usually have a diameter of about 2-20 nm.

### 1.3.3 Noble metal based nanocomposites

Many techniques for incorporating metal NPs into the polymeric matrix have been published in the literature [51]. Such combinations require blending or mixing the components with the polymer in solution or in melt form. However, conducting polymers are not fusible and are generally insoluble in common solvents. Therefore, synthesis techniques had to be developed to

incorporate inorganic components into the conducting polymer. There are two main kinds of nanosized composites of conducting polymers with metals: metal core NPs covered with a conducting polymer shell; and metal NPs embedded into a conducting polymer matrix [52]. Metal core nanoparticles covered with a conducting polymer shell are usually prepared by the chemical or electrochemical polymerization of a thin, nanometer sized layer of a conducting polymer onto colloid metal NPs. There are many techniques for the deposition of nanometer-sized conducting polymer layers onto different substrates, including nanosized ones [53]. Metal nano-particles embedded into a conducting polymer matrix can be easily obtained by the chemical reduction of metal ions from their salt solution in the conducting polymer/solution interface.

### 1.3.4 TiO<sub>2</sub> based nanocomposites

Titanium dioxide (TiO<sub>2</sub>) is most studied and widely used as an efficient photocatalytic material for photo-inactivation of bacteria, decomposing toxic organic molecules to H<sub>2</sub>O, CO<sub>2</sub> and other harmless molecules. Due to its unique properties like photo-stability, chemical structure, physical, optical, and electrical properties [54]. This ability of decomposing organic material has been applied in photo-inactivation of bacteria from water and air, as well as this property can be applicable in self-cleaning or self-sterilizing surfaces for places such as medical center [55].

TiO<sub>2</sub> NPs are photoactive nanomaterial, these did not show reactivity in the absence of light. Interfacial electron transfer reactions on the surface of TiO<sub>2</sub> NPs have focused attention in strategic applications for solving several problems such as photo-inactivation of bacteria, purification of air and water, solar energy conversion, etc. To solve this problem TiO<sub>2</sub> NPs required unique properties like crystalline phase with an adequate particle size, morphology, and optoelectronic properties [56]. TiO<sub>2</sub> NPs have a wide band gap, which shows photo activity under UV light irradiation, [57]. Thus, the photocatalytic

## Chapter 1

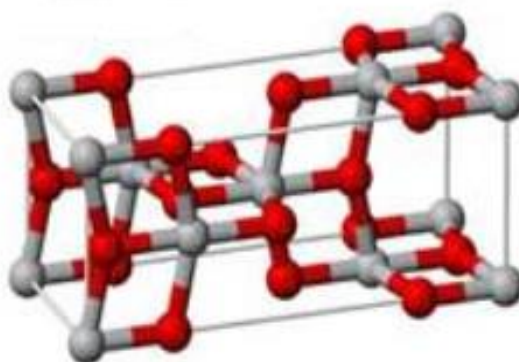
activity of TiO<sub>2</sub> NPs are very less under sunlight because solar spectrum contain less than 5% UV light. The photocatalytic properties of TiO<sub>2</sub> NPs are depend on electronic processes occurring inside and on the surface of TiO<sub>2</sub> NPs [58]. Therefore implanting impurities into the semiconductor photo catalyst greatly influence it activity. Thus, there is necessary to modify TiO<sub>2</sub> NPs to change its optical properties from UV active material to visible light active material for enhancing photo-inactivation of bacteria under visible light irradiation [59].

### 1.3.4.1 Structure of TiO<sub>2</sub> nanoparticles

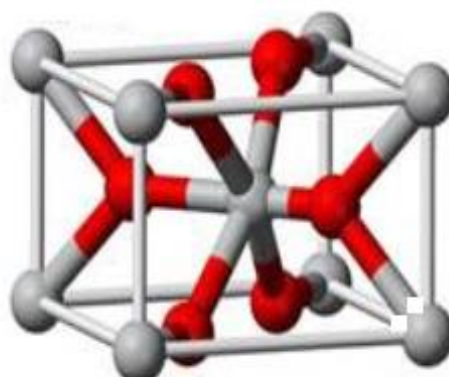
The photoactive TiO<sub>2</sub> NPs are one of the transition metal oxides. It is basically found in four polymorphs: anatase (tetragonal), brookite (orthorhombic), and rutile (tetragonal), and TiO<sub>2</sub> (B) (monoclinic) as shown in Fig. 1.5 (a to c) [60]. The anatase, rutile and brookite are the most studied polymorphs of TiO<sub>2</sub> NPs and their properties are listed in Table 1.1 [61].

**Table 1.1 structural properties of anatase, rutile and brookite TiO<sub>2</sub> NPs.**

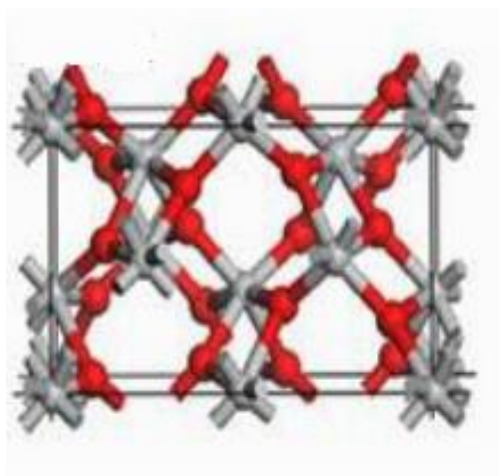
Properties	Anatase	Rutile	Brookite
Crystal structure	Tetragonal	Tetragonal	Orthorhombic
Lattice constant (Å)	a = 3.784 c = 9.515	a = 4.5936 c = 2.9587	a = 9.184 b = 5.447 c = 5.154
Space group	I4 <sub>1</sub> /amd	P4 <sub>2</sub> /mnm	Pbca
Molecule (cell)	2	2	4
Volume/molecule (Å <sup>3</sup> )	34.061	31.2160	32.172
Density (g cm <sup>-3</sup> )	3.79	4.13	3.99
Ti–O bond length (Å)	1.937(4) 1.965(2)	1.949 (4) 1.980 (2)	1.87–2.04
O–Ti–O bond angle	77.7° 92.6°	81.2° 90.0°	77.0°–105°



(a)



(b)



(c)

**Fig. 1.5 Crystal structure of  $\text{TiO}_2$  (a) anatase, (b) rutile and (c) brookite**

Researchers found that the anatase phase is more stable than the other structure preferred for photocatalytic applications because of its higher electron mobility, low dielectric constant. The increased photo reactivity is because of the slightly higher fermi level, lower capacity to adsorb oxygen and a higher degree of hydroxylation in the anatase phase [62]. The rutile phase as a photocatalyst is generally very poor. Brookite phase of  $\text{TiO}_2$  is more complicated, has a larger cell volume and is also the least dense of the 3 forms and is not often used for experimental investigations [63].  $\text{TiO}_2$  NPs has been fervently researched over the past few decades due to its potential applications across many different areas.  $\text{TiO}_2$  has seen considerable use as a white pigment in paint, food coloring, and personal care products and as a UV absorber in sunscreens [64].  $\text{TiO}_2$ -based nanomaterials have been investigated for in vivo imaging, cancer therapy, and protein separation purification and as bactericides [64].

### 1.3.4.2 $\text{TiO}_2$ -metal oxide nanocomposites

Appropriate positioning and thickness of the introduced material result in enhanced charge transfer. This process extends the photo response of the  $\text{TiO}_2$  NPs to visible light wavelengths [65]. Different materials are coupled with  $\text{TiO}_2$ , common semiconductors and metal oxides coupled to  $\text{TiO}_2$  include:  $\text{WO}_3$ ,  $\text{ZnO}$ ,  $\text{MnO}_2$  and  $\text{In}_2\text{O}_3$ , when coupled to  $\text{TiO}_2$  NPs, have also been shown to increase the photocatalytic capability of  $\text{TiO}_2$  NPs [66, 67]. Semiconductor or semiconductor-metal composite nanoparticles facilitate charge rectification in these systems.

### 1.3.4.3 $\text{TiO}_2$ -metal nanocomposites

Noble metal when deposited on semiconductor NPs maximizes the efficiency of photocatalytic reactions. The noble metal acts as a sink for photo-induced charge carriers, promoting interfacial charge-transfer processes [68].

Studies with regard to TiO<sub>2</sub>–metal nanocomposites involving different materials (Au, Ag, Pt) revealed that these metal domains induces charge equilibrium in photo excited TiO<sub>2</sub> NPs affecting the energetics of nanocomposites by shifting the Fermi level to more negative potentials [69, 70]. This corresponding shift in the nanocomposites is indicative of improved charge separation in TiO<sub>2</sub> metal systems and is effective towards enhanced photo catalysis [65]. Therefore, if one wants to use sunshine to promote photo-catalytic reactions there are two possibilities: preparing photocatalyst which are active in visible irradiation or enhancing the already existing activity in UV irradiation.

### 1.4 TiO<sub>2</sub>-MWCNTs nanocomposites

Since the landmark discovery by Iijima [71], Multi-walled carbon nanotubes (MWCNTs) have attracted significant attention in a variety of scientific fields because of their unique; structural, chemical, thermal and electrical properties [72]. Indeed, MWCNTs show the potential to contribute in enhancement of high-surface area and high quality active sites, retardation of electron–hole pair recombination as well as increase in visible light photocatalytic activity by modification of band-gap or sensitization [73]. There has been an increasing number of studies over the past decade seeking to develop TiO<sub>2</sub>-MWCNTs mixtures or nanocomposites with enhanced photocatalytic activity [74]. A literature search under the term “carbon nanotube and TiO<sub>2</sub> NPs retrieves over 1000 articles, TiO<sub>2</sub>-MWCNTs NCs can be prepared showing elevated photocatalytic activity. Despite of the extensive research there is still no definite explanation regarding this activity enhancing effect, but several theories already exist. According to these theories MWCNTs can either act as electron “sinks” and conductive channels for the photo generated electrons thus reducing e<sup>-</sup>/h<sup>+</sup> pair recombination rate, or MWCNTs can act as a photo-sensitizer [75]. For provision of surface reaction sites, the total specific surface area of as grown MWCNTs between 200 and 400 m<sup>2</sup>g<sup>-1</sup> [76]. Thus MWCNTs have the

potential to provide reactive surface areas approaching those obtained using activated carbon [77]. In addition, MWCNTs provide scope for greater control of morphology, and a variety of different structural forms of MWCNT-TiO<sub>2</sub> NCs photocatalyst have been reported. These include TiO<sub>2</sub> NPs on MWCNTs [78] and MWCNTs on TiO<sub>2</sub> NPs [79].

Among various the most published configuration, TiO<sub>2</sub> NPs bound to the surface of MWCNTs, is usually achieved by nucleating and growing TiO<sub>2</sub> NPs on MWCNTs dispersed in a liquid medium [80]. Selection of precursor is important for these routes (usually sol–gel based) because the reactivity of the precursor with the solvent affects whether nucleation is homogeneous in solution or heterogeneous on the MWCNTs [81]. It also affects the growth rate, and fast condensation rates usually result in large particle-size distributions. Acids or bases may be added to alter the reaction rate [82]. The largest challenge in solution based routes is the dispersion of the MWCNTs in the liquid medium such as alcohol (e.g. ethanol or isopropanol). Some groups have used surface charges from acid groups introduced by treatment in hot mineralizing acids to render the MWCNTs soluble in water [83].

### 1.4.1 Plausible photocatalytic mechanism for TiO<sub>2</sub>-MWCNTs nano-composites

In addition to control the morphology of surface chemistry of MWCNTs may be tailored to promote specificity towards adsorbents as shown in Fig. 1.6 This represents an advantage over activated carbons, which are usually non-selective and therefore have a lower photocatalytic activity due to the breakdown of both target and neutral species [84]. Functionalization has been used to achieve strong absorbance and surface contact with TiO<sub>2</sub> NPs without the need for complex/costly multi-stage preparation [85]. MWCNTs are widely reported to synergistically enhance the photocatalytic activity of TiO<sub>2</sub> NPs through the retardation of electron–hole pair recombination [86]. MWCNTs



(which may be metallic, semiconducting or insulating) are capable of forming a Schottky barrier at the  $\text{TiO}_2$ -MWCNT NCs interface, where there is a space charge region.  $\text{TiO}_2$  is an n-type semiconductor, but in the presence of MWCNTs, photo generated electrons may move freely towards the MWCNTs surface, which may have a lower Fermi level. This leaves an excess of holes in the valence band of the  $\text{TiO}_2$  NPs, which can migrate to the surface and react; the  $\text{TiO}_2$  NPs therefore effectively behaving as a p-type semiconductor [87]. Exhibiting high electrical conductivity and high electron storage capacity (one electron for every 32 carbon atoms), MWCNTs may act as extremely effective electron sinks. It has been shown that generating nanoscale  $\text{TiO}_2$  morphologies with high aspect ratio may also play a role in retardation of electron–hole pair recombination [88]. A similar mechanism may be promoted through the use of MWCNTs. Indeed, Xu et al. [89] suggest that the high aspect ratio and nanoscale geometry allow electron accumulation at the ends of MWCNTs, providing highly effective reduction sites.

Another mechanism of enhancement, proposed by Wang et al. [90], is based on the premise that MWCNTs may enhance photocatalytic activity of  $\text{TiO}_2$  NPs by acting as a photosensitizer, transferring electrons to the  $\text{TiO}_2$  NPs. This may be responsible for extending photocatalytic activity into the visible light range. In this mechanism, the photo generated electron in the MWCNTs is transferred into the conduction band of the  $\text{TiO}_2$  NPs, permitting a reduction process, such as the formation of superoxide radicals by adsorbed molecular oxygen. The positively charged MWCNTs then remove an electron from the valence band of the  $\text{TiO}_2$  NPs, leaving a hole. The positively charged  $\text{TiO}_2$  NPs can then take part in an oxidation process; for example, with water to form hydroxyl radicals. These two mechanisms are now widely cited, although there are conflicting views as to whether simple mixing [91] or intimate contact [86] is sufficient to enable such effects; or whether chemical bonding is required [92]. Alternatively, it has been suggested that  $\text{TiO}_2$ -MWCNTs NCs

may be more complex, consisting of two distinct effects leading to enhanced photocatalytic activity. The first is the presence of the C-O-Ti bond, similar to the case for carbon-doped  $\text{TiO}_2$ , which extends light absorption to longer wavelengths [93].

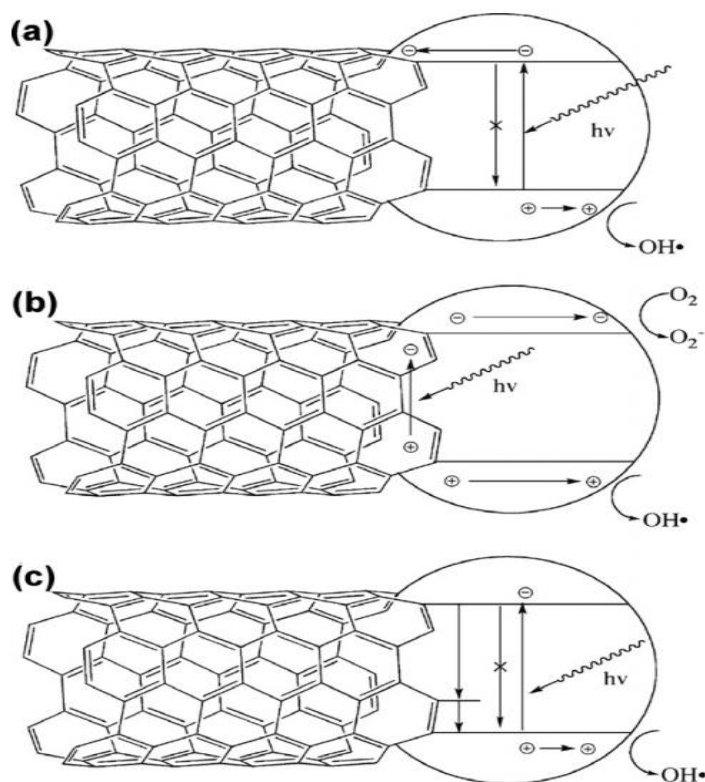


**Fig. 1.6 Proposed mechanisms of synergistic enhancement in  $\text{TiO}_2$ -MWCNTs NCs (a) MWCNTs inhibit recombination by acting as sinks for Photo-generated electrons in  $\text{TiO}_2$  (b) Photosensitizing mechanism based on electron-hole pair generation in the MWCNTs (c) MWCNTs act as impurities through the Ti-O-C bonds. Reproduced from Ref. [93] Copyright (2009), with permission from Wiley VCH Verlag GmbH & Co. KGaA. (License Number 4132320582465)**

The second effect is proposed to result from the electronic configuration of the MWCNTs, with greater numbers of mid band-gap states introduced by defects resulting in higher photocatalytic activity. Scientist Pyrgiotakis et al.

[94] propose that the electronic-band structure of the MWCNTs is more important for photocatalytic activity than the bond between the TiO<sub>2</sub> NPs and MWCNTs. They also suggest that during photocatalysis, some degree of MWCNTs oxidation is expected to occur, and that oxidized portions of MWCNTs may initially permit defect states, allowing for enhanced photo generation of electron–hole pairs. This aspect has received little attention in the literature, with the recent notable exception of the suggested self-photocatalytic activity of MWCNTs in the visible range by Luo et al. [95]. This was observed using highly defective MWCNTs, prepared using a heat treatment technique, which was deliberately intended to introduce defect states. It also observed that vacancies, local lattice reordering and inter-tube reorientation could initiate defect states in the band-gap, leading to visible light photocatalytic activity in the MWCNTs. Although the observed enhancement in the degradation of hydrogen peroxide was modest, ongoing general interest in the modification of the electronic properties of MWCNTs by introduction of defects may contribute to progress and growth in attention regarding self-photocatalytic properties. It may also provide an alternative approach to understanding of TiO<sub>2</sub>-MWCNTs NCs synergistic mechanisms.

### **1.4.2 Effect of MWCNTs on photocatalytic properties of TiO<sub>2</sub> nanoparticles**

In most cases of TiO<sub>2</sub> NPs loaded onto or randomly mixed with MWCNTs, photocatalytic activity increased up to 85 wt. % MWCNTs, after which it decreased [79, 96]. However, the optimum percentage of MWCNTs appears to be highly dependent on the morphology of the photocatalyst: for mixtures/composites of MWCNTs loaded onto larger TiO<sub>2</sub> NPs optimal activity has been found at around 20 wt. % MWCNTs. Conversely, Yen et al. [97] also found 20 wt.% MWCNTs to be optimum for TiO<sub>2</sub> NPs loaded on MWCNTs. In either case, there exists a compromise between increased syner-

gistic effect from higher MWCNTs loadings and insufficient amounts of TiO<sub>2</sub> NPs. The apparently contradictory findings could be partially explained based on whether the MWCNTs is acting as an electron sink or as a photosensitizer. If the former mechanism is active, since the TiO<sub>2</sub> NPs is the photoactive phase, it may be beneficial to have higher percentages of TiO<sub>2</sub> NPs and to promote exposed TiO<sub>2</sub> NPs surface area. If either of the later mechanisms are active, the MWCNTs is the photoactive phase, and optimal activity may be achieved at higher MWCNTs loadings and promotion of exposed MWCNTs surface area. However, since the photocatalytic activity also relates to other factors such as the nature of the inter-phase contact, variations of relative exposed surface areas in different morphologies and the variable importance of the MWCNTs for adsorption of reactants. There is need to fine dispersion of TiO<sub>2</sub> NPs on MWCNTs [97]. They found higher photocatalytic activity for fine, well-dispersed coatings in sol-gel derived MWCNT-TiO<sub>2</sub> NCs, as opposed to those produced by a hydrothermal route, which tended to lead TiO<sub>2</sub> particle agglomeration at MWCNTs junctions. Yao et al. [91] compared MWCNTs loading in both fine (5 nm) TiO<sub>2</sub> NPs deposited on MWCNTs and MWCNTs deposited on larger (100 nm) TiO<sub>2</sub> NPs using both SWCNTs and MWCNTs. They found optimal activity in SWCNTs deposited on 100 nm TiO<sub>2</sub> NPs, suggesting that this morphology and the use of SWCNTs provides optimal dispersion and inter-phase contact. However, while studies such as these empirically demonstrate the need for adequate provision of active sites and inter-phase contact, it may require better understanding of the mechanisms of enhancement before morphologies, proportions and synthesis routes can be optimally designed. With appropriate synthesis and TiO<sub>2</sub>-MWCNTs NCs may provide high-surface area. This approach has also shown promise for the synthesis of titanium oxycarbides and carbon-doped TiO<sub>2</sub>. Recently, the molten salt route has been used to produce Ti-C-coated MWCNTs, which have then been oxidatively converted into carbon-doped TiO<sub>2</sub>-MWCNTs. The NCs

formed in this way may be expected to show high photocatalytic activity, because they could achieve enhancement by both band-gap tuning due to the carbon doping effects in  $\text{TiO}_2$ , and through the electron scavenging or photosensitization enhancement mechanisms induced by the MWCNTs.

### 1.5 Statement of the problem

In recent years, hospital-acquired infection (HAI) has become a very important issue, with the appearance of resistant bacteria and have thus attracted much great attention. Improving the hospital environment is recognized as a highly effective counter measure to combat this problem. In response to the problem, we will be develop  $\text{TiO}_2$ -MWCNTs NCs materials, which are visible light-sensitive photocatalyst, for better antibacterial efficiency against microorganisms.

Among various  $\text{TiO}_2$ -MWCNTs NCs remained in the forefront of intense research because of MWCNTs not only support to anchor  $\text{TiO}_2$  NPs on the surface, but also to assist electron transport with tuning of band energy gap for photocatalytic transformations. Additionally, little studies have been devoted to  $\text{TiO}_2$ -MWCNTs NCs for bacterial treatment. Therefore, our aim to modify  $\text{TiO}_2$  with MWCNTs to realize visible light absorbance and improve the charge separation efficiency thus enhancing its photocatalytic bacterial activity. The aim of this study was to investigate the antibacterial activity of  $\text{TiO}_2$ -MWCNTs NCs in visible light. In the present proposed work an attempt is typically focused on preparation of nanocomposites of functionalized MWCNTs and  $\text{TiO}_2$  host lattices. Different methods like sol-gel or hydrothermal methods were used to prepare  $\text{TiO}_2$  NPs and subsequently used for the preparation of nanocomposites with MWCNTs. The preparation of nanocomposites was optimized in the aim to get better photocatalytic, electrical and optical properties for photo-inactivation of bacteria. Lastly, we will be tested several pathogens, including *E. Coli*, *S. aureus* and *P. aeruginosa* etc. Visible light photo-inactivation of different bacteria on the surface of  $\text{TiO}_2$ -MWCNTs

NCs with various MWCNTs contents were studied.

### 1.6 Objectives of the proposed research work

Following were the objectives of the proposed research work:

#### Part –I

1. To synthesize of doped/undoped TiO<sub>2</sub> NPs with desirable size, morphology, crystallinity, and phase composition, using sol-gel or hydrothermal methods.
2. To use chemical methods adopted for functionalization of commercial MWCNTs. Then, the nanocomposites between TiO<sub>2</sub> nanoparticles with functionalized MWCNTs will be formed.
3. To characterize these nanocomposites by various spectroscopic methods such as TGA, XRD, FTIR, Raman, UV–visible measurement, TEM, EDAX and XPS etc.
4. To prepare visible light assisted antibacterial paint

#### Part-II

1. To test the visible light response and biological activity of these nanocomposites.
2. To study antibacterial activity of nanocomposites using dilution method.
3. To optimize the photo-inactivation of bacteria by various techniques such as statistical analysis & CFU count etc.

### 1.7 Plan of work

With this aim, we would like to explore NCs for photocatalytic bactericidal application. From the application point of view, we developed potential visible light active TiO<sub>2</sub>-MWCNTs NCs. The fundamental point of view, our motivation was to study the photocatalytic properties, TiO<sub>2</sub>-MWCNTs NCs, photo-killing mechanisms, effects of MWCNTs on the photocatalytic properties of TiO<sub>2</sub> NPs.

### **Step: I**

In light of this problem, the work is executed in five steps, first step is a literature survey for synthesis of doped/undoped TiO<sub>2</sub> NPs. Find out suitable method for functionalization of MWCNTs and also find out method to synthesis the nanocomposite between TiO<sub>2</sub> and MWCNTs and in detail methods to study of photo-inactivation of bacteria.

### **Step: II**

Synthesis of doped/undoped TiO<sub>2</sub> NPs and TiO<sub>2</sub>-MWCNTs NCs. Sol-gel method was used for synthesis of TiO<sub>2</sub> NPs and TiO<sub>2</sub>-MWCNTs NCs. The Sol-gel is very simple and cost effective method in the synthesis of phase pure, high quality oxide nanomaterials, hence is the method of choice. The effect of preparative parameters in sol-gel synthesis on the structural, morphological and optical properties on TiO<sub>2</sub>-MWCNTs NCs are studied thoroughly. To prepare NCs of MWCNTs are functionalized with acid treatment, which is help full for form depictive side's form on the surface of MWCNTs. This improving the bond formation between TiO<sub>2</sub> NPs and MWCNTs. To enhance the photocatalytic properties of TiO<sub>2</sub>-MWCNTs NCs the various concentration of MWCNTs are used for synthesis of NCs.

### **Step: III**

This step include the characterization of synthesized nanomaterial with various structural and surface technique like XRD, TEM, SEM EDAX, and XPS etc. To determine the structure and morphology of synthesized nanomaterial. After-word the spectroscopic analysis also carried out with UV-Vis DRS, FTIR Raman and PL analysis. The spectroscopic analysis give direct idea about the optical properties of material which will directly effect on photocatalytic properties.

### Step: IV

The determination of photocatalytic bactericidal ability of synthesized material under various conditions like in dark, in UV light and in visible light irradiation. The standard plate count method is used for determination of photo-inactivation ability of synthesized nanomaterials. The photocatalytic bactericidal study is carried out against common pathogenic bacteria. The effect of nano-material amount and the time of exposure etc. are investigated for their possible use as antibacterial material also In-vitro cytotoxicity studies of synthesized nanomaterial have been studied with the MTT assay on *NIH 3T3* cell lines.

### Step: V

Coating of this material on plane surface and generate antibacterial surface for in hospitals, homes etc. To increase the applicability synthesized nanomaterial. Visible Light Assisted Antibacterial Paint is prepared with synthesized nanomaterial and dye as a coloring agent. The photocatalytic bactericidal activity tested against common pathogenic bacteria with standard plate count method.

This study was expected to yield an appropriate nanocomposites for antibacterial application.



---

### References

- [1] U. Ahmad and F. Md, J. Nanomedine Biotherapeutic Discov. 6 (2016) e140.
- [2] P. K. Tyagi, Int. J. Curr. Microbiol. App. Sci 5 (2016) 548.
- [3] S. Biran Ay and N. Kosku Perkgoz, J. Nanomater. 2015 (2015) 20.
- [4] M. J. Hajipour, K. M. Fromm, A. A. Ashkarran, D. J. de Aberasturi, I. R. de Larramendi, T. Rojo, V. Serpooshan, W. J. Parak, and M. Mahmoodi, Trends in Biotechnol. 30 (2012) 499.
- [5] S. Benayache, F. Benayache, S. Benyahia, J. C. Chalchat, and R. P. Garry, J. Essent. Oil Res. 13 (2001) 210.
- [6] R. G. Bachir and M. Benali, Asian Pac. J. Trop. Biomed. 2 (2012) 739.
- [7] J. W. Liou and H. H. Chang, Arch. Immunol. Ther. Ex. 60 (2012) 267.
- [8] H. A. Foster, I. B. Ditta, S. Varghese, and A. Steele, Appl. Microbiol. Biotechnol. 90 (2011) 1847.
- [9] D. M. Blake, P. C. Maness, Z. Huang, E. J. Wolfrum, J. Huang, and W. A. Jacoby, Sep. Purif. Methods 28 (1999) 1.
- [10] V. B. Koli, S. D. Delekar, and S. H. Pawar, J. Mater. Sci. Mater. Med. 27 (2016) 177.
- [11] C. C. Okpala, Int. J. Adv. Engg. Tech. 12 (2014) 18.
- [12] J. M. Berthelot, Composite materials: mechanical behavior and structural analysis, Springer Science & Business Media, (2012).
- [13] G. Dhorali, Nanomaterials and Nanocomposites: Zero to Threedimaenstional Materials and their composites (2016)
- [14] X. Sauvage, P. Jessner, F. Vurpillot, and R. Pippan, Scr. Mater. 58 (2008) 1125.
- [15] S. Bose, V. Bhattacharya, K. Chattopadhyay, and P. Ayyub, Acta Mater. 56 (2008) 4522.
- [16] V. Bhattacharya and K. Chattopadhyay, Acta Mater. 52 (2004) 2293.
- [17] I. Sabirov and R. Pippan, Scr. Mater. 52 (2005) 1293.

## Chapter 1

- 
- [18] N. A. Luechinger, R. N. Grass, E. K. Athanassiou, and W. J. Stark, Chem. Mater. 22 (2009) 155.
- [19] M. Rosso, J. Mater. Process. Technol. 175 (2006) 364.
- [20] M. Sternitzke, J. Eur. Ceram. Soc. 17 (1997) 1061.
- [21] M. W. Barsoum and T. El-Raghy, J. Am. Ceram. Soc. 79 (1996) 1953.
- [22] R. A. Vaia and E. P. Giannelis, MRS Bull. 26 (2001) 394.
- [23] H. Zou, S. Wu, and J. Shen, Chem. Rev 108 (2008) 3893.
- [24] M. Schwartz and M. Schwartz, Ballistic protection for ground vehicles, human personnel, and habitats, CRC Press Boca Raton, FL, (2010).
- [25] Y. Rao, S. Ogitani, P. Kohl, and C. Wong, J. Appl. Polym. Sci. 83 (2002) 1084.
- [26] T. Kokubo, H.-M. Kim, and M. Kawashita, Biomater. 24 (2003) 2161.
- [27] J. Pyun and K. Matyjaszewski, Chem. Mater. 13 (2001) 3436.
- [28] H. Duan, M. Kuang, D. Wang, D. G. Kurth, and H. Möhwald, Angew. Chem. Int. Ed. 44 (2005) 1717.
- [29] S. Sharma, R. Khosla, D. Deva, H. Shrimali and S. Sharma, Sens. Actuators, A 261(2017) 94.
- [30] D. Krug and R. Laine, ACS Appl. Mater. Interfaces, 9 (2017) 8378.
- [31] L. Nicole, L. Rozes, and C. Sanchez, Adv. Mater. 22 (2010) 3208.
- [32] G. L. Drisko and C. Sanchez, Eur. J. Inorg. Chem. 2012 (2012) 5097.
- [33] S. Bera, M. Ghosh, M. Pal, N. Das, S. Saha, S. K. Dutta, and S. Jana, RSC Adv. 4 (2014) 37479.
- [34] L. Dai, Q. Zhang, J. Li, X. Shen, C. Mu, and K. Cai, ACS Appl. Mater. Interfaces. 7 (2015) 7357.
- [35] M. Biswas and S. S. Ray, in New polymerization techniques and synthetic methodologies, Springer, (2001).
- [36] E. P. Giannelis, Appl. Organomet. Chem. 12 (1998) 675.
- [37] R. Xu, E. Manias, A. J. Snyder, and J. Runt, Macromol. 34 (2001) 337.
-

- 
- [38] S. Bourbigot, M. L. Bras, F. Dabrowski, J. W. Gilman, and T. Kashiwagi, *Fire Mater.* 24 (2000) 201.
  - [39] S. S. Ray, K. Yamada, M. Okamoto, and K. Ueda, *Nano Lett.* 2 (2002) 1093.
  - [40] E. Manias, H. Chen, R. Krishnamoorti, J. Genzer, E. Kramer, and E. Giannelis, *Macromol.* 33 (2000) 7955.
  - [41] E. Manias, V. Kuppa, D. K. Yang, and D. Zax, *Colloids Surf., A* 187 (2001) 509.
  - [42] B. K. G. Theng, *Formation and properties of clay-polymer complexes*, Elsevier, (2012).
  - [43] R. A. Vaia, H. Ishii, and E. P. Giannelis, *Chem. Mater.* 5 (1993) 1694.
  - [44] C. Ruales-Lonfat, J. Barona, A. Sienkiewicz, M. Bensimon, J. Vélez-Colmenares, N. Benítez, and C. Pulgarín, *Appl. Catal., B* 166 (2015) 497.
  - [45] O. Tan, W. Cao, W. Zhu, J. Chai, and J. Pan, *Sens. Actuators B* 93 (2003) 396.
  - [46] A. Pérez-Larios, R. Lopez, A. Hernandez-Gordillo, F. Tzompantzi, R. Gómez, and L. Torres-Guerra, *Fuel* 100 (2012) 139.
  - [47] R. Sui and P. Charpentier, *Chem. Rev.* 112 (2012) 3057.
  - [48] J. K. Wassei and R. B. Kaner, *Acc. Chem. Res.* 46 (2013) 2244.
  - [49] X. Qu, J. Brame, Q. Li, and P. J. Alvarez, *Acc. Chem. Res.* 46 (2012) 834.
  - [50] K. Li, G. Eres, J. Howe, Y. J. Chuang, X. Li, Z. Gu, L. Zhang, S. Xie, and Z. Pan, *Sci. Rep.* 3 (2013) 2353.
  - [51] T. Bein and G. Stucky, *Chemistry of Materials* 8 (1996) 1569.
  - [52] A. Malinauskas, J. Malinauskiene, and A. Ramanavičius, *Nanotechnology* 16 (2005) R51.
  - [53] A. Malinauskas, *Polymer* 42 (2001) 3957.
  - [54] Y. Zhang, Z. R. Tang, X. Fu, and Y. J. Xu, *ACS Nano* 4 (2010) 7303.
-

- 
- [55] S. Chaturvedi, P. N. Dave, and N. Shah, J. Saudi Chem. Soc.16 (2012) 307.
- [56] T. D. Nguyen-Phan, S. Luo, Z. Liu, A. D. Gamalski, J. Tao, W. Xu, E. A. Stach, D. E. Polyansky, S. D. Senanayake, and E. Fujita, Chem. Mater. 27 (2015) 6282.
- [57] R. Lee, Y. Kumaressn, S. Young Yoon, S. Ho Um, K. Kwon and G.Y. Jung, RSC Adv. 7 (2017) 7469
- [58] R. Daghrir, P. Drogui, and D. Robert, Ind. Eng. Chem. Res. 2 (2013) 3581.
- [59] V. B. Koli, A. G. Dhodamani, A. V. Raut, N. D. Thorat, S. H. Pawar, and S. D. Delekar, J. Photochem. Photobiol. A, 328 (2016) 50.
- [60] M. D. Hernández-Alonso, F. Fresno, S. Suárez, and J. M. Coronado, Energy & Environ. Sci. 2 (2009) 1231.
- [61] S. M. Gupta and M. Tripathi, Chin. Sci. Bull. 56 (2011) 1639.
- [62] R. R. Yeredla and H. Xu, Nanotechnology 19 (2008) 055706.
- [63] J.Schneider, M.Mastuoka, M. Takeuchi, J. Zhang, Y. Horiuchi, M. Anpo and D. W. Bahnemann, Chem. Rev. 114 (2014) 9919.
- [64] M. Dahl, Y. Liu, and Y. Yin, Chem. Rev. 114 (2014) 9853.
- [65] O. Ola and M. M. Maroto-Valer, J. Photochem. Photobiol. C 24 (2015) 16.
- [66] H. Kim, J. Kim, W. Kim, and W. Choi, J. Phys.Chem. C 115 (2011) 9797.
- [67] J. Tian, Z. Zhao, A. Kumar, R. I. Boughton, and H. Liu, Chemi. Soc. Rev. 43 (2014) 6920.
- [68] P. V. Kamat and D. Meisel, C. R. Chim. 6 (2003) 999.
- [69] V. Subramanian, E. E. Wolf, and P. V. Kamat, J. Am. Chem. Soc. 126 (2004) 4943.
- [70] J. Yang and J. Y. Ying, Angew. Chem. Int. Ed. 50 (2011) 4637.
- [71] S. Iijima, Physica B 323 (2002) 1.
-

- 
- [72] X. Liu, X. Wang, X. Xing, Q. Li, and J. Yang, *Adv. Powder Technol.* 26 (2015) 8.
- [73] Y. J. Xu, Y. Zhuang, and X. Fu, *J. Phys. Chem. C* 114 (2010) 2669.
- [74] R. Leary and A. Westwood, *Carbon* 49 (2011) 741.
- [75] P. Zeng, Q. Zhang, T. Peng, and X. Zhang, *Phys. Chem. Chem. Phys.* 13 (2011) 21496.
- [76] Y. T. Ong, A. L. Ahmad, S. H. S. Zein, K. Sudesh, and S. H. Tan, *Sep. Puri. Technol.* 76 (2011) 419.
- [77] B. Stoner, B. Brown, and J. Glass, *Diamond Relat. Mater.* 42 (2014) 49.
- [78] N. O. Ramoraswi and P. G. Ndungu, *Nanoscale Res. Lett.* 10 (2015) 427.
- [79] W. Feng, Y. Feng, Z. Wu, A. Fujii, M. Ozaki, and K. Yoshino, *J. Phys.: Condens. Matter.* 17 (2005) 4361.
- [80] Y. Yan, J. Miao, Z. Yang, F. X. Xiao, H. B. Yang, B. Liu, and Y. Yang, *Chem. Soc. Rev.* 44 (2015) 3295.
- [81] Y. Luo, J. Liu, X. Xia, X. Li, T. Fang, S. Li, Q. Ren, J. Li, and Z. Jia, *Mater. Lett.* 61 (2007) 2467.
- [82] B. Verheggen and M. Mozurkewich, *J. Geophys. Res. Atmos.* 07 (2002).
- [83] J. Hilding, E. A. Grulke, Z. George Zhang, and F. Lockwood, *J. Dispersion Sci. Technol.* 24 (2003) 1.
- [84] O. Carp, C. L. Huisman, and A. Reller, *Prog. Solid Chem.* 32 (2004) 33.
- [85] P. Clemens, X. Wei, B. L. Wilson, and R. L. Thomas, (2013).
- [86] B. S. Huang, F. Y. Chang, and M. Y. Wey, *J. Nanopart. Res.* 12 (2010) 2503.
- [87] Y. Chen, J. C. Crittenden, S. Hackney, L. Sutter, and D. W. Hand, *Environ. Sci. Technol.* 39 (2005) 1201.
- [88] S. Z. Kang, Z. Xu, Y. Song, and J. Mu, *J. Dispersion Sci. Technol.* 27 (2006) 857.
-

- [89] Z. Xu, Y. Long, S. Z. Kang, and J. Mu, J. Dispersion Sci. Technol. 29 (2008) 1150.
- [90] W. Wang, P. Serp, P. Kalck, and J. L. Faria, J. Mol. Catal. A: Chem. 235 (2005) 194.
- [91] Y. Yao, G. Li, S. Ciston, R. M. Lueptow, and K. A. Gray, Environ. Sci. Technol. 42 (2008) 4952.
- [92] O. Akhavan, M. Abdollahad, Y. Abdi, and S. Mohajerzadeh, Carbon 47 (2009) 3280.
- [93] K. Woan, G. Pyrgiotakis and W. Sigmund, Adv. Mater. 21(2009) 2233.
- [94] G. Pyrgiotakis, S. H. Lee, and W. Sigmund, MRS Proceedings, 876 (2005) 7.
- [95] Y. Luo, Y. Heng, X. Dai, W. Chen, and J. Li, J. Solid State Chem. 182 (2009) 2521.
- [96] Y. Yu, C. Y. Jimmy, C. Y. Chan, Y. K. Che, J. C. Zhao, L. Ding, W. K. Ge, and P. K. Wong, Appl. Cata. B: Environ. 61 (2005) 1.
- [97] C. Y. Yen, Y. F. Lin, C. H. Hung, Y. H. Tseng, C. C. M. Ma, M. C. Chang, and H. Shao, Nanotechnology 19 (2008) 045604.

## Chapter 2

# **Photocatalytic nanocomposites for antibacterial agent: Theoretical Background**







### 2.1 Introduction

Nowadays infectious diseases mainly caused due to pathogenic bacteria may cause permanent damage to humans when diagnostics and medical treatment are not punctually managed [1]. The most of these diseases are caused by bacterial infections that may lead to sepsis, pneumonia endocarditis, bacteremia, or even death of the patient occurs [2]. Production and high environmental survival of bacteria can lead to serious diseases. Pathogenic bacterial mainly two types Gram-negative bacteria (*Escherichia coli*, *Salmonella enterica*, *Salmonella typhi*, *Pseudomonas aeruginosa*,) and Gram-positive bacteria (*Staphylococcus aureus*, [3-7].

To control these bacterial infection microbiologists distinguishes two types of antimicrobial agents, antibiotics, which are natural substances produced by certain groups of microorganisms, and chemo-therapeutic agents, which are chemically synthesized. The chemotherapeutic antimicrobial began was first discovered in 1929, by Fleming's powerful bactericidal substance, such as penicillin, and Domagk's discovery in 1935 of synthetic chemicals (sulfonamides) with broad antimicrobial activity. There were various antibacterial agents which kill the bacterial or stop the growth of bacteria. However, many pathogenic bacteria have developed resistance against antibiotics because of the extensive use of these antibacterial agents [2, 8]. The WHO report 2015 [9] reveals that the U.S. Centers for Disease Control and Prevention (CDC) estimates that antibiotic resistance is responsible for more than 2 million infections and 23,000 deaths each year in the United States, at a direct cost of \$20 billion and additional productivity losses of \$35 billion (CDC 2013) [10]. In Europe, an estimated 25,000 deaths are attributable to antibiotic-resistant infections, costing €1.5 billion annually in direct and indirect costs (EMA and ECDC 2009). Although reliable estimates of economic losses in the developing world are not available, it is estimated that 58,000 neonatal sepsis deaths are attributable to drug resistant infections in India alone [10]. Studies from Tanzania and

## Chapter 2

---

Mozambique indicate that resistant infections result in increased mortality in neonates and under five years old children's [11, 12]. Therefore, necessary to develop new types of antibiotics and effective therapeutic strategies to solve this emerging problem.

To overcome this emerging problem various disinfectants, are used to kill effectively harmful microorganisms, which are also powerful oxidants that oxidize the organic matter and bromide naturally present in most source waters, but they forming disinfection by products (DBPs) [13-15]. Chlorine, ozone, chlorine dioxide, and chloramines are the most common disinfectants in use, and each produces its own suite of chemical DBPs in finished drinking water. Pathogenic organisms provide the primary human health risk from drinking water, while chemical DBPs also provide an unintended health hazard [16, 17]. Therefore, the development of more effective sterilization technologies or anti-bacterial agents which having less DBPs has become an urgent issue [16].

Surface disinfection by photo-catalyzed reactions on  $\text{TiO}_2$  NPs is a possible popular alternative to using chemical disinfectants such as bleach powder because it avoids the use of chemicals for which there are currently concerns about possible toxicity and mutagenesis [17-20]. Subsequently, scientist and engineers are engaged in developing  $\text{TiO}_2$  based antibacterial techniques. In the last decade, immobilized  $\text{TiO}_2$  has been utilized as a self-cleaning and self-sterilizing material for coating many clinical tools including sanitary ware, food packaging, tableware, building materials, and medical devices.

Since the discovery of the "Honda-Fujishima effect" [21]  $\text{TiO}_2$  has proved to one of the most efficient materials for environmental remediation because of its various desirable properties. In 1985, Matsunaga et al. first reported photocatalytic inhibition of *Saccharomyces cerevisiae* (yeast), *Lactobacillus acidophilus* and *E. coli* (bacteria), and *Chlorella vulgaris* (green algae) in water using a Pt- $\text{TiO}_2$  photocatalyst [22]. They also demonstrated the photo

killing mechanism for microbial cell. Since then, much research has been performed on the photocatalytic antimicrobial effect of TiO<sub>2</sub>. The larger energy provided to the material larger than the band gap, then the electron (e<sup>-</sup>)/hole (h<sup>+</sup>) pairs are generated and reacts with O<sub>2</sub> and H<sub>2</sub>O to form superoxide anion radical (O<sub>2</sub><sup>•-</sup>) and hydroxyl radical (•OH). These oxygen species (•OH, and O<sub>2</sub><sup>•-</sup>) are all highly reactive, which are considered to be the dominant oxidative or reductive species contributing to the mineralization of microorganism cells [23]. However, bare anatase TiO<sub>2</sub> photocatalyst is active under ultraviolet light due to its wide band gap energy of 3.2 eV. Recent research has identified chemically modified TiO<sub>2</sub>-based photocatalyst, which work under visible and UV.

**Table. 2.1 List of bacterial species with causing diseases**

Sr. No.	Species	Diseases produced	Reference
1	<i>Escherichia coli</i> (generally)	Diarrhea Urinary tract infections (UTI) Meningitis in infants Hospital-acquired pneumonia Hospital-acquired sepsis	[23, 24]
2	<i>Enteropathogenic E. coli</i>	Diarrhea in infants	[23]
3	<i>Enteroinvasive E. coli</i> (EIEC)	bloody diarrhea and fever	[24, 25]
4	<i>Enterohemorrhagic (EHEC), including E. coli O157:H7</i>	bloody diarrhea Hemolytic-uremic syndrome	[23, 24]
5	<i>Pseudomonas aeruginosa</i>	Pneumonia Urinary tract infection Corneal infection Endocarditis Osteomyelitis Burn wound infection	[23, 24]
6	<i>Salmonella typhi</i>	Typhoid fever type salmonellosis (fever, abdominal pain, hepatosplenomegaly, rose	[23, 24]

## Chapter 2

		spots) Chronic carrier state	
7	<i>S. typhimurium</i>	Salmonellosis with gastroenteritis Paratyphoid fever Osteomyelitis in people with sickle cells Sepsis	[23, 24]
8	<i>Staphylococcus aureus</i>	Coagulase-positive staphylococcal infections: Skin infections, including impetigo Acute infective endocarditis Septis Necrotizing pneumonia Meningitis	[23, 24]
9	<i>Epidermidis</i>	Infections of implanted prostheses(e.g. heart valves and joints) and catheters	[23, 24]
10	<i>Saprophyticus</i>	Cystitis in women	[23, 24]
11	<i>pneumoniae</i>	Acute bacterial pneumonia & meningitis in adults Otitis media and sinusitis in children Sepsis	[23, 24]
12	<i>pyogenes</i>	Streptococcal pharyngitis Sepsis Scarlet fever Rheumatic fever Impetigo and erysipelas Puerperal fever	[23, 24]
14	<i>S. sonnei</i>	Shigellosis (bacillary dysentery)	[23, 24]
15	<i>Klebsiella pneumoniae</i>	Klebsiella pneumonia, with significant lung necrosis and hemoptysis Hospital-acquired Urinary tract infection and sepsis	[24, 26]

Photocatalytic antibacterial property of TiO<sub>2</sub> NPs would help to promote its photocatalyst based research for the development of efficient photocatalytic disinfection technology. Compared with other photocatalyst, TiO<sub>2</sub> is much more promising due to its highly stable nature, non-corrosive, environmentally benign, ubiquitous component and cost effectiveness. Based on recent research works, enhancement methods for photocatalytic antibacterial applications of TiO<sub>2</sub>-MWCNTs NCs are reviewed and summarized.

### 2.2 Infectious diseases and antibacterial surfaces

Infectious diseases are caused by organisms such as bacteria, viruses, fungi or parasites. Many organisms live in and on our bodies. They're normally harmless or even helpful, but under certain conditions, some organisms may cause disease. Some infectious diseases can be passed from person to person. Some are transmitted by bites from insects or animals. The others are acquired by ingesting contaminated food or water or being exposed to organisms in the environment. Signs and symptoms vary depending on the organism causing the infection, but often include fever and fatigue. Mild infections may respond to rest and home remedies, while some life-threatening infections may require hospitalization. The common bacterial species with causing diseases listed in Table 2.1.

An antimicrobial surface contains an antimicrobial agent that inhibits or reduces the ability of microorganisms to grow on the surface of a material [27]. Such surfaces are becoming more widely investigated for possible use in various settings including clinics, industry, and even the home. The most common and most important use of antimicrobial coatings has been in the healthcare setting for sterilization of medical devices to prevent hospital associated infections, which have accounted for almost 100,000 deaths in the United States [28]. In addition to medical devices, linens and clothing can provide a suitable environment for many bacteria, fungi, and viruses to grow

when in contact with the human body which allows for the transmission of infectious diseases. Antimicrobial surfaces are functionalized in a variety of different processes. A coating may be applied to a surface that has a chemical compound which is toxic to microorganism. Other surfaces may be functionalized by attaching a polymer [29], or polypeptide to its surface an innovation in antimicrobial surfaces is the discovery that copper and its alloys are natural antimicrobial materials that have intrinsic properties to destroy a wide range of microorganism. But instead of this photoactive nanomaterials coating on surfaces and develop the surface as antibacterial surfaces have been much interest in the microbial contamination of the inanimate environment within a healthcare setting and the effect this may have on the epidemiology of hospital-acquired infections. Application of antimicrobial surface technologies to mitigate this contamination, has been reviewed elsewhere [18]. However, recent studies have surveyed patients and staff within hospital environments and have recovered microorganisms from various devices. Literature shows that in the period 2005–2009 all studies in this field reported contamination of devices with microorganisms, with up to 40% of studied devices having *Staphylococcus aureus* present a microbe of clinical significance in nosocomial hospital infections [18, 30].

### 2.3 Photocatalytic inactivation of bacteria by using nanocomposites

Energy received from Sun in the form of photons is a great gift for humans. The photons have energy related to wavelength from the high energy sources like X-ray, gamma ray relation given by  $h\nu = hc/\lambda$ . Where  $h$  is planks constant,  $C$  is velocity constant. In the nature photon energy used to clean the environment including bacterial infection in continuation with the nanomaterials have been predicted to be the effective source of inactivation of bacteria. Photo-inactivation of bacteria with nanomaterial is attracted great attention due to the unique physical, chemical and biological properties of photoactive NCs.

Although, photo inactivation of bacteria first time demonstrated in 1985 by Manstunga et al. [22] against pathogenic bacteria, by using UV light irradiation on TiO<sub>2</sub>/Pt hybrid nanostructures. Afterword's TiO<sub>2</sub> photo-catalyst is used for photo-inactivation of a large number of bacterial species. But use of UV light is also one of limitation to use of photoactive materials. Currently, visible light photoactive nanomaterials are used for photo-inactivation of bacteria by exposing visible light to material in the presence of bacteria, for generation of reactive oxygen species (ROS) which damages the cell wall bacteria.

Microbial contamination and proliferation hospitals (HAI) surfaces are the key cause of associated infection. One potential means by which bacterial surface contamination can be reduced is the use of photosensitization, utilising photoactive nanomaterials. These nanomaterials are non-toxic, however, when irradiated with visible light, the nanomaterials is generated to the reactive oxygen species and subsequently undergoes photochemical reactions either involving electron transfer with substrate molecules such as water (type I), or energy transfer with triplet state molecule oxygen (type II). Overall, these photocatalytic processes generate a wide range of cytotoxic ROS such as hydroxyl radicals, superoxide radicals (type I) and singlet oxygen (type II), which can affect [31] the oxidation of biological molecules including nucleic acids, lipids, polysaccharides and proteins. Moreover, the antimicrobial activity demonstrated by the generated ROS utilises a specific “multi-site” mechanistic mode of attack against microorganisms in the vicinity, rendering the incidence of microbial resistance extremely unlikely. In clinical applications, it is important that the photoactive nanomaterial and illumination conditions employed to effect the lethal photo-inactivation of bacteria, do not demonstrate a similar photo toxicity towards host cells. Investigations have indicated that both the photoactive nanomaterial concentrations and irradiation times required to inactivate bacteria, is not sufficient to cause damage to mammalian cells.

This chapter focus on photo-inactivation of bacteria and the detail photo-inactivation mechanism explained in this chapter.

### 2.4 Controlling of infectious diseases with photo-inactivation

Infectious diseases are transferred from a source to a receiver through surfaces or the air and water. Airborne and waterborne transfer are harder to measure and control with the traditional system. Recent advances in air and water cleaning technology are helping experts understand how the pathogens are transferred and how they can be controlled. The result is generally safer, healthier environments. Traditional system has a limited ability to capture and hold airborne and waterborne pathogens. A new technology called photo-inactivation of bacteria is able to neutralize a wide range of airborne and waterborne pathogens into Hospital Acquired Infections (HAI) [31].

#### 2.4.1 Mechanism for photo inactivation of bacteria

The different types of interaction are shown nanomaterials and bacterial cell wall interaction Fig. 2.1. Overall it is hydrodynamic interactions between the catalyst and the microorganism. This is related with particle size, the possible three ways of interaction shown in Fig. (1) The nanoparticles are larger than the microbial cells. This may be the case when catalyst particles agglomerate forming relatively large aggregates or when the nanoparticles forms a continuous immobilized surface (e.g., thin film applications); (2) the nanoparticles are much smaller than the microbial cells as is the case for ultra-fine catalysts in suspension; (3) the nanoparticles and the microbial cells are of equal size and mutually interact.



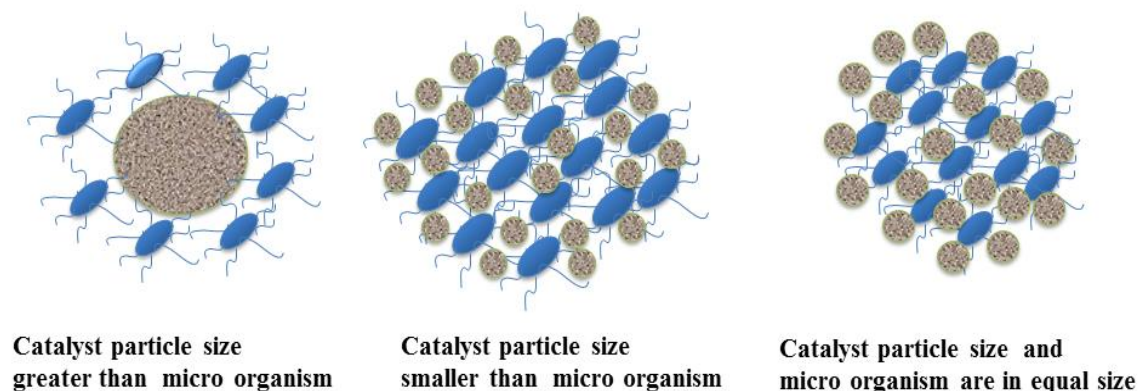


**Fig. 2.1 Size dependent interaction of photo induced nanomaterials with microbial cell**

### **2.4.2. Extracellular target sites**

In photo-induced disinfection cell membrane and cell wall are the first targets in the extracellular environment. However, cell membrane and cell wall were made up of complex structures and also multiple sites were available for the attack. In the bacterial study mainly external layers mainly divided in three classes: (1) the peptidoglycan layer, present in both Gram-negative and Gram-positive bacteria; (2) the lipopolysaccharide layer (LPS), the outermost layer found only in Gram-negative bacteria; and (3) the phospholipid bilayer two in Gram-negative and one in Gram-positive organisms.

### **Peptidoglycan**

In literature, very few reports available on the effects of photo induced activity of the peptidoglycan layer. Peptidoglycan is one of a peptide-cross linked polysaccharide matrix which surrounds the cell. The basic function is sheet formation from individual elements by adjusting peptidoglycan layer. Peptidoglycan layer is plays very important role in Gram-positive bacteria,

## Chapter 2

---

because about 90% of the cell wall made up of peptidoglycan with several sheets stacked upon each other. As compared to Gram-positive, the Gram-negative bacteria, cell wall contain only 10% of the peptidoglycan. So it is possible that peptidoglycan layer may be susceptible to radical attack [32].

But, peptidoglycan layer is very porous which allows nanoparticles of approximately (2 nm) to pass through layer in both Gram-negative as well as Gram-positive bacteria [33]. Whereas, peptidoglycan layer pores are enough to pass the oxidative species, likes superoxide and hydroxyl radical, If photo induced inactivation were is depends upon thickness of peptidoglycan layer then, Gram-positive bacteria having more advantage as compared to Gram-negative bacteria. This result has been suggested in literature by researchers who have already done the comparative study of Gram-positive and Gram-negative bacteria same photocatalytic conditions [34, 35]. But, the comparison of inactivation rates between Gram-positive and Gram-negative bacteria based was not simply depends upon on peptidoglycan layer thickness. And also comparison is totally based on the complexity and density of the cell wall. So it is clear that thick peptidoglycan layer in Gram-positive bacteria to possibly having greater resistance than the outer membrane of the Gram-negative bacteria, while some researchers did observe a decrease in inactivation rate with increased layer density and complexity [35]. Although still it is very difficult to make final conclusions regarding the role of peptidoglycan in the inactivation mechanism (or in the resistance thereof), so cell wall complexity is an unclear parameter.

### **Lipids and polysaccharides**

Up to the present time, the many researchers have shown that the, particularly polyunsaturated fatty acids (PUFA), are the major targets for oxidative radical attack. The inhibiting effects of lipid peroxidation in cells have been

confirmed both in photocatalytic experiments [36, 37] and other reactions involving radicals [38-40]. Polyunsaturated fatty acids are among the most oxygen sensitive molecules in nature.

Previously the effect of ROS, especially free radicals, on cellular molecules has been well reported. These free radicals are naturally occurring in biological systems, but when the free radicals are not controlled, they damage to important cell content likely Nucleic acids, lipids and proteins. The lipid peroxidation has also linked to degenerative diseases in human like Alzheimer's, cancer, immune system decline and cardiovascular disease. In photo induced activity lipid peroxidation attracting much interest because the LPS layer and the phospholipid bilayer contain fatty acids, which may be susceptible to peroxidation. In photo induced activity ROS like hydroxyl radicals were generated in the extracellular environment and they have ability to travel only very short distances before meeting oxidizable substrate like fatty acids [41]. The presence of complex and multilayer membrane decrease the changes of the radical reaching intracellular components such as DNA. The repeating arrangement of lipids forms predominantly composed phospholipids membrane. And chain reaction is started by which allow to damage the cell at sites comparatively different that initiation sites. This whole chain reaction due to the reaction of an unsaturated fatty acid with a free radical in the presence of oxygen, which causes the formation of a peroxy radical, so there is possibility of react with other nearby lipid molecules to generate additional lipid radicals. The continuous process shows newly produced lipid radicals react with other unsaturated lipids. So the chain reaction ultimately results in the oxidation of biomolecules at sites different sites rather than initial sites.

---

### 2.4.3. Intracellular target sites

The cytoplasm is made up of a complex mixture of chemicals and structures in the cell. The main components present in cytoplasm, are RNA, DNA and ribosomes with other dissolved or suspended materials. These entire components are very important for the proper functioning of the organism. The cell membrane plays important role for cytoplasm is protected by the cell membrane, which is not give permission to enter any molecules and ions. Only water and a few other small, uncharged molecules like oxygen and carbon dioxide diffuse freely across the membrane. All other substances enter through active transport or diffuse through trans-membrane proteins, whose channels open and close according to the needs of the cell.

There is few major factors which avoids the possibility of intracellular target sites being reached: (1) in the presence of water at a typical pH 5-8 , nanoparticles get aggregated and formed nanocomposites greater than 300 nm [42, 43]; (2) it is typically considered that oxidation of bacterial cell takes place through surface-bound radicals which are not free to diffuse into the cell [22, 44] (3) if consider some radicals are free or detached in solution, they are highly reactive and imminently they found the oxidizable substrate on the cytoplasmic membrane. This is clearly shown that the attack of intracellular components gives with generation of other oxidants, such as, hydrogen superoxide peroxide lipid radicals and, surface-bound radicals on particles. Photo-induced apart from direct attack, superoxide and hydrogen peroxide can produce hydroxyl radicals in the intracellular environment through the Fenton reaction involving “free” iron [45-47]. Many cells tend to regulate their iron uptake as a mechanism of defense against the formation of the more active hydroxyl radical formed from the Fenton reaction [47]. However, once generated within the cell, the hydroxyl radical is free to attack biomolecules and decomposition occurs.

### Enzymes and coenzymes

The most vital substance in the cytoplasm is enzyme. Enzymes catalyze a wide variety of chemical reactions in the cell. No study has investigated the complete degradation of vital enzymes as part of a photocatalytic inactivation mechanism. Though its effect has not been substantially studied in photochemical disinfection, superoxide is capable of directly inactivating a select group of enzymes [48, 49].

However, initial studies in photocatalytic disinfection pointed to the oxidation of coenzyme A as the mechanism of inactivation [22]. Coenzymes (small non-protein molecules) participate in catalytic reactions as part of an enzyme. Coenzyme A was isolated as a target to be observed largely because the same research group had previously shown that coenzyme. A mediates electron transfer between cells and an electrode [50]. It could be possible that an attack of coenzyme plays a role in cell inactivation.

### **Nucleic acids**

DNA is particularly susceptible to oxidative stress. ROS may attack DNA either at sugar or at the base, giving rise to a large number of products [51]. Attack at sugar ultimately leads to sugar fragmentation, base loss, and a strand break with a terminal garmented sugar residue. Damage to nucleic acid in photocatalytic systems appears as an indirect result from the generation of superoxide. By using strains of *E. coli*, deficient in genes known to confer resistance to ROS and regulate iron uptake. Gogniat and Dukan et al. [52] suggested that DNA damage resulted from hydroxyl radical attack generated by the Fenton reaction. They observed an increase in susceptibility to photocatalysis by the mutant strains, particularly during recovery. In addition, this may support the observation that DNA can be attacked by at least two different modes, which include direct hydrogen peroxide or superoxide attack and Fenton reaction-generated radicals [52]. The schematic representation for mechanism of photo-inactivation bacteria shown in Fig. 2.2.

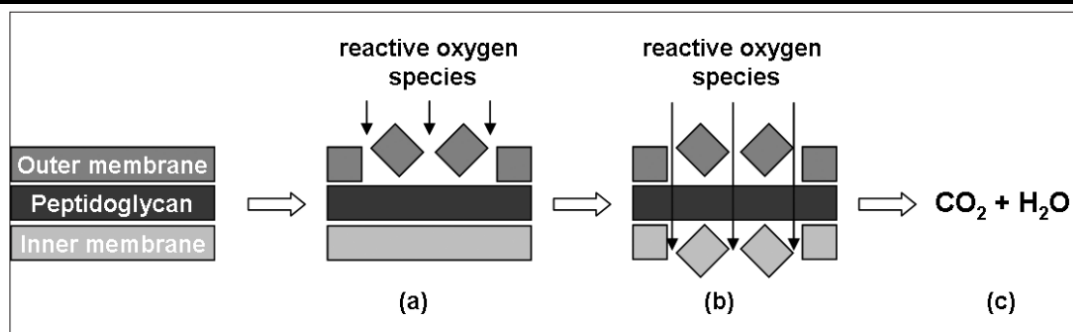


**Fig. 2.2 Three-step proposed mechanism for photo-inactivation of bacteria on antibacterial surfaces.**

## 2.5 Photoactive nanomaterials

Photoactive nanomaterials are one of the most important nanomaterials for functioning as highly sensitive labelling reagents in various bio applications [53]. Current developments have demonstrated that photoactive nanomaterials provide significant strong and photo-stable optical properties which help to photo-inactivation of bacteria. In comparison with bare photoactive materials, modified hybrid demonstrated great potential as highly efficient photo-inactivation of bacteria.

Regarding the suitability of nanomaterials (NMs) to be used as nano disinfectant, they have to compile with the above mentioned properties; however, the proper use of any NMs should also include: (1) Physical (i.e. no aggregation or settling) and chemical stability in aqueous phase; (2) for photo-excitation NPs must be active under light illumination. Therefore, researchers are seeking to develop new multifunctional NMs to improve disinfection systems as well as to remove organic and inorganic pollutants from water. Although it will take some time to understand the full potential of NMs, it shows to be a promising approach for water disinfection processes. As a result, a noticeable number of NMs have been proposed such as photocatalytic titanium dioxide (TiO<sub>2</sub>), zinc oxide (ZnO), Carbon nanotubes (CNTs).

---

### 2.5.1 Zinc oxide (ZnO)

ZnO has been proved as strong antimicrobial agent by exhibiting the activity in the 7.0–8.0 pH range, which are favorable for the treatment of drinking water [54, 55]. ZnO is a semiconductor with a large band gap. Hence high energy is applied for the formation of holes ( $h^+$ ) and free electrons. The holes react with water to form  $\bullet OH$  and electrons in CB react with oxygen to form  $\bullet O^{2-}$  and  $\bullet OH$ . All these reactions will ultimately end on forming  $H_2O_2$  [56]. Shi et al. observed that ZnO worked as a bacteria growth inhibitor and this effect was more on Gram-positive bacteria.  $H_2O_2$  formation was linearly proportional to the concentration of ZnO [56]. Electrostatic forces might play an important role by promoting the binding of bacteria on particle surface [57]. Moreover, Zhang et al. [58] concluded that ZnO could inhibit the growth of Gram-positive and Gram-negative bacteria even some high temperature and pressure resistance spores.

### 2.5.2 Carbon nanotubes (CNTs)

Carbon nanotubes (CNTs) are one of the most important NMs with their unique physical, chemical and mechanical properties [59]. These NMs has different industrial applications including its passive or active use in concrete technology, textiles, conductor and semiconductor technology, solar cell, water treatment, air purification, biotechnology, mechanical engineering and medicine. Kang and his research group worked extensively on CNTs application as antimicrobial agents. They found that purified single walled-nanotubes (SWNTs) could be strong antimicrobial through severe damage of cell membrane and contact of the nanotubes (NTs) with bacteria (i.e. *E.coli*). Contact with bacteria might increase the cell permeability and facilitate the release of cytoplasmic fluid into the solution of SWNTs. The concentration of plasmid materials such as DNA and RNA was increased by 5 times and 2 times, respectively, in the presence of SWNTs. Damage of cell membranes was indicated by these high

concentrations of DNA and RNA in solutions. Other two possible mechanisms of bacteria inactivation might be metal toxicity and oxidation stress (i.e. lipid peroxidation in cell). The observed toxicity effect was related with incubation period of SWNTs and bacteria [60].

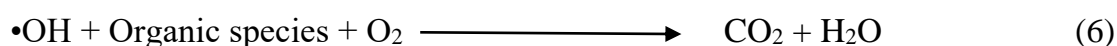
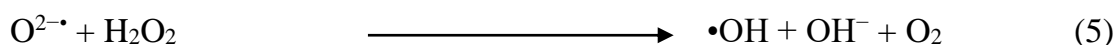
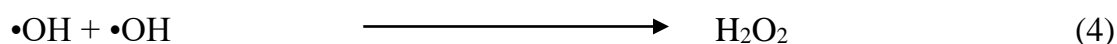
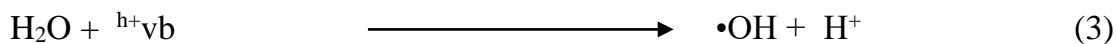
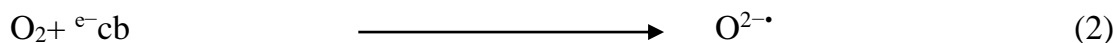
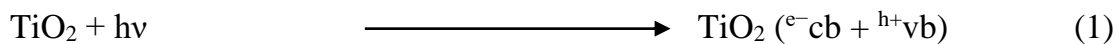
### 2.5.3. TiO<sub>2</sub> nanoparticles

TiO<sub>2</sub> is the most commonly used nanoparticle to inactivate pathogens in water. It has a wide range of industrial applications that include: food industry, photocatalytic media, gas sensor, paint and cosmetic industry as white pigment, water treatment, air purification, solar energy, UV absorber, semiconductor industry and agricultural industry [61]. Inactivation of microorganisms depends on several factors, e.g., concentration of TiO<sub>2</sub>, type of microorganism, intensity and wavelength of light, degree of hydroxylation, pH, temperature, availability of oxygen and ROS and retention time [62, 63].

In photocatalysis, a light of sufficient energy is incident on semiconducting material to generate ROS which are responsible for photochemical transformations. Traditional TiO<sub>2</sub> photocatalyst shows activity under UV light only. In TiO<sub>2</sub> photocatalytic process, when light energy is greater than its band gap, it ejects an electron from the valence band to the conduction band, creating a negatively charged free electron and a positively charged hole. The electrons are then free to migrate within the conduction band and the holes may be filled by an electron from an adjacent molecule. This process can be repeated. Thus, holes are also mobile. The electrons and holes generated by the reactions have strong reducing and oxidizing power. Electrons and holes may recombine (bulk recombination) a non-productive reaction, or, when they reach the surface, react to give ROS such as superoxide anion radical ( $O_2^{\cdot-}$ ) and hydroxyl radical ( $\cdot OH$ ). The hydroxyl radicals combine together to form hydrogen peroxide ( $H_2O_2$ ); which further reacts with superoxide anion radical to produce hydroxyl ion and hydroxyl radical [61]. Reaction of these ROS with



organic compounds results in the mineralization with the formation of CO<sub>2</sub> and H<sub>2</sub>O. The various reactions involved in TiO<sub>2</sub>-based photocatalytic process are shown below:



ROS are extremely reactive hence the destruction of microorganism in air and water can be achieved when they come into contact with the surfaces of a photocatalyst. Photocatalysis has been shown to be capable of killing a wide range of organisms including Gram-negative and Gram-positive bacteria, including endospores, fungi, algae, protozoa and viruses [64].

Different mechanisms for killing of bacteria have been proposed in the literature, which include the killing mechanism implies an oxidation of the intracellular coenzyme A (CoA) due to direct contact with TiO<sub>2</sub> in presence of photon, which inhibits cell respiration and subsequently causes cell death [22, 65]. Another mechanism is bacterial death due to significant disorder in the cell permeability and decomposition of the cell walls [66]. It is suggested that the cell wall damage might take place prior to cytoplasmic membrane damage. During the photo-oxidation process, the UV light irradiation also causes cell damage. Oguma et al. [67] reported that long wavelength UV light (i.e., 320–400 nm) mainly damages microorganisms by exciting photosensitive molecules within the cell, and the generated ROS adversely affect the genome and other intracellular molecules sub-lethally or lethally causing cell mutations, growth delay. Sunada et al. [68] reported cell membrane damage due to the photoca-

talytic degradation of endotoxin from *E. coli* with TiO<sub>2</sub> thin films. Maness et al. [36] showed the photo-oxidation of bacterial cell components responsible for cell death. Damage of the cell membrane directly leads to leakage of minerals, proteins, and genetic materials, causing cell death. Keller et al. [69] disputed that many parameters acting significantly at the biological level are not taken into account for chemicals. The adsorption was consistently associated with reduction in bacterial membrane integrity, as revealed by flow cytometry. They suggested that adsorption of cells onto aggregated TiO<sub>2</sub>, followed by loss of membrane integrity, and were the key to the bactericidal effect of photo catalysis.

### **2.6. Strategies for improving photocatalytic properties of TiO<sub>2</sub> nano-particles**

Different approaches have been adopted for improving TiO<sub>2</sub> photocatalytic efficiency; all of them consist of either morphological modifications, such as increasing surface area and porosity, or the incorporation of additional components, such as metals or semiconductor material. However, contradictory reports available in the literature are devoted to TiO<sub>2</sub> improvement, very likely because changing composition or morphology unavoidably modifies other parameters which also affect efficiency of TiO<sub>2</sub>. The major drawback in the semiconductor photocatalysis is the recombination of photo generated charge carriers as it lowers the activity [70]. Also, the potential applicability of TiO<sub>2</sub> photocatalyst is prevented by its wide band gap, which lies in the UV light region. For making visible light driven photocatalyst and retard possible electron-hole pair recombination, doping of TiO<sub>2</sub> with transition metal ions is one of the most successful strategies. These strategies can alter the optical as well as electronic properties and, thus, enhance the efficiency of TiO<sub>2</sub> in the presence of photon for various applications.

### 2.6.1. Transition metal doping

Transition metal ions can provide additional energy levels, called as density of states, within the band gap of a semiconductor. Electron transfer from one of these levels to the conduction band requires lower photon energy than in the situation of an unmodified semiconductor [71, 72].

### 2.6.2. Noble metal loading

Addition of noble metals is another approach for the modifying photocatalyst. Active antimicrobial noble metals (silver, gold, & platinum) were incorporated in TiO<sub>2</sub> photocatalyst to enhance the bactericidal activity. Because the Fermi levels of these noble metals are lower than that of TiO<sub>2</sub>, photo excited electrons can be transferred from the conduction band of TiO<sub>2</sub> to metal particles deposited on the surface of TiO<sub>2</sub>, while photo generated holes in the valence band remain on TiO<sub>2</sub>. This greatly reduces the possibility of electron-hole pair recombination, resulting in efficient separation and higher photocatalytic activity [71, 73].

### 2.6.3. Non-metal doping

Among the many chemical modifications adopted for shifting the TiO<sub>2</sub> band gap to lower energy, currently the most promising route seems to be the partial substitution of oxygen with non-metals (N, C and S). Extensive research on non-metal doping for enhancement of bactericidal activity of TiO<sub>2</sub> has been reported in literature. In particular, most of the studies have focused on non-metal doped TiO<sub>2</sub>, which show remarkable photoactivity under visible illumination. Doping of non-metal ions (N, C, S etc.) in TiO<sub>2</sub> host lattice could shift its photo-response in the visible region [74-78].

---

### 2.6.4. Hybrid nanocomposites

It is possible to create coupled colloidal structures, in which illumination of one semiconductor produces a response in the other semiconductor at the interface between them and such nanocomposites exhibit very high photocatalytic activity [79]. The geometry of particles, surface texture, and particle size plays a significant role in inter particle electron transfer [71]. A ternary hybrid CdS/Pt–TiO<sub>2</sub> nanotube photo electrode developed by dipping and deposition technique and ionic layer adsorption and reaction (SILAR) showed higher bactericidal activity for *E.coli* [80, 81]. Hamal et al. [81] demonstrated that TiO<sub>2</sub> co-doped with Silver, Carbon, and Sulphur can serve as a multifunctional generic biocide as well as a visible light activated photo-catalyst. It shows strong antimicrobial properties without light activation against both *E. coli* and *B. subtilis* spores. The antibacterial activity of various TiO<sub>2</sub> based NCs against the Gram-positive and Gram-negative bacteria is reviewed in detail and it shown in Table 2.2

Table 2.2 Antibacterial activity of TiO<sub>2</sub> based nanocomposites

Sr. No.	Bacteria	Material	Activity in		Reference
			Dark	light	
	<b>Gram-positive</b>				
1	<i>Micrococcus luteus</i>	Apatite/TiO <sub>2</sub>	✓	✓	[82]
2	<i>Staphylococcus aureus</i>	Apatite/TiO <sub>2</sub>	✓	✓	[82]
		N-TiO <sub>2</sub> :PTFE	X	✓	[83]
		Cu/TiO <sub>2</sub> /Cs	✓	✓	[84]
		TiO <sub>2</sub> -MWCNTs	✓	✓	[59]
3	<i>Bacillus subtilis</i>	TiO <sub>2</sub> -MWCNTs	X	✓	[85]
		Fe-TiO <sub>2</sub> -MWCNTs	X	✓	[86]
	<b>Gram-negative</b>				
1	<i>Aeromonas hydrophila</i> (BCRC 13018)	Fe <sub>3</sub> O <sub>4</sub> /TiO <sub>2</sub>	--	✓	[87]
2	<i>Edwardsiella tarda</i> (BCRC 10670)	Fe <sub>3</sub> O <sub>4</sub> /TiO <sub>2</sub>	--	✓	[87]
3	<i>Escherichia coli</i>	CNT-TiO <sub>2</sub>	✓	✓	[88]
		Apatite/ TiO <sub>2</sub>	✓	✓	[82]
		Ag-N-TiO <sub>2</sub>	✓	✓	[89]
		TiO <sub>2</sub> -MWCNTs	X	✓	[59]
4	<i>Escherichia coli</i> (8099)	Cu/TiO <sub>2</sub> /C	✓	✓	[84]
5	<i>Escherichia coli</i> (AN 387)	Ag <sub>2</sub> O/TiON	✓	✓	[90]
6	<i>Escherichia coli</i> (DH 5R)	Au-TiO <sub>2</sub>	X	✓	[91]
7	<i>Escherichia coli</i> (IFO 3301)	Cu/TiO <sub>2</sub>	✓	✓	[68]
8	<i>Escherichia coli</i> (NBRC 3972)	N-TiO <sub>2</sub> : PTFE	X	✓	[83]

9	<i>Escherichia coli</i> k-12 (ATCC 29181)	Nd <sup>3+</sup> -TiO <sub>2</sub> / NiFe <sub>2</sub> O <sub>4</sub>	--	√	[92]
10	<i>Photobacterium damsela</i> <i>subsp. piscicida</i>	TiO <sub>2</sub> /Fe <sub>3</sub> O <sub>4</sub>	X	√	[93]
11	<i>Pseudomonas aeruginosa</i>	Fe-TiO <sub>2</sub> - MWCNTs	X	√	[86]

### 2.7 Future prospects of photo-induced nanomaterials in antibacterial studies

Photocatalytic antibacterial activity is a hot cake of environmental, bio-medical research and an alternative technique for inhibition of bacteria. Since 1985, photocatalytic disinfection technology by TiO<sub>2</sub> still retains its importance in research because of the unique physiochemical properties of TiO<sub>2</sub> NPs, and its ability to mineralize pollutants and microorganisms. TiO<sub>2</sub> NPs possesses a large surface area with small particle size, which is useful in photocatalytic disinfection. Generation of ROS by photocatalysis on TiO<sub>2</sub> is responsible for killing a wide range of organisms in water, in air and on surfaces. Different modified TiO<sub>2</sub> based photocatalyst have been synthesized and found to be effective for the photocatalytic disinfection. Surface coating is another option for developing real systems, which is promising for the commercialization of the technology. Modified TiO<sub>2</sub> photocatalyst were investigated to achieve absorption from the visible region by reducing the band gap of the doped catalyst. There is urging to develop standard method for the testing of the antimicrobial efficiency of photocatalytic processes. Future advances in nanotechnology will present great opportunities for designing more effective photocatalytic disinfection systems, particularly the visible light driven ones. Photocatalytic systems that use low cost visible lamp light and solar light to achieve adequately high output are of great interest. Photo-catalytic bactericidal

technology has great potential applications in biomedical and environment remediation and further research is necessary.

---

### Reference

- [1] T. Denis, A. C. Dai T, R. Anderson, and M. Hamblin, *Virulence*, 2 (2011) 509.
- [2] J. A. Byrne, P. S. M. Dunlop, J. W. J. Hamilton, P. Fernández-Ibáñez, I. Polo-Lopez, P. K. Sharma, and A. S. M. Vennard, *Molecules*, 20 (2015) 5574.
- [3] C. McCullagh, J. M. Robertson, D. W. Bahnemann, and P. K. Robertson, *Res. Chem. Intermed.* 33 (2007) 359.
- [4] O. Planas, R. Bresoli-Obach, J. Nos, T. Gallavardin, R. Ruiz-González, M. Agut, and S. Nonell, *Molecules* 20 (2015) 6284.
- [5] S. H. Zinner, *Expert. Rev. Anti. Infect. Ther.* 3 (2005) 907.
- [6] R. A. Bohara and S. H. Pawar, *Appl. Biochem. Biotechnol.* 176 (2015) 1044.
- [7] J. B. Lamb1, J. A. van de, D. G. Bourne, C. Altier, M. Y. Hein, E. A. Fiorenza1, J. Jompa, and C. Drew Harvell, *Science* , 355(2017) 6326.
- [8] I. Yacoby and I. Benhar, *Future Medi.* 3 (2008) 329.
- [9] H. Gelband, P. Molly Miller, S. Pant, S. Gandra, J. Levinson, D. Barter, A. White, and R. Laxminarayan, *Wound Healing Southern Africa* 8 (2015) 30.
- [10] R. Laxminarayan, A. Duse, C. Wattal, A. K. Zaidi, H. F. Wertheim, N. Sumpradit, E. Vlieghe, G. L. Hara, I. M. Gould, and H. Goossens, *Lancet Infect. Dis.* 13 (2013) 1057.
- [11] N. Kayange, E. Kamugisha, D. L. Mwizamholya, S. Jeremiah, and S. E. Mshana, *BMC Pediatrics.* 10 (2010) 39.
- [12] A. Roca, L. Quintó, F. Abacassamo, L. Morais, X. Vallès, M. Espasa, B. Sigaúque, J. Sacarlal, E. Macete, and A. Nhacolo, *Trop. Med. Int. Health* 13 (2008) 818.
- [13] M. Herz, *Nw. UL Rev.* 99 (2004) 297.
- [14] A. Talaiekhosani, M. R. Talaei, and S. Rezania, *J. Environ. Chem. Eng.* 5 (2017) 1828.



- [15] S. Sharma and A. Bhattacharya, Appl. Water Sci. 7 (2017) 1043.
- [16] E. W. Rice, J. C. Hoff, and F. W. Schaefer III, Appl. Environ. Microbiol. 43 (1982) 250
- [17] W. Q. Betancourt and J. B. Rose, Vet. Parasitol. 126 (2004) 219.
- [18] K. Page, M. Wilson, and I. P. Parkin, J. Mater. Chem. 19 (2009) 3819.
- [19] A. Vohra, D. Goswami, D. Deshpande, and S. Block, J. Ind. Microbiol. Biotechnol. 32 (2005) 364.
- [20] R. J. Watts, S. Kong, M. P. Orr, G. C. Miller, and B. E. Henry, Water Res. 29 (1995) 95.
- [21] A. Fujishima, Nature 238 (1972) 37.
- [22] T. Matsunaga, R. Tomoda, T. Nakajima, and H. Wake, FEMS Microbiol. Lett. 29 (1985) 211.
- [23] M. R. Hoffmann, S. T. Martin, W. Choi, and D. W. Bahnemann, Chem. Rev. 95 (1995) 69.
- [24] R. Herriman, List of common pathogenic bacteria that affect the human body system Sep (2011).
- [25] S. S. Kaufman, C. A. Loseke, J. V. Lupo, R. J. Young, N. D. Murray, L. W. Pinch, and J. A. Vanderhoof, J. Pediatr. 131 (1997) 356.
- [26] R. E. Lundgren and A. H. McMakin, Risk communication: A handbook for communicating environmental, safety, and health risks, John Wiley and Sons, (2013).
- [27] G. McDonnell and A. D. Russell, Clin. Microbiol. Rev. 12 (1999) 147.
- [28] R. Dastjerdi and M. Montazer, Colloids Surf., B 79 (2010) 5.
- [29] A. Raut, R. Satvekar, S. Rohiwal, A. Tiwari, A. Gnanamani, S. Pushpavanam, S. Nanaware, and S. Pawar, Des. Monomers Polym. 19 (2016) 445.
- [30] E. R. Sydnor and T. M. Perl, Clin. Microbiol. Rev. 24 (2011) 141.
- [31] W. Thomas, The Royal College of Surgeons of England, (2008).
- [32] Z. . Lu, L. Zhou, Z. L. Zhang, W. L. Shi, Z. X. Xie, H. Y. Xie, D. W.

- 
- Pang, and P. Shen, *Langmuir* 19 (2003) 8765.
- [33] P. Demchick and A. L. Koch, *J. Bacteriol.* 178 (1996) 768.
- [34] A. Pal, S. O. Pehkonen, E. Y. Liya, and M. B. Ray, *J. Photochem. Photobiol. A* 186 (2007) 335.
- [35] K. P. Kuhn, I. F. Chaberny, K. Massholder, M. Stickler, V. W. Benz, H.G. Sonntag, and L. Erdinger, *Chemosphere* 53 (2003) 71.
- [36] P.C. Maness, S. Smolinski, D. M. Blake, Z. Huang, E. J. Wolfrum, and W. A. Jacoby, *Appl. Environ. Microbiol.* 65 (1999) 4094.
- [37] J. Kiwi and V. Nadtochenko, *J. Phys. Chem. B* 108 (2004) 17675.
- [38] B. R. Moser and S. Z. Erhan, *Eur. J. Lipid Sci. Technol.* 109 (2007) 206.
- [39] I. Tejero, À. González-Lafont, J. M. Lluch, and L. A. Eriksson, *J. Phys. Chem. B* 111 (2007) 5684.
- [40] B. Halliwell and S. Chirico, *Am. J. Clin. Nutr.* 57 (1993) 715S.
- [41] S. Veremeichenko and G. Zdorovenko, *Microbiol.* 73 (2004) 260.
- [42] R. A. French, A. R. Jacobson, B. Kim, S. L. Isley, R. L. Penn, and P. C. Baveye, *Environ. Sci. Technol.* 43 (2009) 1354.
- [43] S. Yurdakal, V. Loddò, B. Bayarri Ferrer, G. Palmisano, V. Augugliaro, J. Giménez Farreras, and L. Palmisano, *Ind. Eng. Chem. Prod. Res.* 46 (2007) 7620.
- [44] A. Mills and S. Morris, *J. Photochem. Photobiol., A* 71 (1993) 75.
- [45] S. I. Liochev and I. Fridovich, *IUBMB life* 48 (1999) 157.
- [46] I. J. Monod, U. Paris, P. Jussieu, Isolation of superoxide dismutase, *Free Radical Biol. Med.* 5 (1986) 623.
- [47] S. Dubrac and D. Touati, *Microbiol.* 148 (2002) 147.
- [48] Y. Kono and I. Fridovich, *J. Biol. Chem.* 257 (1982) 5751.
- [49] J. Blum and I. Fridovich, *Arch. Biochem. Biophys.* 240 (1985) 500.
- [50] T. Matsunaga and Y. Namba, *Anal. Chim. Acta.* 159 (1984) 87.
- [51] H. Hidaka, S. Horikoshi, N. Serpone, and J. Knowland, *J. Photochem. Photobiol. A* 111 (1997) 205.
-

- 
- [52] G. Gogniat and S. Dukan, Appl. Environ. Microbiol. 73 (2007) 7740.
  - [53] T. A. Faunce, Med. J. Aust. 190 (2009) 463.
  - [54] S. Baruah, S. K Pal, and J. Dutta, Nanosci. Nanotechnol. Asia 2 (2012) 90.
  - [55] O. Yamamoto, Int. J. Inorg. Mater. 3 (2001) 643.
  - [56] L. E. Shi, L. Xing, B. Hou, H. Ge, X. Guo, and Z. Tang, Current Research, Technology and Education Topics in Appl. Microbiol. Microbi (2010).
  - [57] P. K. Stoimenov, R. L. Klinger, G. L. Marchin, and K. J. Klabunde, Langmuir 18 (2002) 6679.
  - [58] L. Zhang, Y. Ding, M. Povey, and D. York, Prog. Nat. Sci. 18 (2008) 939.
  - [59] V. B. Koli, A. G. Dhodamani, A. V. Raut, N. D. Thorat, S. H. Pawar, and S. D. Delekar, J. Photochem. Photobiol., A 328 (2016) 50.
  - [60] S. Kang, M. Pinault, L. D. Pfefferle, and M. Elimelech, Langmuir 23 (2007) 8670.
  - [61] H. M. Yadav, S. V. Otari, V. B. Koli, S. S. Mali, C. K. Hong, S. H. Pawar, and S. D. Delekar, J. Photochem. Photobiol. A 280 (2014) 32.
  - [62] C. Wei, W. Y. Lin, Z. Zainal, N. E. Williams, K. Zhu, A. P. Kruzic, R. L. Smith, and K. Rajeshwar, Environ. Sci. Technol. 28 (1994) 934.
  - [63] A. Markowska-Szczupak, K. Ulfig, and A. Morawski, Catal. Today 169 (2011) 249.
  - [64] H. A. Foster, I. B. Ditta, S. Varghese, and A. Steele, Appl. Microbiol. Biotechnol. 90 (2011) 1847.
  - [65] T. Matsunaga, R. Tomoda, T. Nakajima, N. Nakamura, and T. Komine, Appl. Environ. Microbiol. 54 (1988) 1330.
  - [66] T. Saito, T. Iwase, J. Horie, and T. Morioka, J. Photochem. Photobiol., B 14 (1992) 369.
  - [67] K. Oguma, H. Katayama, and S. Ohgaki, Appl. Environ. Microbiol. 68
-

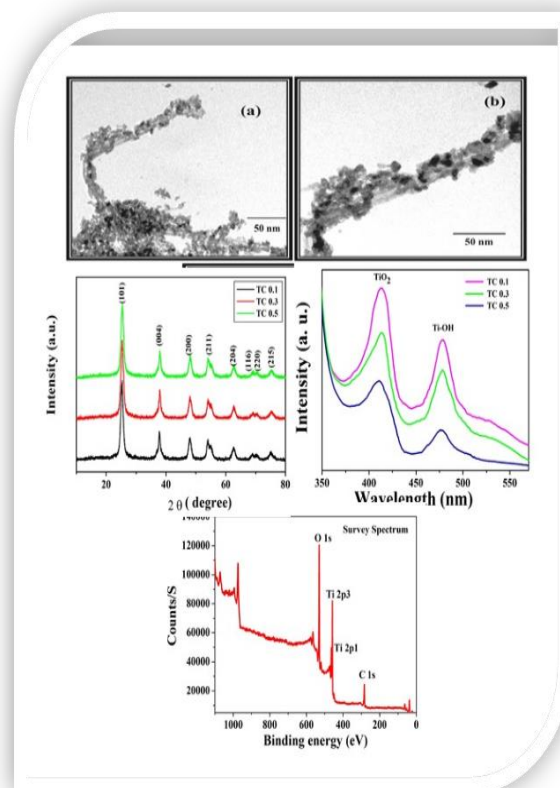
- (2002) 6029.
- [68] K. Sunada, T. Watanabe, and K. Hashimoto, *Environ. Sci. Technol. Lett.* 37 (2003) 4785.
- [69] S. Josset, N. Keller, M.C. Lett, M. J. Ledoux, and V. Keller, *Chem. Soc. Rev.* 37 (2008) 744.
- [70] W. Choi, A. Termin, and M. R. Hoffmann, *J. Phys. Chem.* 98 (1994) 13669.
- [71] S. M. Gupta and M. Tripathi, *Chin. Sci. Bull.* 56 (2011) 1639.
- [72] S. Delekar, H. Yadav, S. Achary, S. Meena, and S. Pawar, *Appl. Surf. Sci.* 263 (2012) 536.
- [73] S. Deshmukh, R. Dhokale, H. Yadav, S. Achary, and S. Delekar, *Appl. Surf. Sci.* 273 (2013) 676.
- [74] P. He, J. Tao, X. Huang, and J. Xue, *J. Sol-Gel Sci. Technol.* 68 (2013) 213.
- [75] V. Etacheri, G. Michlits, M. K. Seery, S. J. Hinder, and S. C. Pillai, *ACS Appl. Mater. Interfaces* 5 (2013) 1663.
- [76] W. Wang, Y. Yu, T. An, G. Li, H. Y. Yip, J. C. Yu, and P. K. Wong, *Environ. Sci. Technol.* 46 (2012) 4599.
- [77] J. C. Yu, W. Ho, J. Yu, H. Yip, P. K. Wong, and J. Zhao, *Environ. Sci. Technol.* 39 (2005) 1175.
- [78] R. Barkul, V. Koli, V. Shewale, M. Patil, and S. Delekar, *Mater. Chem. Phys.* 173 (2016) 42.
- [79] A. Mills and S. Le Hunte, *J. Photochem. Photobiol. A* 108 (1997) 1.
- [80] Q. Kang, Q. Z. Lu, S. H. Liu, L. X. Yang, L. F. Wen, S. L. Luo, and Q. Y. Cai, *Biomater.* 31 (2010) 3317.
- [81] D. B. Hamal, J. A. Haggstrom, G. L. Marchin, M. A. Ikenberry, K. Hohn, and K. J. Klabunde, *Langmuir* 26 (2009) 2805.
- [82] W. Kangwansupamonkon, V. Lauruengtana, S. Surassmo, and U. Ruktanonchai, *Nanomed. Nanotechnol. Biol. Med.* 5 (2009) 240.

- [83] K. Yamauchi, Y. Yao, T. Ochiai, M. Sakai, Y. Kubota, and G. Yamauchi, *J. Nanotechnol.* (2011).
- [84] S. Chen, Y. Guo, S. Chen, H. Yu, Z. Ge, X. Zhang, P. Zhang, and J. Tang, *J. Mater. Chem.* 22 (2012) 9092.
- [85] V. B. Koli, A. G. Dhodamani, S. D. Delekar, and S. H. Pawar, *J. Photochem. Photobiol. A* 333 (2017) 40.
- [86] V. B. Koli, S. D. Delekar, and S. H. Pawar, *J. Materi. Sci. Mater. Medi.* 27 (2016) 177.
- [87] N. Yeh, Y. Lee, C. Chang, and T. Cheng, *Thin Solid Films* 549 (2013) 93.
- [88] O. Akhavan, R. Azimirad, S. Safa, and M. Larijani, *J. Mater. Chem.* 20 (2010) 7386.
- [89] A. A. Ashkarran, H. Hamidinezhad, H. Haddadi, and M. Mahmoudi, *Appl. Surf. Sci.* 301 (2014) 338.
- [90] P. Wu, R. Xie, K. Imlay, and J. K. Shang, *Environ. Sci. Technol.* 44 (2010) 6992.
- [91] G. Fu, P. S. Vary, and C.T. Lin, *The J. Phys. Chem. B* 109(2005) 8889.
- [92] S. Rana, J. Rawat, M. Sorensen, and R. Misra, *Acta Biomater.* 2 (2006) 421.
- [93] T. Cheng, K. Yao, N. Yeh, C. Chang, H. Hsu, F. Gonzalez, and C. Chang, *Thin Solid Films* 519 (2011) 5002.



# Chapter 3

## Characterization Techniques







---

### 3.1 Introduction

The fundamental of nanotechnology lies in the fact that properties of nanomaterials change dramatically when their size is reduced to nanometer range. But measuring this nano dimension is not a very easy task. Although research is going on synthesis of nanostructured and monophasic materials, characterization of this nanosized materials are an emerging fields, posing lot of challenges to scientist and technology, Thus nanotechnology has motivated in upsurge in development and discovery of sophisticated characterization techniques to allow better control of morphology, size and dimensions of nanomaterials. The important characterization techniques used for analysis of TiO<sub>2</sub> NPs and TiO<sub>2</sub>-MWCNTs NCs explained in this chapter. The phase analysis, compositional analysis, surface characterization, structural analysis and the toxicity of formed NCs towards pathogenic microorganisms and mammalian cells were analyzed by techniques such as X-ray diffraction (XRD), UV-visible (UV-Vis) spectroscopy, Transmission Electron Microscopy (TEM), Fourier Transform Infra-Red (FTIR) Spectroscopy photoluminescence spectroscopy (PL), and Raman analysis. This chapter is dedicated to explain of basic principles of the techniques used for characterization of materials.

### 3.2 Structural and Surface Techniques

#### 3.2.1 X-Ray powder Diffraction (XRD)

X-ray powder diffraction (XRD) is a rapid analytical technique, typical XRD unit is shown in Fig.3.1 (a). It provides information on phases, structures, preferred crystal orientations (texture), and other structural parameters like crystallinity, average crystallite size, crystal defects and strain [1]. In this technique, diffraction of X-ray radiation occurs only when the wavelength of the wave motion is same order of magnitude with specific planes of material. The diffraction condition known as Bragg's law and represented by equation [2]

---

$$2d\sin\theta = n\lambda \quad \dots\dots\dots 3.1$$

Where, d = crystallite size

$\theta$  = diffraction angle

$\lambda$  = wavelength of X-ray, n = order of diffraction



**Fig.3.1 (a) Photograph of XRD Unit**

The X-ray powder diffraction method is thus ideally used for characterization on and identification of crystalline phases. The synthesized material is finely ground, homogenized, and average bulk composition is determined [3]. Most of all solid materials can be described as crystalline. In this study when X-rays interact with a crystalline substance (Phase), diffraction pattern is observed. In 1919 scientist A.W. Hull discovered that “Every crystal-line substance gives a pattern; the same substance always gives the same pattern; and in a mixture of substances each produces its pattern independently of the others [4]. Therefore the X-ray diffraction pattern of a pure substance is, like as a fingerprint of the substance. These patterns are wholly depend up on constructive interference of monochromatic X-rays and a crystalline nature of sample. The source used in this technique for generation of X-rays is cathode ray tube,

which is filtered to produce monochromatic radiation, collimated to concentrate, and directed towards the sample.

An electron in an alternating electromagnetic field will oscillate with the same frequency as the field. When an X-ray beam irradiated on atom, the electrons around the atom start to oscillate with the same frequency as the incoming beam [5]. There is destructive interference, that is, the combining waves are out of phase. The atoms in a crystal are arranged in a systematic regular pattern, and constructive interference observed in very few directions [6]. The waves will be in phase and there will be well defined X-ray beams leaving the sample at various directions. Hence, diffracted beam may be described as a beam composed of a large number of scattered rays mutually reinforcing one another. However the crystallites having reflecting planes (hkl) parallel to the specimen surface will contribute to the reflected intensities. These diffracted X-rays are then detected, processed and counted. By scanning the sample through a range of  $2\theta$  angles, all possible diffraction directions of the lattice should be attained due to the random orientation of the powdered material [7]. While conversion of the diffraction peaks to d-spacing permits identification of the mineral because each mineral has a set of unique d-spacing. Typically, this is achieved by comparison of d-spacing of sample with standard reference patterns.

Typical diffractometer is based on the Bragg-Brentano geometry. It commonly contains a source of X-ray and a detector for the detection of diffracted X-rays. There are three types of diffraction methods, viz. Laue method, rotating crystal method and powder method. From these, powder method is used for whole proposed work. A schematic diagram of X-ray diffractometer is shown in Fig. 3.1 (b).

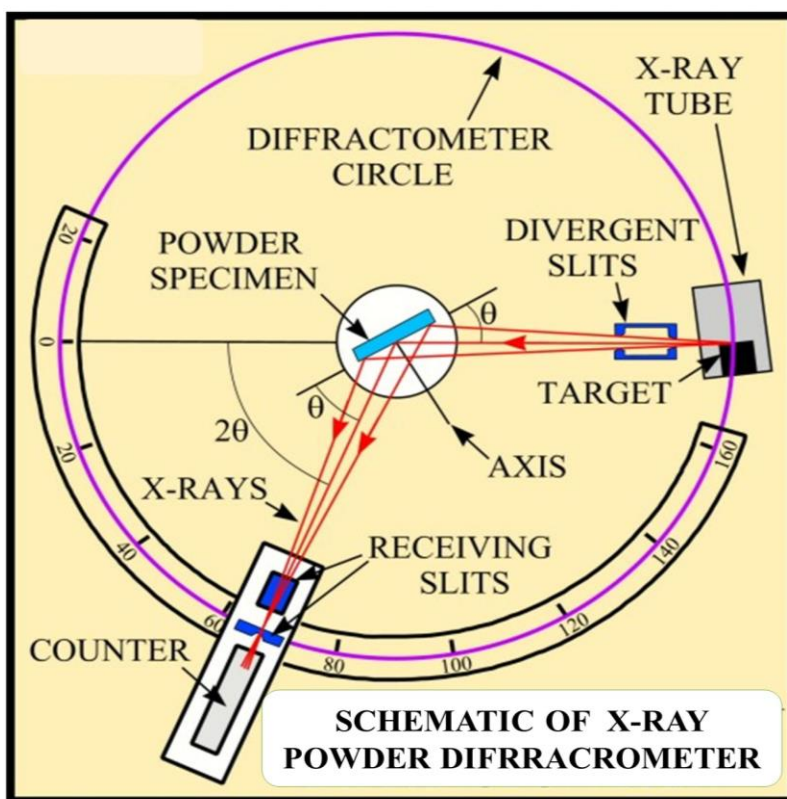


**Fig. 3.1 (b) Schematic of the X-ray diffractometer.**

[Source: <https://www.spec2000.net/09-xrd.htm>]

Scheme of Phase identification and structural analysis of the  $\text{TiO}_2$  NPs under investigation were studied by XRD (Mini Flex 600 Rigaku) in the  $2\theta$  range from 10 to  $80^\circ$ . The patterns were evaluated by Panalytical X'pert high-score software and compared with Joint Committee on Powder Diffraction Standards (JCPDS). The crystallite size (D) was calculated from the Full Width at Half Maximum (FWHM) of high intensity diffraction peak of pattern using Debye formula.

### 3.2.2 Transmission Electron Microscopy (TEM)

Transmission Electron Microscopy (TEM) is one of an important tool for the characterization of NPs. Although XRD can provide information about the average crystallite size of the crystallites from peak broadening, advantage of TEM is useful for the actual visualization of the NPs size and morphology. Furthermore, TEM studies provide pertinent information about the particle size distribution [8]. A TEM uses a high-powered beam to essentially shoot electrons through the object. Electron beam first passes through a condenser lens in order to concentrate the beam on the object. Further the beam goes through the object, some electrons pass all the way through, while others hit molecules in the object and scatter.



**Fig. 3.2 (a) Photograph of TEM unit**

This high powered beam passes through an objective lens, a projector lens and strike onto a fluorescent screen where the final image is observed [9]. As the electron beam passes entirely through the object, the scatter pattern gives the observed and comprehensive view of the interior of the object [10]. The ray diagram of TEM is shown in Fig. 3.2 (a) and (b). Conventional TEM uses

## Chapter 3

only the transmitted beams or some of the forward scattered beams to create a diffraction contrast image. High resolution transmission electron microscopy (HRTEM) uses the transmitted and the scattered beams to create an interference image. HRTEM also used for phase analysis by measuring the interplanar distance. TEM also provides selected area electron diffraction (SAED) pattern. Which confirm the crystalline nature of nanomaterials. TEM images of prepared  $\text{TiO}_2$  NPs and  $\text{TiO}_2$ -MWCNTs NCs were recorded on a (Philips CM 200, operating voltages: 20–200 kV, Resolution: 2.4 Å).

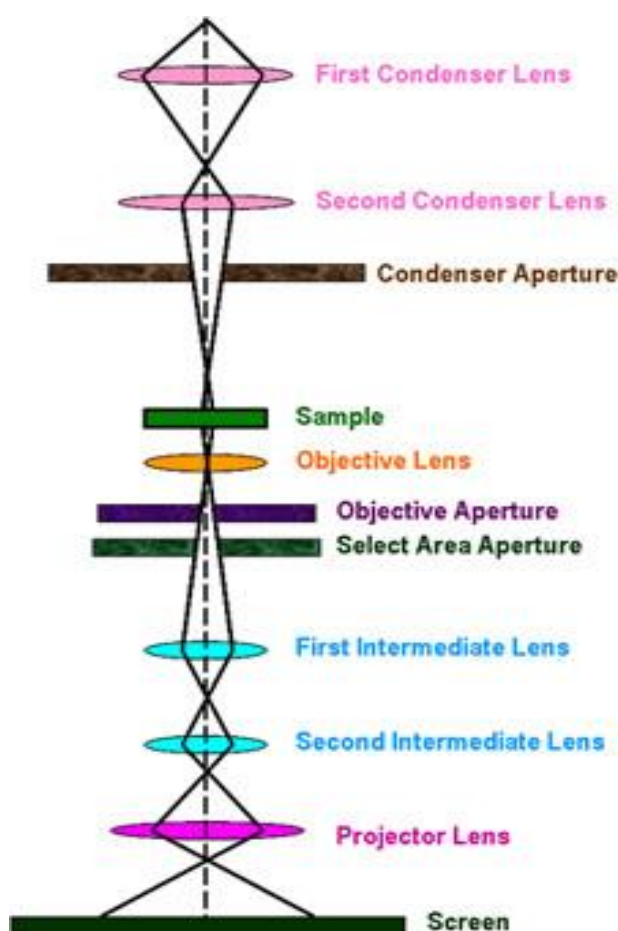


**Fig. 3.2. (b) Ray Diagram for a TEM**

[Source: <http://www.nanoscience.gatech.edu/zwang/research/tem.html>]

### 3.2.3 X-ray photoelectron spectroscopy (XPS)

In XPS, we are bothered with a special form of photoemission, i.e., the ejection of an electron from a core level by an X-ray photon of energy  $h\nu$ . The energy of the emitted photoelectrons are analyzed by the electron spectrometer and the data presented as a graph of intensity (usually expressed as counts or Counts/S) versus electron energy of the X-ray induced photoelectron spectrum [11]. The kinetic energy (KE) of the electron is the experimental quantity measured by the spectrometer, but this is dependent on the photon energy of the X-rays employed and is therefore not an intrinsic material property [12]. The binding energy of the electron (BE) is the parameter which identifies the electron specifically, both in terms of its parent element and atomic energy level. The relationship between the parameters involved in the XPS experiment is: [13]

$$BE = h\nu - KE - W \quad \dots\dots\dots 3.2$$

Where  $h\nu$  is the photon energy, KE is the kinetic energy of the electron, and W is the spectrometer work function.

As all three quantities on the right-hand side of the equation are known or measurable, it is a simple matter to calculate the binding energy of the electron. In practice, this task will be performed by the control electronics or data system associated with the spectrometer and the operator merely selects a binding or kinetic energy scale whichever is considered the more appropriate. The process of photoemission is shown schematically in Fig. 3.4. (a) Where an electron from the K shell is ejected from the atom (1s photoelectron). The photoelectron spectrum will reproduce the electronic structure of an element quite accurately since all electrons with a binding Ejected K electron (1s electron) Vacuum.

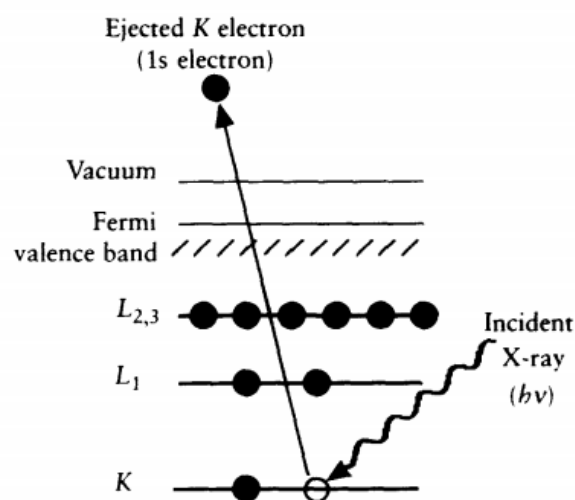


**Fig. 3.4. (a) Schematic diagram of the XPS process, showing photoionization of an atom by the energy less than the photon energy will feature in the spectrum.**

The other possibility is the ejection of an Auger electron. Thus, Auger electrons are produced as a consequence of the XPS process often referred to as X-AES (X-ray induced Auger electron spectroscopy) [14]. X-AES, although not widely practised, can yield valuable chemical information about an atom. For the time being we will restrict our thoughts to AES in its more common form, which is when a finely focused electron beam causes the emission of Auger electron. The photograph of XPS unit shown in in Fig. 3.4. (b)

XPS has broadly used technique for studying the properties of atoms, molecules, solids and surfaces. XPS spectra are gained by irradiating a material with a beam of X-rays while simultaneously measuring the kinetic energy and number of electrons that escape from the top 0 to 10 nm of the material is being analyzed [15]. It is based on the principle of photoelectric effect. In the working of XPS, electrons are released from the sample as a result of photoemission process. An electron is emitted from an atomic energy level by an X-ray photon, mostly from an Al-K $\alpha$  or Mg-K $\alpha$  primary source, and



its energy is analyzed by the spectrophotometer [16]. The schematic of an XPS Spectrophotometer shown in Fig. 3.4. (c).



**Fig 3.4. (b) Photograph of XPS unit**

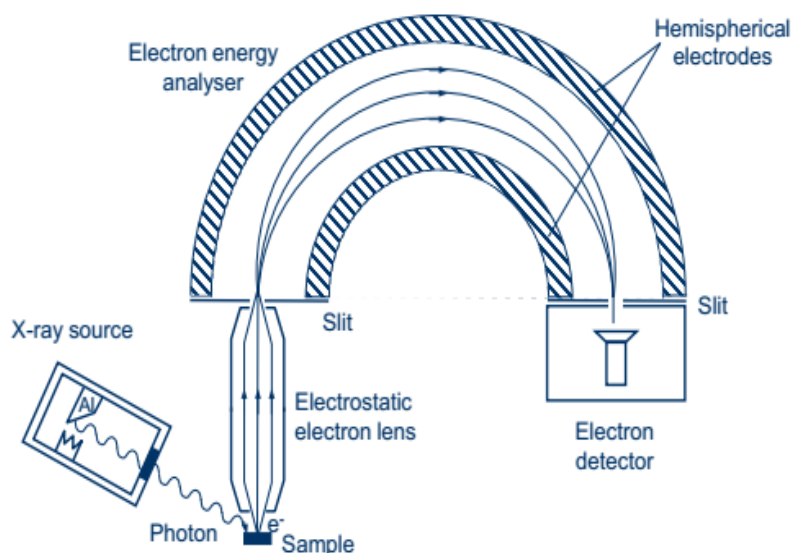


**Fig 3.4. (c) Schematic of an XPS spectrometer**

[Source:[https://www.google.co.in/search?q=Schematic+of+an+XPS+spectrometer&source=lnms&tbm=isch&sa=X&ved=0ahUKEwiv6t\\_MHTAhUIvo8KHX3jDJAQ\\_AUIBigB&biw=1517&bih=708#imgrc=y\\_J05WfbdPOtPM](https://www.google.co.in/search?q=Schematic+of+an+XPS+spectrometer&source=lnms&tbm=isch&sa=X&ved=0ahUKEwiv6t_MHTAhUIvo8KHX3jDJAQ_AUIBigB&biw=1517&bih=708#imgrc=y_J05WfbdPOtPM)]

### 3.3 Spectroscopic and Thermal Analysis Technique

#### 3.3.1 UV-vis Diffuse reflectance spectroscopy

The energy gap ( $E_g$ ) is an important feature of semiconductors which determines their applications in optoelectronics [17, 18]. The UV-vis absorption spectroscopy is frequently used to characterize semiconductors thin films [19]. Due to low scattering in solid films, it is easy to extract the  $E_g$  values from their absorption spectra knowing their thickness. However, in colloidal samples, the scattering effect is enhanced since more superficial area is exposed to the light beam. In normal incidence mode, dispersed light is counted as absorbed light and the technique (optical absorption) does not distinguish between the two phenomena. On the other hand, it is common to obtain powdered samples instead of thin films or colloids, and frequently UV-vis absorption spectroscopy is carried out dispersing the sample in liquid media like water, ethanol or methanol. If the particle size of the sample is not small enough, it precipitates and the absorption spectrum is even more difficult to interpret. In order to avoid these complications, it is desirable to use diffuse reflectance spectroscopy (DRS), which enables to obtain  $E_g$  of unsupported materials [20]. The synthesized material was analyzed by using UV-3092 lab India model as shown in Fig. 3.5. (a)



**Fig.3.5. (a) Photograph of UV-visible DRS (UV 3092 Lab India)**

## Chapter 3

The theory which makes possible to use DR spectra was proposed by Kubelka and Munk [21]. Originally they proposed a model to describe the behavior of light traveling inside a light-scattering specimen, which is based on the following differential equations:

$$\begin{aligned} -di &= -(S + K) i dx + S j dx \\ dj &= -(S + K) j dx + S i dx \end{aligned} \dots\dots\dots 3.3$$

Where  $i$  and  $j$  are the intensities of light traveling inside the sample towards its unilluminated and illuminated surfaces, respectively;  $dx$  is the differential segment along the light path;  $S$  and  $K$  are the so called K-M scattering and absorption coefficients, respectively. These last two quantities have no direct physical meaning on their own, even though they appear to represent portions of light scattered and absorbed, respectively, per unit vertical length [22]. This model holds when the particle size is comparable to, or smaller than the wavelength of the incident light, and the diffuse reflection no longer allows to separate the contributions of the reflection, refraction, and diffraction (i.e. scattering occurs). In the limiting case of an infinitely thick sample, thickness and sample holder has no influence on the value of reflectance ( $R$ ). In this case, the Kubelka-Munk equation at any wavelength becomes:

$$K/S = (1 - R_\infty)^2 / 2R_\infty \equiv F(R_\infty) \dots\dots\dots 3.4$$

$F(R_\infty)$  is the so-called remission or Kubelka-Munk function, where  $R_\infty = R_{\text{sample}} / R_{\text{standard}}$  [23]. In the parabolic band structure, the band gap  $E_g$ , and absorption coefficient  $\alpha$  of a direct band gap semiconductor are related through the well-known equation [24].

$$\alpha h\nu = C_1 (h\nu - E_g)^{1/2} \dots\dots\dots 3.4$$

Where,  $\alpha$  is the linear absorption coefficient of the material,  $h\nu$  is the photon energy and  $C_1$  is a proportionality constant. When the material scatters

## Chapter 3

in perfectly diffuse manner (or when it is illuminated at  $60^\circ$  incidence), the K-M absorption coefficient  $K$  becomes equal to  $2\alpha$  ( $K=2\alpha$ ). In this case, considering the K-M scattering coefficient  $S$  as constant with respect to wavelength, and using the remission function in Eq. (3) we obtain the expression:

$$[F(R_\infty) h\nu]^2 = C_2 (h\nu - E_g) \dots \dots \dots 3.5$$

Therefore, obtaining  $F(R_\infty)$  from Eq. (2) and plotting the  $[F(R_\infty) h\nu]^2$  against  $h\nu$ , the band gap  $E_g$  of a powder sample can be extracted easily. Fig 3.5. (b)

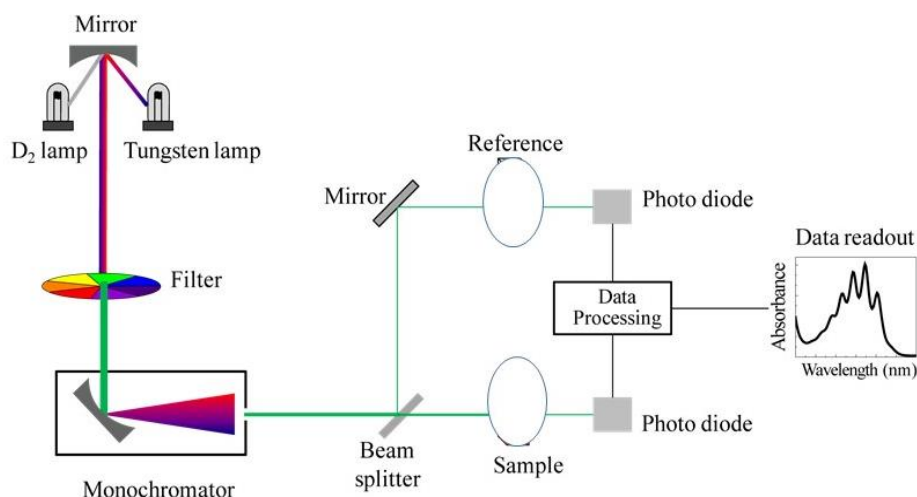


**Fig 3.5. (b) Ray diagram of UV-visible spectroscopy**

[Source: <https://orgspectroscopyint.blogspot.in/p/basics-of-uv-visible-spectroscopy.html>]

### 3.3.2 Fourier transform infrared spectroscopy (FTIR)

FTIR is extensively used technique for characterization of both organic and inorganic compounds. Presence of some specific functional moieties can be determined by using FTIR spectra. Specific chemical bonds or functional groups show selective transmittance bands. Hence this technique is used to confirm presence of a compound in the sample. In the proposed work, functionalization of MWCNTs confirmed by this technique. Also the TiO<sub>2</sub> NPs coated on the surface of MWCNTs studied. FTIR was used to confirm coating of TiO<sub>2</sub> NPs on surface of MWCNTs. The nature of chemical binding can be well understood using this technique.

The infrared technique is working on the simple fact that, a chemical substance shows selective absorption in the infrared region [25]. Block diagram of FTIR showed in Fig. 3.6. (a) The wavelength of absorption depends on relative masses of the atoms, force constants of the bonds and geometry of atoms. Then molecules of the chemical substance vibrate at many rates giving rise to close packed absorption bands. Band intensities are expressed either as transmittance (T) or absorbance (A). IR encompasses a spectral region from red end of visible spectrum ( $12,500\text{ cm}^{-1}$ , 0.75mm) to the microwave ( $10\text{ cm}^{-1}$ , 1000 mm) in the electromagnetic spectrum [26].

The FTIR analysis helps to understand the successful attachment of TiO<sub>2</sub> NPs on the surface MWCNTs. The interferometer consists of two perpendicularly plane mirrors, one of which can travel in a direction perpendicular to the plane. A semi-reflecting film, known as beam splitter, bisects the planes of these two mirrors. The beam splitter material is decided according to the region to be examined. For the mid or near-infrared regions materials like germanium or iron oxide are covered onto an “infrared-transparent” substrate as like potassium bromide or caesium iodide to produce beam splitters. In this technique mainly, a chemical substance shows selective absorption in the infrared region. The wavelength of absorption depends on relative masses of the atoms,

force constants of the bonds and geometry of atoms. Then the molecules of the chemical substance vibrate at many rates of vibrations, giving rise to close packed absorption bands. The IR absorption spectrum may extend over a wide range of wavelength. In spectrum each band corresponds to the characteristic functional groups and bonds present in a compound. The FTIR unit used for characterization of  $\text{TiO}_2$  NPs and  $\text{TiO}_2$ -MWCNTs NCs shown in Fig. 3.6 (b).

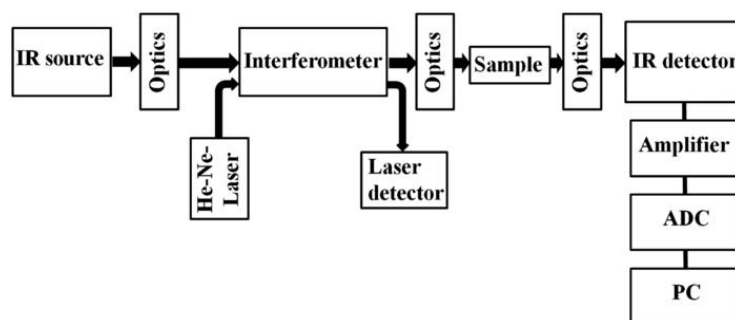


**Fig 3.6 (a) Block diagram of FTIR Spectrophotometer**

[Source: <http://iopscience.iop.org/article/10.1088/0143-0807/34/6/S123>]



**Fig 3.6 (b) Photograph of alpha Bruker FT-IR Spectrophotometer**

### 3.3.3 Raman spectroscopy

The Raman spectroscopy measures the vibrational motions of a molecule like the infrared spectroscopy. However, Raman spectroscopy deals with the light scattering while the infrared spectroscopy is based on absorption of photons. Raman spectroscopy is a complementary technique to IR spectroscopy because some chemical compound exhibits a center of symmetry. Certain normal vibrations will be only Raman active and certain normal vibrations will be only IR active, as per mutual exclusion principle [27]. Thus, to record complete vibrational spectrum of a compound both techniques are required. Additionally, the bands that are weak in IR are generally strong in Raman, and vice versa if the normal modes are allowed [28]. Generally, strong IR bands are related to polar functional groups, whereas non-polar functional groups give rise to strong Raman bands.

The Raman phenomenon was detected in 1928 by the Indian physicist Sir Chandrasekhara Venkata Raman and Kariamanikkam Srinivasa Krishnan [29]. Independently of this work, the phenomenon was also reported by Grigory Landsberg and Leonid Mandelstam [30]. However, the phenomenon was predicted theoretically even earlier by using the classical model [31]. After the end of 1920's the method was forgotten for several decades because the signal is very weak. Raman spectroscopy experienced a renaissance in the 1960's when the lasers were invented and started to be used as light sources in spectroscopy.

In Raman spectroscopy, sample is illuminated with a monochromatic laser beam which interacts with the scattering centers of sample and originates a scattered light. The scattered light having a frequency different from that of incident light (stokes/ anti stokes scattering) is used to construct a Raman spectrum. Raman spectra arise due to inelastic collision between incident monochromatic radiation and centers of sample. When a monochromatic radiation strikes at sample, it scatters in all directions after its interaction with

## Chapter 3

---

sample scattering centers. Much of this scattered radiation has a frequency which is equal to frequency of incident radiation and constitutes Rayleigh scattering. Only a small fraction of scattered radiation has a frequency different from frequency of incident radiation and constitutes Raman scattering. When the frequency of incident radiation is higher than frequency of scattered radiation Stokes lines appear in Raman spectrum. But when the frequency of incident radiation is lower than frequency of scattered radiation, anti-Stokes lines appear in Raman spectrum. Scattered radiation is usually measured at right angle to incident radiation [32, 33].

Stokes shifted Raman bands involve the transitions from lower to higher energy vibrational levels and therefore, Stokes bands are more intense than anti-Stokes bands and hence are measured in conventional Raman spectroscopy [33]. While anti-Stokes bands are measured with fluorescent samples because fluorescence causes interference with Stokes bands [32]. The magnitude of Raman shifts does not depend on wavelength of incident radiation. Raman scattering depends on wavelength of incident radiation [26]. A change in polarizability during molecular vibration is an essential requirement to obtain Raman spectrum of sample. Since Raman scattering due to water is low, water is an ideal solvent for dissolving samples. Glass can be used for optical components (mirror, lens, sample cell) in Raman spectrophotometer [34]. A Raman spectrum is presented as an intensity-versus wavelength shift. Raman spectra can be recorded over a range of  $4000\text{--}10\text{ cm}^{-1}$ . However, Raman active normal modes of vibration of organic molecules occur in the range of  $4000\text{--}400\text{ cm}^{-1}$ . Depending on spectrophotometers design and optical components, typical Raman spectra cover the wavenumber region between  $400\text{--}5\text{ cm}^{-1}$  and  $4000\text{--}3800\text{ cm}^{-1}$ . A Raman spectrum is significantly simpler than its Infrared (IR) counterparts because in normal Raman overtones, combination and difference bands are rare.



## Chapter 3

An instrument capable to function as Raman spectrometer (Fig. 3.7 (a)) must comprise (1) a laser source for excitation, (2) a collecting optical system for the emitted radiation, (3) filtering system to cut out the Rayleigh scattering— notch filter, edge pass filter, or a band pass filter, (4) 166 pectos grating for Raman spectral decomposition and a (5) detector for photon counting, most suitably CCD devices. Excitation sources (1) are lasers (diodes or Nd: YAG) in the ultra-violet, visible and near-infrared regions of electromagnetic radiation (wavelengths of 633 nm, 660 nm, 785 nm and 1064 nm). Also the Fig. 3.7. (b) Shows the photograph of Raman spectroscopy unit.

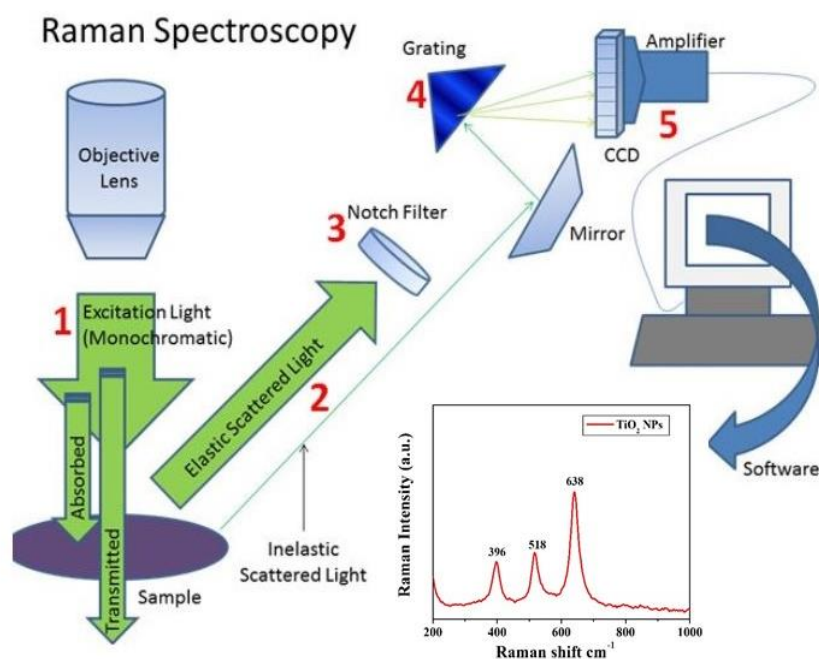


**Fig. 3.7 (a) Shechatic represntion of Raman Spectroscopy**

[Source : <http://www.unexmin.eu/wp-content/uploads/2017/02/D2.1-PARAMETER-FRAMEWORK-REPORT.pdf?x49778>]



**Fig. 3.7. (b) Photograph of Raman spectroscopy unit.**

### **3.3.4 Photoluminescence (PL) spectroscopy**

Photoluminescence (PL) spectroscopy is a very efficient, contactless, nondestructive, widely used technique for the analysis of the optoelectronic properties of semiconductors, which requires very little sample manipulation [35]. Photoluminescence is defined as the spontaneous emission of light from a material under optical excitation and can be therefore used to provide detailed information on discrete electronic states involving both intrinsic optical processes and about the wide variety of defect. Which are endemic in practical semiconductor materials and extrinsic optical processes (internal transitions involving defects and their energy levels) by applying an external light with energy  $h\nu \gtrsim E_g$ ; where  $E_g$  denotes the energy band gap, and observing the re-emitted photons. The schematic layout of a high-sensitivity photoluminescence Spectrofluorometer system shown in Fig.3.8. (a) Also the photograph of PL unit shown in Fig. 3.8. (b).The main uses of photoluminescence are [36].

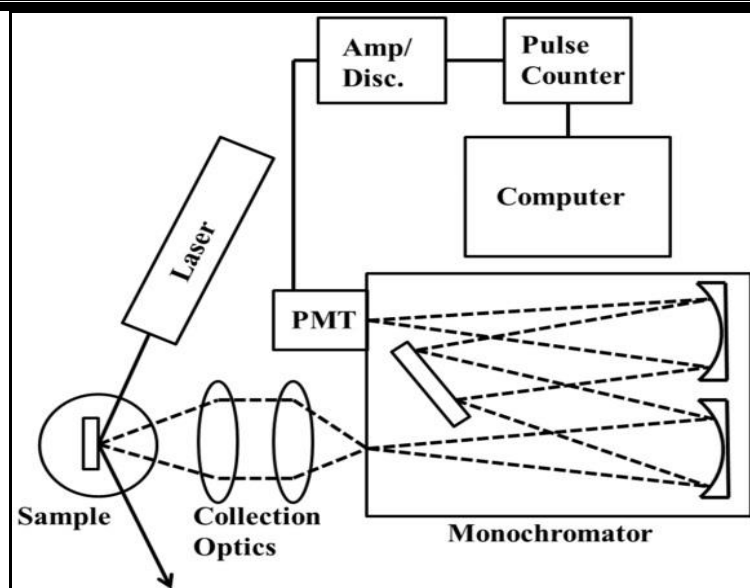


**Fig. 3.8. (a) A schematic layout of PL instrument.**



**Fig. 3.8. (b) Photograph of PL unit.**

- (1) Understanding of recombination mechanisms: Analysis of Photoluminescence helps to understand the underlying physics of recombination processes.
- (2) Identification of surface, interface, and impurity levels.

- 
- (3) Band gap determination: Most common radiative transitions in semiconductors occur between states in the conduction and valence bands, with the energy difference known as band gap ( $E_g$ ).
  - (4) Assessment of the material quality: Material quality can be measured by quantifying the amount radiative recombination, keeping in mind that non-radiative recombination is associated to localized defect levels that are detrimental to material quality and subsequently to device performance

**3.3.4.1** Detection of defect and impurity levels: Radiative transitions can also involve localized defects and the photoluminescence energy associated to these levels can be used to identify these specific defects.

**(a) Donor- acceptor pair recombination (DAP)**

A semiconductor is referred to as n- or p- type, when it may contain both donor and acceptor impurities according to the dominant impurity [37]. These donors and acceptors can form pairs and act as stationary molecules imbedded in the host material. The recombination energy of a donor- acceptor pair

( $D^0 + A^0 \rightarrow D^- + A^+ + h\nu$ ) is given by:

$$h\nu = E_g - (E_A + E_D) + \frac{e^2}{4\pi\epsilon_0\epsilon_r r} - E_{vdW} \dots\dots\dots 3.6$$

Where  $e$  is the electronic charge,  $\epsilon_r$  the static dielectric constant,  $r$  is the separation between donors and acceptors and  $E_{vdW}$  is a polarization interaction term dominated by the intercenter interaction in the initial state of the transition and the first order term,  $\frac{e^2}{4\pi\epsilon_r}$  is the Coulomb interaction between donor and acceptor impurities, and this term influences the binding energies of isolated impurities. Due to the Coulomb term the peak maximum energy of the donor acceptor emission shifts towards higher energies as the power excitation intensity,  $P_{exc}$ ; increases, since with increasing power excitation the separation,  $r$ ; between donors and acceptors is reduced with the

blue shift characterized by the factor  $\beta$  [meV=DeK]. : A blue shift is suggestive of donor- acceptor transitions.

$$h\nu_{DA}(P_{exc}) = h\nu_{DA}(P_0) + \beta \log_{10} (P_{exc} / P_0) \dots\dots\dots 3.7$$

### (b) Photon-related recombinations

The energy released from the recombination of an electron and hole can be transformed into photons and or optical phonons, the phonons being the collective vibrational modes of the atoms forming the crystal [38]. The electron-phonon interaction can induce simultaneous emission of one or more phonons, leading to replicas or satellites of the main recombination peak in the photoluminescence spectrum displaced by the energies of the most important phonons, therefore strong phonon coupling can lead to the observation of multiple orders of phonon replicas.

At the temperature  $T=0K$  the shape of the emission band due to the phonon replicas is given by equation 3.8

$$I_{em}(E) = I_0 \sum_n \frac{\exp(-S) S^n}{n!} \delta(E_0 - n\hbar\omega - E) \dots\dots\dots 3.8$$

Where  $S$  is the Huang-Rhys coupling factor representing the average number of phonons involved,  $E_0$  the energy of the zero-phonon transition, and  $I_0$  is the intensity in the zero phonon line.

### 3.3.5 Thermogravimetric analysis (TGA)

TGA is a method of thermal analysis in which changes observed in weight/mass and of materials is measured as a function of increasing temperature (with constant heating rate), or as a function of time (with constant temperature and/or constant mass loss [39]. The physical phenomena, such as second order phase transitions, including absorption, sublimation, adsorption, vaporization and desorption can be obtained using this technique. Also, it can

## Chapter 3

provide information about chemical phenomena including chemisorption's, desolation (especially dehydration), decomposition and solid-gas reactions (e.g., oxidation or reduction). Measurements are used primarily to determine the composition of materials and to predict their thermal stability at temperatures up to 1000 °C.

The results from thermogravimetric are usually reported in the form of curves relating the mass lost from the sample against temperature. In this form the temperature at which certain processes begin and are completed are graphically demonstrated. The Fig. 3.9. (a) shows the photo graph of TGA Unit. Fig. 3.9. (b) shows the schematic of TGA instrument.



**Fig. 3.9. (a) Photograph of TGA unit.**

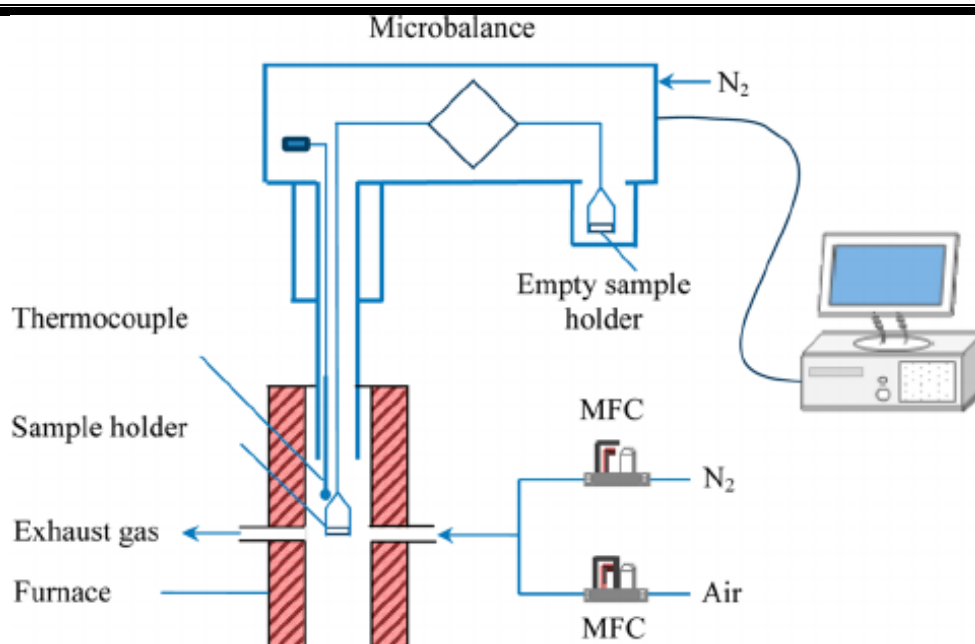


**Fig. 3.9. (b) Schematic layout of TGA instrument.**

[Source: [https://www.researchgate.net/figure/263958136\\_fig2\\_Figure-2-Schematic-of-the-TGA](https://www.researchgate.net/figure/263958136_fig2_Figure-2-Schematic-of-the-TGA)]

### 3.4 Cytotoxicity studies

The biocompatibility study is carried for TiO<sub>2</sub> and TiO<sub>2</sub>-MWCNTs NCs with MTT assay as follows:

Measurement of cell viability and proliferation forms the basis for numerous in vitro assays of cell population's response to external factors. The reduction of tetrazolium salts is widely accepted as a reliable way to examine cell proliferation. The yellow 3-(4, 5-dimethylthiazolyl-2)-2, 5- diphenyl tetrazolium bromide (tetrazolium MTT) is reduced by metabolically active cells in turn by dehydrogenase enzymes, to generate reducing equivalents such as NADH and NADPH. The reduction process forms intracellular purple formazan which can be solubilized and quantified by spectrophotometrically [40]. The MTT assay measures the cell proliferation rate when metabolic events lead to necrosis or apoptosis, the reduction in cell viability. In the absence of cells,

## Chapter 3

---

the MTT reagent dose not yield high background absorbance values. The whole assay carried out in dark condition of synthesized nanomaterial.



---

### Reference

- [1] R. Das, E. Ali, and S. B. Abd Hamid, *Rev. Adv. Mater. Sci.* 38 (2014) 95.
- [2] J. M. Zuo and J. H. Spence, *The geometry of electron diffraction patterns* (2017).
- [3] A. R. West, *Solid State Chemistry and its Applications*, John Wiley & Sons, (2007).
- [4] J. Hanawalt, H. Rinn, and L. Frevel, *Ind. Eng. Chem. Anal. Ed.* 10 (1938) 457.
- [5] S. Thomas, D. Rouxel, and D. Ponnamm, *Spectroscopy of Polymer Nanocomposites*, William Andrew, (2016).
- [6] J. P. Glusker, M. Lewis, and M. Rossi, *Crystal structure analysis for chemists and biologists*, John Wiley & Sons, (1994).
- [7] Y. V. Pathak and J. N. Lokhande, *Handbook of Metallonutraceuticals*, CRC Press, (2014).
- [8] R. Matyi, L. Schwartz, and J. Butt, *Catal. Rev. Sci. Eng.* 29 (1987) 41.
- [9] D. B. Williams and C. B. Carter, in *Transmission electron microscopy*, Springer, (1996).
- [10] F. Krumeich, *Laboratory of Inorganic Chemistry*, disponível em <http://www.microscopy.ethz.ch/downloads/Interactions.pdf>, consultado em (2011).
- [11] E. Jagst, *Surface functional group characterization using Chemical Derivatization X-ray Photoelectron Spectroscopy (CD-XPS)*. Diss. Freie Universität Berlin, (2010).
- [12] Z.K. Xu, X.J. Huang, and L.S. Wan, *Surface engineering of polymer membranes*, Springer Science and Business Media, (2009).
- [13] J. F. Watts and J. Wolstenholme, *An Introduction to Surface Analysis by XPS and AES*, by John F. Watts, John Wolstenholme, Wiley-VCH, (2003).

## Chapter 3

- 
- [14] M. Chen, X. Wang, Y. Yu, Z. Pei, X. Bai, C. Sun, R. Huang, and L. Wen, *Appl. Surf. Sci.* 158 (2000) 134.
  - [15] J. M. Wagner, *X-ray photoelectron spectroscopy*, Nova Science Publishers, (2011).
  - [16] K. Janssens and R. Van Grieken, *Non-destructive micro analysis of cultural heritage materials*, Elsevier, (2004).
  - [17] U. OZG, *J. Appl. Phys.* 98 (2005) 041301.
  - [18] C. Boemare, T. Monteiro, M. Soares, J. Guilherme, and E. Alves, *Physica B* 308 (2001) 985.
  - [19] U. Pal, D. Samanta, S. Ghorai, and A. Chaudhuri, *J. Appl. Phys.* 74 (1993) 6368.
  - [20] D. G. Barton, M. Shtein, R. D. Wilson, S. L. Soled, and E. Iglesia, *The J. Phys. Chem. B* 103 (1999) 630.
  - [21] P. Kubelka and F. Munk, *Z. Tech. Phys* 12 (1931) 593.
  - [22] L. Yang and B. Kruse, *J. Opt. Soc. Am. A* 21 (2004) 1933.
  - [23] J. Torrent and V. Barrón, *Diffuse reflectance spectroscopy of iron oxides. Encyclopedia of surface and Colloid Science* (2002).
  - [24] R. A. Smith, *Semiconductor*, (1978).
  - [25] A. Lagashetty and A. Venkataraman, *Resonance* 10 (2005) 49.
  - [26] F. A. Settle, *Handbook of instrumental techniques for analytical chemistry*, Prentice Hall PTR, (1997).
  - [27] D. Lin-Vien, N. B. Colthup, W. G. Fateley, and J. G. Grasselli, *The handbook of infrared and Raman characteristic frequencies of organic molecules*, Elsevier, (1991).
  - [28] B. Sharma, *Instrumental methods of chemical analysis*, Krishna Prakashan Media, (2000).
  - [29] S. Bhagavantam, *Biographical Memoirs of Fellows of the Royal Society* 17 (1971) 565.
  - [30] G. Landsberg, *Naturwiss.* 16 (1928) 558.
-

- [31] C. Raman and K. Krishnan, Nature 121 (1928) 501.
- [32] D. A. Skoog, F. J. Holler, and S. R. Crouch, Principles of instrumental analysis, Thomson Brooks/Cole, (2007).
- [33] E. Smith and G. Dent, Modern Raman spectroscopy: a practical approach, John Wiley and Sons, (2013).
- [34] S. Califano, Vibrational states, John Wiley & Sons, (1976).
- [35] J. E. Toney, in Characterization of Materials, John Wiley & Sons, Inc., (2002).
- [36] M. Anpo and M. Che, Adv. Cata. 44 (1999) 119.
- [37] B. Guo, Z. Qiu, and K. Wong, Appl. Phys. Lett. 82 (2003) 2290.
- [38] J. I. Pankove, Optical processes in semiconductors, Courier Corporation, (2012).
- [39] S. Devasahayam, K. Dowling, and M. K. Mahapatra, Sustainability in the Mineral and Energy Sectors, CRC Press, (2016).
- [40] A. Aysun, K., Yagmur and B. Yusuf, Current Pharm. Biotechnol. 17 (2016) 1213.



# Chapter 4

## Synthesis and characterization of photocatalytic TiO<sub>2</sub>-MWCNTs nanocomposites

Journal of Photochemistry and Photobiology A: Chemistry 328 (2016) 50–58



Contents lists available at ScienceDirect  
Journal of Photochemistry and Photobiology A:  
Chemistry

journal homepage: [www.elsevier.com/locate/jphotochem](http://www.elsevier.com/locate/jphotochem)



Visible light photo-induced antibacterial activity of TiO<sub>2</sub>-MWCNTs nanocomposites with varying the contents of MWCNTs



Valmiki B. Koli<sup>a,b</sup>, Ananta G. Dhodamani<sup>b</sup>, Abhinav V. Raut<sup>a</sup>, Nanasaheb D. Thorat<sup>c</sup>, Shivaji H. Pawar<sup>a</sup>, Sagar D. Delekar<sup>a,b,d,\*</sup>

<sup>a</sup> Center for Interdisciplinary Research, D.Y. Patil University, Kolhapur 416 006, India

<sup>b</sup> Department of Chemistry, Shivaji University, Kolhapur 416 004, India

<sup>c</sup> Department of Physics and Energy, University of Limerick, Limerick, Ireland

<sup>d</sup> Department of Chemistry and Biochemistry, Florida State University, Tallahassee 32306-4390, United States

Journal of Photochemistry and Photobiology A: Chemistry 333 (2017) 40–48



Contents lists available at ScienceDirect  
Journal of Photochemistry and Photobiology A:  
Chemistry

journal homepage: [www.elsevier.com/locate/jphotochem](http://www.elsevier.com/locate/jphotochem)



*In situ* sol-gel synthesis of anatase TiO<sub>2</sub>-MWCNTs nanocomposites and their photocatalytic applications



Valmiki B. Koli<sup>a</sup>, Ananta G. Dhodamani<sup>b</sup>, Sagar D. Delekar<sup>a,b,\*</sup>, Shivaji H. Pawar<sup>a,\*</sup>

<sup>a</sup> Center for Interdisciplinary Research, D.Y. Patil University, Kolhapur 416 006, India

<sup>b</sup> Department of Chemistry, Shivaji University, Kolhapur 416 004, India



---

### 4.1 Introduction

The selection of synthetic method plays an important role for determining the effectiveness of the photocatalyst. The methods need for preparation of nanomaterials mainly classified into two categories; physical and chemical methods. Due to various advantages from this wet chemical methods are useful to control desired structural and morphological properties of materials on a nanometer scale. There are numerous chemical methods to produce TiO<sub>2</sub> NPs and TiO<sub>2</sub>-MWCNTs NCs such as hydrothermal method [1, 2], solvothermal [3] sol-gel technique [4] electrochemical synthesis [5] sonochemical synthesis [6], microemulsion method and [7], microwave method [8, 9].

This chapter includes the various chemical methods used for synthesis of doped/undoped TiO<sub>2</sub> NPs and TiO<sub>2</sub>-MWCNTs NCs. Here, in addition, main emphasis on sol-gel method is given in detail for synthesis of nanomaterials. However, an overview of other much used techniques is also provided.

### 4.2 Synthesis methods

#### 4.2.1 Hydrothermal method

Hydrothermal synthesis is normally conducted in steel pressure vessels called autoclaves with or without Teflon liners under controlled temperature or pressure with the reaction in aqueous solutions. The temperature can be elevated above the boiling point of water, reaching the pressure of vapor saturation. The temperature and the amount of solution added to the autoclave largely determine the internal pressure produced. This method is widely used for the production of small particles in the ceramics industry. The hydrothermal method has been used to synthesize TiO<sub>2</sub>-MWCNTs NCs [10, 11]. The hydrothermal method can be useful to control grain size, particle morphology, crystalline phase and surface chemistry through regulation of the solution composition, reaction temperature, pressure, solvent properties, additives and aging time [12]. The drawbacks of this technique are the difficulty in

controlling the growth process and requirement of expensive autoclaves.

### 4.2.2 Solvothermal method

The solvothermal method is almost same to the hydrothermal method except that the solvent used usually in this method non-aqueous solvent is used. However, the temperature can be elevated much higher than that in hydrothermal method, since a variety of organic solvents with high boiling points can be chosen. The solvothermal method normally has better control of the size and shape distributions and the crystallinity of the material. The solvothermal method has been found to be a versatile method for the synthesis than hydrothermal method. A variety of NPs with narrow size distribution and dispersity. The solvothermal method has been employed to synthesize TiO<sub>2</sub>-MWCNTs NCs [13]. However, the disadvantage of this method is also apparent that a relative long time is required to raise the temperature of solution in the autoclave to a target value [14].

### 4.2.3 Electrochemical method

Electrochemical synthesis is commonly used to produce a coating, usually metallic, or metal oxides on a surface by the action of reduction at the cathode. The substrate to be coated is used as cathode and immersed into a solution which contains a salt of the metal to be deposited. The metallic ions are attracted to the cathode and reduced to metallic form. Electrochemical synthesis is actively studied as a science and also has many industrial applications. The main advantage of electrochemical synthesis over an ordinary redox reaction is the ability to precisely tune the required potential. Various energy storages devices of TiO<sub>2</sub> NPs have been synthesized by electrochemical method [15, 16]. Electrochemical synthesis method mostly used for fabrication of nanostructured energy materials, and various nanostructures, such as nanorods, nanowires, nanotubes, nanosheets, and composite nanostructures [17,



18]. The advantages of this method are low cost, low synthetic temperature, high purity, and simplicity [19]. With this advantages this method suffering with few limitation such as electrolysis cells are unreliable, consume large energy for large scale process and the performance of electrochemical process suffers from mass transport limitations and the size of the specific electrode area. Similarly the electrochemical synthesis method has been used to synthesize  $\text{TiO}_2$ -MWCNTs NCs [16].

### 4.2.4 Sonochemical method

Ultrasound has been very useful in the synthesis of a wide range of nanostructured materials, including high-surface area transition metals, alloys, carbides, oxides, and colloids. The effects of ultrasound do not come from a direct interaction with molecular species. Instead, sonochemistry arises from acoustic cavitation: the formation, growth, and implosive collapse of bubbles in a liquid [20]. Abdulrazzak et al. [21] decorated Pt- $\text{TiO}_2$  NPs on the surface of CNTs with sonochemical method.

### 4.2.5 Microwave method

A dielectric material can be processed with energy in the form of high-frequency electromagnetic waves. The principal frequencies of microwave heating are between 900 and 2450 MHz, at lower microwave frequencies, conductive currents flowing within the material due to the movement of ionic constituents can transfer energy from the microwave field to the material. At higher frequencies, the energy absorption is primarily due to molecules with a permanent dipole which tend to reorientate under the influence of a microwave electric field. Microwave radiation is applied for rapid synthesis of  $\text{TiO}_2$ -MWCNTs NCs [22, 23]. However, there are few drawbacks of microwave over the conventional heating. The monitoring of the reaction course or, in the case of inorganic species, the time dependent monitoring of the particles growth is

not possible.

### 4.2.6 Microemulsion methods

Aqueous in non-aqueous microemulsion has been successfully used for the synthesis of NPs. The advantages of microemulsion synthesis are thermodynamically stable systems, optically isotropic solutions of two immiscible liquids composed of micro domains of one or both stabilized by an interfacial film of surfactant. The surfactant molecule generally has a polar (hydrophilic) head and a long-chained aliphatic (hydrophobic) tail [12]. The basis behind the microemulsion technique is very simple: two reactants are introduced in two identical microemulsions. After mixing both micro-emulsions, droplets collide and interchange the reactants. Then the reaction can take place inside the nanoreactors [24]. Advantage of this method is the biocompatibility and biodegradability of synthesized materials. A large number of NPs of metals and semiconductors have been synthesized using microemulsions method [25]. Recently, ultrafine TiO<sub>2</sub> NPs have been generated in water in oil microemulsions developed by researchers [25, 26]. Even though promising early studies, there have been only limited reports of controlled TiO<sub>2</sub> NPs synthesis from these microemulsions [27].

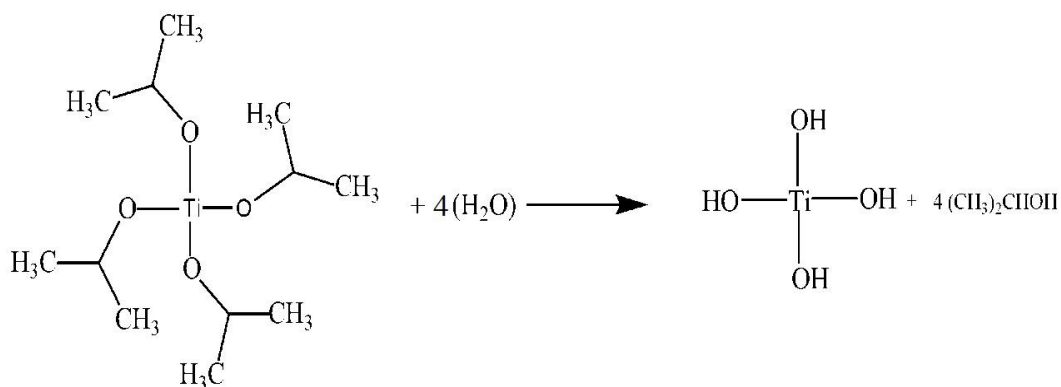
### 4.3 Sol-gel method

The sol-gel method is a versatile wet chemical process for synthesis of nanomaterials. This synthesis technique involves the transition of a system from a colloidal liquid, named sol, into a solid gel phase [28, 29]. The sol-gel method allows to prepare nanomaterials in various forms such as ultra-fine or spherical shaped NPs, thin film coatings, ceramic fibres, micro-porous inorganic membranes, monolithic, or extremely porous aerogels. The starting materials used in the preparation of the sol are usually inorganic metal salts or metal organic compounds that by hydrolysis and poly condensation reactions

form the sol [30]. Further processing of the sol enables one to make ceramic materials in different forms. Thin films can be produced by spin-coating or dip-coating. When the sol is cast into a mould, a wet gel will form. By drying and heat-treatment, the gel is converted into dense ceramic or glass materials. If the liquid in a wet gel is removed under a supercritical condition, a highly porous and extremely low density aerogel material is obtained. The details steps involved in sol-gel synthesis of nanomaterials given as follows.

### Step 1: Hydrolysis

In this step a suspension of colloidal powder, or sol, is formed by mechanical mixing of metal precursor in solvent at a pH that prevents precipitation. The different metal precursor alkoxide precursor, such as Ti (OR)<sub>n</sub>, where R is CH<sub>3</sub>, C<sub>2</sub>H<sub>5</sub>, or C<sub>3</sub>H<sub>7</sub>, is hydrolyzed by mixing with water as follows.

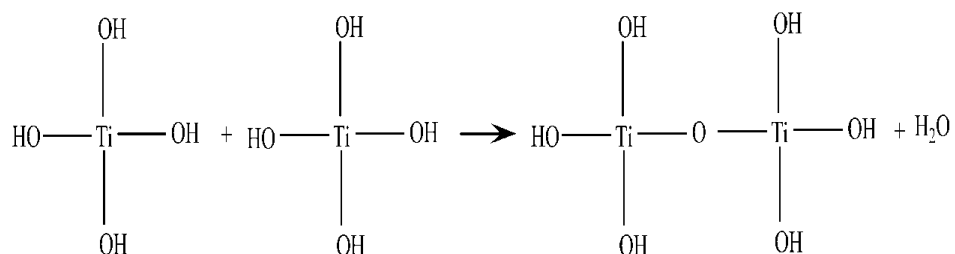


### Step 2: Condensation and polycondensation

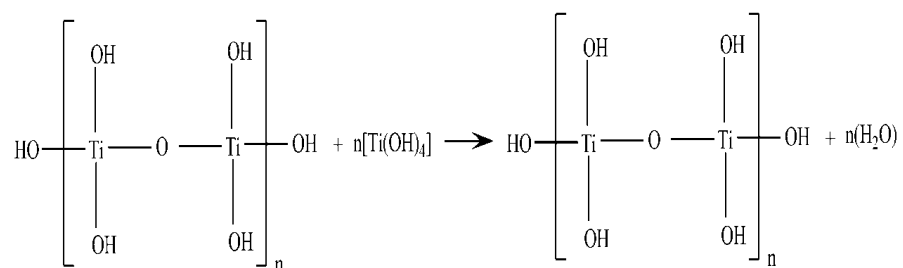
In this step, hydrolyzed precursor condensed to gathers in presence of acidic medium, which shown in following reaction. The physical characteristics of the gel network depend greatly upon the size of particles and extent of cross-linking prior to gelation. Condensation reactions between two hydroxylated metal species leads to formation of Ti –O–Ti bonds under release of water (oxolation), whereas the reaction between a hydroxide and an alkoxide leads to

## Chapter 4

formation of Ti–O–Ti bonds under release of an alcohol (alkoxolation). Condensation reactions can proceed to form large chains of molecules through polycondensation. The electrophilicity of the metal, the strength of the entering nucleophile and the stability of the leaving group all have an influence over the thermodynamics of the hydrolysis and condensation reactions.



By polycondensation process, sols are nucleated and ultimately sol is formed. Furthermore, polycondensation or esterification reaction results in a dramatic increase in the viscosity of the solution. Additional linkage of Ti–OH tetrahedral occurs as a result of polycondensation reaction and ultimately results in a TiO<sub>2</sub> network. The alcohol and water expelled from the reaction remains in the pores of the network. When sufficient interconnected network of Ti–O–Ti bonds are formed in a region, they respond cooperatively as colloidal particles in the scale of sub micrometer. The size of the colloidal particles and the cross-linking within the particles mainly depend upon the pH and the amount water and alkoxide precursor

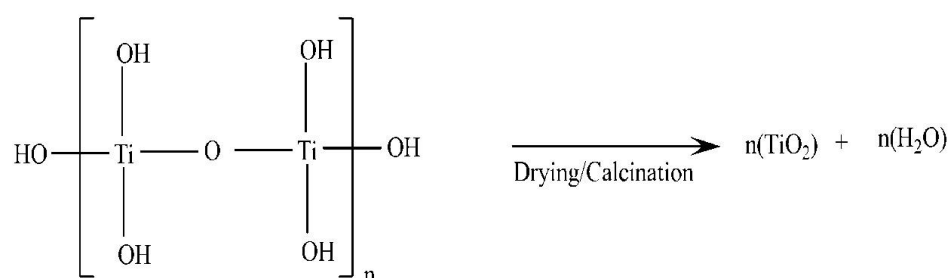


### Step 3: Aging

Aging of a gel, also called syneresis, involves maintaining the cast object for a period of time, hours to days, completely immersed in liquid. During aging, polycondensation continues along with localized solution and re precipitation of the gel network, which increases the thickness of inter particle necks and decreases the porosity. Aging process also increases the strength of the gel.

### Step 4: Drying

During drying the liquid is removed from the interconnected pore network. This process is complicated due to fundamental changes in the structure of the gel. The pH of solvent plays an important role in the kinetics of gelation [31]. Heating the porous gel at high temperature causes densification to occur [32]. The pores are removed to get xerogel.



### Step 5: Dehydration or Chemical Stabilization

Dehydration, during which surface-bound M–OH groups are removed, there by stabilizing the gel against rehydration. This is normally achieved by calcinating the material at high temperatures.

### Step 6: Densification

Densification and decomposition of the gels at high temperatures. The pores of the gel network are collapsed, and remaining organic species are volatilized. The typical steps that are involved in sol–gel processing are shown in the Fig. 4.1

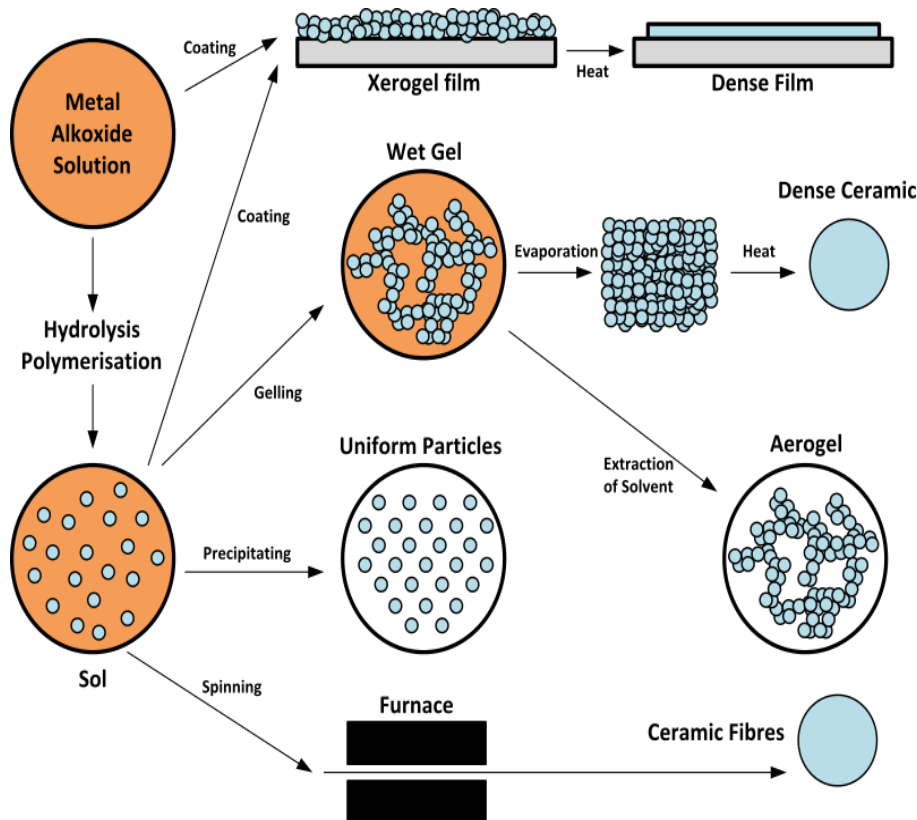


**Fig 4.1 Sol–gel processing options.**

[Source:[https://en.wikipedia.org/wiki/Sol-gel#/media/File:Sol-Gel\\_Scheme.svg](https://en.wikipedia.org/wiki/Sol-gel#/media/File:Sol-Gel_Scheme.svg)]

#### 4.4 Synthesis of TiO<sub>2</sub> NPs with sol-gel method.

Fig. 4.2 shows a flow diagram for the synthesis of TiO<sub>2</sub> NPs by so-gel method at low temperature. To synthesis of TiO<sub>2</sub> NPs, 5 mL glacial acetic acid and 5 mL titanium (IV) isopropoxide were taken in a 250 mL round-bottom flask, content was stirred at room temperature for 15 min followed by addition of aqueous solution of sodium dodecyl sulfate (SDS) and 100 mL of deionized water is added with 2-3 drops of HNO<sub>3</sub>. The content was stirred at room temperature for 4h. The pH of the resulting solution was adjusted to approximately 10.00 ( $\pm 1$ ) using ammonia solution. The solution was stirred at 60 °C for 3 h and then cooled to room temperature and filtered. The residue was slurred in 80 mL distilled water at room temperature for 1 h, followed by constant stirring at 60 °C for 3 h. The content was cooled to room temperature, filtered and washed with 50 mL of ethanol. Residue was dried at 110 °C and calcinated in air at 450 °C for 5 h, which resulted in white colored TiO<sub>2</sub> NPs [33].

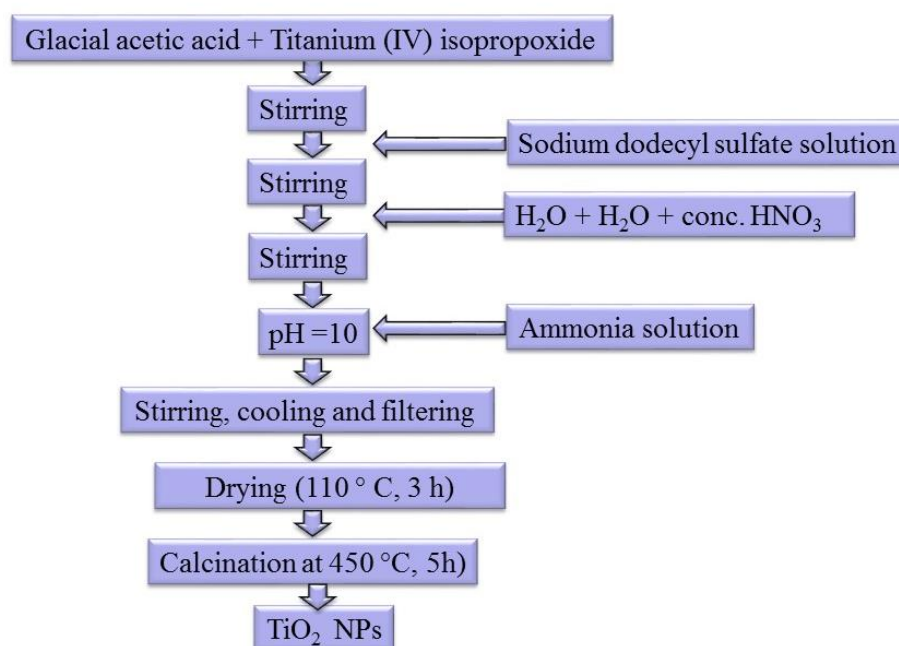


**Fig 4.2 Flow diagram for synthesis of TiO<sub>2</sub> NPs**

### 4.5 Functionalization of MWCNTs

The MWCNTs were functionalized using earlier reported method [34]. The commercial MWCNTs was refluxed in mixture of  $\text{H}_2\text{SO}_4\text{:HNO}_3$  (3:1 volume ratio) at 100 °C for 5 h. Then, the content was cooled, centrifuged, and washed with distilled water several times to maintain its neutralization. Further, it was dried at 80 °C in the electric oven for obtaining its functionalized form as shown in Fig. 4.3. These functionalized MWCNTs were dispersed in water with ultra-sonication for longer times.

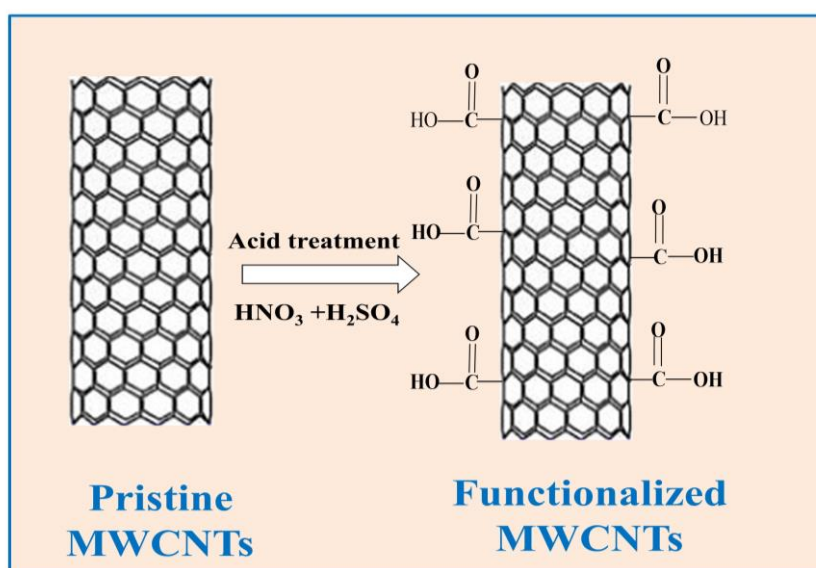


**Fig. 4.3 Schematic of MWCNTs functionalization**



### 4.6 Synthesis of TiO<sub>2</sub>-MWCNTs nanocomposites

The TiO<sub>2</sub>-MWCNTs (TC) NCs were synthesized by *in situ* sol-gel methods. As shown in flow diagram Fig. 4.2, Stoichiometric (1:1) amounts of 5 mL titanium (IV) isopropoxide and 5 mL glacial acetic acid were mixed in aqueous solution, and then 5 mL aqueous sodium dodecyl sulphate (5 wt. %) was added. Afterward, a stoichiometric amount of FMWCNTs suspension was added; later 100 mL distilled water was added with 2-3 drops of HNO<sub>3</sub> and stirred magnetically for 2 h. Then, 40 mL ammonia solution was added and in the mixture to maintain the pH 10 of whole mixture and stirred for 2 h at 60 °C. The precipitate was centrifuged and washed with deionized water and ethanol several times. The product was dried at 110 °C and calcinated in air at 450 °C for 4 h, nanocomposite with different concentration of FMWCNTs (0.1, 0.3 and 0.5 wt. %) were synthesized and are denoted as TC 0.1, TC 0.3 and TC 0.5. The TC NCs changes color from white to whitish black [35].

### 4.7 Characterization of TiO<sub>2</sub> NPs and TiO<sub>2</sub>-MWCNTs nanocomposites

#### 4.7.1 Characterization of TiO<sub>2</sub> NPs

X-ray diffraction pattern of the TiO<sub>2</sub> NPs and TiO<sub>2</sub>-MWCNTs NCs were recorded on BRUKER D8-ADVANCE diffractometer using Cu K $\alpha$  (K $\alpha$ 1 = 1.5406 and K $\alpha$ 2 = 1.5444 Å) radiation. The diffraction data were collected in the 2 $\theta$  range of 10°– 80° in step scan mode at a rate of 2.0°/min. TEM image of the samples were recorded on a Tecnai F30 field emission transmission electron microscope operating at 300 kV. Morphological analysis carried out by SEM with model JEOL JSM-6360, Mira-3, Tescan, Brno-Czech Republic. Thermogravimetric analysis (TGA) of the sample was carried out using METTLER-TOLEDO TG TGA/SDTA851e thermos balance system. The TGA trace for the powder sample was recorded from 35°C– 1000°C at heating rate of 10 °C min<sup>-1</sup>.

**4.7.1.1 Thermal analysis (TGA)**

TGA analysis of  $\text{TiO}_2$  NPs is shown in Fig. 4.4. The total weight loss observed in the whole temperature range was 37.80% for  $\text{TiO}_2$ . The total weight loss occurs in three different stages. The first stage of weight loss is in between room temperature to 150 °C, which is caused by the loss of physically adsorbed water. The second stage of weight loss is from 150 °C to 400 °C and is due to loss of chemisorbed water, solvent and organic groups attached to sample [36]. The third stage is from 450 °C to 900 °C, where the mass loss is less than 0.80 %. Taking into consideration of TGA studies, all the samples are calcinated at 450 °C for their further characterization.

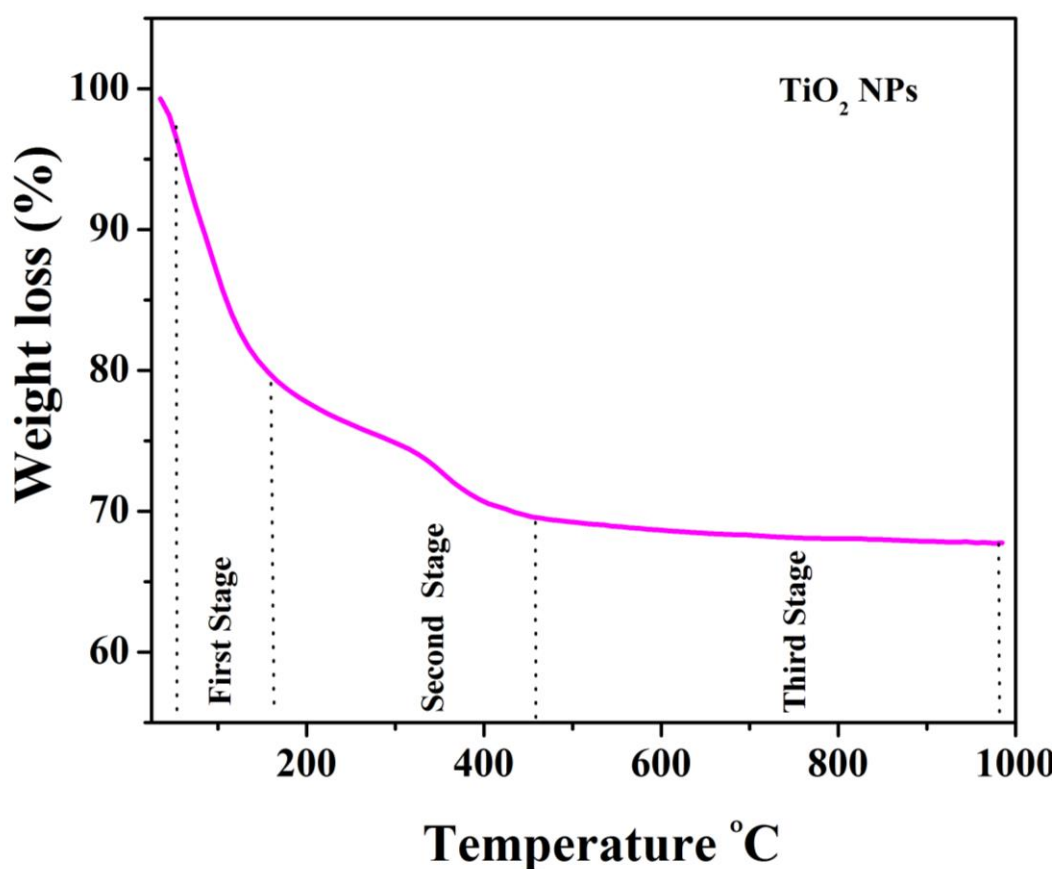


**Fig. 4.4. TGA thermogram of pure  $\text{TiO}_2$  NPs**

#### 4.7.1.2 X-ray diffraction studies

The experimental XRD pattern of synthesized TiO<sub>2</sub> NPs shown in Fig. 4.5 All peaks were indexed in the tetragonal anatase phase of TiO<sub>2</sub>. No peaks observed for rutile and brookite phase of TiO<sub>2</sub> NPs. Also the various structural parameters are calculated from XRD pattern and listed in Table 4.1. The XRD pattern of TiO<sub>2</sub> sample is clearly matches with the standard anatase phase (Joint Committee for Powder Diffraction Standard, #21–1272) [37]. The lattice parameter calculated from XRD pattern closely matches with literature data of anatase tetragonal structure TiO<sub>2</sub> ( $a = 3.7822 \text{ \AA}$ ,  $c = 9.5023 \text{ \AA}$  and  $V = 135.93 \text{ \AA}^3$ ). The diffractogram does not shows any extra peaks confirming that the anatase phase only without any impurity. The crystallite size of the TiO<sub>2</sub> NPs was estimated from the full-width at half-maximum (FWHM) of the strongest diffraction plane (101) using the Scherrer's formula. Crystallite size of TiO<sub>2</sub> NPs is found to 7 nm. The crystallite particle size of TiO<sub>2</sub> NPs increases the probability for reactions of the photogenerated electrons and holes with reactant molecules and ultimately enhances the photocatalytic activity [38].

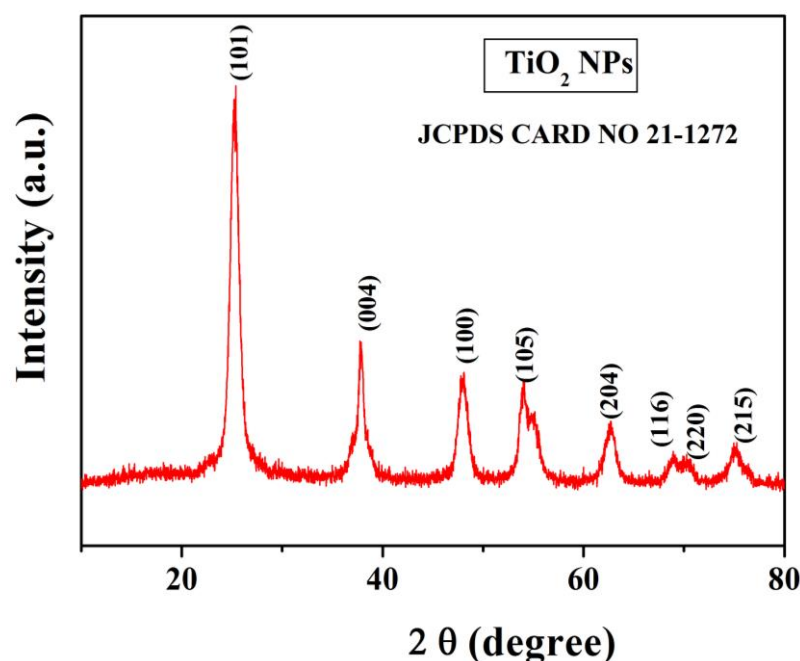


**Fig. 4. 5. XRD pattern of TiO<sub>2</sub> NPs**

**Table 4.1 Summary of structural parameters of TiO<sub>2</sub> NPs**

Samples	(h k l)	Standard 'd' values (Å)	Calculated 'd' values (Å)	Cell cons. a and c (Å) V Å <sup>3</sup>	Crystallite size (nm)
TiO <sub>2</sub> NPs	(1 0 1)	3.51	3.50	'a' = 3.78	7.0
	(0 0 4)	2.37	2.36	'c' = 9.48	
	(2 2 0)	1.33	1.33	'V' = 136.40	

#### 4.7.1.3 Transmission electron microscopy (TEM) studies

The transmission electron micrograph (TEM) of TiO<sub>2</sub> NPs is shown in Fig. 4.6. (a) The particle size of TiO<sub>2</sub> NPs was observed in the range of 7-15 nm. It is seen that the particles are of non-uniform size and shape. The observed particle size closely approaches with XRD results. The structural behavior of TiO<sub>2</sub> NPs was also confirmed by selected area electron diffraction (SAED) and these patterns are shown in Fig. 4.6 (b). In SAED pattern diffraction rings are indexed and perfectly match the anatase phase of TiO<sub>2</sub> NPs [39].

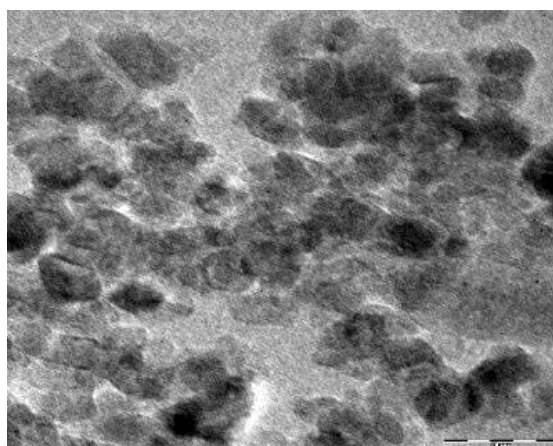


**Fig. 4.6. (a) TEM image of Pure TiO<sub>2</sub> NPs**

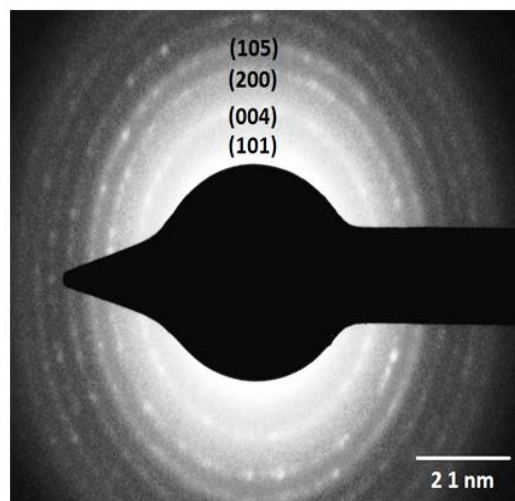


**Fig. 4.6. (b) SAED pattern of Pure TiO<sub>2</sub> NPs**

## **4.7.2 Characterization of TiO<sub>2</sub>-MWCNTs NCs**

### **4.7.2.1 Thermal analysis (TGA)**

TGA curve of the representative ‘as-prepared’ sample, TC 0.5 NCs is shown in Fig. 4.7. The first minor weight loss observed between initial ambient temperature and 100 °C due to the loss of physically adsorbed moisture, found to be 18.04 wt. %. The highest weight loss observed in between 100 °C and 200 °C, because the transformation of hydroxides into their corresponding amorphous oxide [36]. Also the weight loss observed in the range 200 °C to 450 °C due to loss of coordinated water as well as organic moieties. The Fig. 4.7 shows the TC 0.5 NC is thermally stable in the range of 450 °C to 1000 °C [40]. Therefore the synthesized TC NCs are calcinated at 450 °C temperature.

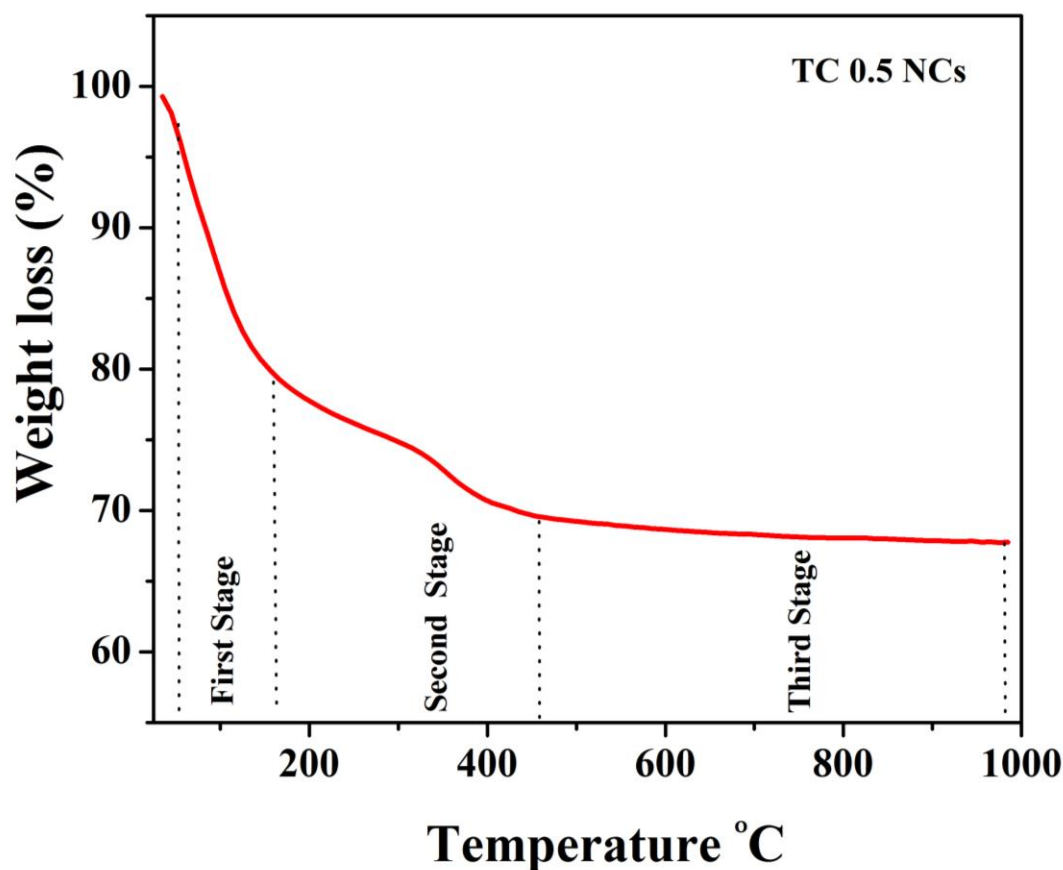


Fig. 4.7. TGA thermogram of TC 0.5 NCs

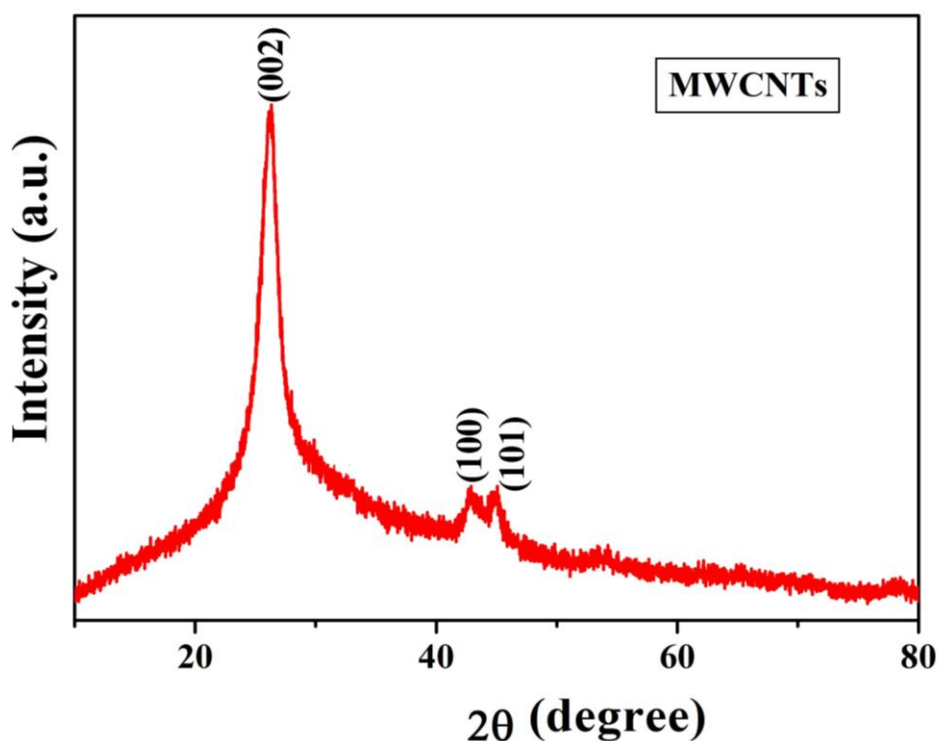
#### 4.7.2.2 X-ray diffraction studies

Fig. 4.8.(a) shows XRD pattern of MWCNTs, the characteristics intense peak at  $26.34^\circ$  corresponding to the (002) reflection with other peaks at  $42.90^\circ$ ,  $45.04^\circ$  correspond to (100), (101) reflections, respectively. All these peaks are also clearly matched with the characteristic peaks of standard graphite carbon (JCPDS 75-1621) [41]. Fig. 4.8. (b) Shows XRD pattern of  $\text{TiO}_2$ -MWCNTs (TC) NCs. The most intense peak at  $25.3^\circ$  with reflection plane (101) which conformance the presence of anatase phase in TC NCs. The characteristic peaks of TC NCs exactly matches with (JCPDS 21-1272) this reveals that the TC NCs having only anatase phase of  $\text{TiO}_2$  NPs [42]. No peaks observed for

rutile and brookite phase of TiO<sub>2</sub> NPs. Also, the characteristic peak of MWCNTs at 26.3° was overlapped with a characteristic peak of anatase TiO<sub>2</sub> NPs [43] No other characteristic peaks of MWCNTs were observed in TC NCs due to the very low concentration.. The intensity of peaks is increased with the presence of MWCNTs due to the interaction between TiO<sub>2</sub> and MWCNTs. [41]. The crystallite size (D) was calculated by Scherrer's equation (4.1) and the crystallite size is mentioned in Table 1.

$$D = 0.9\lambda / \beta \cos \theta \dots\dots\dots(4.1)$$

Where  $\lambda$  is the wavelength of X-ray diffraction ( $\lambda = 1.5406 \text{ \AA}$ ),  $\beta$  is full width at half maximum (FWHM),  $\theta$  is the Bragg's angle and structural parameters calculated from XRD patterns listed in Table 4.2.



**Fig. 4.8. (a) XRD pattern of MWCNTs**

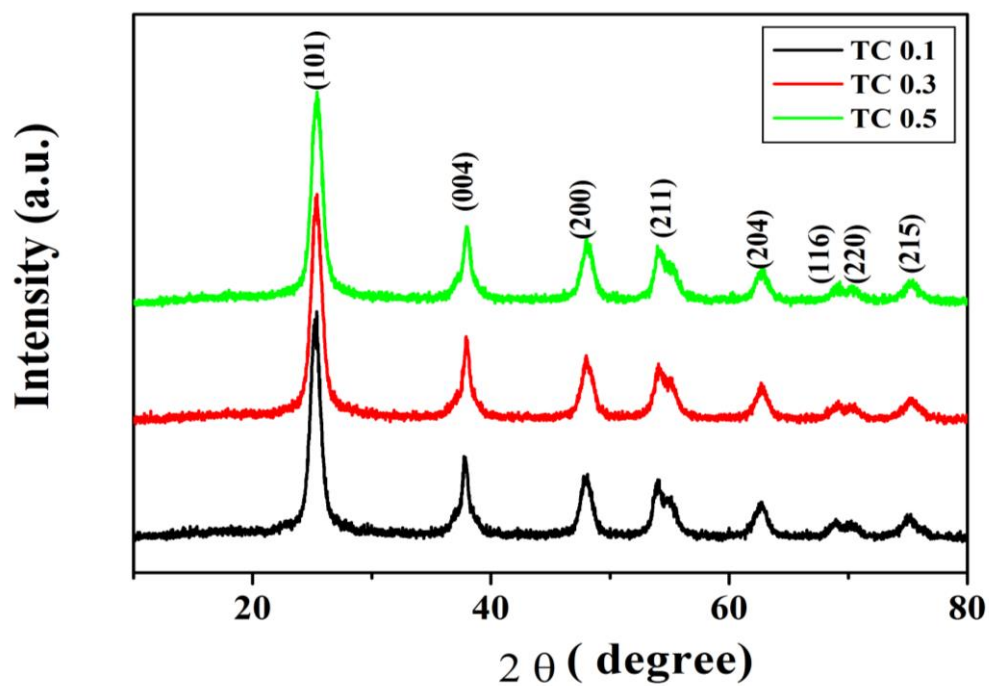


Fig. 4.8. (b) XRD patterns of TiO<sub>2</sub>-MWCNTs NCs

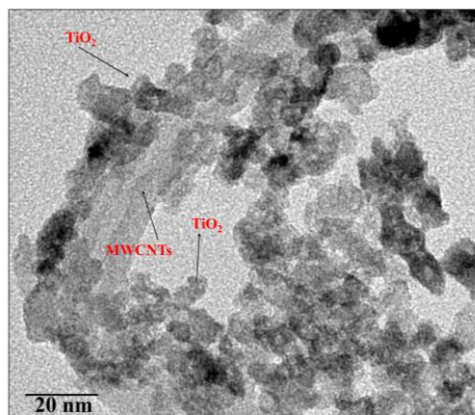


**Table 4.2 Summary of structural parameters of TiO<sub>2</sub>-MWCNTs NCs**

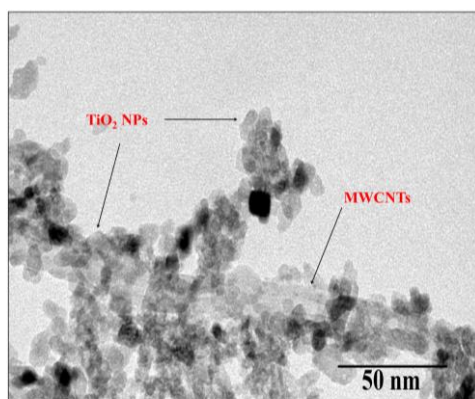
Samples (NCs)	(h k l)	Standard 'd' values (Å)	Calculated values (Å)	Cell cons. 'a' and 'c' (Å) 'V' Å <sup>3</sup>	Crystallite size (nm)
TC 0.1	(1 0 1)	3.51	3.50	a = 3.78, c = 9.50 & V = 136.50	9.0
	(0 0 4)	2.37	2.37		
	(2 2 0)	1.33	1.33		
TC 0.3	(1 0 1)	3.51	3.50	a = 3.78, c = 9.48 & V = 136.40	11.3
	(0 0 4)	2.37	2.37		
	(2 2 0)	1.33	1.33		
TC 0.5	(1 0 1)	3.51	3.50	a = 3.78, c = 9.46 & V = 136.55	11.8
	(0 0 4)	2.37	2.37		
	(2 2 0)	1.33	1.33		

#### 4.7.2.3. Transmission electron microscopy (TEM) studies

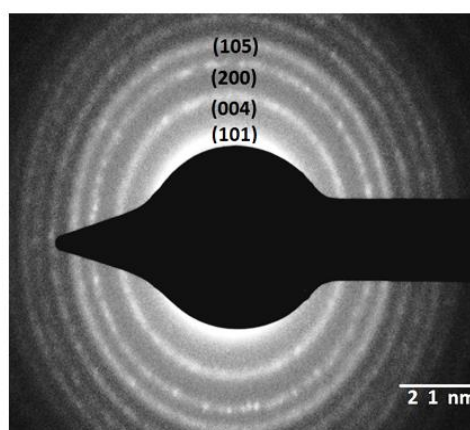
Fig. 4.9 shows the morphology and inner structure of representative TC 0.5 NCs, Fig. 4.9 (a) and (b) shows the MWCNTs were homogenously decorated by TiO<sub>2</sub> NPs. The diameter of nanotubes was in the range of 7-15 nm and less aggregation of TiO<sub>2</sub> NPs. The good decoration of TiO<sub>2</sub> NPs on the surface of MWCNTs has occurred due the presence of abundance hydroxyl groups, carboxyl groups, on the surface of MWCNTs and the particle size observed in the range of 7-15 nm [44]. The selected area electron diffraction (SAED) pattern of TC 0.5 NCs shown Fig. 4. (c) for confirming the structural phase. The diffraction rings are indexed and perfectly matches to the anatase phase of TiO<sub>2</sub> NPs.



(a)



(b)



(c)

**Fig. 4.9. (a) and (b) TEM image; (c) SAED pattern; of TC 0.5 NCs**

### 4.8 Conclusions

In this chapter the various chemical methods were highlighted in detail for synthesis of  $\text{TiO}_2$  NPs and  $\text{TiO}_2$ -MWCNTs NCs. Also we have successfully synthesized  $\text{TiO}_2$  NPs and  $\text{TiO}_2$ -MWCNTs NCs by simple sol–gel method and characterized by various techniques. X-ray diffraction studies confirm the presence of pure anatase phase with crystallite size 7 nm for  $\text{TiO}_2$  NPs and also of 7 to 12 nm for  $\text{TiO}_2$ -MWCNTs NCs. Morphological studies were carried out by TEM which revealed well decoration of  $\text{TiO}_2$  NPs on the surface MWCNTs with particle size in the range of 7-15 nm. Thermal analysis showing approximately 38% weight loss in both sample.

---

### Reference

- [1] M. Andersson, L. Osterlund, S. Ljungström, and A. Palmqvist, J. Phys. Chem. B 106 (2002) 10674.
- [2] B. Boro, B. Gogoi, B. Rajbongshi, and A. Ramchiary, Renew. Sustainable Energy Rev. (2017) <https://doi.org/10.1016/j.rser.2017.06.035>.
- [3] R. K. Wahi, Y. Liu, J. C. Falkner, and V. L. Colvin, J. Colloid Interface Sci. 302 (2006) 530.
- [4] M. H. Bazargan, M. M. Byranvand, and A. N. Kharat, Int. J. Mater. Res. 103 (2012) 347.
- [5] L. Kavan, N. Tetreault, T. Moehl, and M. Grätzel, J. Phys. Chem. C, 118 (2014) 16408.
- [6] H. Arami, M. Mazloumi, R. Khalifehzadeh, and S. Sadrnezhad, Mater. Lett. 61 (2007) 4559.
- [7] K. T. Lim, H. S. Hwang, W. Ryoo, and K. P. Johnston, Langmuir 20 (2004) 2466.
- [8] E. Stathatos, P. Lianos, F. Del Monte, D. Levy, and D. Tsiourvas, Langmuir 13 (1997) 4295.
- [9] D. Zhang, L. Qi, J. Ma, and H. Cheng, J. Mater. Chem. 12 (2002) 3677.
- [10] S. Muduli, W. Lee, V. Dhas, S. Mujawar, M. Dubey, K. Vijayamohanan, S.H. Han, and S. Ogale, ACS Appl. Mater. Interfaces. 1 (2009) 2030.
- [11] L. Song and S. Zhang, Chem. Eng. J. 166 (2011) 779.
- [12] O. Carp, C. L. Huisman, and A. Reller, Prog. Solid State Chem. 32 (2004) 33.
- [13] L. Tian, L. Ye, K. Deng, and L. Zan, J. Solid State Chem. 184 (2011) 1465.
- [14] H. Chen, S. M. Yu, D.-W. Shin, and J. B. Yoo, Nanoscale Res. Lett. 5 (2010) 217.
- [15] H. Zhou and Y. Zhang, J. Phys. Chem. C 118 (2014) 5626.
- [16] L. C. Jiang and W. D. Zhang, Electroanalysis 21 (2009) 988.

- 
- [17] B. Murray, Q. Li, J. Newberg, E. Menke, J. Hemminger, and R. Penner, Nano Lett. 5 (2005) 2319.
  - [18] J. K. McDonough and Y. Gogotsi, Electrochem. Soc. Interface, 22 (2013 ) 61.
  - [19] G. R. Li, H. Xu, X. F. Lu, J. X. Feng, Y. X. Tong, and C. Y. Su, Nano-scale 5 (2013) 4056.
  - [20] M. Malekshahi Byranvand, A. Nemati Kharat, L. Fatholahi, and Z. Malekshahi Beiranvand, J. Nanostruct. 3 (2013) 1.
  - [21] F. H. Abdulrazzak, F. H. Hussein, A. F. Alkaim, I. Ivanova, A. V. Eme-line, and D. W. Bahnemann, Photochem. Photobiol. Sci. 15 (2016)1347.
  - [22] F. Alosfur, H. Jumali, S. Radiman, N. J. Ridha, M. A. Yarmo, and A. A. Umar, Int. J. Electrochem Sci. 8 (2013) 2977.
  - [23] M. H. H. Jumali, F. K. M. Alosfur, S. Radiman, N. J. Ridha, M. A. Yarmo, and A. A. Umar, Mater. Sci. Semicond. Process. 25 (2014) 207.
  - [24] B. Corain, G. Schmid, and N. Toshima, Metal nanoclusters in catalysis and materials science: the issue of size control, Elsevier, (2011).
  - [25] V. Chhabra, V. Pillai, B. Mishra, A. Morrone, and D. Shah, Langmuir 11 (1995) 3307.
  - [26] J. Xie, L. F. Mei, L. B. Liao, G. C. Lv, Z. G. Xia, and G. X. Du, in Key Engineering Materials, Vol. 602, Trans Tech Publ, (2014).
  - [27] R. Zhang and L. Gao, Mater. Res. Bull. 37 (2002) 1659.
  - [28] C. J. Brinker and G. W. Scherer, Sol-gel science: the physics and chemistry of sol-gel processing, Academic press, (2013).
  - [29] S. G. Ullattil and P. Periyat, Sol-Gel Materials for Energy, Environment and Electronic Applications, Springer, (2017).
  - [30] C. Brinker, B. Bunker, D. Tallant, K. Ward, and R. Kirkpatrick, ACS Publications, (1988).
  - [31] G. W. Scherer, J. Non-Cryst. Solids 100 (1988) 77.
  - [32] L. L. Hench and J. K. West, Chem. Rev. 90 (1990) 33.

- 
- [33] V. B. Koli, A. G. Dhodamani, A. V. Raut, N. D. Thorat, S. H. Pawar, and S. D. Delekar, *J. Photochem. Photobiol. A* 328 (2016) 50.
  - [34] A. Ramar, T. Soundappan, S.-M. Chen, M. Rajkumar, and S. Ramiah, *Int. J. Electrochem. Sci* 7 (2012) 11734.
  - [35] V. B. Koli, A. G. Dhodamani, S. D. Delekar, and S. H. Pawar, *J. Photochem. Photobiol. A* 333 (2017) 40.
  - [36] K. Nagaveni, M. Hegde, and G. Madras, *J. Phys. Chem. B* 108 (2004) 20204.
  - [37] V. B. Koli, A. G. Dhodamani, K. V More, S. F. A. Acquahc, D. K. Panda, S. H. Pawar, S.D. Delekar, *Sol. Energy* 149 (2017) 188.
  - [38] H. M. Yadav, S. V. Otari, V. B. Koli, S. S. Mali, C. K. Hong, S. H. Pawar, and S. D. Delekar, *J. Photochem. Photobiol. A* 280 (2014) 32.
  - [39] B. Liu and H. C. Zeng, *Chem. Mater.* 20 (2008) 2711.
  - [40] K. Lin, W. Liou, T. Yang, H. Lin, C. K. Lin, S. Chien, W. Chen, and S. Wu, *Diamond Relat. Mater.* 18 (2009) 312.
  - [41] K. M. Samant, J. S. Suroshe, and S. S. Garje, *Eur. J. Inorg. Chem.* 2014 (2014) 499.
  - [42] Y. Cong, X. Li, Y. Qin, Z. Dong, G. Yuan, Z. Cui, and X. Lai, *Appl. Catal. B.* 07 (2011) 128.
  - [43] H. M. Yadav, T. V. Kolekar, S. H. Pawar, and J. S. Kim, *J. Mater. Sci.: Mater. Medi.* 27 (2016) 1.
  - [44] A. Corrias, G. Mountjoy, D. Gozzi, and A. Latini, *Nanotechnology* 18 (2007) 485610.

# Chapter 5

## Effect of MWCNTs content on photocatalytic properties of TiO<sub>2</sub> nanoparticles

Journal of Photochemistry and Photobiology A: Chemistry 328 (2016) 50–58



Contents lists available at ScienceDirect  
Journal of Photochemistry and Photobiology A:  
Chemistry  
journal homepage: [www.elsevier.com/locate/jphotochem](http://www.elsevier.com/locate/jphotochem)



### Visible light photo-induced antibacterial activity of TiO<sub>2</sub>-MWCNTs nanocomposites with varying the contents of MWCNTs



Valmiki B. Koli<sup>a,b</sup>, Ananta G. Dhodamani<sup>b</sup>, Abhinav V. Raut<sup>a</sup>, Nanasaheb D. Thorat<sup>c</sup>, Shivaji H. Pawar<sup>a</sup>, Sagar D. Delekar<sup>a,b,d,\*</sup>

<sup>a</sup>Center for Interdisciplinary Research, D.Y. Patil University, Kolhapur 416 006, India

<sup>b</sup>Department of Chemistry, Shivaji University, Kolhapur 416 004, India

<sup>c</sup>Department of Physics and Energy, University of Limerick, Limerick, Ireland

<sup>d</sup>Department of Chemistry and Biochemistry, Florida State University, Tallahassee 32306-4390, United States

Journal of Photochemistry and Photobiology A: Chemistry 333 (2017) 40–48



Contents lists available at ScienceDirect  
Journal of Photochemistry and Photobiology A:  
Chemistry  
journal homepage: [www.elsevier.com/locate/jphotochem](http://www.elsevier.com/locate/jphotochem)



### *In situ* sol-gel synthesis of anatase TiO<sub>2</sub>-MWCNTs nanocomposites and their photocatalytic applications



Valmiki B. Koli<sup>a</sup>, Ananta G. Dhodamani<sup>b</sup>, Sagar D. Delekar<sup>a,b,\*</sup>, Shivaji H. Pawar<sup>a,\*</sup>

<sup>a</sup>Center for Interdisciplinary Research, D.Y. Patil University, Kolhapur 416 006, India

<sup>b</sup>Department of Chemistry, Shivaji University, Kolhapur 416 004, India





### 5.1 Introduction

The NCs with carbon nanostructures, especially multi-walled carbon nanotubes (MWCNTs) found to tune the optical band gap of  $\text{TiO}_2$  into the visible region and improve its photoactivity [1, 2]. Generally MWCNTs has two roles plausibly. As per the literature, MWCNTs may acts as electron scavengers in the NCs. This is due to its highly conductive nature; which accepts the excited electrons from the conduction band of  $\text{TiO}_2$  resulting in the well separation of charge carriers. The nature of MWCNTs, as an electron sink, in combination with the other semiconductors and also shown the enhancement in life-time of photogenerated carriers due to their well separations as the Fermi level of MWCNTs is lower as compared to  $\text{TiO}_2$  NPs. Another role of MWCNTs is concerned to the photosensitizer and hence itself absorbs the photon energy and thereafter the electrons are transferred to the conduction band of  $\text{TiO}_2$  NPs. In the NCs, the introduction of MWCNTs into  $\text{TiO}_2$  remarkably increased the photocatalytic activity. The synergetic effect, induced by a strong interphase interaction between MWCNTs and  $\text{TiO}_2$  NPs, was ascribed to MWCNTs acting as photosensitizers rather than as adsorbent or dispersing agent in the composites. These two possible ways ultimately decrease the probability of the recombination of the electron-hole pairs and hence which may results the absorption of visible light. Therefore, MWCNTs act as absorber or sensitizer and hence which enhances the oxidative reactivity of particles in contact to bacteria with the damage of its cell-walls [3]. When  $\text{TiO}_2$  NPs was decorated on the surface of MWCNTs, the particles are well dispersed and hence would have the large specific surface area to bind bacteria effectively. Also, in presence of light, the electron-hole recombination rate was diminished at the interfaces of  $\text{TiO}_2$ -MWCNTs (TC NCs), which resulting the superior activity as compared to bare particles[3, 4]. The activity of NCs is also enhanced due to the formation of even more reactive oxygen species, like

hydroxyl and other radicals. The overall effect of MWCNTs concentration on photocatalytic properties of TiO<sub>2</sub> NPs is included in this chapter.

### 5.2. Spectroscopic properties of TiO<sub>2</sub>

#### 5.2.1 UV–visible diffuse reflectance spectroscopy (UV-DRS) studies

UV–visible diffuse reflectance spectrum of TiO<sub>2</sub> NPs is shown in Fig. 5.1 (a). TiO<sub>2</sub> NPs show a well-defined optical absorption edge in the range of 340-420 nm with the extrapolation of tangent to the X-axis at around 387 nm; The optical band gap of the TiO<sub>2</sub> NPs was determined by the following tauc equation [5].

$$\alpha h\nu = A (h\nu - E_g)^2 \quad (5.1)$$

Where A is the proportionality constant,  $\alpha$  is the absorption coefficient,  $E_g$  is the optical band gap, and  $n=2$  for direct transition.

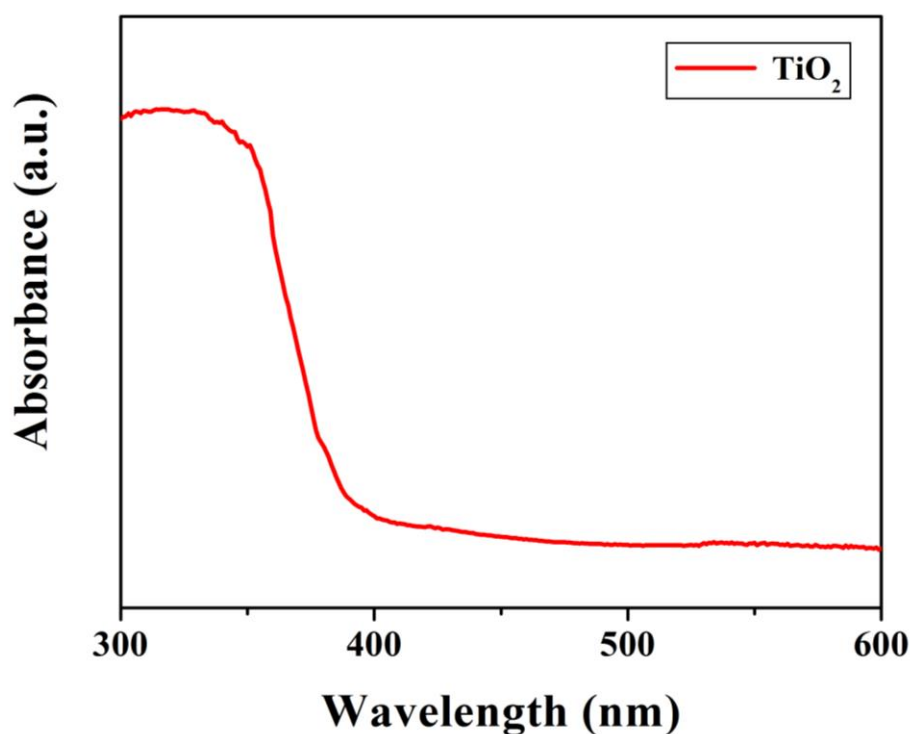


**Fig.5.1. (a) UV–Visible diffuse reflectance spectrum of TiO<sub>2</sub> NPs**

Based on the above equation, the optical band gap of the samples is determined through a graph of  $(\alpha h\nu)^2$  eV vs  $h\nu$ ; which is shown in Fig.5.1 (b). It is observed that the optical band gap  $\text{TiO}_2$  NPs is 3.2 eV, optical band gap value of  $\text{TiO}_2$  NPs is in good agreement with the reported earlier [6, 7].

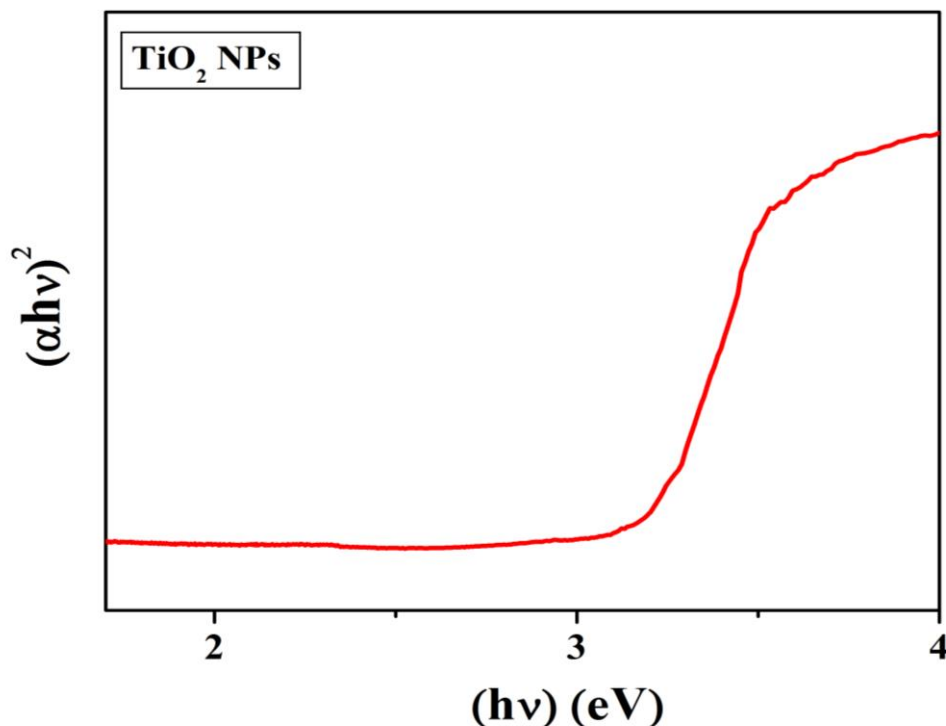


**Fig 5.1 (b) Plot of  $(\alpha h\nu)^2$  versus  $h\nu$  for  $\text{TiO}_2$  NPs**

### 5.2.2 Fourier transform infrared spectroscopy (FTIR) studies

The FTIR spectrum of  $\text{TiO}_2$  NPs represented in Fig. 5.2 A broad peak observed in between  $3500 \text{ cm}^{-1}$  to  $2900 \text{ cm}^{-1}$  can be assigned to stretching vibration mode of the  $-\text{OH}$  group on the surface  $\text{TiO}_2$  NPs; which show the coordination vacancies in the presence of water [8, 9]. The bending vibration band of the  $-\text{OH}$  group is observed at  $1629 \text{ cm}^{-1}$ . A broad band in between  $400 \text{ cm}^{-1}$  to  $1000 \text{ cm}^{-1}$  region with peaks at about  $475 \text{ cm}^{-1}$ , and  $590 \text{ cm}^{-1}$  are characteristic peaks of anatase  $\text{TiO}_2$  NPs [10]. These low Low-frequency and in the range  $<600 \text{ cm}^{-1}$  have been assigned to bending vibrations of the  $\text{Ti}-\text{O}-\text{Ti}$

network of the anatase TiO<sub>2</sub> NPs [11].

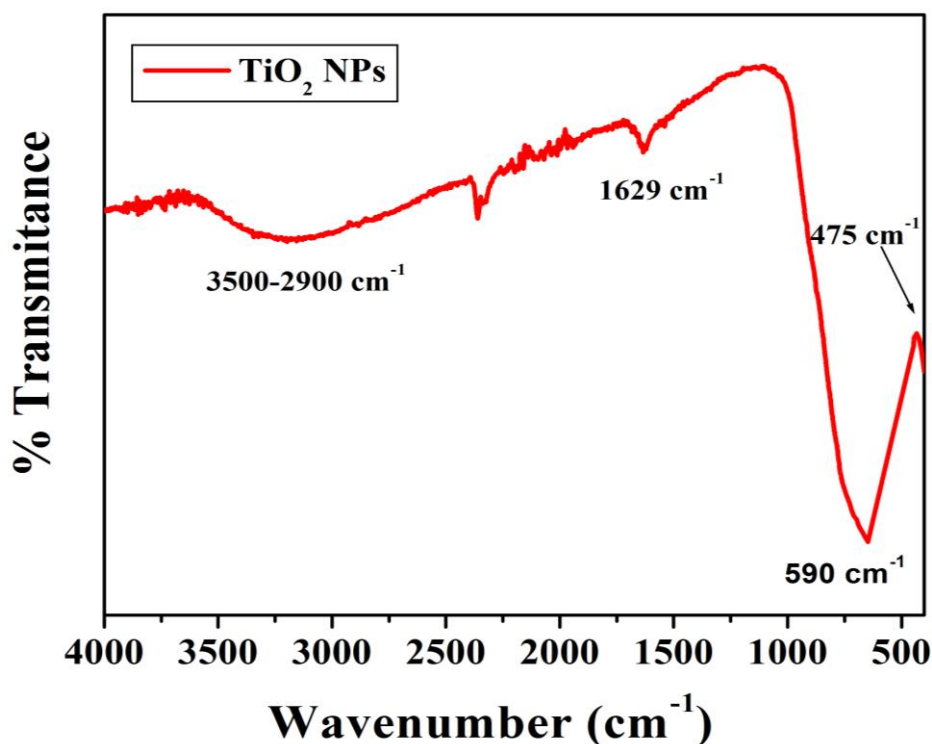


Fig. 5.2 FTIR spectrum of TiO<sub>2</sub> NPs

### 5.2.3 Raman spectroscopy

Raman spectroscopic studies of TiO<sub>2</sub> NPs were carried out for further investigation of its structural phases. Raman spectrum of TiO<sub>2</sub> NPs is shown in the Fig. 5.3 TiO<sub>2</sub> NPs show a Raman peaks similar to the characteristic feature of anatase TiO<sub>2</sub> NPs [12]. Tetragonal anatase structured TiO<sub>2</sub> NPs belongs to  $D_{4h}^{19}$  ( $I4_1/amd$ ) space group and may have following normal lattice vibration modes.

$$\text{Anatase} = A_{1g} + B_{1g} + B_{2g} + E_g \dots\dots\dots (5.2)$$

TiO<sub>2</sub> NPs show the characteristic bands at 396, 518 and 638 cm<sup>-1</sup> correspond to the B<sub>1g</sub> (1), A<sub>1g</sub>+B<sub>1g</sub> (2) and E<sub>g</sub> (3) modes, respectively [13]. This is also confirms the presence of anatase phase of TiO<sub>2</sub> in the all composites; without rutile or other phases. The absence of the Raman bands at

612, 447 and  $235\text{ cm}^{-1}$  corresponding to the rutile phase of  $\text{TiO}_2$  again confirmed that the anatase phase purity of pure  $\text{TiO}_2$  sample. The observed results are reliable with the XRD measurements.

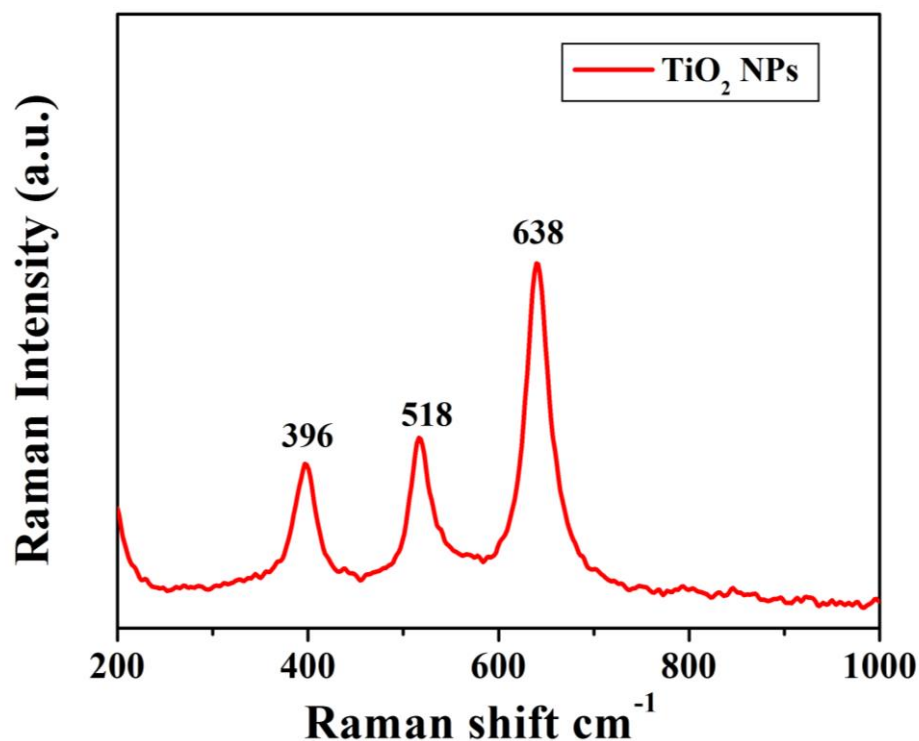
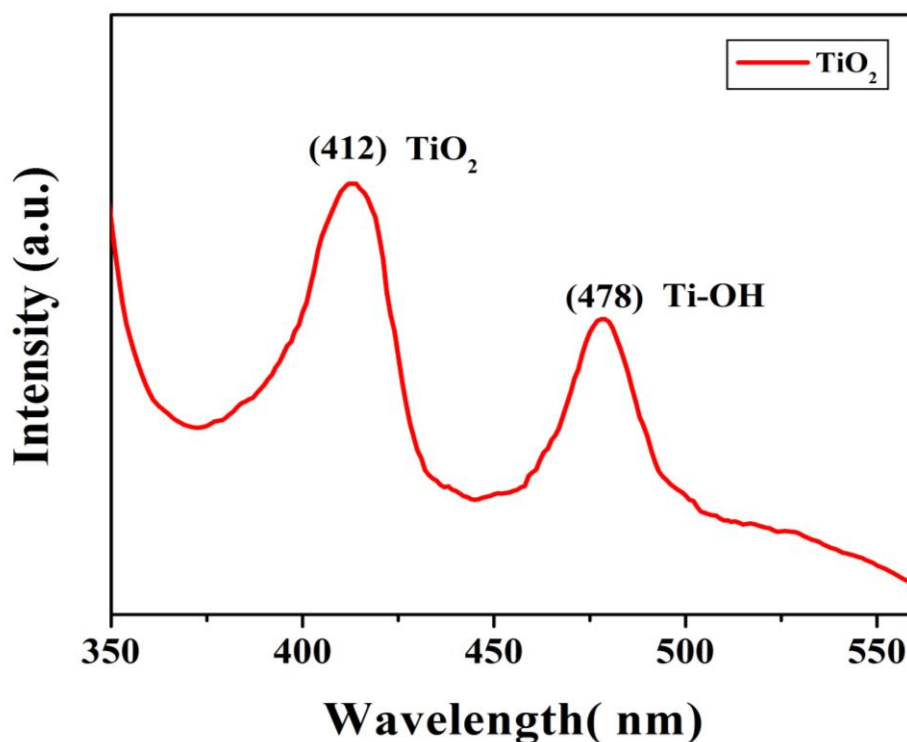


Fig. 5.3 Raman Spectrum of  $\text{TiO}_2$  NPs

#### 5.2.4 Photoluminescence spectroscopy (PL)

PL spectrum of  $\text{TiO}_2$  NPs is shown in Fig. 5.4, The PL emission study of semiconductor NPs gives the efficiency of charge carrier trapping, immigration, and transfer. This study also helpful for understanding the rate of electrons and holes recombination of free carriers [14, 15].  $\text{TiO}_2$  NPs show the good intense emission peaks which confirms that electrons and holes are more easily recombined. The intensity of PL peaks suggest the rate of recombination of electrons and hole [16, 17]. The PL emission mainly results from the recombination of excited electrons and holes, and the lower PL intensity attributed to the decrease in recombination rate. When the recombination rate

decreases, more photogenerated charge carriers can participate in the photocatalytic activity, resulting in the enhancement of photocatalytic activity. PL spectrum shows two emission peaks at 412 nm and 478 nm; due to free exciton emission of  $\text{TiO}_2$  and the surface  $\text{Ti-OH}$  bonds, respectively [18] The energy difference between band gap and emission peak energy is caused by the Stokes shift due to the Franck-Condon effect. The change of defect state on the shallow level of the  $\text{TiO}_2$  NPs surface is also responsible for the variation of PL intensity [19].



**Fig. 5.4 PL spectrum of  $\text{TiO}_2$  NPs (excitation wavelength 285 nm)**

### 5.2.5 X-ray photoelectron spectroscopy

Quantitative analysis of the electronic structures and chemical properties of the representative  $\text{TiO}_2$  NPs was analyzed by XPS. Fig. 5.5. (a) shows survey spectrum of  $\text{TiO}_2$  NPs. Fig. 5.5.(b) shows XPS spectrum for  $\text{Ti}2p$  configuration with two bands are observed at 459.4 and 465.1 eV, which are

the characteristics of Ti 2p<sub>3/2</sub> and Ti 2p<sub>1/2</sub> peaks respectively. The splitting between the Ti 2p<sub>1/2</sub> and Ti 2p<sub>3/2</sub> is 5.8 eV, indicating a presence of Ti<sup>4+</sup> oxidation state in the TiO<sub>2</sub> NPs [20, 21]. Fig. 5.5. (c) shows XPS of O 1s configuration. The two peaks are observed at the binding energies of 529 eV and 532 eV. Former peak is assigned for the characteristic of Ti–O bond in lattice oxide; while latter is for –OH bond due to surface adsorbed water molecules [22].

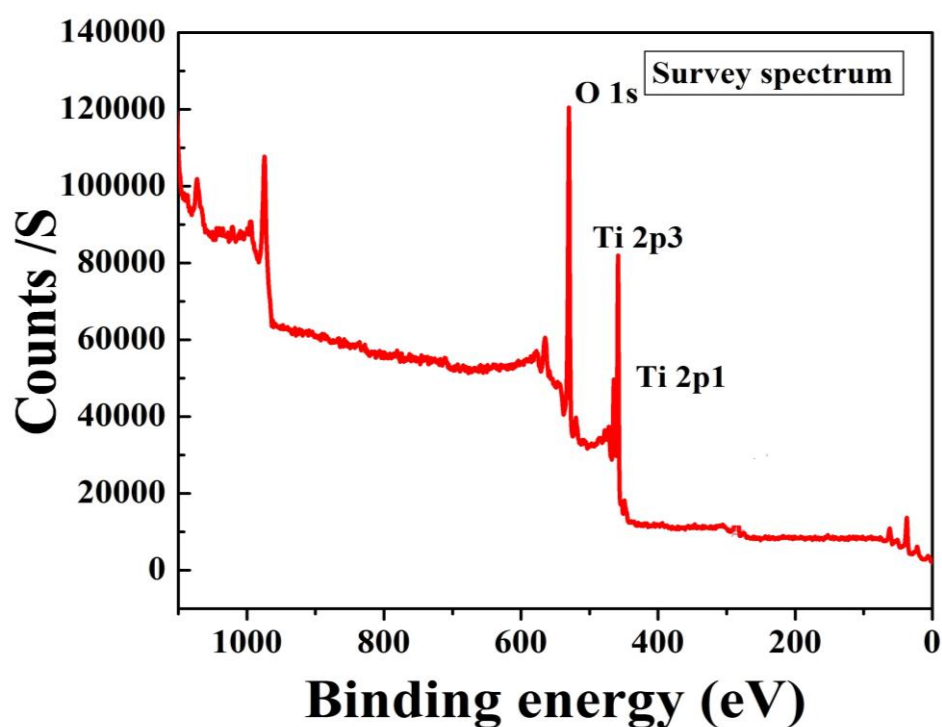
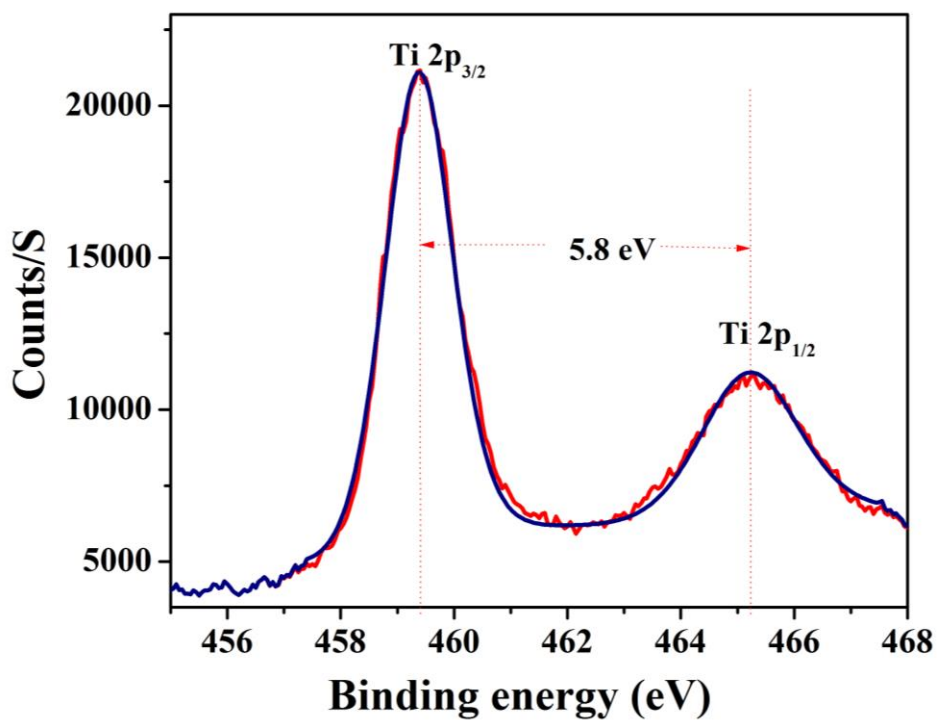
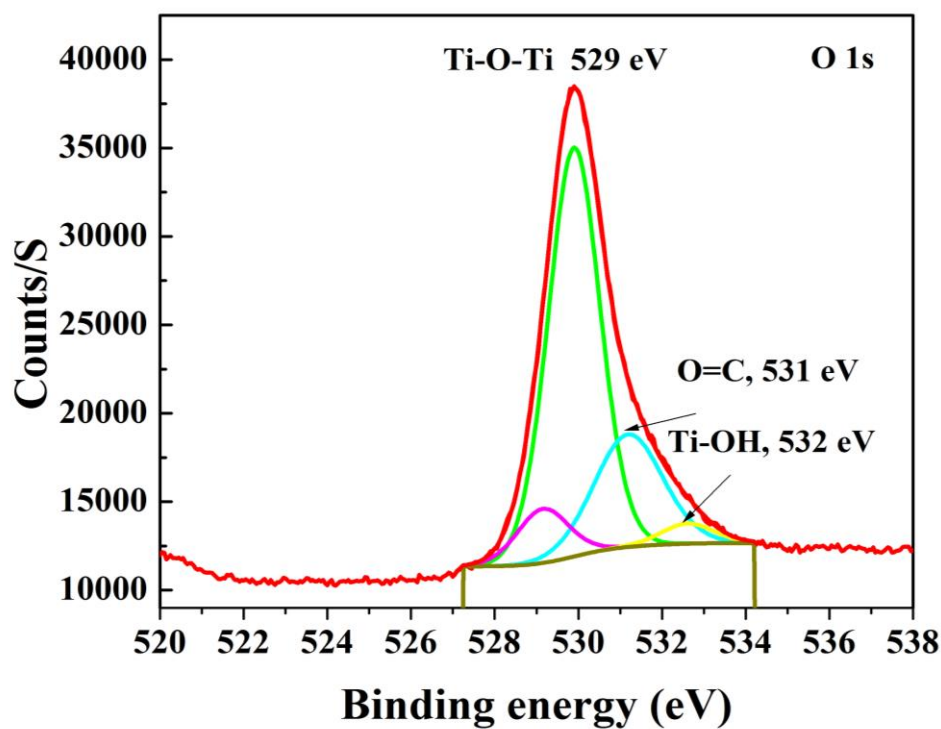


Fig. 5.5. (a) Survey spectrum of TiO<sub>2</sub> NPs

Fig. 5.5 (b) Ti 2p configuration of TiO<sub>2</sub> NPsFig. 5.5 (c) O 1s configuration of TiO<sub>2</sub> NPs



### 5.3 Cytotoxicity study of TiO<sub>2</sub> NPs.

The mouse embryonal fibroblast NIH 3T3 cell line was plated in 96-well culture plates (PAA) at an initial density of 1104 cells/well, and incubated (at 37 °C in humidified 5% CO<sub>2</sub> atmosphere) in 100 µL of culture medium Dulbecco's Modified Eagle Medium, High Glucose (DMEM, PAA, Austria) supplemented with 10% heat-inactivated fetal bovine serum (FBS, Thermo Scientific), 0.4% penicillin–streptomycin (Sigma) and L-glutamine (2 mM, Sigma)]. After a 24 h incubation period, the culture medium was removed and suspensions of TiO<sub>2</sub> were added at different concentrations such as 100 µg/mL, 50 µg/mL, 25 µg/mL, 12.5 µg/mL, 6.25 µg/mL. Then the content was agitated homogeneously for 15 min on a shaker to ensure adequate dissolution. Again, after a 24 h incubation period with the studied TiO<sub>2</sub> NPs, the absorbance of the suspension was measured at 450 nm using a micro plate spectrophotometer. The absorbance values were hence analyzed (calculating the average value from three wells per each experimental point in the case of the studied nanomaterials and from nine wells in the case of free medium PBS) to determine cell proliferation compared to control wells [23].

Cytotoxicity of the representative TiO<sub>2</sub> NPs was tested in Mouse embryonal fibroblast NIH 3T3 cells lines. Fig. 5.6 shows the cell viability of TiO<sub>2</sub> NPs for their varying range of concentrations (mean ± S.E. for n=3); and the relative cell viability (%) compared with control well containing cells without TiO<sub>2</sub> NPs is calculated by the equation:

$$\frac{[A]_{\text{tested}}}{[A]_{\text{control}}} \times 100 \quad 5.3$$

Fig. 5.6 shows increase in cytotoxicity for TiO<sub>2</sub> NPs with their concentrations ranges from 6.25 µg/mL to 100 µg/mL. Lowest concentration 6.25 µg/mL showing 86% cell viability while the highest concentration 100 µg/mL showing only 28.85 % cell viability. It suggest that the pure TiO<sub>2</sub> NPs are

biocompatible in certain concentration range.

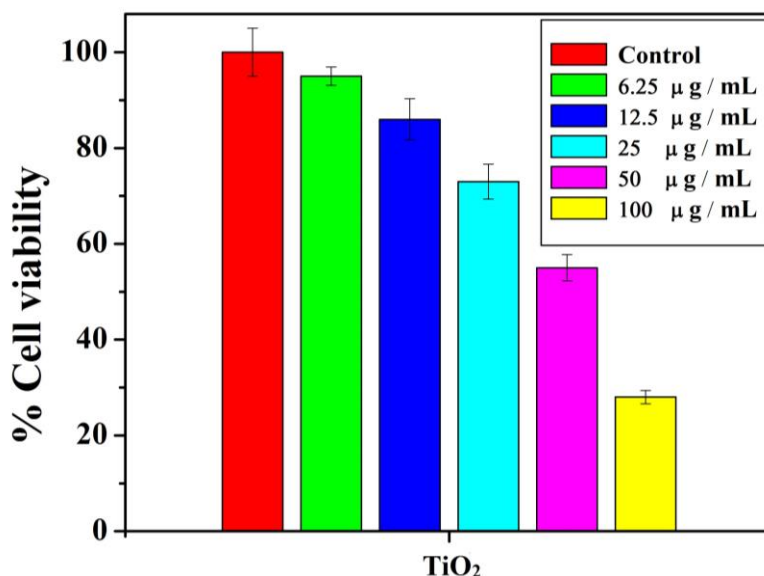


**Fig. 5.6 Cell viability studies of TiO<sub>2</sub> NPs with their varying concentrations against Mouse embryonal fibroblast *NIH 3T3* cells lines**

#### 5.4 Spectroscopic properties of TiO<sub>2</sub>-MWCNTs (TC) NCs

##### 5.4.1 UV–visible diffuse reflectance spectroscopy (UV-DRS) studies

Fig. 5.7 (a) shows the UV-vis diffuse reflectance spectra (UV-vis DRS) of TC NCs. The presence of MWCNTs content affects the optical properties of NCs significantly. The increase in concentration of MWCNTs in TiO<sub>2</sub> host lattice has two-fold advantages. The optical absorption property, directly correlated to absorption intensity, of the NCs is enhanced as compared to that of pure TiO<sub>2</sub> NPs (Fig 5.3. (a)). Also, the optical absorption edge of the NCs is observed in the 390-430 nm; which shifted towards the higher wavelength of electromagnetic spectrum with increase in MWCNTs content. This red shifting would be better for electron transfer from the conduction band of TiO<sub>2</sub> to the MWCNTs surface [24]. The high surface area of MWCNTs allows photogenerated electrons move easily; which helps for better photocatalytic inactivation bacteria.

The optical band gap of the all samples was calculated by using the standard tauc equation. Based on this equation, the optical band gap of the samples is determined through a graph of  $(\alpha h\nu)^2$  vs  $h\nu$ ; which is shown in Fig. 5.7 (b). It is observed that the optical band gap of the NCs decreases from 3.0 eV to 2.6 eV with increase in MWCNTs content. The optical band gap of values of TC NCs are in good agreement with the similar compositions reported earlier [25, 26]. It is suggested that it acts as either photon absorber or scavenger in the NCs samples. In former case, MWCNTs absorb the photon energy with the formation of the charge carriers and then the photogenerated electrons is transferred to the conduction band of the  $\text{TiO}_2$  through the formed Ti–C bonds [27]. In latter case, the generated charge carriers in  $\text{TiO}_2$  host lattice are transferred towards MWCNTs; which ultimately reduces the optical band gap as well as the rate of electron–hole pair recombination. Therefore, the NCs can result the higher photo inactivation of bacteria as compared to pure  $\text{TiO}_2$ .

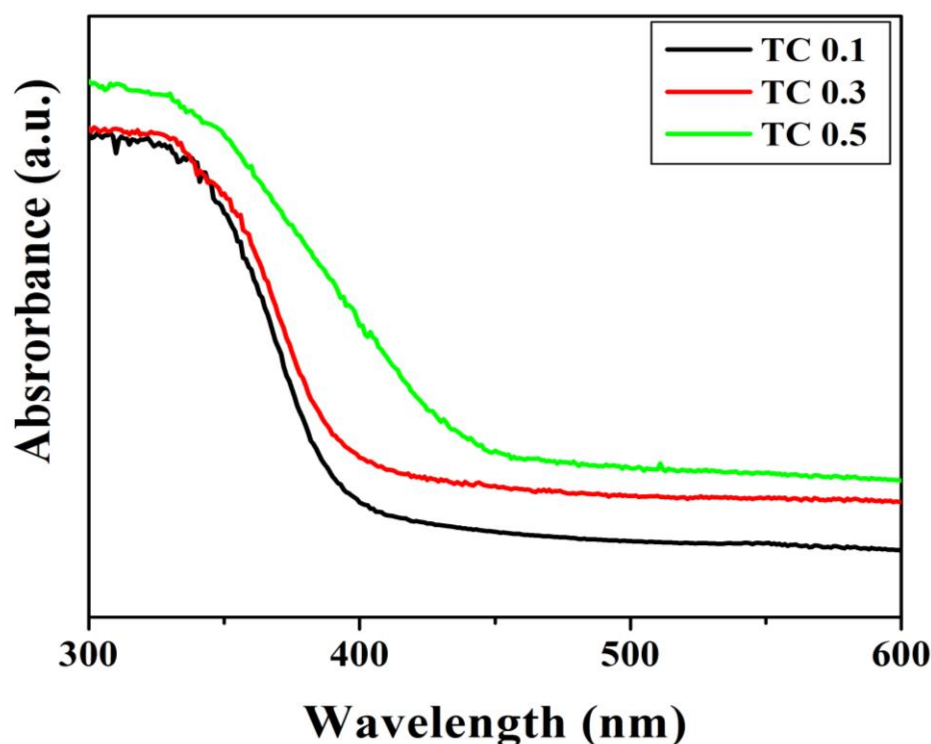


**Fig.5.7. (a) UV–visible diffuse reflectance spectra of TC NCs**

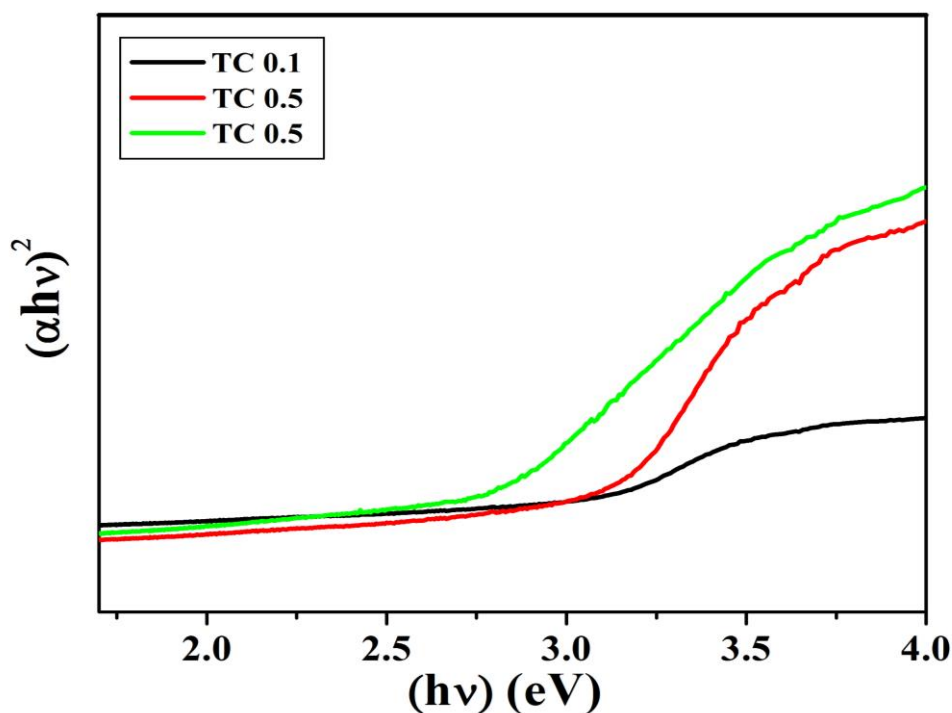
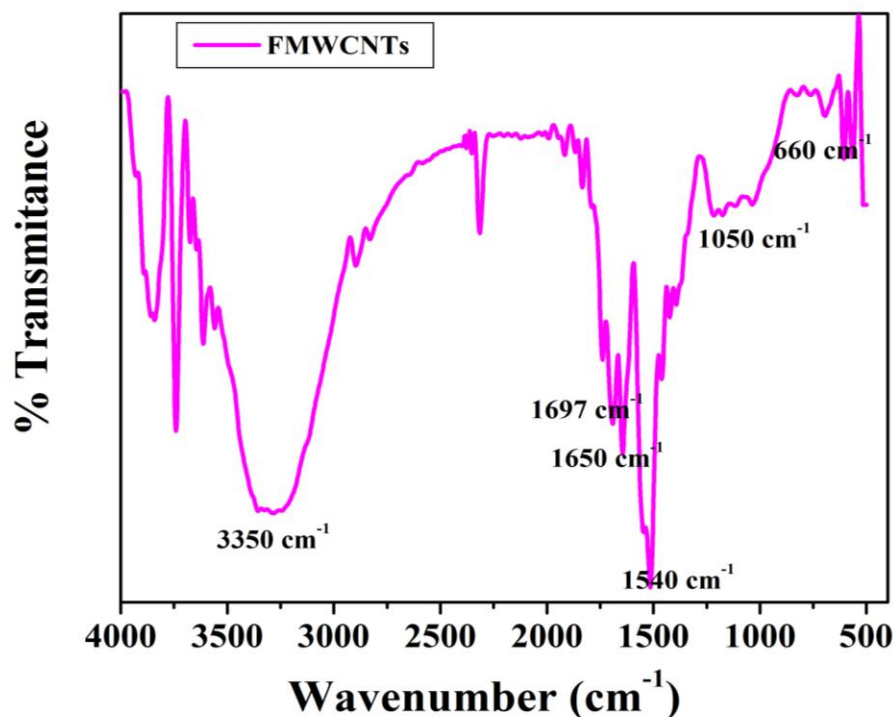


Fig 5.7. (b) The plot of  $(\alpha h\nu)^2$  versus  $h\nu$  for TC NCs

#### 5.4.2 Fourier transform infrared spectroscopy (FTIR) studies

FTIR studies were used to identify the surface functionalized groups. In the FT-IR spectrum of MWCNTs is shown in Fig. 5.8. (a) Which gives the valuable information about the behavior of the attached functional groups to the MWCNTs. The presence of band at  $3450\text{ cm}^{-1}$ , corresponding to stretching vibrations of -OH group with another band at  $1697\text{ cm}^{-1}$  for stretching vibration of the carbonyl group. These bands confirm the presence of -COOH group on the surfaces of MWCNTs. These results indicate pristine MWCNTs were successfully functionalized with acids treatment.



**Fig. 5.8. (a) FTIR spectrum of FMWCNTs**

Fig.5.8.(b) shows FTIR spectra of TC NCs; which consists of a broad band from  $3500\text{--}2900\text{ cm}^{-1}$  for stretching vibrations of  $\text{-OH}$  group with another band at  $1701\text{ cm}^{-1}$  for stretching vibration of the carbonyl group. As compared to pure  $\text{TiO}_2$  NPs (Fig. 5.2) TC NCs shows more functional groups present on the surface of TC NCs. These bands confirm the presence of  $\text{-COOH}$  group on the surfaces of TC NCs. Also, the band at  $1564\text{ cm}^{-1}$  reveals the presence of  $\text{C=C}$  stretching of MWCNTs [28]. The absorption band at  $1629\text{ cm}^{-1}$  is due to the bending vibration of  $\text{-OH}$  group either in coordinated  $\text{H}_2\text{O}$  or  $\text{Ti-OH}$  bonding. The broad peak from  $3500\text{--}2900\text{ cm}^{-1}$  corresponds to the stretching vibrations of surface adsorbed  $\text{-OH}$  groups, and the broad band in the range from  $400\text{--}900\text{ cm}^{-1}$  with peaks at  $475\text{ cm}^{-1}$ ,  $590\text{ cm}^{-1}$ ,  $645\text{ cm}^{-1}$  confirming  $\text{O-Ti-O}$  bonding of anatase  $\text{TiO}_2$  [29]. The synthesized NCs clearly show the characteristics bands of  $\text{TiO}_2$  NPs without characteristics bands of MWCNTs due to its low content in all NCs.

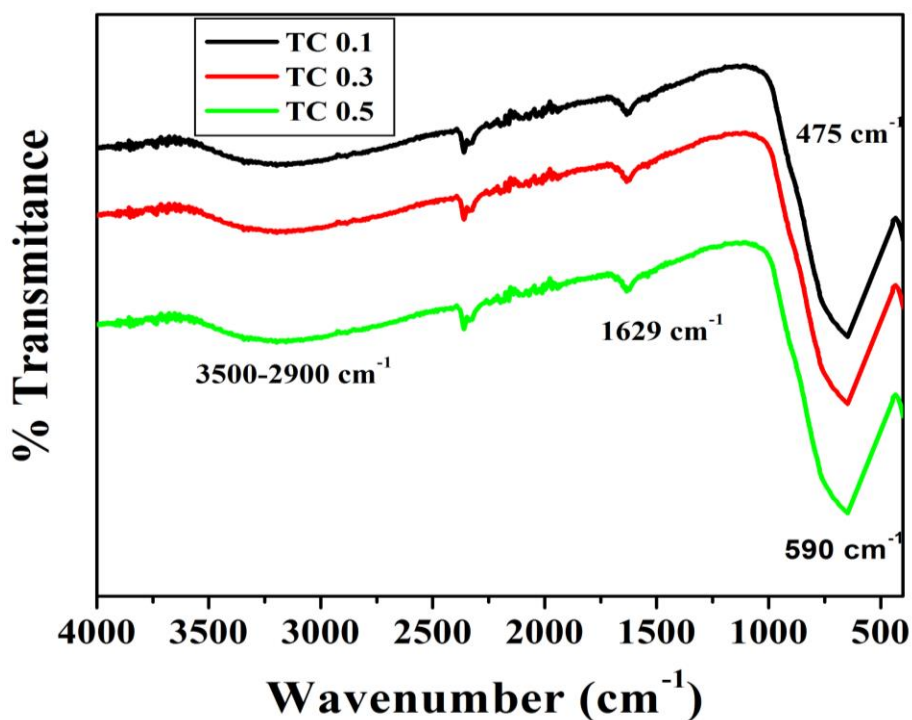


Fig. 5.8. (b) FTIR spectra of TC NCs

#### 5.4.3 Raman spectroscopy

Raman spectrum of pristine MWCNTs is shown in Fig. 5.9 (a). The two peaks at 1286  $\text{cm}^{-1}$  (D-band) and 1589  $\text{cm}^{-1}$  (G band) are correspond to MWCNTs [23]. Fig. 5. 9. (b) shows the Raman spectra of TC NCs consists of; five peaks from this three peaks at 396  $\text{cm}^{-1}$ , 518  $\text{cm}^{-1}$  and 638  $\text{cm}^{-1}$  are associated with  $\text{TiO}_2$  NPs [30, 31] and reaming two peaks at 1286  $\text{cm}^{-1}$  (D-band) and 1589  $\text{cm}^{-1}$  (G band) are correspond to MWCNTs. TC NCs are shows same peak position as observed in pristine MWCNTs. This confirms the formation of nanocomposite between  $\text{TiO}_2$  NPs and MWCNTs.

However, the peaks corresponds to  $\text{TiO}_2$  NPs exactly matches with anatase phase of  $\text{TiO}_2$  NPs. This confirms the presence of anatase phase of  $\text{TiO}_2$  NPs in the all TC NCs; without rutile or other phases.

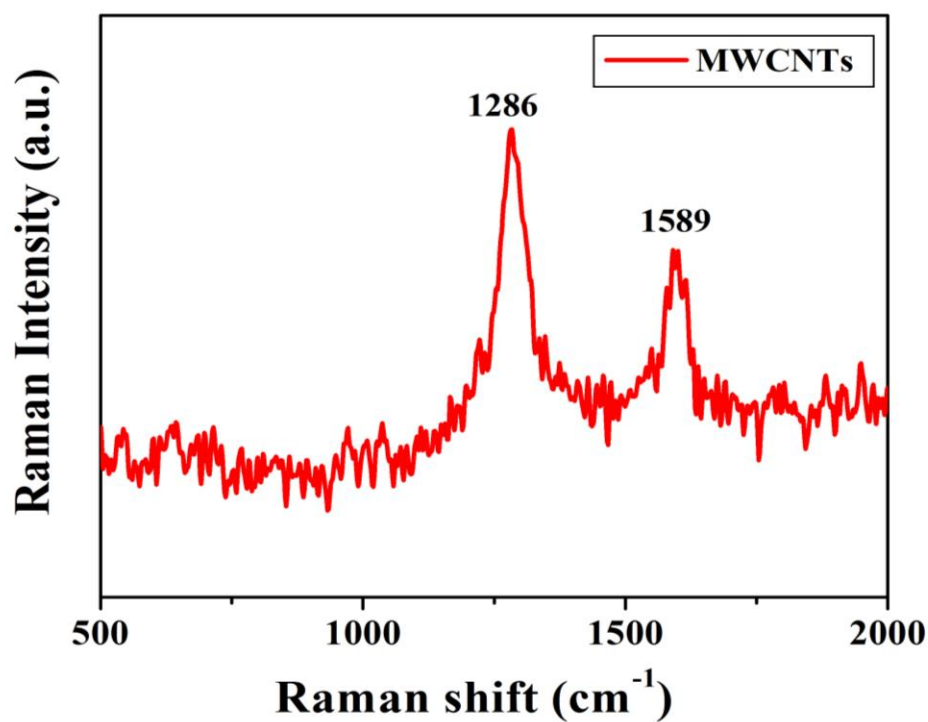


Fig. 5.9. (a) Raman Spectrum of MWCNTs

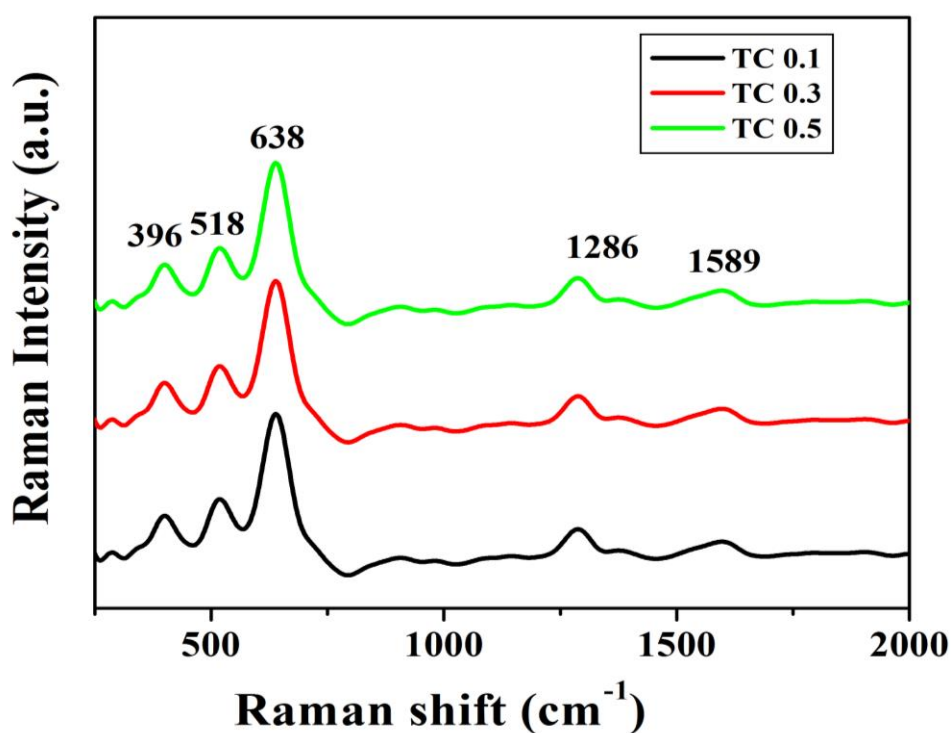


Fig. 5.9. (b) Raman spectra of TC NCs

#### 5.4.4 Photoluminescence spectroscopy (PL)

Fig. 5.10 shows the PL emission spectra of TC NCs at excitation wavelength 285 nm at room temperature. The spectra show two emission peaks at 412 nm and 478 nm; due to free exciton emission of  $\text{TiO}_2$  and the surface Ti–OH bonds, respectively [32, 33]. In addition, the intensity of these peaks in NCs is significantly decreases as compared to PL Intensity of Pure  $\text{TiO}_2$  NPs (Fig. 5.4) with increasing MWCNTs contents. This reveals that the decrease in the rate of electron-hole pair recombination in NCs with increasing amount of MWCNTs up to 0.5 wt. % in TC 0.5 NCs [34].

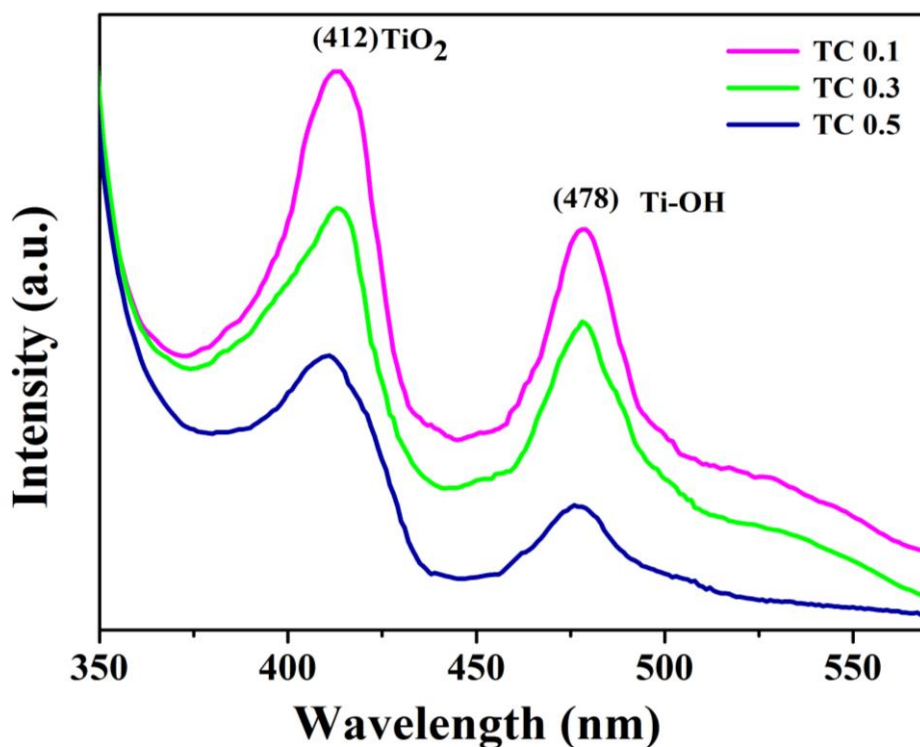


Fig. 5.10 PL Spectra of TC NCs



### 5.4.5 X-ray photoelectron spectroscopy

The qualitative information regarding chemical bonding of TC 0.5 NCs was determined by XPS analysis. Fig. 5.11 (a) shows the survey spectrum for TC 0.5 NCs, XPS spectrum for Ti 2p configuration of TC 0.5 NCs shown in Fig. 5.11.(b). which shows two peaks at 459.37 eV (Ti 2p<sub>3/2</sub>) and 465.22 eV (Ti 2p<sub>1/2</sub>) indicates that Ti element exists in Ti<sup>4+</sup> state [20, 21]. XPS spectrum for O1s configuration shown in Fig.5.11 (c). The three peaks at 529 eV, 531 eV, and 532 eV have been observed, which are attributed to Ti-O-Ti (lattice O), C=O (and COO), and Ti-OH, species, respectively [35, 36]. XPS spectrum for C content in TC 0.5 NCs is shown in Fig.5.11. (d) C 1s configuration was not shows peak at 281 eV for Ti-C bond [37], this observation reveals that the chemical environments for Ti and O are not changed, strongly, it confirms the carbon atom does not directly enter into bulk TiO<sub>2</sub> lattice [38]. MWCNTs shows a most intense peak at 284 eV for graphitic C=C bonds. There was also two other peaks with binding energies located at 285 eV and 288 eV; which correspond to C-C, and O-C=O bonds, these chemical bonds were present in TC NCs due to functionalized form of MWCNTs [39]. In synthesized TC NCs, TiO<sub>2</sub> NPs grafted onto the MWCNTs surface by C-O-Ti bond with such structure preferring the desired charge transfer upon light excitation and C-O-Ti bond extends the light absorption to longer wavelengths [38].

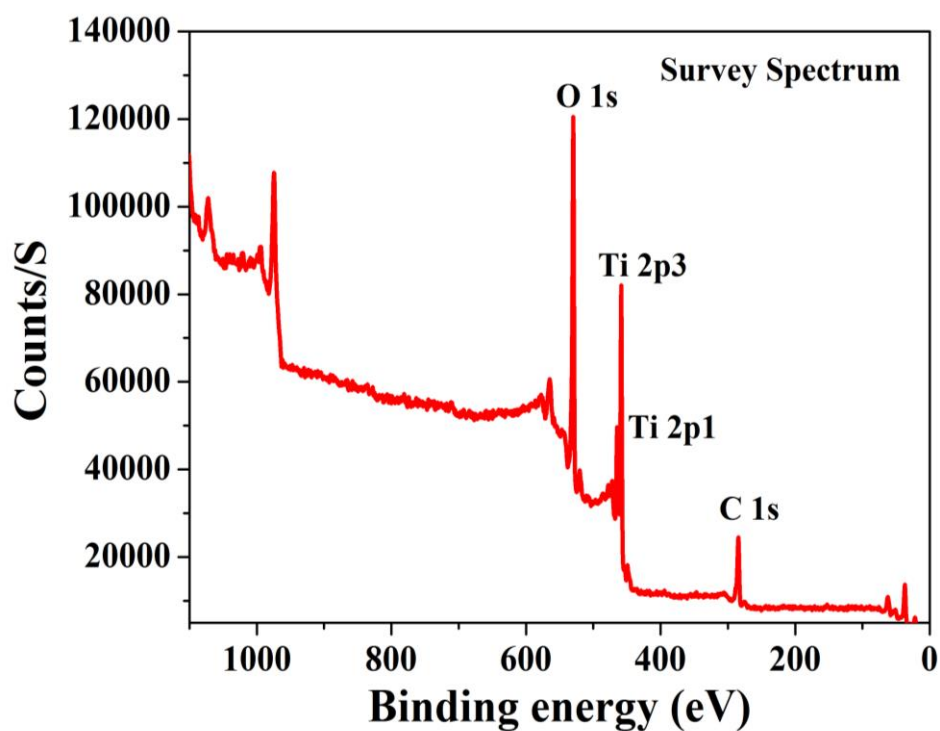


Fig. 5.11. (a) Survey spectrum of TC NCs

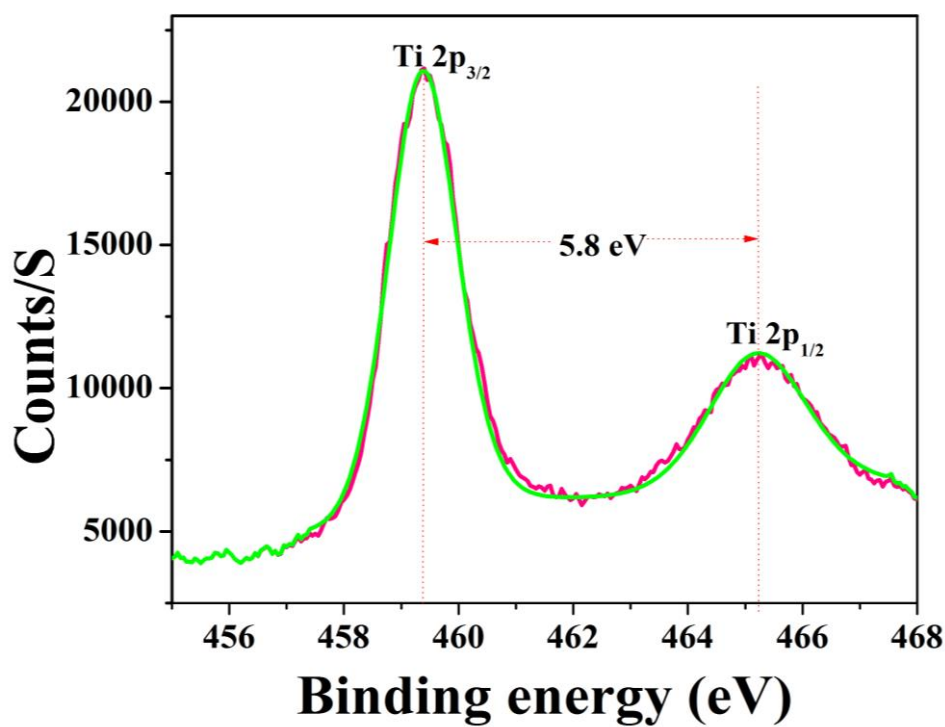


Fig. 5.11. (b) Ti2p configuration of TC NCs

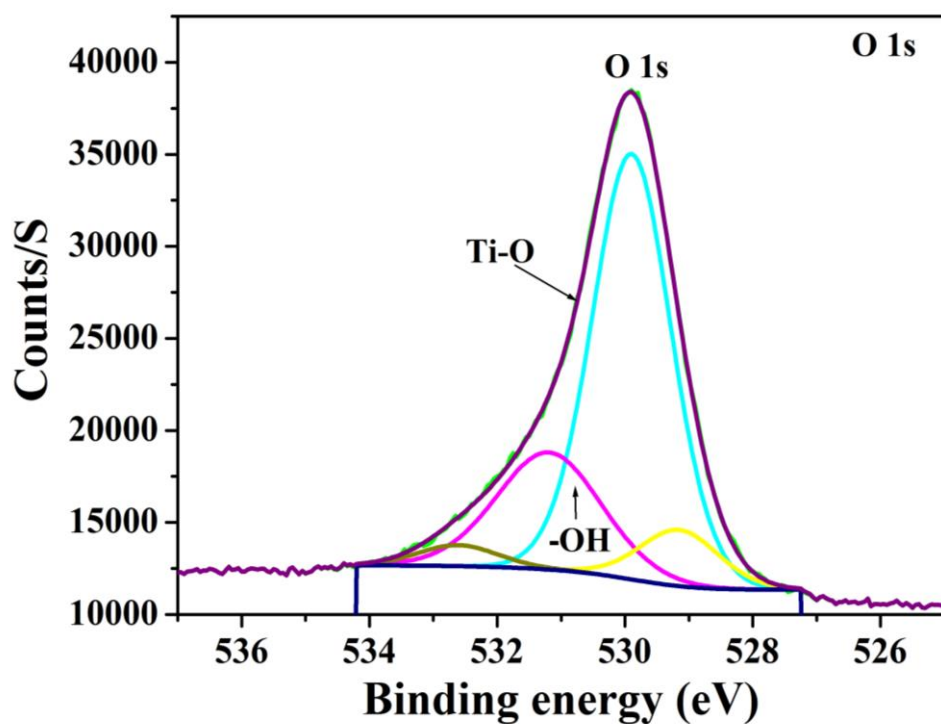


Fig. 5.11. (c) O 1s configuration of TC NCs

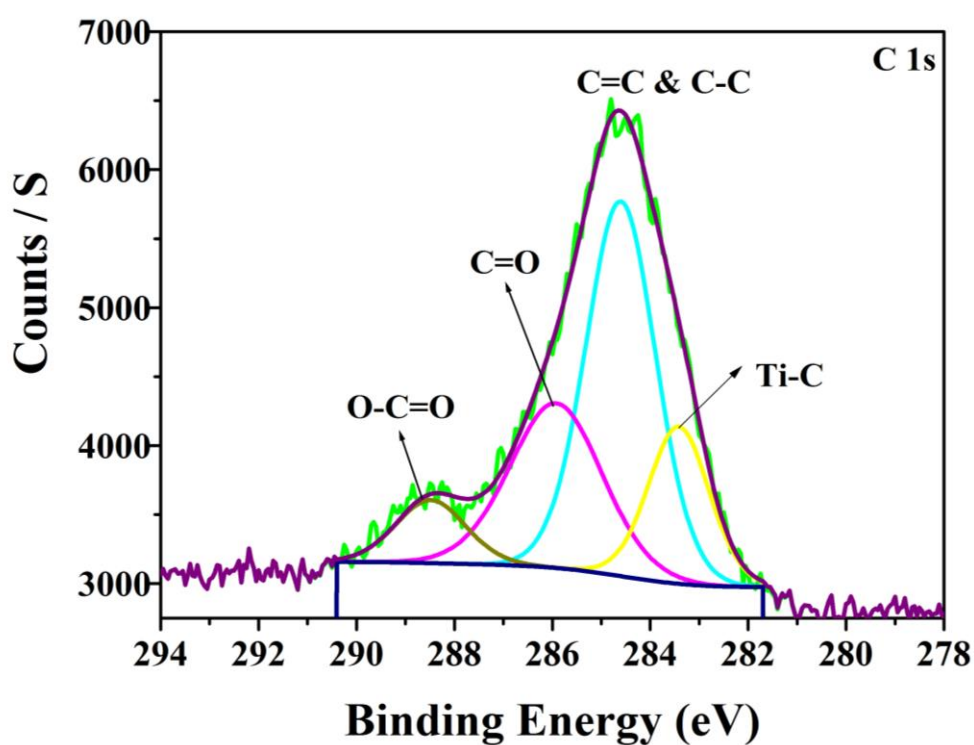
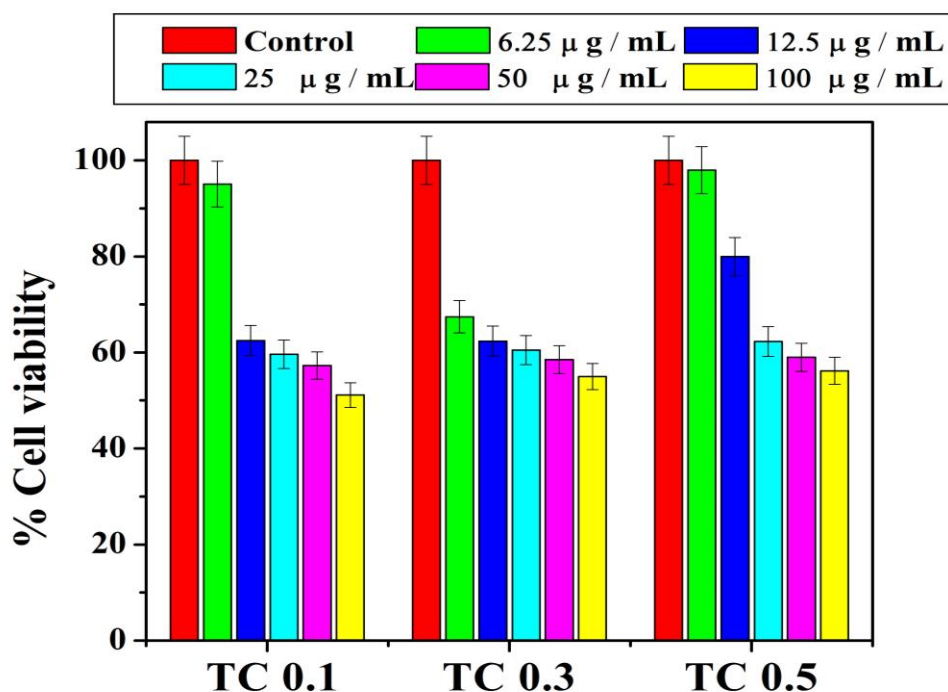


Fig. 5.11. (d) C 1s configuration of TC NCs

### 5.5 Toxicology study of TC NCs.

To study the cytotoxicity of TC NCs the similar standard experimental procedure was used. Cytotoxicity of the representative TC NCs was tested in Mouse embryonal fibroblast NIH 3T3 cells lines. Fig. 5.12 shows the cell viability of various NCs for their varying range of concentrations (mean  $\pm$  S.E. for  $n=3$ ); and the relative cell viability (%) compared with control well containing cells without TC NCs is calculated by the equation (5.3).

Fig. 5.12 shows increase in cytotoxicity for all NCs with their concentrations ranges from 6.25  $\mu\text{g/mL}$  to 100  $\mu\text{g/mL}$ . However, the cytotoxicity effect was lower towards fibroblast *NIH 3T3* cells lines against TC 0.5 sample as compared to other NCs or Pure  $\text{TiO}_2$  NPs. This reveals that TC0.5 sample is more biocompatible as compared to others [39][40].



**Fig. 5.12 Cell viability studies of TC NCs with varying concentrations against Mouse embryonal fibroblast *NIH 3T3* cells lines**

### 5.6 Conclusions

This chapter deals with effect of MWCNTs content on photo-catalytic properties of  $\text{TiO}_2$  NPs. UV-vis DRS analysis confirmed that TC NCs possessed stronger absorption bands in the visible range of 400–800 nm compared to pure  $\text{TiO}_2$  NPs. As the concentration of MWCNTs increase in TC NCs, the band gap decreases from 3.2 to 2.6 eV. The prepared TC NCs were active under visible light due to the tunable optical band gap with efficient charge transfer. FTIR data revealed that the -COOH groups open up on the surface of MWCNTs under acid treatments and the resulting TC NCs was formed through -COOH groups. Raman analysis confirmed the presence of anatase phase only of  $\text{TiO}_2$  NPs as well as TC NCs. PL study interprets the decrease in intensity of PL emission peaks with concentration of MWCNTs with reduction in recombination rate of electron-hole pair for increase in the rate of photocatalytic activity. XPS study of  $\text{TiO}_2$  NPs and TC NCs, confirms the elemental composition of  $\text{TiO}_2$  NPs and TC NCs as Ti present  $\text{Ti}^{+4}$  with no doping of C in  $\text{TiO}_2$  host lattice. Cytotoxicity study shows the TC 0.5 NCs is more biocompatible to cell line as compared pure  $\text{TiO}_2$  NPs and TC NCs.

---

### Reference

- [1] A. Kyaw, H. Tantang, T. Wu, L. Ke, C. Peh, Z. Huang, X. Zeng, H. Demir, Q. Zhang, and X. Sun, *Appl. Phys. Lett.* 99 (2011) 021107.
- [2] R. Naira, A. Dasa, S. Paulb, B. Rajbongshib, and S. Samdarshic. *J Alloys Compd.* 695 (2017) 3511.
- [3] M. Dahl, Y. Liu, and Y. Yin, *Chem. Rev.* 114 (2014) 9853.
- [4] F. J. Zhang, M. L. Chen, and W. C. Oh, *Korean J. of Mater. Res.* 18 (2008) 583.
- [5] C. H. Wei and C. M. Chang, *Mater. Trans.* 52 (2011) 554.
- [6] S. D. Delekar, H. M. Yadav, S. N. Achary, S. S. Meena, and S. H. Pawar, *Appl. Surf. Sci.* 263 (2012) 536.
- [7] H. M. Yadav, S. V. Otari, R. A. Bohara, S. S. Mali, S. H. Pawar, and S. D. Delekar, *J. Photochem. Photobiol. A* 294 (2014) 130.
- [8] K. Nagaveni, M. Hegde, N. Ravishankar, G. Subbanna, and G. Madras, *Langmuir* 20 (2004) 2900.
- [9] T. Lopez, J. Moreno, R. Gomez, X. Bokhimi, J. Wang, H. Yee-Madeira, G. Pecchi, and P. Reyes, *J. Mater. Chem.* 12 (2002) 714.
- [10] K. Bhattacharyya, S. Varma, A. Tripathi, S. Bharadwaj, and A. Tyagi, *J. Phys. Chem. C* 112 (2008) 19102.
- [11] G. d. A. Soler-Illia, A. Louis, and C. Sanchez, *Chem. Mater.* 14 (2002) 750.
- [12] V. B. Koli, A. G. Dhodamani, K.V. More, S. F.A. Acquahc, D.K. Panda, S. H. Pawar, S. D. Delekar, *Sol. Energy* 149 (2017) 188.
- [13] S. Liu, J. Yu, and S. Mann, *J. Phys. Chem. C* 113 (2009) 10712.
- [14] J. G. Yu, H. G. Yu, B. Cheng, X. J. Zhao, J. C. Yu, and W. K. Ho, *J. Phys. Chem. B* 107 (2003) 13871.
- [15] F. Li and X. Li, *Chemosphere* 48 (2002) 1103.
- [16] M. Yang, C. Hume, S. Lee, Y.H. Son, and J. K. Lee, *J. Phys. Chem. C* 114 (2010) 15292.

- 
- [17] Y. F. Li, D. Xu, J. I. Oh, W. Shen, X. Li, and Y. Yu, *Acs Cata.* 2 (2012) (391).
- [18] O. Akhavan, E. Ghaderi, and K. Rahimi, *J. Mater. Chem.* 22 (2012) 23260.
- [19] F. Li and X. Li, *Appl. Cata. A* 228 (2002) 15.
- [20] D. Gu, Y. Lu, and B. Yang, *Chem. Comm.* (2008) 2453.
- [21] C. Su, L. Liu, M. Zhang, Y. Zhang, and C. Shao, *Cryst. Eng. Comm.* 14 (2012) 3989.
- [22] X. Yan, B. K. Tay, and Y. Yang, *J. Phys. Chem. B* 110 (2006) 25844.
- [23] V. B. Koli, A. G. Dhodamani, A. V. Raut, N. D. Thorat, S. H. Pawar, and S. D. Delekar, *J. Photochem. Photobiol. A* 328 (2016) 50.
- [24] B. Reti, K. Mogyorósi, A. Dombi, and K. Hernadi, *Appl.Cata. A* 469 (2014) 153.
- [25] J. Yu, T. Ma, and S. Liu, *Phys. Chem. Chem. Phys.* 13 (2011) 3491.
- [26] S. S. Mali, C. A. Betty, P. N. Bhosale, and P. Patil, *ECS J. Solid State Sci. Technol.* 1 (2012) M15.
- [27] O. Akhavan, R. Azimirad, S. Safa, and M. Larijani, *J. of Mater. Chem.* 20 (2010) 7386.
- [28] K. R. Reddy, B. C. Sin, K. S. Ryu, J.-C. Kim, H. Chung, and Y. Lee, *Synth. Met.* 159 (2009) 595.
- [29] G. Hu, X. Meng, X. Feng, Y. Ding, S. Zhang, and M. Yang, *J. Mater. Sci.* 42 (2007) 7162.
- [30] J. Yu, J. Fan, and B. Cheng, *J. Power Sources* 196 (2011) 7891.
- [31] T. Sawatsuk, A. Chindaduang, C. Sae-Kung, S. Pratontep, and G. Tumcharern, *Diamond and Relat. Mater.* 18 (2009) 524.
- [32] O. Akhavan and E. Ghaderi, *Nanoscale* 5 (2013) 10316.
- [33] O. Akhavan and E. Ghaderi, *J. Mater. Chem. B* 1 (2013) 6291.
- [34] V. B. Koli, S. D. Delekar and S. H. Pawar, *Mater Sci: Mater Med* 27 (2016) 177.
-

- [35] E. Papirer, R. Lacroix, J.B. Donnet, G. Nansé, and P. Fioux, Carbon 33 (1995) 63.
- [36] W. Ren, Z. Ai, F. Jia, L. Zhang, X. Fan, and Z. Zou, Appl. Cata. B 69 (2007) 138.
- [37] S. Sreekantan, K. A. Saharudin, Z. Lockman, and T. W. Tzu, Nanotechnology 21 (2010) 365603.
- [38] D. Zhao, G. Sheng, C. Chen, and X. Wang, Appl. Cata.B 111 (2012) 303.
- [39] K. Cendrowski, M. Jedrzejczak, M. Peruzynska, A. Dybus, M. Drozdik, and E. Mijowska, Jo.Alloys Compd. 605 (2014) 173.
- [40] L. Yan, G. Li, S. Zhang, F. Sun, X. Huang, Q. Zhang, L. Dai, F. Lu, and Y. Liu, Chin. Sci. Bull.58 (2013) 2347.



# Chapter 6

## Photocatalytic inactivation of bacteria

Journal of Photochemistry and Photobiology A: Chemistry 328 (2016) 50–58



Contents lists available at ScienceDirect  
Journal of Photochemistry and Photobiology A:  
Chemistry

journal homepage: [www.elsevier.com/locate/jphotochem](http://www.elsevier.com/locate/jphotochem)



### Visible light photo-induced antibacterial activity of TiO<sub>2</sub>-MWCNTs nanocomposites with varying the contents of MWCNTs



Valmiki B. Koli<sup>a,b</sup>, Ananta G. Dhodamani<sup>b</sup>, Abhinav V. Raut<sup>a</sup>, Nanasahab D. Thorat<sup>c</sup>, Shivaji H. Pawar<sup>a</sup>, Sagar D. Delekar<sup>a,b,d,\*</sup>

<sup>a</sup>Center for Interdisciplinary Research, D.Y. Patil University, Kolhapur 416 006, India

<sup>b</sup>Department of Chemistry, Shivaji University, Kolhapur 416 004, India

<sup>c</sup>Department of Physics and Energy, University of Limerick, Limerick, Ireland

<sup>d</sup>Department of Chemistry and Biochemistry, Florida State University, Tallahassee 32306-4390, United States

Journal of Photochemistry and Photobiology A: Chemistry 333 (2017) 40–48



Contents lists available at ScienceDirect  
Journal of Photochemistry and Photobiology A:  
Chemistry

journal homepage: [www.elsevier.com/locate/jphotochem](http://www.elsevier.com/locate/jphotochem)



### *In situ* sol-gel synthesis of anatase TiO<sub>2</sub>-MWCNTs nanocomposites and their photocatalytic applications



Valmiki B. Koli<sup>a</sup>, Ananta G. Dhodamani<sup>b</sup>, Sagar D. Delekar<sup>a,b,\*</sup>, Shivaji H. Pawar<sup>a,\*</sup>

<sup>a</sup>Center for Interdisciplinary Research, D.Y. Patil University, Kolhapur 416 006, India

<sup>b</sup>Department of Chemistry, Shivaji University, Kolhapur 416 004, India



---

### 6.1 Introduction

Human beings are continuously suffering with infection from micro-organism and hence can lead to several serious problems [1]. Antibacterial agents are extensively used to kill bacteria in a wide variety of domestic and healthcare settings and hence they play a vital role in controlling infection [2, 3]. In recent years, nanomaterials, like  $\text{TiO}_2$  NPs, have been attracted as an antibacterial agent, due to their strong oxidizing power, high photo-stability and low toxicity [4-6]. However,  $\text{TiO}_2$  NPs are active under ultraviolet (UV) light due to its wide band gap energy ( $\sim 3.2$  eV) [7]. Initially, the antibacterial activity of  $\text{TiO}_2/\text{Pt}$  powder under a near-UV light irradiation was reported by Matsunaga et al. for killing of microbial cells in water [8]. Afterward, considerable research has been continued for the enhancement of antibacterial performance of  $\text{TiO}_2$ -based photocatalyst [9]. It is of our interest to find a  $\text{TiO}_2$ -based photocatalyst; which is sensitive to visible light in order to make efficient antibacterial agents for potential applications in our living environments. Fortunately, it has been demonstrated that the photocatalytic efficiency of  $\text{TiO}_2$  NPs in the visible light absorption can be effectively improved by various modifications such as metal/non-metal doping, formation of NCs [10, 11]. The NCs with carbon nanostructures, specially multi-walled carbon nano-tubes (MWCNTs) found to tune the optical band gap of  $\text{TiO}_2$  into the visible region very effective and improve its photoactivity [12, 13]. In general, MWCNTs in NCs plays dominant role in photo-inactivation of bacteria. Overall, MWCNTs is not only providing a large surface area to support  $\text{TiO}_2$  catalyst; but also stabilizing the charge separation by trapping the electrons transferred from  $\text{TiO}_2$ , thereby hindering the charge recombination. Therefore, the photogenerated electrons are transferred from  $\text{TiO}_2$  to the MWCNTs with the decrease in recombination-rate of charge carriers; which enhances the oxidative reactivity of particles in contact with bacteria to the damage of its cell walls [14].

When TiO<sub>2</sub> NPs was decorated on the surface of MWCNTs, the particles were well dispersed and hence would have the large specific surface area to bind bacteria effectively. Also, in presence of light, the electron-hole pair recombination rate was diminished at the interfaces of TiO<sub>2</sub>-MWCNTs (TC NCs), which resulting the superior activity as compared to bare particles. [14, 15]. The activity of NCs is also enhanced due to the formation of even more reactive oxygen species, like hydroxyl and other radicals.

These NCs are regularly known materials for degradation of various contaminants [16, 17], oxidative reactions [18]. These are also used in sensitized solar cells [19] and water splitting fuel cells [20, 21]. In all these investigations, these are actively tested under UV-lamp irradiation to enhance their activity. As concerned to their antibacterial studies, few reports have been found in the literatures. Akhavan et al. [9] reported the visible light photo-inactivation of bacteria using CNT-doped TiO<sub>2</sub> thin films formed by a dip-coating method. This study is limited to Gram-negative bacteria *Escherichia coli* (*E. coli*) as well. Also, the stability of thin films as well as the vast diversity in morphology of thin films, formed by dip coatings, are the major ambiguity of this work; which indirectly hamper the antibacterial performance. Bose et al. reported a unique method for the incorporation of various nanostructures such as TiO<sub>2</sub> decorated CNTs, Ag-decorated TiO<sub>2</sub> and Ag@TiO<sub>2</sub> decorated CNTs into PVDF/ PMMA (poly (vinylidene fluoride)/poly(methyl methacrylate)) blends in membrane forms to test the antimicrobial activity [21]. Also, investigators have claimed that, due to well electron-hole separation and high specific interfacial area, this composite may gain quicker entry into cells and thereby promote photo-oxidation of critical cellular components [22]. The increase in the *E. coli* bacterial colonies was reported for hybrid materials due to synergistic effects of combined constituents but polymer blending may not results in the effective killing of bacteria. Akhavan et al. [23] reported the formation of titania/carbon nanotube heterojunction arrays on the Si substrate

by using plasma enhanced chemical vapor deposition at 650 °C for photo-inactivation of *E. coli* in visible light irradiation. This chapter is focused on the testing antibacterial activity of TiO<sub>2</sub> NPs and TC NCs against gram positive bacteria *staphylococcus aureus* (*S. aureus*) and *Bacillus* (*B. subtilis*) and gram negative bacteria *Escherichia coli* (*E. coli*) and *Pseudomonas aeruginosa* (*P. aeruginosa*) in different conditions such as dark, UV light and visible light irradiation.

### 6.2 Experimental details

#### 6.2.1 Materials

Required chemicals such as nutrient agar, bacterial agar, distilled water, saline solution and bacterial stains etc.

#### 6.2.2 Photocatalytic bactericidal activity

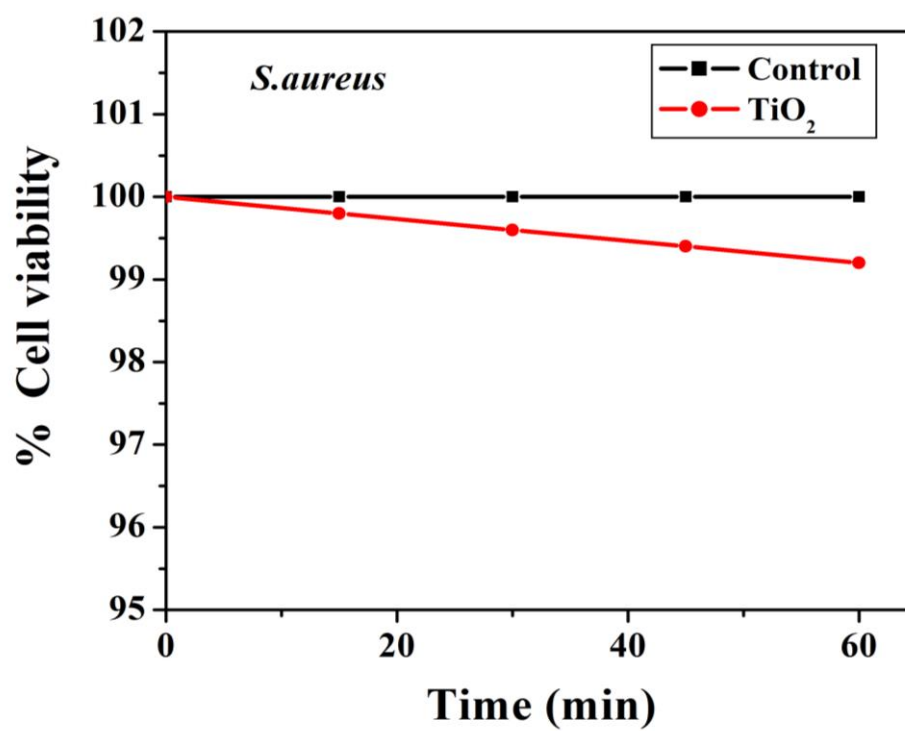
The antibacterial activity of TiO<sub>2</sub> NPs and TC NCs against common pathogenic bacteria was carried out in a systematic way. The bacteria such as *S. aureus* NCIM 2654 and *B. subtilis* NCIM-2712 (Gram-positive) and *E.coli* NCIM 2066 and *P. aeruginosa* NCIM-2036 (Gram-negative) were purchased from NCIM (National Collection of Industrial Microorganisms), National Chemical Laboratory (NCL), Pune, India. Before carrying out microbial evolutions, all samples and glassware were sterilized by autoclaving at 120 °C for 20 min. In all antibacterial experiments, a suspension of each bacterial species having concentration of  $1 \times 10^{-8}$  cfu/mL was used. The bactericidal testing was carried out in a multi lamp borosilicate glass reactor with eight fluorescent tubes (Philips make, 8 W,  $\lambda > 400$  nm, light intensity  $5 \text{ mW cm}^{-2}$ ) [11]. To study photo-inactivation of bacteria, 1 mg of TiO<sub>2</sub> NPs or TC NCs photocatalyst was stirred with a bacterial suspension in saline solution (5 mL, 0.9 % NaCl at pH 7.0) and irradiated to visible light in a photo-reactor. From this, 100  $\mu\text{L}$  of suspension was taken with regular time intervals and spread on

freshly prepared Mueller-Hinton agar plates. These plates were incubated at 37 °C for 24 h. The standard plate count method was used to determine viable number of cells as cfu/mL<sup>-1</sup>. A similar experiment was conducted for TiO<sub>2</sub> NPs with UV light irradiations (Philips make, 8 W,  $\lambda=365$  nm). A dark experiment was performed similarly with photocatalyst without light irradiations for all samples. Control runs were also carried out under the same irradiation conditions without photocatalyst. The attempts were made for getting the effective antibacterial properties of NCs through the optimization of various parameters. All antibacterial experiments were done under sterile conditions.

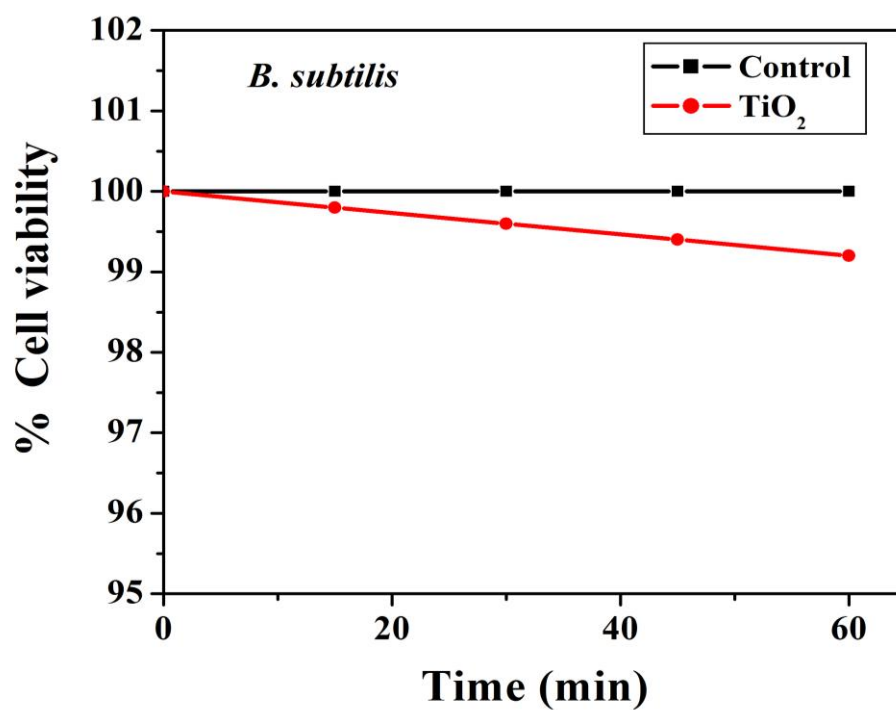
### 6.3 Effect of TiO<sub>2</sub> nanoparticles on photo-inactivation of bacteria

#### 6.3.1. Under dark condition

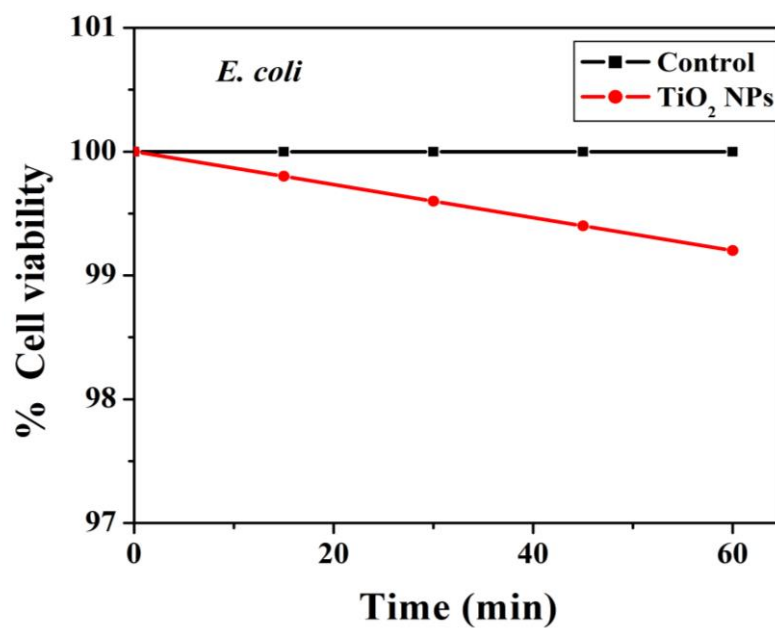
For dark condition experiment, Gram-positive such as *S. aureus*, *B. subtilis* and Gram-negative such as *E. coli*, *P. aeruginosa* species was used to perform experiment. The experiment was carried out for 1 h. in dark condition with constant stirring. After that the inoculum spared in petri plates and kept in incubator for 24 h at 37 °C. The effect of TiO<sub>2</sub> NPs on photocatalytic bacterial inactivation is shown in Fig. 6.1. (a) to (d). The bacterial growth was the same as at the beginning of the experiment. The cell survival of TiO<sub>2</sub> NPs treated cells was determined by CFU counting after 24 h of incubate. It showed that, the inactivation of bacterial cells with NPs under dark condition did not occur. Significantly less than 1-2% bacteria get killed in the experiment, this may be due to stirring with NPs.



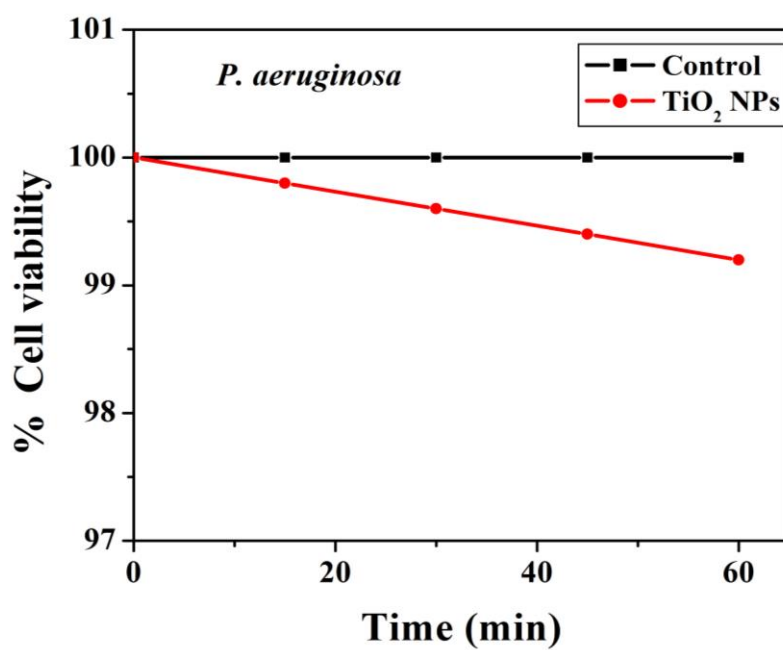
(a)



(b)



(c)



(d)

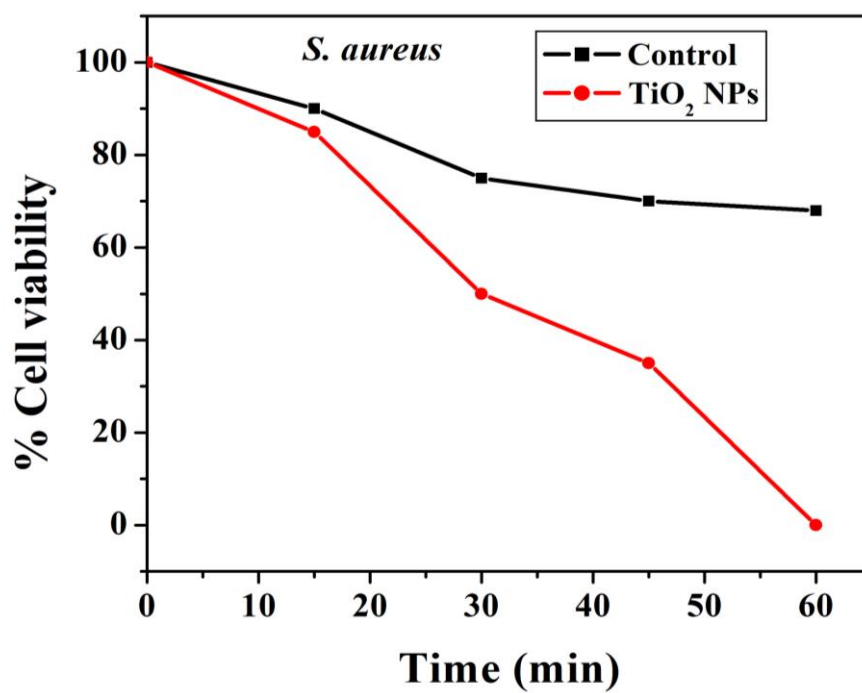
**Fig 6.1 Effect of TiO<sub>2</sub> NPs on photocatalytic inactivation of (a) *S. aureus* (b) *B. subtilis*, (c) *E. coli* and (d) *P. aeruginosa* under dark condition**



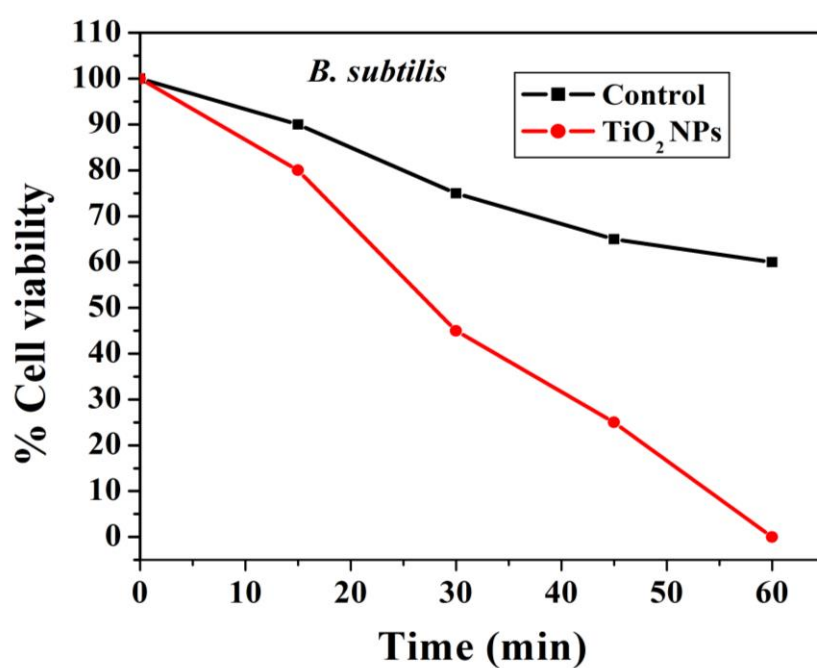
### 6.3.2. Under UV light irradiation

To determine the effect of UV light on the growth of the bacteria, bacterial suspension exposed to UV light without NPs (control). When bacteria were exposed to UV light, there was decrease in the number of viable cells up to certain extents only. In the UV light irradiation only, viable cell count was decreased up to 30% for *S. aureus* and 35% *B. subtilis* after 60 min exposure without TiO<sub>2</sub> NPs. While Gram-negative bacteria showing less than 20% killing of bacteria in presence of UV light alone for 1 h. The Gram-positive bacteria having high rate of photo-inactivation as compared due Gram-negative bacteria. This due to the cell wall nature of bacteria. Our results are in good agreement with some previous reports [24, 25]. The photo-inactivation of bacteria with TiO<sub>2</sub> was strongly enhanced in the presence of UV light radiations, followed to complete killing of bacteria within 1 h. A relatively high rate of bacterial inactivation was found when irradiated with UV-light in the presence of TiO<sub>2</sub> as compared to that of UV-light alone. This observed pattern for both Gram-positive as well as Gram-negative bacteria, and associated with the principle photocatalytic antibacterial activity of TiO<sub>2</sub> NPs as shown in Fig. 6.2.(a) to (d). It is usually known that the reactive oxygen species (ROS) generated in TiO<sub>2</sub> NPs during UV light irradiation and these are responsible for oxidative damage of cell membrane and further attack on internal cellular components ultimately results in cell death.

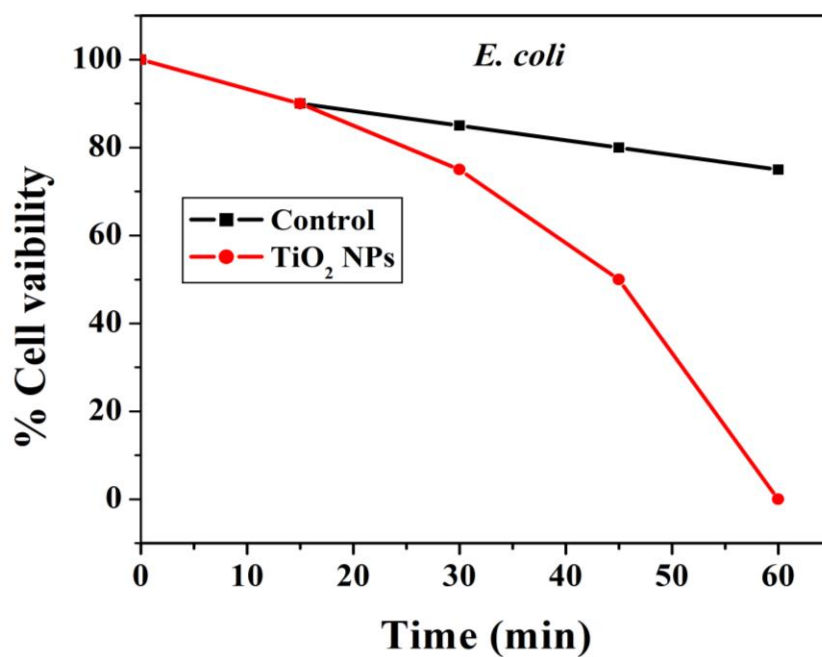
In present investigation UVA radiation we used and having wavelength in range of 350-400 nm. All types of UV-radiations such as UVA (400-320 nm), UVB (320-290 nm) and UVC (290-100) able to damage collagen fibers and thus accelerate aging of the skin [26]. In general, UVA is the least harmful, but can contribute to the aging of skin, DNA damage and possibly skin cancer. It penetrates deeply and does not cause sunburn [27, 28]. So, there is a strong need of the development of system which will excellently work in the visible region of electromagnetic spectrum of light.



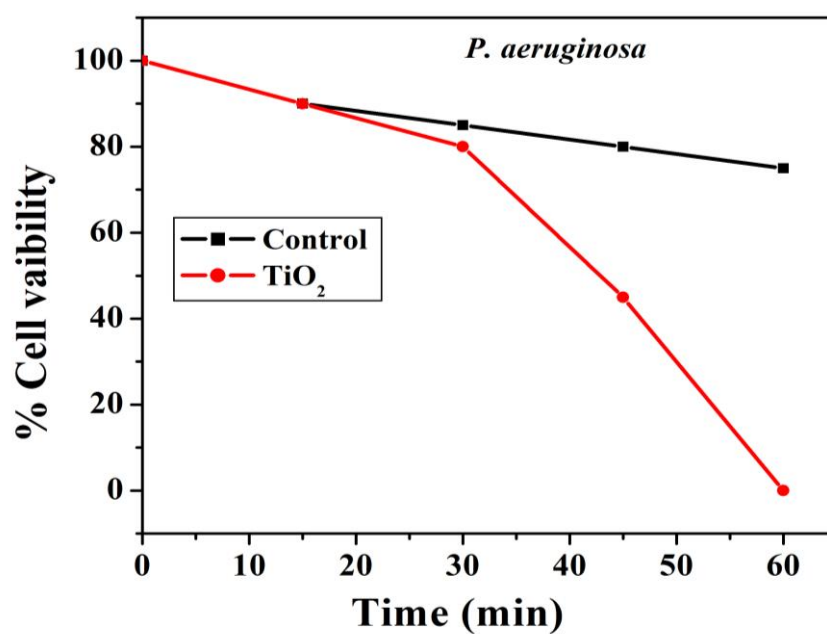
(a)



(b)



(c)



(d)

**Fig 6.2.** The effect of TiO<sub>2</sub> NPs on photocatalytic inactivation of (a) *S. aureus* (b) *B. subtilis*, (c) *E. coli* and (d) *P. aeruginosa* under UV light irradiation

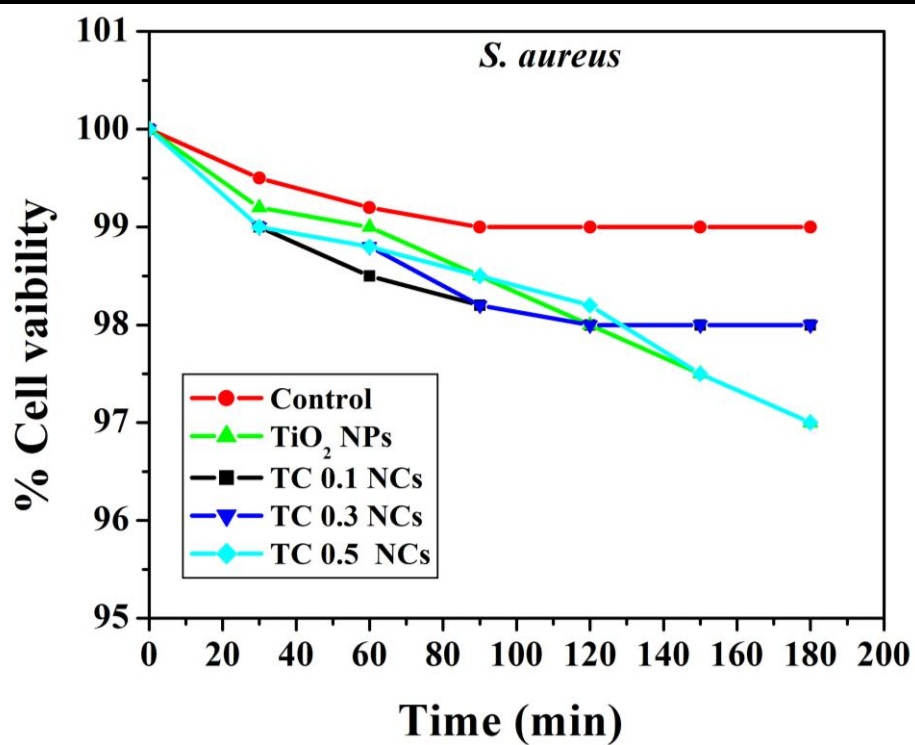
---

### 6.4 Effect of TiO<sub>2</sub> nanoparticles and TC nanocomposites on photo-inactivation of bacteria

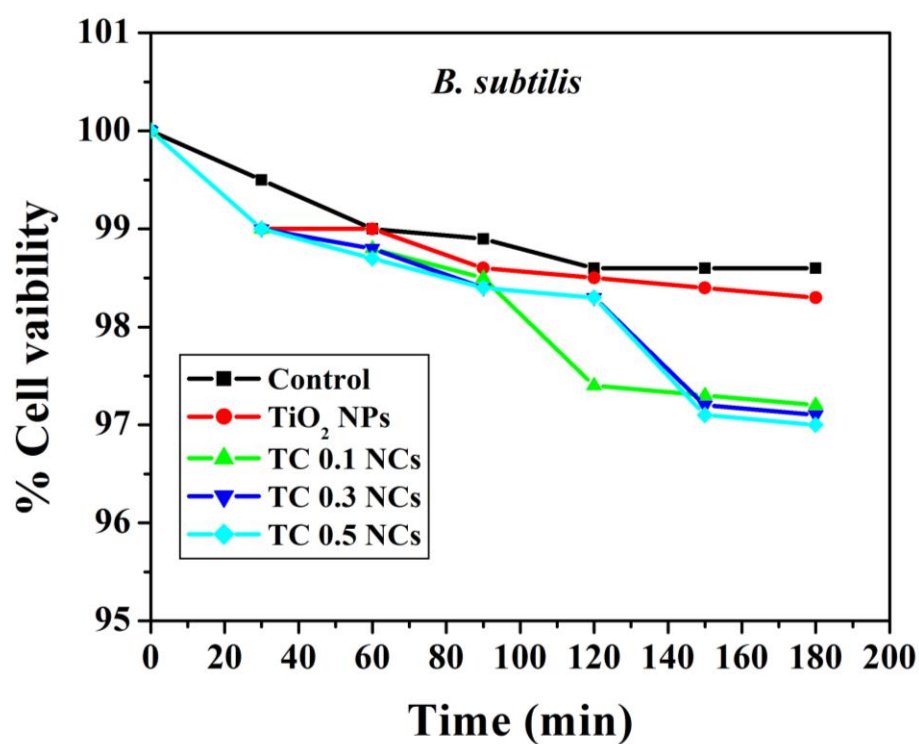
Similar experiment performed under visible light as mentioned experimental method.

#### 6.4.1. Under dark condition

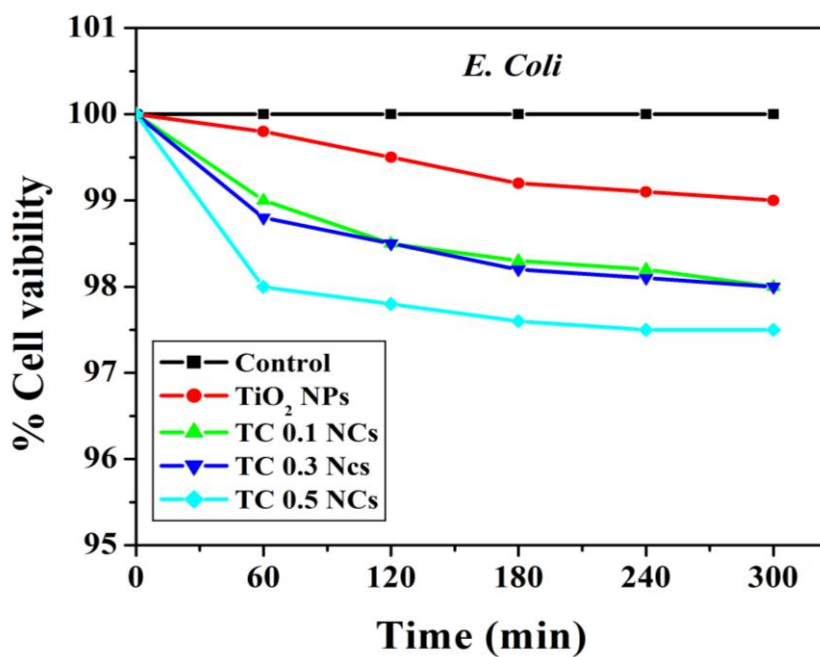
To study the effect of TC NCs on bacterial inactivation whole experiment carried out in dark with consistent stirring the earlier selected Gram-positive *S. aureus*, *B. subtilis* and Gram-negative *E. coli*, *P. aeruginosa* species were used to perform experiment. The experiment were carried out for 3 h for gram-positive bacteria and 5 h Gram-negative bacteria in dark condition with constant stirring. After that the inoculum spared in petri plates and kept in incubator for 24 h at 37°C. The observed results are shown in Fig. 6.3 (a) to (d). There is no inactivation of bacteria was observed. The cell survival of TC NCs treated cells was determined by CFU counting after 24 h of incubate. It showed that, the inactivation of bacterial cells with TC NCs under dark condition did not occur effectively. Less than 1-3% bacteria get killed in the experiment this may be due to stirring with TC NCs.



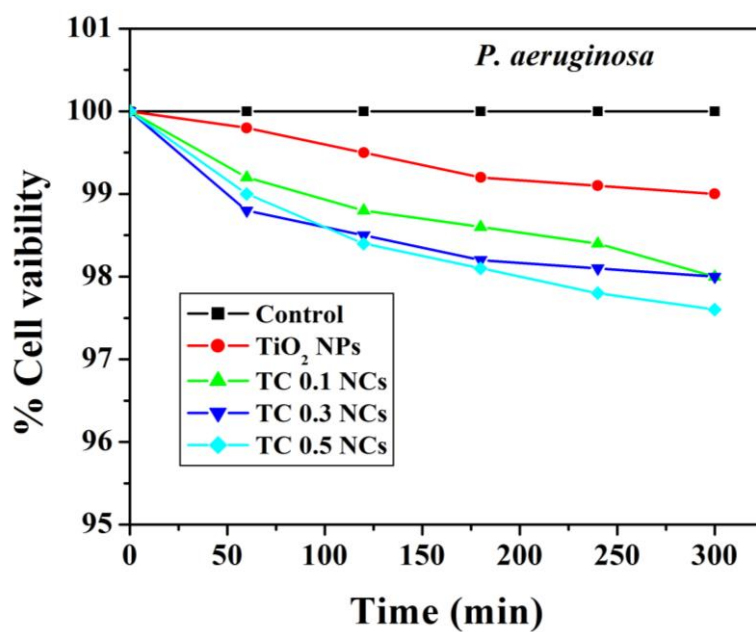
(a)



(b)



(c)



(d)

Fig. 6.3. The effect of TC NCs on photocatalytic inactivation of (a) *S. aureus* (b) *B. subtilis*, (c) *E. coli* and (d) *P. aeruginosa* under dark condition.

---

### 6.4.2. Under Visible light irradiation

To study the photocatalytic inactivation, the common pathogenic bacteria was treated with pure TiO<sub>2</sub> NPs as well as TC NCs under visible light. The experimental conditions were optimized for these samples in presence of visible light. In the dark experiment, the bacterial cell suspension with TC NCs or pure TiO<sub>2</sub> NPs were placed in the incubator; which did not show any bactericidal effect on microorganisms. In visible light irradiations with pure TiO<sub>2</sub> NPs, the bacterial growth was not inhibited. Our results are in good agreement with some previous reports [25, 29] Fig. 6.4.(a) shows percent survival of *S. aureus* under visible light irradiation in presence of TC NCs as a function of time. The visible light irradiation without TC NCs, no bacterial cell inactivation was observed. It clearly reveals that the light irradiation does not show any photocatalytic inactivation effect on the microorganisms in absence of TC NCs. Among various TC NCs, TC 0.5 NCs showed 100% inhibition for *S. aureus* within 180 min. under visible light irradiation as no colony grew on Muller-Hinton medium after 24 h of incubation. However, at 180 min., 80% and 90% inhibition was observed for TC 0.3 and TC 0.1 NCs, respectively [30]. Fig. 6.4 (b) shows the photographs of bactericidal effect on *S. aureus* with TC NCs under visible light exposure.

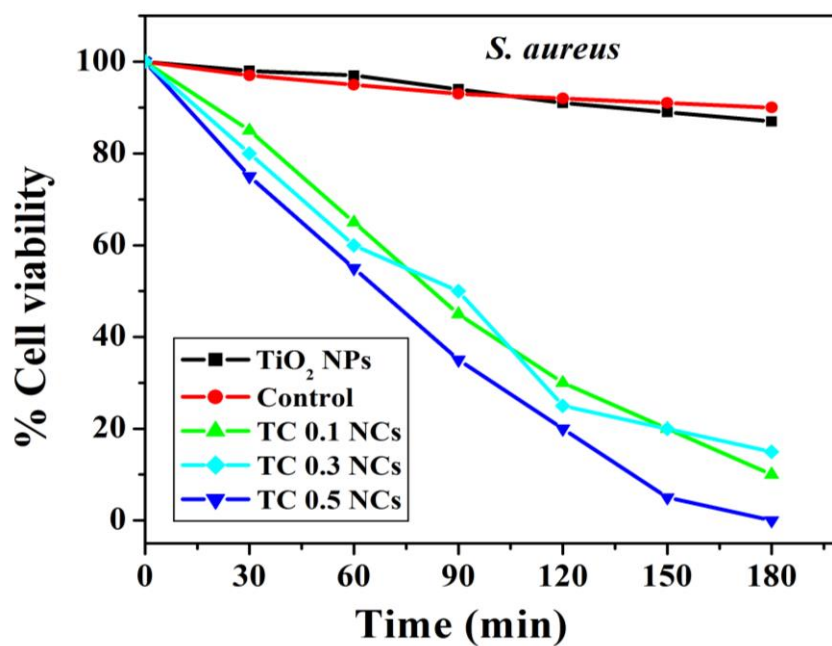


Fig. 6.4. (a) % survival of *S. aureus* with TC NCs samples as function of time.

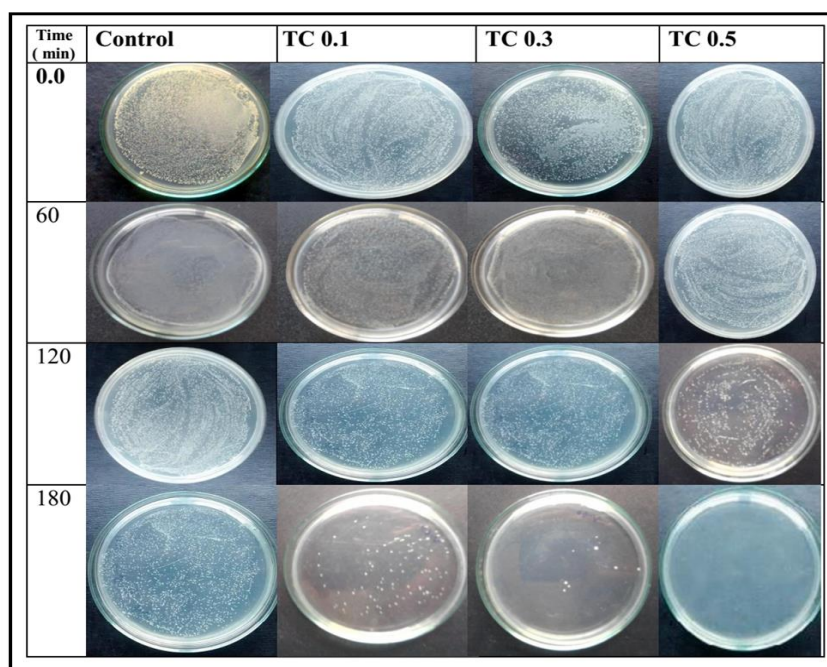
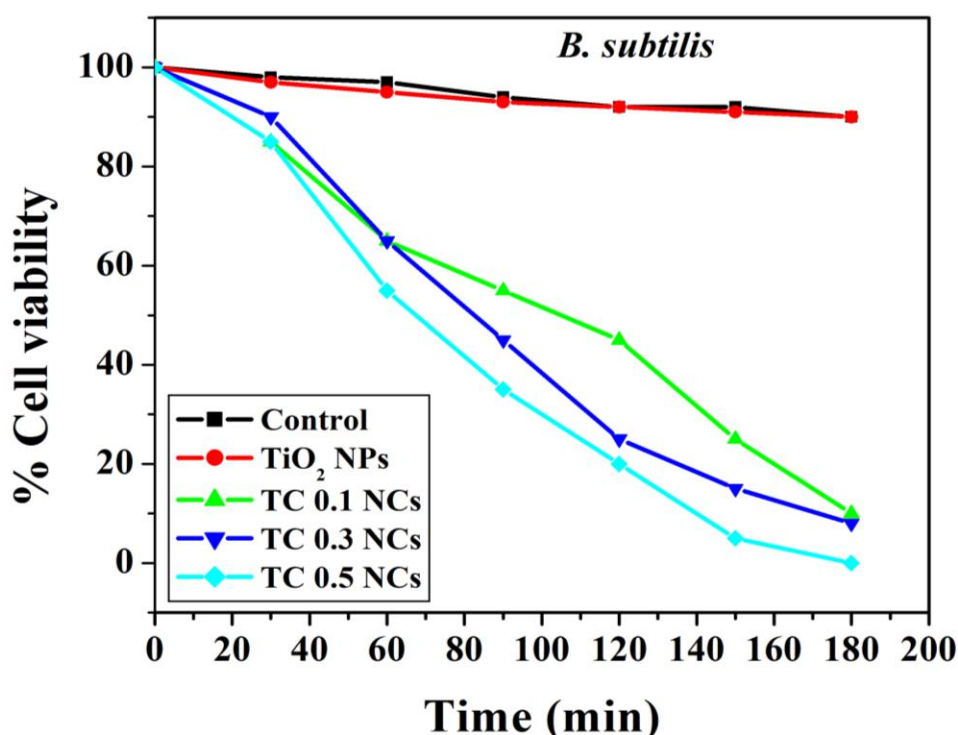


Fig. 6.4. (b) Photographs of antimicrobial effect on *S. aureus* with TC NCs under visible light exposure.



Fig. 6.4.(c) shows percent survival of *B. subtilis* under visible light irradiation in presence on TC NCs as a function of time. There is no effect of light on bacteria without TC NCs. It clearly reveals that the light irradiation does not show any photocatalytic inactivation effect on the microorganisms in the absence of TC NCs. while TC 0.5 NCs showed complete inhibition for *B. subtilis* within 180 min. in presence of visible light irradiation as no colony grew on Muller-Hinton medium after 24 h of incubation [31]. Fig. 6.4.(c) shows percent survival of *B. subtilis* under visible light irradiation in presence on TC NCs as a function of time.



**Fig. 6.4. (c) % survival of *B. subtilis* with TC NCs samples as function of time.**

A similar experiment was performed for *E. coli*. Fig. 6.4. (d) shows percent survival of *E. coli* as function of time. From the plot, 100% cell inhibition was observed in 300 min. irradiation for TC 0.5 NCs, while 90% and 95% cell inhibitions of *E. coli*. was observed after 24 h on Muller-Hinton

medium [30]. Fig. 6.4. (e) shows the photographs of antimicrobial effect on *E. coli* with TC NCs under visible light exposure.

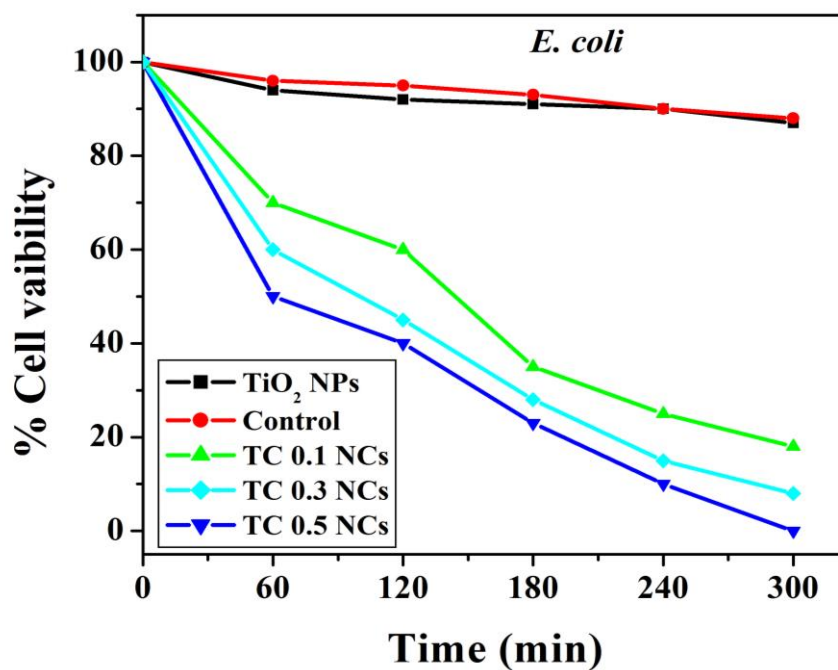


Fig. 6.4. (d) shows percent survival of *E. coli* as function of time.

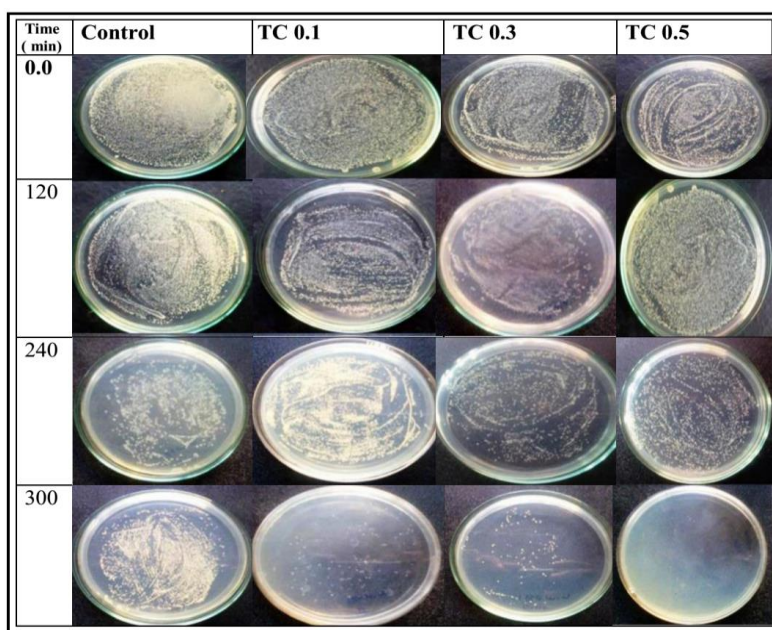


Fig 6.4. (e) Photographs of antimicrobial effect on *E. coli* with TC NCs under visible light exposure

Fig. 6.4. (f) shows percent survival of *P. aeruginosa* as function of time. from the Fig. it is boserved that the compltete cell inhibition was observed in 300 min. irradiation for TC 0.5 NCs, while other TC NCs required more time for complete cell inhibitions of *P. aeruginosa*. were observed after 24 h on Muller-Hinton medium.

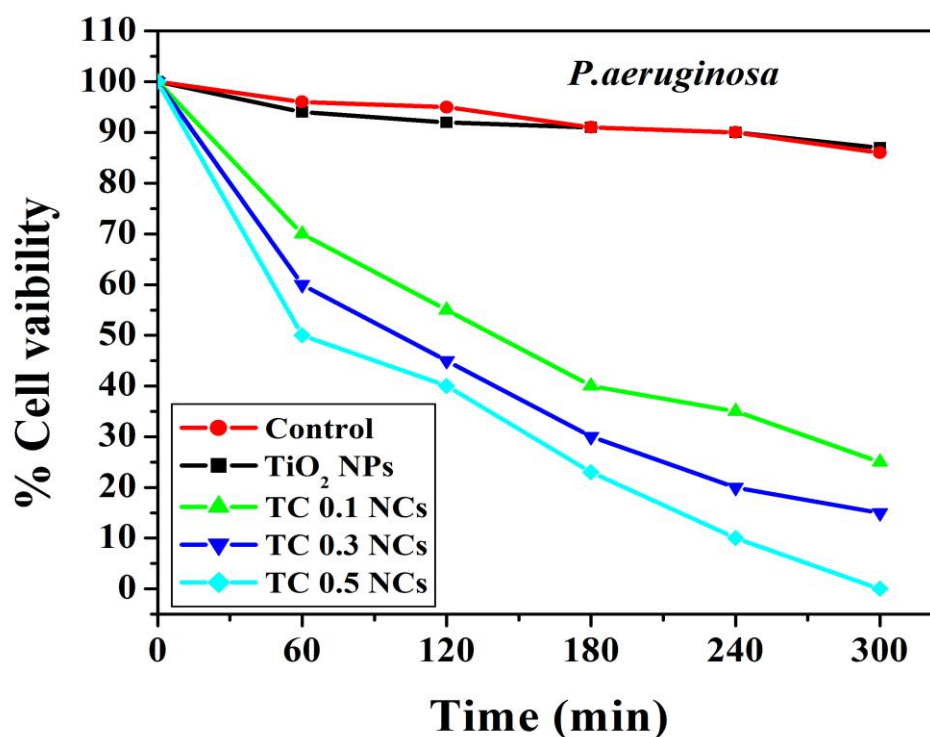


Fig 6.4. (f) % survival of *P. aeruginosa* with TC NCs as function of time

The photocatalytic inactivation of Gram-negative bacteria requires long time exposure as compared to gram-positive bacteria. The Gram-negative bacteria is relatively more resistant because of the nature of their cell wall, which restricts absorption of many molecules to movements through the cell membrane [32]. The antibacterial studies reveal that the photo-killing activity of TC NCs is increased with increasing MWCNTs contents. This is due to increase the reactive surface area of the TiO<sub>2</sub> NPs anchored on the surfafces (sic) of

MWCNTs, and hence the intimate interphase contact between TiO<sub>2</sub> NPs and MWCNTs leads the tuning of optical properties into visible region and hence the overall synergistic due to well-dispersed more surface with visible active particles resulting the photo-inhibition of bacteria [33, 34].

### 6.5 Conclusions

The photocatalytic inactivation of Gram-positive bacteria *S. aureus*, *B. subtilis* and Gram-negative bacteria such as *E. coli*, *P. aeruginosa* using TiO<sub>2</sub> NPs/TiO<sub>2</sub>-MWCNTs NCs are carried out under various conditions such as dark, UV light and artificial visible light irradiation. The observed results reveals that in dark bacterial inhibition is not observed, while in UV light, TiO<sub>2</sub> NPs have high rate of photo-inactivation. The modified with MWCNTs used effectively for photocatalytic inactivation against both type of bacteria. TC 0.5 NCs was antibacterial agent against bacteria as compared to the others; TC 0.1 and TC 0.3 NCs. This is due to its more visible activation as well more functional moieties present on the surface of TC NCs. These NCs would be highly beneficial to prevent and control the persistence and spreading of bacterial infections.

---

**Reference**

- [1] A. van Belkum, D. C. Melles, J. Nouwen, W. B. van Leeuwen, W. van Wamel, M. C. Vos, H. F. Wertheim, and H. A. Verbrugh, *Infection, Genet.Evol.* 9 (2009) 32.
- [2] C. Dipankar and S. Murugan, *Colloids Surf., B* 98 (2012) 112.
- [3] H. Kong, J. Song, and J. Jang, *Chem. Commun.* 46 (2010) 6735.
- [4] S. Li, T. Zhu, J. Huang, Q. Guo, G. Chen, and Y. Lai, *Int. J. Nanomedicine.* 12 (2017)2593.
- [5] J. Du, X. Lai, N. Yang, J. Zhai, D. Kisailus, F. Su, D. Wang, and L. Jiang, *ACS Nano* 5 (2011) 590.
- [6] R. Daghrir, P. Drogui, and D. Robert, *Ind. Eng. Chem. Res.* 52 (2013) 3581.
- [7] S. Xu, D. Feng, and W. Shangguan, *J. Phys. Chem. C* 113 (2009) 2463.
- [8] T. Matsunaga, R. Tomoda, T. Nakajima, and H. Wake, *FEMS Microbiol. Lett.* 29 (1985) 211.
- [9] O. Akhavan, R. Azimirad, S. Safa, and M. Larijani, *J. Mater. Chem.* 20 (2010) 7386.
- [10] K. Rajasekar, S. Thennarasu, R. Rajesh, R. Abirami, K. B. Ameen, and A. Ramasubbu, *Solid State Sci.* 26 (2013) 45.
- [11] H. M. Yadav, S. V. Otari, V. B. Koli, S. S. Mali, C. K. Hong, S. H. Pawar, and S. D. Delekar, *J. Photochem. Photobiol., A* 280 (2014) 32.
- [12] L. Chetibi, T. Busko, N. P. Kulish, D. Hamana, S. Chaieb and S. Achour, *J. Nanopart. Res.* 19 (2017)129.
- [13] Y. Cong, X. Li, Y. Qin, Z. Dong, G. Yuan, Z. Cui, and X. Lai, *Appl. Catal., B*, 107 (2011) 128.
- [14] M. Dahl, Y. Liu, and Y. Yin, *Chem. Rev.* 114 (2014) 9853.
- [15] F. J. Zhang, M. L. Chen, and W. C. Oh, *Korean J. Mater. Res.* 18 (2008) 583.

- 
- [16] Y. Zhang, Z. R. Tang, X. Fu, and Y. J. Xu, *ACS Nano* 4 (2010) 7303.
- [17] Y. J. Xu, Y. Zhuang, and X. Fu, *J. Phys. Chem. C* 114 (2010) 2669.
- [18] A. D. Gronewold, M. E. Borsuk, R. L. Wolpert, and K. H. Reckhow, *ACS Publications*, (2008).
- [19] V. Manthina, J. P. Correa Baena, G. Liu, and A. G. Agrios, *J. Phys. Chem. C* ,116 (2012) 23864.
- [20] J. Yu, L. Qi, and M. Jaroniec, *J. Phys. Chem. C* 114 (2010) 13118.
- [21] M. Sharma, G. Madras, and S. Bose, *J. Mater. Chem. A* 3 (2015) 5991.
- [22] W. C. Oh, A. R. Jung, and W. B. Ko, *Mater. Sci. Eng. C* 29 (2009)1338.
- [23] O. Akhavan, M. Abdolahad, Y. Abdi, and S. Mohajerzadeh, *Carbon* 47 (2009) 3280.
- [24] G. Veréb, L. Manczinger, G. Bozsó, A. Sienkiewicz, L. Forró, K. Mogyorósi, K. Hernádi, and A. Dombi, *Appl. Catal., B*, 129 (2013) 566.
- [25] J. M. Robertson, P. K. Robertson, and L. A. Lawton, *J. Photochem. Photobiol., A* 175 (2005) 51.
- [26] F. Pescheck, K. T. Lohbeck, M. Y. Roleda, and W. Bilger, *J. Photochem. Photobiol., B* , 132 (2014) 85.
- [27] Y. Matsumura and H. N. Ananthaswamy, *Toxicol. Appl. Pharmacol.* 195 (2004) 298.
- [28] C. Puglia, A. Offerta, A. Saija, D. Trombetta, and C. Venera, *J. Cosmet Dermatol.* 13 (2014) 151.
- [29] K. Nagaveni, M. Hegde, and G. Madras, *J. Phys. Chem. B* 108 (2004) 20204.
- [30] V. B. Koli, A. G. Dhodamani, A. V. Raut, N. D. Thorat, S. H. Pawar, and S. D. Delekar, *J. Photochem. Photobiol.* 328 (2016) 50.
- [31] V. B. Koli, A. G. Dhodamani, S. D. Delekar, and S. H. Pawar, *J. Photochem. Photobiol., A* 333 (2017) 40.
-

- [32] L. Caballero, K. Whitehead, N. Allen, and J. Verran, *J. Photochem. Photo -biol., A* 202 (2009) 92.
- [33] W. Wang, P. Serp, P. Kalck, and J. L. Faria, *J. Mol. Catal. A: Chem.* 235 (2005) 194.
- [34] F. J. Zhang and W. C. Oh, *Bull. Korean Chem. Soc.* 31 (2010) 1981.





## Chapter 7

# Fe-doped TiO<sub>2</sub>-MWCNTs nanocomposites as an antibacterial agent

J Mater Sci: Mater Med (2016)27:177  
DOI 10.1007/s10856-016-5788-0



CLINICAL APPLICATIONS OF BIOMATERIALS

Original Research

### Photoinactivation of bacteria by using Fe-doped TiO<sub>2</sub>-MWCNTs nanocomposites

Valmiki B. Koli<sup>1</sup> · Sagar D. Delekar<sup>1,2</sup> · Shivaji H. Pawar<sup>1</sup>



### 7.1 Introduction

In 1970, first time Fujishima and Honda discovered the photocatalytic water splitting based on the photocatalytic material. Since then, photoactive materials have attracted extensive scientific interest for environmental applications, such as antibacterial agent, removal of chemical pollutant from water and air [1]. TiO<sub>2</sub> nanoparticles (NPs) having excellent properties such as abundance, non-toxicity, low cost, high absorption coefficient and well structural stability [2]. TiO<sub>2</sub> is a semiconductor material with low efficiency and active under UV light irradiation only due to its wide band gap energy (3.2 eV.) [3]. Thus, TiO<sub>2</sub> NPs have limitation to apply for a wide range of applications. To overcome these obstacles, several research groups have been developed various strategies including metal doping, non-metal doping, and preparing nanocomposites. TiO<sub>2</sub> NPs have been found to modified with some transition metals (V, Cr, Mn, Fe, and Co), non-metals (N, C, and S) and nano-composites (NCs) with metal oxides, polymers and carbon nanostructures to improve its photocatalytic efficiency [4-9].

Recently, multi-walled carbon nanotubes (MWCNTs) have attracted significant attention due to their excellent electrical, mechanical, magnetic properties, high surface area, and high chemical stability [10, 11]. TiO<sub>2</sub>-MWCNTs (TC) NCs have considerable attention due to their unique properties. These types of NCs are widely used in wastewater treatment, remove a large number of chemical pollutant [12-14], as well as used in solar energy harvesting and antibacterial agent [9, 15, 16]. These NCs have excellent properties such as high adsorption capacity, large surface area, and ability to tune optical absorption band edge of TiO<sub>2</sub> NPs in the visible region [17-19]. Nanocomposites of TiO<sub>2</sub> with MWCNTs are found to decrease the rate of electron-hole pair recombination rate which ultimately yields superior photocatalytic activity compared with individual analogous [16]. The structural

morphology of MWCNTs allows them to prepare NCs with metal and metal oxide NPs [20]. The NCs of MWCNTs with NPs are specifically used in antibacterial study, catalysis, energy storage, waste water treatment etc. [17, 21, 22]. Earlier studies were carried out to find a low-cost, stable, non-toxic and visible light photoactive NCs to apply in various field like hospitals, homes, environmental clean-up, water disinfection, textiles, packaging, construction, biomedical, and food industries etc. [23-25]. In 1985, Matsunaga et al. first time investigated the killing of microbial cells such as *Lactobacillus acidophilus*, *Saccharomyces cerevisiae*, and *Escherichia coli* by using Pt-TiO<sub>2</sub> under UV light irradiation [25]. In addition, TiO<sub>2</sub> NPs have attracted attention towards the inactivation of a wide range of microbial cells like bacteria, fungi and viruses [26, 27].

The photo-inactivation mechanism of TiO<sub>2</sub> NPs for the micro-organism is well explored. This mechanism includes several complex pathways such as light irradiation, generation of reactive oxygen species (ROS) having strong oxidation ability which interact with the cell wall of microorganism and oxidize the cell wall continent, leading to ultimate cell death [22, 28]. In previous studies, many researchers have reported that the optimum concentrations of Fe<sup>3+</sup>-doping in TiO<sub>2</sub> NPs, which introduce new bands in between the conduction and valence bands of TiO<sub>2</sub> NPs, which powerfully modify the optoelectronic properties of the material towards absorption of visible light [29]. Recently, Our group, demonstrated photocatalytic antibacterial activity of Fe-containing TiO<sub>2</sub> NPs against Gram-negative and Gram-positive bacterium under fluorescent light [29]. Tarapalis et al. reported bactericidal activity of Fe-doped TiO<sub>2</sub> thin film towards *E.coli* under UV light [30]. Similarly, Egerton et al. fabricated Fe-doped TiO<sub>2</sub> electrode by spin coating and tested their antibacterial activity in the presence of UV light [31]. Akhavan et al. reported the visible light photo-inactivation of gram-negative bacteria using CNT-doped

TiO<sub>2</sub> thin films formed by a dip-coating method [18]. Similarly, Ashkarran et al. demonstrated antibacterial activity towards *E. coli* for CNT–TiO<sub>2</sub> hybrid nanostructures prepared by arc discharge method in a liquid [32]. Several reports are available on removable of organic pollutant by using modified TiO<sub>2</sub> photo catalyst under visible light irradiation [30, 33]. However, hardly any attention has been paid for the development metal-doped TiO<sub>2</sub> with MWCNTs as a NCs for photo-inactivation of bacteria under visible light.

In the present chapter, Fe-doped TiO<sub>2</sub>-MWCNTs (Fe-TC) NCs were prepared by a facile sol-gel method and characterized using various techniques. The photo-inactivation of bacteria study was carried out against Gram-positive and Gram-negative bacteria under visible light irradiation. The effect of the iron doping and MWCNT's wt. % ratio on the photocatalytic properties of TiO<sub>2</sub> against bacteria was demonstrated under visible light irradiation. The rate of ROS generation on the surface of nanocomposites was also studied using PL spectroscopy.

## 7.2. Experimental

### 7.2.1 Materials

Required chemicals such as titanium (IV) isopropoxide (TTIP), sodium dodecyl sulfate (SDS), glacial acetic acid, ethanol, Ferric nitrate were of AR grade. MWCNTs (CVD method, diameter: 20-45 nm, length: 10-40  $\mu$ m and surface area: >500 m<sup>2</sup>/gm).

### 7.2.2 Synthesis of Fe doped TiO<sub>2</sub>-MWCNTs nanocomposites

Fe doped TiO<sub>2</sub>-MWCNTs (Fe-TC) NCs were synthesized by using a modified sol-gel method reported previously [29]. Glacial acetic acid and titanium (IV) isopropoxide were taken in a stoichiometric amount. The content was stirred very well followed by addition of capping agent (aqueous solution of sodium dodecyl sulfate) and then add the stoichiometric amount (3 mole %)

of ferric nitrate dissolved in distilled water stirred for 1h. Afterward, the suspension of FWCNTs 0.1 wt. % to 0.5 wt. % (i.e. Fe-TC 0.1, Fe-TC 0.3, Fe-TC 0.5 NCs) with excess deionized water for hydration. Subsequently, pH of the solution was adjusted to 10.00 using ammonia solution. Then, the whole content was stirred at 60 °C for 3 h, and then cooled to room temperature. Then, this precipitate was centrifuged and washed with ethanol followed by deionized water. The NCs was dried in an electric oven at 110 °C and calcinated in air at 450 °C for 5 h. The Fe-doped TiO<sub>2</sub> NPs were prepared by same method without adding the FMWCNTs suspension and denoted as Fe-TiO<sub>2</sub> (Fe-T) NPs.

### 7.2.3 Photocatalytic inactivation of bacteria

Gram-positive *Bacillus subtilis* (*B. subtilis*) and Gram-negative *Pseudomonas aeruginosa* (*P. aeruginosa*) bacterium are selected to evaluate photo-inactivation of bacteria. These selected bacterial species were cultured on nutrient agar plates at 37 °C for 24 h. The bacterial suspensions were prepared in 5 mL saline solution to obtain a final concentration of bacteria of 10<sup>8</sup> CFU/mL<sup>-1</sup>. A borosilicate glass photo reactor system was used to perform photo-inactivation bacteria experiments; consisting of eight fluorescent lamps (Philips TLD 8 W,  $\lambda > 400$  nm) and intensity of 5 mW cm<sup>-2</sup> [29, 34, 35]. The bacterial suspension was placed in a glass vessel and magnetically stirred with Fe-TC NCs. Then, the bacterial suspension was illuminated under visible light. To avoid contamination, all experiments were carried out under sterilized conditions. After a fixed time, 100  $\mu$ L of solution was spread on Mueller–Hinton agar plates and incubated at 37 °C for 24 h. The standard plate count method was used to determine viable numbers of cells as CFU mL<sup>-1</sup>. The experiment at same condition was repeated for three times and the average values are reported here.

---

**7.2.4 Characterization**

To study the effect of iron and MWCNTs on the crystal structure of TiO<sub>2</sub> NPs, X-ray diffraction (XRD) patterns of the samples were recorded on X-ray diffractometer (Bruker D 8-advance) using Cu K $\alpha$  (1.5406 Å) radiation in the 2 $\theta$  range from 20-80°. UV-vis diffuse reflectance spectra (UV-DRS) of the samples were measured using UV- 3092 (lab India) in the range of 300-700 nm. The surface morphologies and particle sizes of samples were observed by using transmission electron microscope (TEM) (Philips CM 200, operating voltages: 20-200 kV, Resolution: 2.4 Å). X-ray photoelectron spectroscopy (XPS) was used for determining the surface compositions of the catalysts, using a (Physical Electronics 5600 Multi-technique System with monochromatic Al K  $\alpha$  radiation). The photoluminescence (PL) spectra of a representative sample, Fe-TC (0.5 wt. %) were recorded on a fluorescence spectrometer (JASCO FP-750).

**7.3 Structural characterization of Fe-T NPs and Fe-TC NCs****7.3.1 X-ray diffraction analysis**

X-ray diffraction patterns of Fe-T NPs, and Fe-TC NCs are shown in Fig. 7.1 All diffraction peaks revealed that the tetragonal anatase phase of synthesized material (JCPDS 21-1272). No peaks were found for Fe and carbon in the synthesized NCs. The most intense peak of TiO<sub>2</sub> was observed for all samples, but characteristic of the peak of MWCNTs and other peaks of MWCNTs are not observed due to its low concentration [36]. There is no peaks for rutile and brookite phases of TiO<sub>2</sub> NPs observed in the XRD patterns of all samples. Doping with Fe<sup>3+</sup> and composite with MWCNTs shows slightly increase in the intensity of diffraction peaks in XRD pattern. This is due to the shift changes in atomic positions of different ions of TiO<sub>2</sub> NPs as well as heterogeneous nucleation of MWCNTs for TiO<sub>2</sub> NPs and the formation of

larger anatase  $\text{TiO}_2$  crystalline particles with higher crystalline degree in NCs [37]. Crystallite size was determined using Scherrer's equation

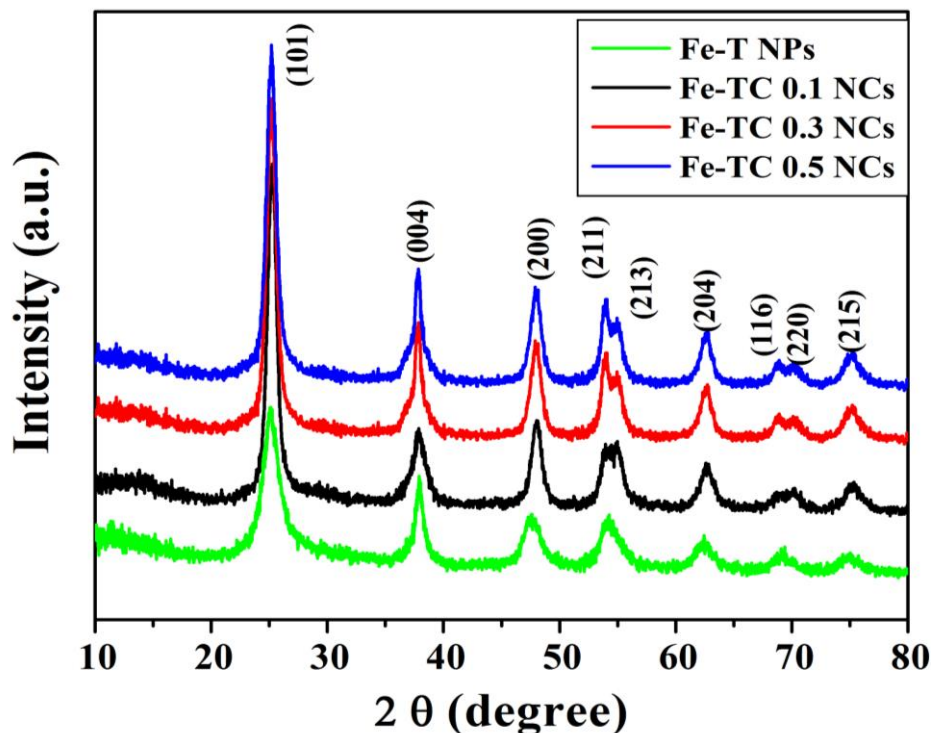


**Fig. 7.1** XRD patterns of, Fe-T NPs and Fe-TC NCs.

The calculated average crystallite sizes of the Fe-T NPs and Fe-TC NCs were found in the range from 7 to 10 nm. The structural parameters of the samples are listed in Table 7.1. The substitution of  $\text{Ti}^{4+}$  with  $\text{Fe}^{3+}$  in the lattice structure of  $\text{TiO}_2$  causes distortion of  $\text{TiO}_6$  octahedral, and the strong charge difference creates oxygen deficiency, which may be responsible for the generation of large dipole moments and internal polarization fields in the structure. Thus, the recombination rate of electron and hole decreases and photocatalytic antibacterial activity of Fe-TC NCs increase [29, 38].



**Table 7.1. Structural parameters with the optical band gap of, Fe-T NPs and Fe-TC NCs.**

Samples	(h k l)	Standard 'd' values (Å)	Calculated d values (Å)	Cell cons. a and c (Å)	Crystallite size (nm)	Optical band gap (eV)
Fe-T NPs	(1 0 1)	3.51	3.52	a = 3.78	7.0	2.78
	(0 0 4)	2.37	2.37	c = 9.50		
	(2 2 0)	1.33	1.33			
Fe-TC 0.1 NCs	(1 0 1)	3.51	3.50	a = 3.77	7.5	2.70
	(0 0 4)	2.37	2.37	c = 9.51		
	(2 2 0)	1.33	1.33			
Fe-TC 0.3 NCs	(1 0 1)	3.51	3.53	a = 3.78	7.5	2.64
	(0 0 4)	2.37	2.37	c = 9.47		
	(2 2 0)	1.33	1.34			
Fe-TC 0.5 NCs	(1 0 1)	3.51	3.53	a = 3.79	9.5	2.42
	(0 0 4)	2.37	2.37	c = 9.48		
	(2 2 0)	1.33	1.33			

### 7.3.2 Transmission electron microscopy (TEM)

Fig. 7.2 (a) and (b) shows TEM image of Fe-TC 0.5 NCs prepared by the modified sol-gel method and calcinated at 450 °C. The image of Fe-TC NCs confirmed the existence of Fe-T NPs decorated on the surface of MWCNTs [39]. The outer diameter of the MWCNTs was found to be 20-45 nm whereas the particle size of Fe-T NPs was found to in the range 7-15 nm. The photo-inactivation of bacteria is mainly influenced by MWCNTs because

it supports to Fe-T NPs as well as intimate interphase contact between Fe-T NPs and MWCNTs leads the tuning of optical properties into visible region and hence the overall synergistic due to well-dispersed more surface with visible active particles resulting the photo-inactivation of bacteria [17, 40].

Fig. 7.2. (c) shows the corresponding selected area electron diffraction (SAED) patterns. It shows that diffraction spots of the MWCNTs were overlaid with the diffraction rings of Fe-T NPs appearing in polycrystalline phases. The SAED shows that the circular rings correspond to plane anatase (101), (004), (200), (105). The presence of Fe-T NPs in anatase phase are photocatalytically superior than rutile and brookite due to its better optical properties and stability [41]. This result is in good agreement with the results obtained from XRD analysis.

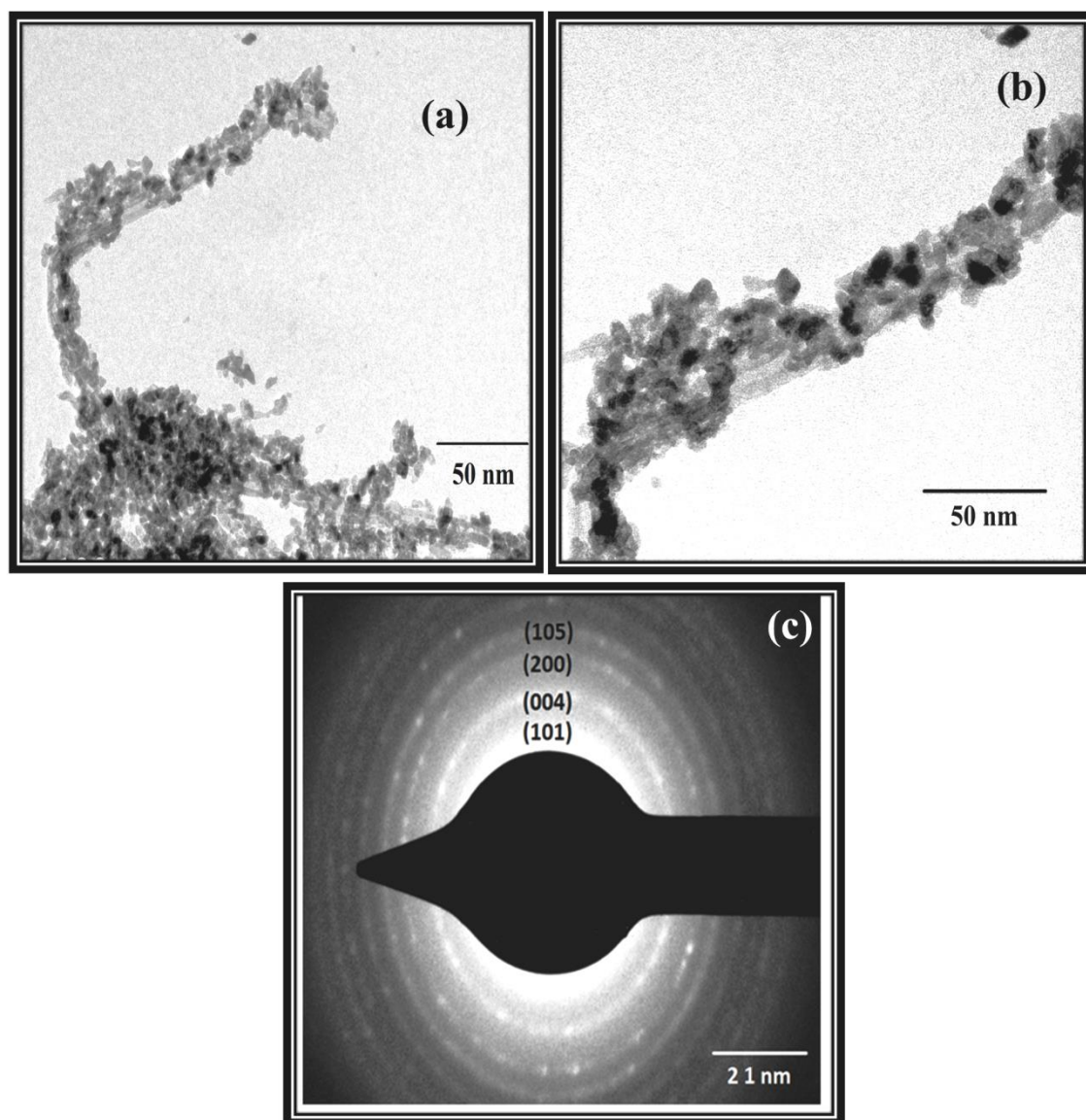
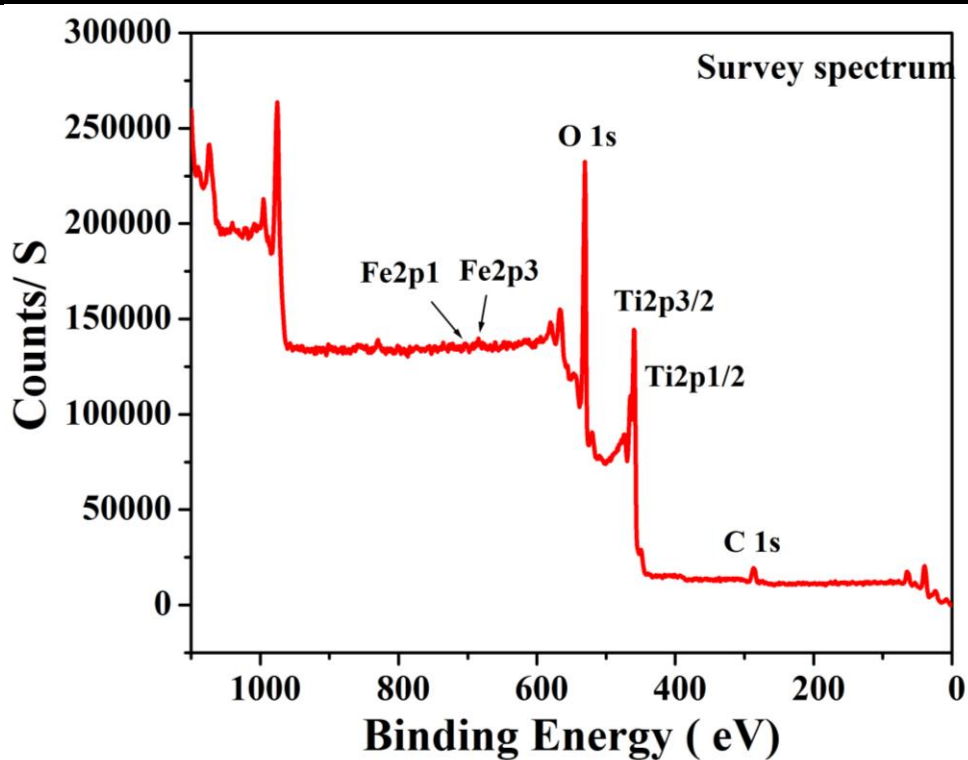


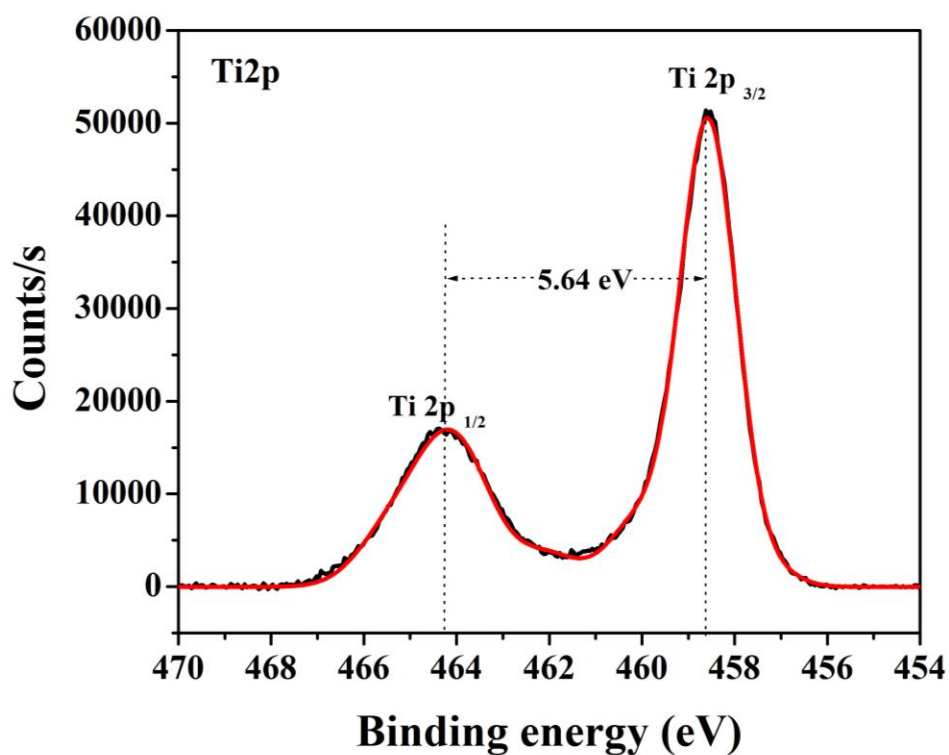
**Fig. 7.2. TEM images: (a) and (b) Fe-TC 0.5 NCs and (c) SAED pattern of Fe-TC 0.5 NCs**

### 7.3.3 X-ray photoelectron spectroscopy

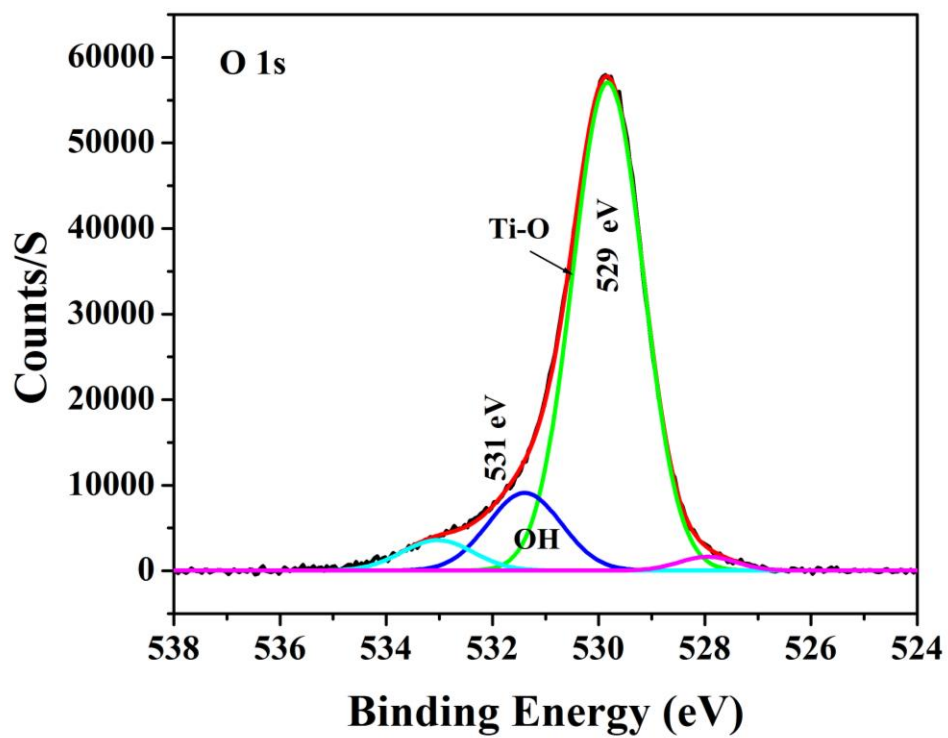
Fig. 7.3 shows the XPS spectrum of Fe-TC 0.5 NCs. Fig.7.3 (a) shows the survey spectrum of Fe-TC 0.5 NCs. Fig.7.3 (b) shows XPS spectrum for Ti2p configuration with two characteristics bands of Ti 2p<sub>3/2</sub> and Ti 2p<sub>1/2</sub> peaks at 458.59 and 464.23 eV respectively. The splitting between the Ti 2p<sub>1/2</sub> and Ti 2p<sub>3/2</sub> is 5.64 eV indicating the presence of Ti<sup>4+</sup> oxidation state in the NCs [42, 43]. Binding energy of TiO<sub>2</sub> was not affected by the addition of dopant and MWCNTs due to low concentration as compare to TiO<sub>2</sub>. The peaks observed for Fe and carbon are very small due to their low concentration. Fig. 7.3 (c) shows XPS spectrum of O1s configuration, the binding energy peak observed at 531 eV reveals the presence of surface hydroxyl groups while the peak at 529 eV arises from the titanium lattice for Ti-O bonding [44, 45]. The sp<sup>2</sup>-hybridized (C=C) carbon peak appeared at 284 eV and other significant peaks observed at 286 and 288 eV are related to oxidation developed C-O and C=O (aromatic) functional groups, which shown in XPS spectrum of C 1s configuration in Fig. 7.3 (d). Similarly, the peak at 289 eV is assigned for COOH functional group present on MWCNTs [46]. In Fig. 7.3.(e), the peak observed for Fe2p configuration confirms formation Ti-O-Fe bonds due to the substitution of Ti<sup>4+</sup> by Fe<sup>3+</sup> in Fe-TC NCs. This alters the electron densities of Ti<sup>4+</sup> cations and O<sub>2</sub><sup>-</sup> anions and changes the charge distributions of the atoms on the surface of photocatalyst. However Fe<sup>3+</sup> ions doping in TiO<sub>2</sub> host lattice introduce a new impurity level into the band gap of TiO<sub>2</sub> NPs. This reduce the band gap of TiO<sub>2</sub> NPs which may improve the visible light absorption of Fe-T NPs which results the better photo-inactivation of bacteria [47].



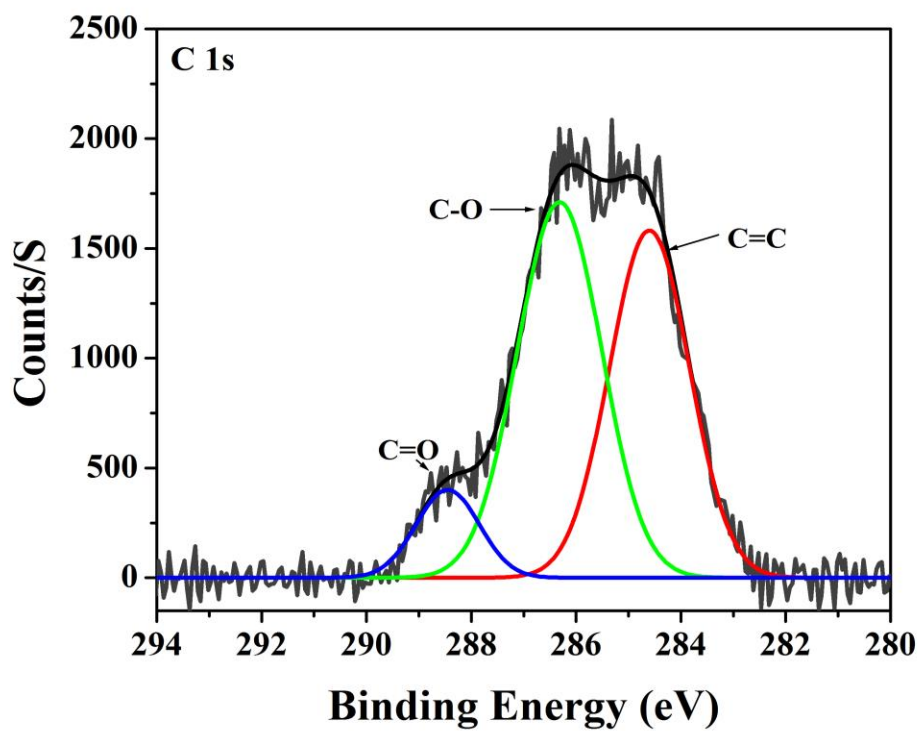
(a)



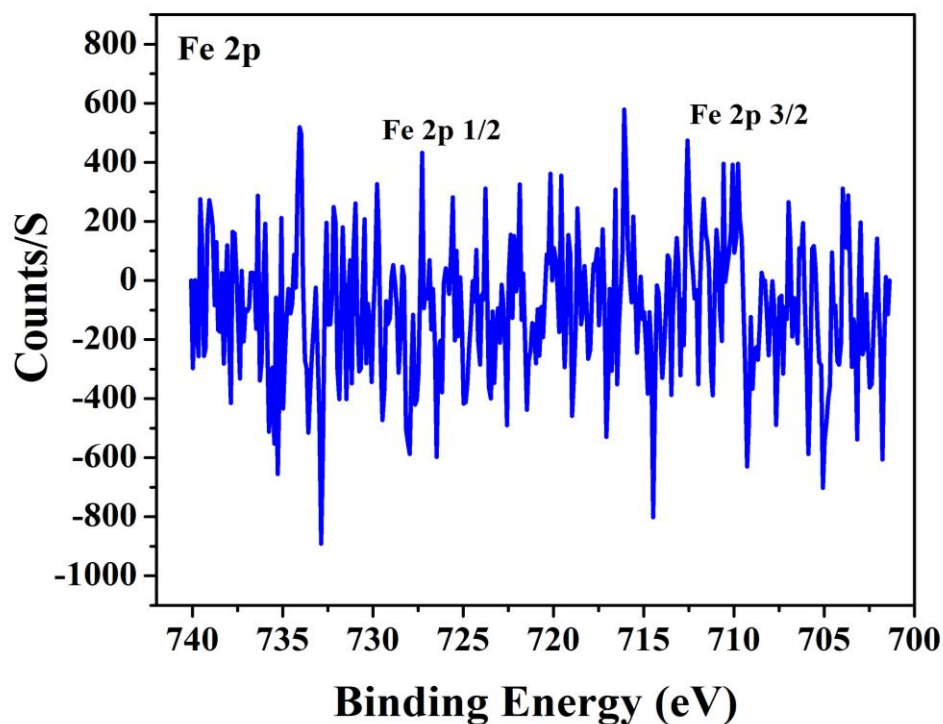
(b)



(c)



(d)



(e)

**Fig.7.3 XPS for Fe-TC 0.5 NCs: (a) survey; (b) Ti 2p; (c) O 1s; (d) C 1s and (e) Fe2p peak configuration**

## 7.4 Spectroscopic characterization of Fe-T NPs and Fe-TC NCs

### 7.4.1 UV-vis diffuse reflectance spectra

UV-vis diffuse reflectance spectra of Fe-T NPs and Fe-TC NCS samples are shown in Fig. 7.4. The optical absorption edge of Fe-TC NCs is shifted to the visible range at 400-500 nm. As expected, the spectrum of Fe-T NPs has a sharp absorption edge at 410 nm while the addition of MWCNTs shifted this absorption edge in the higher wavelength [48]. The band gap of the samples is calculated by using tauc equation. The band gap energy values for Fe-T NPs, Fe-TC 0.1, Fe-TC 0.3 and Fe-TC 0.5 NCs is 2.78, 2.70, 2.64 and 2.42 eV respectively. The band gap of Fe-T NPs decreases with increasing concentration of MWCNTs in NCs. Because MWCNTs present in NCs not only support the Fe-T NPs but also stabilized the charge separation by trapping the

electrons transferred from Fe-T NPs, thereby hindering the charge recombination. Hence, the photogenerated electrons are transferred from Fe-T NPs to the MWCNTs with the decrease in recombination-rate of electron and hole; with reducing the band gap of Fe-T NPs and increases the visible light absorptions which enhances the oxidative reactivity of particles in contact to bacteria with the damage of its cell walls [49, 50].

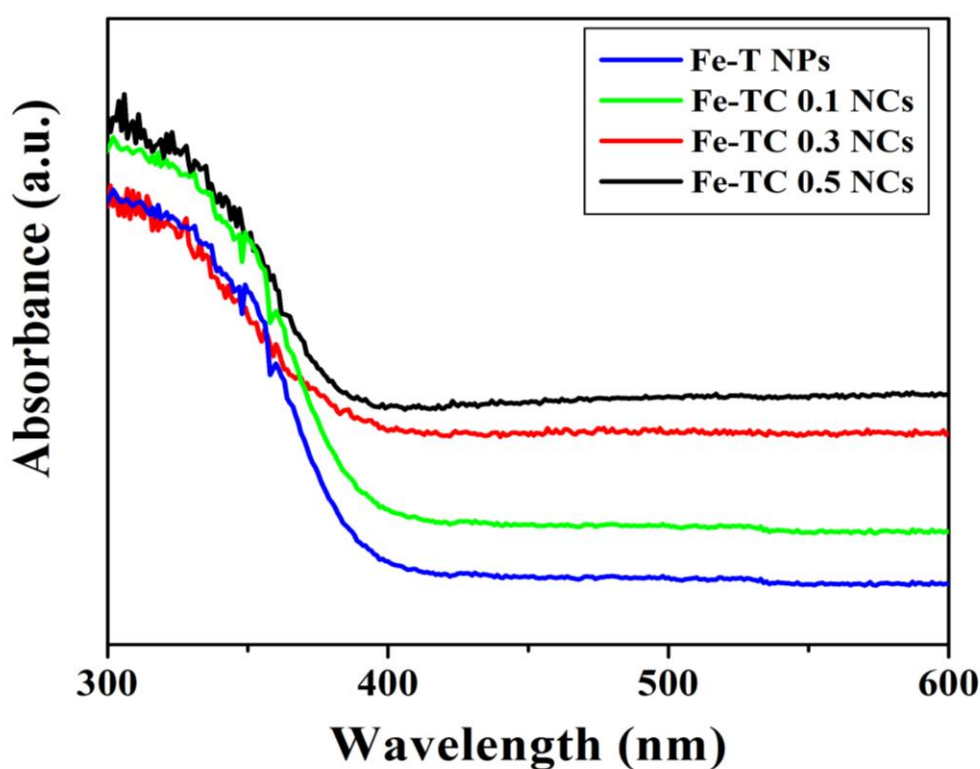
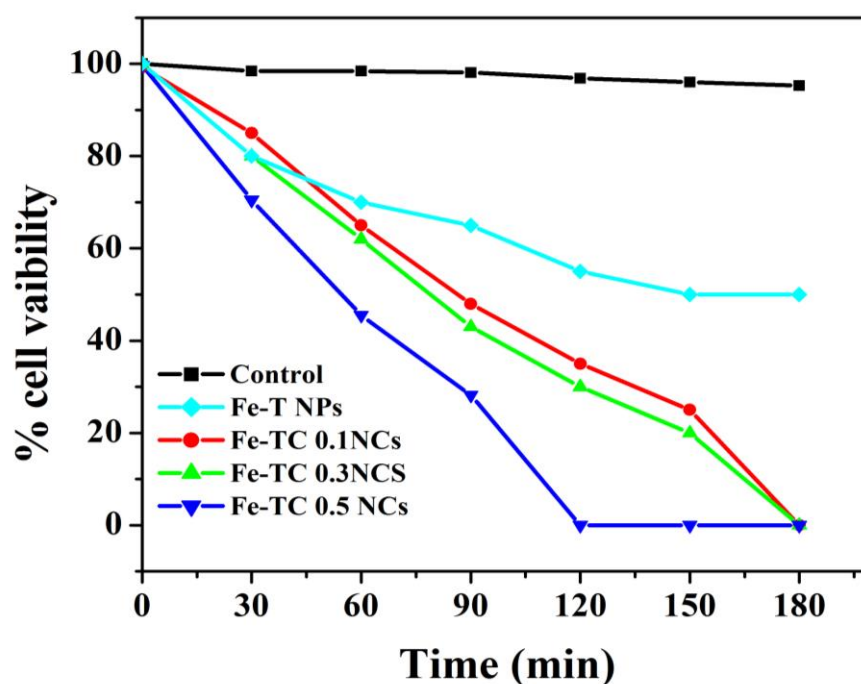


Fig. 7.4 UV-vis DRS of Fe-T NPs and Fe-TC NCs



### 7.5 Photo-inactivation of bacteria

The photocatalytic disinfection study was performed against two model bacteria species, a Gram-positive *B. subtilis* and a Gram-negative *P. aeruginosa*. The bacterial species were incubated with Fe-TC NCs in dark. It is clear that the catalyst will not inhibit the growth of bacteria in the absence of light. Then the effect of light on bacterial growth was studied by light exposure on bacterial suspension without Fe-TC NCs. There was no effect of light on the growth of bacteria. Thus, it reveals that catalysts, as well as visible light, are required for the inactivation of bacterial cells. The photocatalytic disinfection experiments show inactivation of bacteria in the presence of visible light as well as it depends on the concentration of MWCNTs in NCs. Fig. 7.5 shows the complete inhibition of *B. subtilis* bacteria at 120 min for Fe-TC 0.5 NCs. However, the other nanocomposites Fe-TC 0.1 and Fe-TC 0.3 show complete inhibition at 180 min.



**Fig. 7.5** Visible light photocatalytic inactivation of *B. subtilis* with Fe-TC NCs

The similar experiments were performed for the inactivation of gram-negative *Pseudomonas aeruginosa* under visible light irradiation. In Fig. 7.6 after 240 min of visible light treatment by Fe-TC 0.5 NCs, shows almost all cells were destroyed (100%), whereas the use of Fe-TC 0.1 NCs and Fe-TC 0.3 NCs shows complete inhibition at 300 min and at 240 min were as bacterial inhibition up to 85 and 75% cell growth was inhibited respectively.

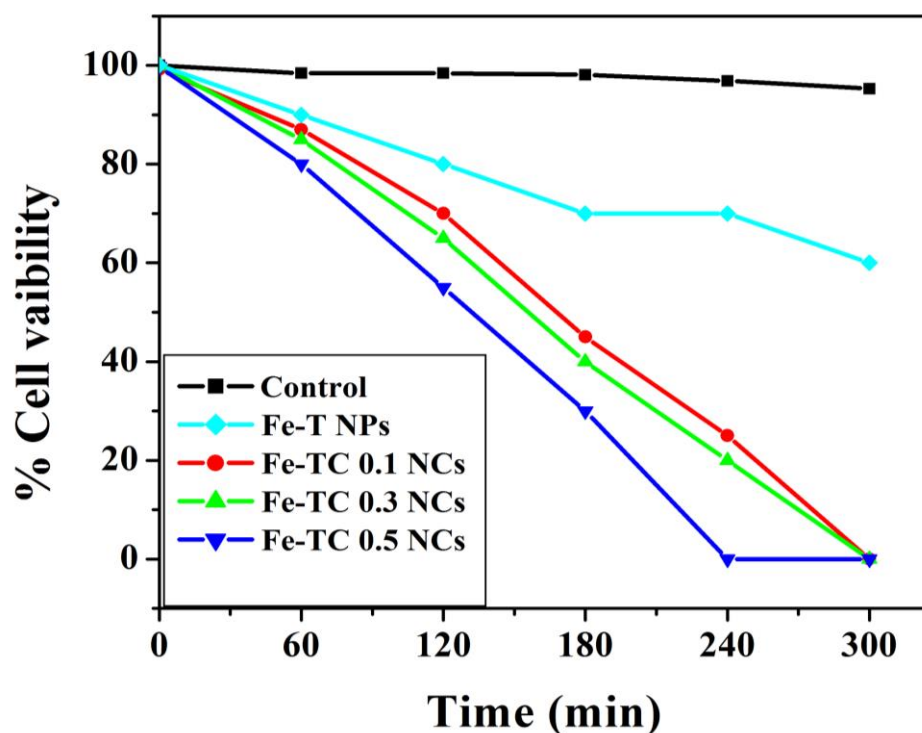


**Fig. 7.6** Visible light photocatalytic inactivation of *P. aeruginosa* with of Fe-TC NCs.

### 7.6. ROS measurement

In the photo-inactivation of bacteria, the rate of ROS generation plays an important role [51, 52]. The ROS species having strong oxidation capacity and it damages the bacterial cell wall. In initial stage, ROS generated by photocatalysis was damaged the surfaces of the bacterial cells, afterward the internal bacterial components leak from the cells through the damaged side of the cell wall. The role of hydroxyl radicals in bacterial inactivation was studied by PL technique using coumarin-based fluorescence probe method [53]. For this, coumarin solution ( $1 \times 10^{-3}$  M) and Fe-TC 0.5 NCs were stirred magnetically and also irradiated under visible light. The fluorescence emission spectrum excited at 332 nm from the coumarin solution was measured for every 3 min during irradiation. Fig. 7.7 shows the fluorescence initiation of Fe-TC 0.5 NCs with coumarin solution. The  $\bullet\text{OH}$  radicals generated was responsible for the photo-catalytic oxidative damage of the bacterial cells. Fig. 7.7 shows the gradual increase in the fluorescence peak intensity at 456 nm. This was observed only when coumarin solution was irradiated with Fe-TC 0.5 NCs. This confirms the fluorescence was due to the generation of  $\bullet\text{OH}$  from 7-hydroxycoumarin during the visible light illumination. In PL studies Fe-TC 0.1 NCs and Fe-TC 0.3 NCs samples, shows a small PL peaks which indicates the lower production of the  $\bullet\text{OH}$  radicals. This attributed that the Fe-TC 0.5 NCs generates higher rate of ROS, because the optimized concentration of MWCNTs present in Fe-TC NCs can enhance the transfer of photo generated electrons and reduce the recombination of photo generated charge carriers to prolong their separation, which is responsible for the enhancement of photocatalytic activity. The ROS measurements results confirms the Fe-TC 0.5 NCs generates more ROS in presence of visible light compared to other NCs. Also in photo-inactivation of bacterial experimental results shows Fe-TC 0.5 NCs having better photo-inactivation as compare to other NCs. Therefore the ROS generation and photo-inactivation of bacteria experimental results

confirms the photo-inactivation of bacteria was due to the ROS generated by Fe-TC NCs in presence of visible light.

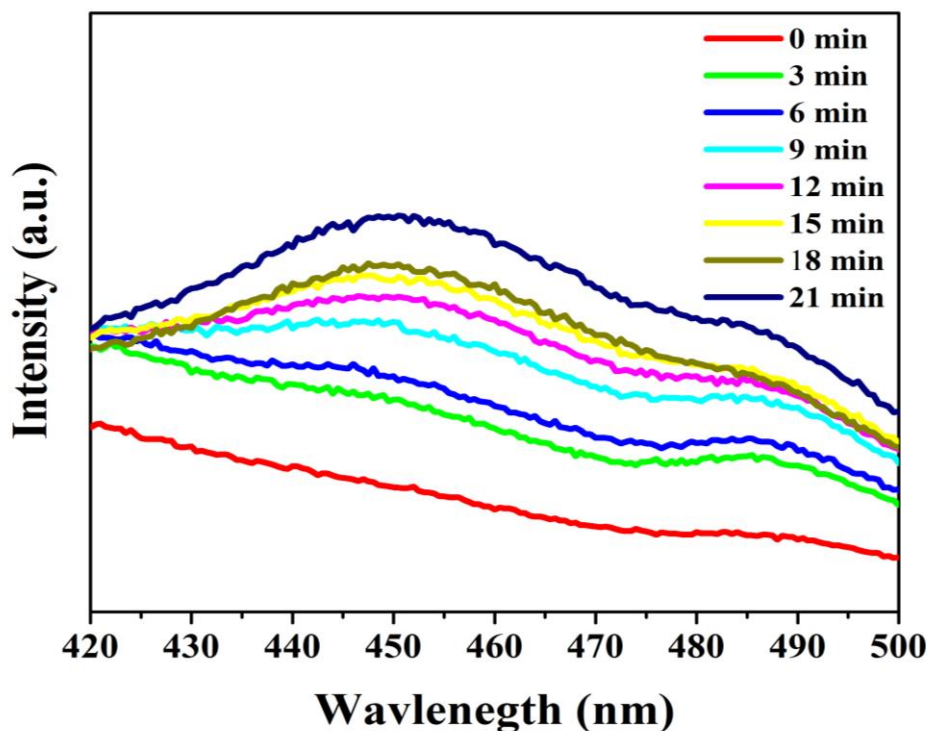


**Fig.7.7 PL spectra of Fe-TC 0.5 NCs in presence of coumarin with different irradiation time**

### 7.7 Overall discussion

The photocatalytic NCs with antibacterial properties are increasingly developed to reduce various bacterial infections and produce alternative to routine antibacterial agent. In photo-inactivation of bacteria,  $\text{TiO}_2$  NPs attracted great attention because it's having ability to generate ROS and kill the wide range bacteria. In the present study the attempt is made for the synthesis of Fe-TC by using simple sol-gel method. The two strategies have been used to decrease the band gap of  $\text{TiO}_2$  NPs, one is appropriate amount of Fe doping in  $\text{TiO}_2$  host lattice and other is preparing NCs with MWCNTs. XRD analysis confirms the crystallite sizes and phase purity of the prepared materials (Fig. 7.1). The Fe-TC NCs shows the characteristic peak of MWCNTs is overlapped

by most intense peak of TiO<sub>2</sub> NPs. UV-DRS study shows the decrease in band gap of Fe-TC NCs with increasing concentration of MWCNTs. Fe-TC NCs of lower band gap applicable for various applications. The morphological study of Fe-TC NCs shows the uniform decoration of Fe-T NPs on the surface of MWCNTs which avoids aggregation of Fe-T NPs and help full for the separation of electron hole pair. The qualitative analysis (XPS) of Fe-TC NCs confirms the presence of Ti, Fe, C and O in NCs. It also confirms the presence of various functional groups on the surface like C-O, C=O, COOH, also shows the Ti-O and Ti-O- Fe etc.

Thus the overall morphological and optical study of Fe-TC NCs reveals that the Fe-TC NCs are the visible light active nanomaterials. To determine its applicability, photo-inactivation of Gram-positive and Gram-negative bacteria was carried out under visible light and results shown in Fig. 7.5 and Fig. 7.6. This results demonstrate that complete inhibition of Gram-positive *B. subtilis* and Gram-negative *P. aeruginosa* in presence Fe-TC 0.5 under visible light. For Gram-positive bacteria inhibition time 120 min while Gram-negative bacteria it required 240 min. This is due to gram negative bacteria is relatively more resistant because of the nature of their cell wall, which restricts absorption of many molecules to movements through the cell membrane. In case of Gram-positive bacteria, 90% of the cell wall made up of peptidoglycan while for the Gram-negative bacteria, cell wall contains only 10% of the Peptidoglycan. This layer is very porous which allows NPs of approximately (2 nm) to pass through layer in both Gram-negative as well as Gram-positive bacteria [54]. Whereas, peptidoglycan layer pores are enough to pass the oxidative species, likes superoxide and hydroxyl radical due to this the Gram-positive bacterial inhibition take place in short time than Gram-negative bacteria. Fe-TC NCs in presence of visible light generates ROS which, cause membrane disorganization, increased membrane permeability as a result of perforation and finally leading to cell death [55, 56].

### 7.8. Conclusion

This chapter is concentrated with the synthesis of Fe-TC NCs with composition (0.0 to 0.5 wt. % MWCNTs) by using sol-gel method. The physicochemical properties of the NCs were investigated by, XRD, UV-vis DRS, XPS analysis, TEM, and PL. Our experimental results demonstrate that the Fe-T NPs are well decorated on surface of MWCNTs which improved interface between Fe-T NPs and MWCNTs. It provides the number of active sites with viable surface area, which was in favor of the separation of electron-hole pairs and lowers the efficiency of their recombination. In photo-inactivation of bacteria two model bacteria, Gram-positive *B. subtilis* and a Gram-negative *P. aeruginosa* are tested in presence of visible light. The both types of studied bacterium species had efficiently inactivated on the surface of NCs under visible light. These finding will have large implication on inhibition of pathogenic bacteria resulting the better health care.

---

### Reference

- [1] B. Pant, H. R. Pant, N. A. Barakat, M. Park, K. Jeon, Y. Choi, and H.Y. Kim, *Ceram. Int.* 39 (2013) 7029.
- [2] K. Rajasekar, S. Thennarasu, R. Rajesh, R. Abirami, K. B. Ameen, and A. Ramasubbu, *Solid State Sci.* 26 (2013) 45.
- [3] H. Li, X. Zhang, Y. Huo, and J. Zhu, *Environ. Sci. Technol.* 41 (2007) 4410.
- [4] S. F. Chen, J. P. Li, K. Qian, W. P. Xu, Y. Lu, W. X. Huang, and S. H. Yu, *Nano Res.* 3 (2010) 244.
- [5] W. Fan, Q. Lai, Q. Zhang, and Y. Wang, *J. Phys. Chem. C* 115 (2011) 10694.
- [6] A. Truppi, F. Petronella, T. Placido, M. Striccoli, A. Agostiano, M. L. Curri, and R. Comparelli *Catalysts* 7 (2017) 100.
- [7] H. M. Yadav, S. V. Otari, V. B. Koli, S. S. Mali, C. K. Hong, S. H. Pawar, and S. D. Delekar, *J. Photochem. Photobiol. A* 280 (2014) 32.
- [8] R. Barkul, V. Koli, V. Shewale, M. Patil, and S. Delekar, *Mater. Chem. Phys.* 173 (2016) 42.
- [9] V. B. Koli, A. G. Dhodamani, A. V. Raut, N. D. Thorat, S. H. Pawar, and S. D. Delekar, *J. Photochem. Photobiol. A* 328 (2016) 50.
- [10] E. T. Thostenson, C. Li, and T.W. Chou, *Compos. Sci. Technol.* 65 (2005) 491.
- [11] K. Lau, C. Gu, and D. Hui, *Composites Part B*, 37 (2006) 425.
- [12] K. Zhang, K. C. Kemp, and V. Chandra, *Mater. Lett.* 81 (2012) 127.
- [13] F. Petronella, A. Truppia, C. Ingrosso, T. Placido, M. Striccoli, M.L. Curri, A. Agostiano, R. Comparelli, *Cata. Today* 281 (2017) 85.
- [14] G. Ghasemzadeh, M. Momenpour, F. Omid, M. R. Hosseini, M. Ahani, and A. Barzegari, *Front. Environ. Sci. Eng.* 8 (2014) 471.
- [15] S. S. Mali, C. A. Betty, P. N. Bhosale, and P. Patil, *ECS J. Solid State Sci.* 1 (2012) M15.

- 
- [16] H. Yu, X. Quan, S. Chen, and H. Zhao, J. Phys. Chem. C, 111 (2007) 12987.
- [17] W. Wang, P. Serp, P. Kalck, and J. L. Faria, J. Mol. Catal. A: Chem. 235 (2005) 194.
- [18] O. Akhavan, R. Azimirad, S. Safa, and M. Larijani, J. Mater. Chem. 20 (2010) 7386.
- [19] W.C. Oh, A.R. Jung, and W.B. Ko, J. Ind. Eng. Chem. 13 (2007) 1208.
- [20] P. C. Ma, B. Z. Tang, and J.K. Kim, Carbon 46 (2008) 1497.
- [21] X. Wang, M. Li, Z. Chang, Y. Yang, Y. Wu, and X. Liu, ACS Appl. Mater. Interfaces ,7 (2015) 2280.
- [22] S. Da Dalt, A. Alves, and C. Bergmann, Mater. Res. Bull. 48 (2013) 1845.
- [23] T. Amna, M. S. Hassan, N. A. Barakat, D. R. Pandeya, S. T. Hong, M.S. Khil, and H. Y. Kim, Appl. Microbiol. Biotechnol. 93 (2012) 743.
- [24] C.Chawengkijwanich and Y. Hayata, Int. J. Food Microbiol. 123 (2008) 288.
- [25] T. Matsunaga, R. Tomoda, T. Nakajima, and H. Wake, FEMS Microbiol. Lett. 29 (1985) 211.
- [26] F. Chen, X. Yang, and Q. Wu, Building and Environment 44 (2009) 1088.
- [27] L. Zan, W. Fa, T. Peng, and Z. Gong, J. Photochem. Photobiol., B 86 (2007) 165.
- [28] Z. X. Lu, L. Zhou, Z. L. Zhang, W.L. Shi, Z. X. Xie, H. Y. Xie, D. W. Pang, and P. Shen, Langmuir 19 (2003) 8765.
- [29] H. M. Yadav, T. V. Kolekar, S. H. Pawar, and J.S. Kim, J. Mater. Scie. Mater. in Medi. 27 (2016) 1.
- [30] C. Trapalis, P. Keivanidis, G. Kordas, M. Zaharescu, M. Crisan, A. Szatvanyi, and M. Gartner, Thin Solid Films 433 (2003) 186.
-



- 
- [31] T. A. Egerton, S. A. Kosa, and P. A. Christensen, *Phys. Chem. Chem. Phys* 8 (2006) 398.
- [32] A. A. Ashkarran, M. Fakhari, and M. Mahmoudi, *RSC Adv.* 3 (2013) 18529.
- [33] S. D. Perera, R. G. Mariano, K. Vu, N. Nour, O. Seitz, Y. Chabal, and K. J. Balkus Jr, *ACS Catal.* 2 (2012) 949.
- [34] H. Yadav, T. Kolekar, A. Barge, N. Thorat, S. Delekar, B. Kim, and J. Kim, *J. Mater. Sci. Mater. Electro.* 27 (2016) 526.
- [35] H. M. Yadav, S. V. Otari, R. A. Bohara, S. S. Mali, S. H. Pawar, and S. D. Delekar, *J. Photochem. Photobiol., A*, 294 (2014) 130.
- [36] W. Feng, Y. Feng, Z. Wu, A. Fujii, M. Ozaki, and K. Yoshino, *J. Phys.: Condens. Matter*, 17 (2005) 4361.
- [37] L. Chen, X. Pang, G. Yu, and J. Zhang, *Adv. Mater. Lett.* 1 (2010) 75.
- [38] K. Gupta, R. Singh, A. Pandey, and A. Pandey, *Beilstein J. Nanotechnol.* 4 (2013) 345.
- [39] A. Corrias, G. Mountjoy, D. Gozzi, and A. Latini, *Nanotechnology* 18 (2007) 485610.
- [40] F.J. Zhang and W.C. Oh, *Bull. Korean Chem. Soc.* 31 (2010) 1981.
- [41] C. Karunakaran, G. Abiramasundari, P. Gomathisankar, G. Manikandan, and V. Anandi, *J. Colloid Interface Sci.* 352 (2010) 68.
- [42] J. Zhu, F. Chen, J. Zhang, H. Chen, and M. Anpo, *J. Photochem. Photobiol., A*, 180 (2006) 196.
- [43] D. Gu, Y. Lu, and B. Yang, *Chem. Commun.* (2008) 2453.
- [44] H.C. Hsu, I. Shown, H.Y. Wei, Y.C. Chang, H.Y. Du, Y.G. Lin, C.A. Tseng, C.H. Wang, L.C. Chen, and Y.C. Lin, *Nanoscale* 5 (2013) 262.
- [45] X. Yan, B. K. Tay, and Y. Yang, *J. Phys. Chem. B* 110 (2006) 25844.
- [46] A. E. Vilian, V. Veeramani, S. M. Chen, R. Madhu, C. H. Kwak, Y. S. Huh, and Y.K. Han, *Sci. Rep.* 5 (2015)
-

- [47] N. D. Abazović, L. Mirengi, I. A. Janković, N. Bibić, D. V. Sojic, B. F. Abramovic, and M. I. Comor, *Nanoscale Res. Lett.* 4 (2009) 518.
- [48] J. Yu, T. Ma, and S. Liu, *Phys. Chem. Chem. Phys.* 13 (2011) 3491.
- [49] T. A. Saleh and V. K. Gupta, *J. Colloid Interface Sci.* 371 (2012) 101.
- [50] M. Dahl, Y. Liu, and Y. Yin, *Chem. Rev.* 114 (2014) 9853.
- [51] Y. S. Kim, E. S. Park, S. Chin, G.N. Bae, and J. Jurng, *Powder Technol.* 215 (2012) 195.
- [52] P.C. Maness, S. Smolinski, D. M. Blake, Z. Huang, E. J. Wolfrum, and W. A. Jacoby, *Appl. Environ. Microbiol.* 65 (1999) 4094.
- [53] K. Ishibashi, A. Fujishima, T. Watanabe, and K. Hashimoto, *Electrochem. Commun.* 2 (2000) 207.
- [54] P. Demchick and A. L. Koch, *J. Bacteriol.* 178 (1996) 768.
- [55] L. K. Adams, D. Y. Lyon, and P. J. Alvarez, *Water. Res.* 40 (2006) 3527.
- [56] Y. H. Tsuang, J. S. Sun, Y. C. Huang, C. H. Lu, W. H. S. Chang, and C. C. Wang, *Artif. Organs.* 32 (2008) 167.

# Chapter 8

## Visible Light Assisted Antibacterial paint (VLAAP)



Photochemical &  
Photobiological  
Sciences

**Engineering the paint with light assisted control of hospital  
acquired infections**

Journal:	Photochemical & Photobiological Sciences
Manuscript ID	Draft
Article Type:	Paper
Date Submitted by the Author:	n/a
Complete List of Authors:	Koli, Valmiki; D. Y. Patil Univeristy, Kolhapur Delekar, Sagar; D. Y. Patil University, Kolhapur Pawar, Shivaji; D.y. Patil Univeristy Kolhapur , Center for Interdisciplinary Research Lab

SCHOLARONE™  
Manuscripts



---

### 8.1 Introduction

Whole world is continuously suffering with Hospital Acquired Infections (HAIs), this directly contributing towards morbidity, mortality and increased medical costs [1, 2]. HAIs are caused due to range of microorganisms including Methicillin resistant *Staphylococcus aureus* (MRSA), *Clostridium difficile* (*C. difficile*) and *Escherichia coli* (*E. Coli*) [3, 4]. The European Centre for Disease Prevention and Control (2013) estimated more than 4,000,000 HAIs occur across the Europe every year and of these approximately 37,000 die as a direct consequence [5, 6]. Similar condition of HAIs found in the whole world. The United States Center for Disease Control and Prevention (CDC), found that approximately 4% of patients in the United States acquire HAIs, equivalent to 7,28,000 infections per year, and 75,000 of patients die during hospitalization [5, 7]. Since a last decade, CDC has implemented many strategies, including surveillance, inspection, and improved guidelines to reduce the rate of HAIs [8, 9]. Especially, there are mainly three types of infection such as central line-associated bloodstream infections, catheter-associated urinary tract infections and surgical site infections. MRSA infections, and *C. difficile* infections are increased the HAIs rate. In addition, surfaces are also potential reservoirs of other bacteria to cause HAIs and therefore, in hospitals, contaminated surfaces make an important contribution to HAIs and other diseases [10]. Pathogenic micro-organisms are capable of surviving on surfaces of healthcare facilities for long time, and they can be transmitted through touch by hospital staff and patients [11-13]. Researchers revealed that, the bacterial colonization occurs on a variety of hospital surfaces such as: beds operation tables, walls, door handles, mops, telephones, computers and keyboards, taps, pens, stethoscopes, X-ray cassettes, and sterile packaging, etc. [11, 13, 14]. Number of cleaning and disinfection strategies are used to control HAIs caused by pathogenic bacteria, although the common cleaning and disinfection strategies were unbaled to remove complete patho-

genic bacteria as these pathogens were rapidly reproduce in moist and warm conditions [15]. Therefore, it is necessary to think seriously and develop the best alternative techniques to thwart or diminish pathogen transmission in healthcare facilities. To control bacterial contamination completely, the self-sterilizing surfaces are capable way to reduce complete bacterial infection from contaminated surfaces and also an alternative approach to inhibit the spread of HAIs in healthcare facilities as an extra strategy to cleaning.

In self-sterile surfaces, the various techniques such as soft and hard surfaces, including silver or copper-coated surface [16], self-cleaning surfaces, and enzyme or bacteriophage-immobilized surfaces [17], TiO<sub>2</sub> coated surfaces, attract great attention from the all above methods. Among them, TiO<sub>2</sub> coated surfaces use TiO<sub>2</sub> as the host materials for killing a wide range of micro-organisms including bacteria, fungi, viruses, and algae, and researchers have also proven that TiO<sub>2</sub> NPs are commonly applicable in medical devices, such as film, glass and polymers, for different purposes [18]. Photo-inactivation activity of TiO<sub>2</sub> NPs is depends on generation of reactive oxygen species (ROS) which damage the bacterial cell wall and ultimately cell death occurred [19, 20]. But, TiO<sub>2</sub> NPs or its surfaces require UV light active material in photo-inactivation of bacteria; which is the serious ambiguity for killing the bacteria. Hence, in the literature, there are many strategies to modify it for its visible activity and these are metal doping, non-metal doping, and the formation of nanocomposite with carbon nanostructures, polymers, etc. [19-21].

Recently, our group revealed photocatalytic antibacterial activity of Fe-containing TiO<sub>2</sub> NPs against gram-negative and gram-positive bacteria under fluorescent light [22]. Akhavan et al. reported the visible light photo-inactivation of Gram-negative bacteria using CNT-doped TiO<sub>2</sub> thin films formed by a dip-coating method [23]. After modification TiO<sub>2</sub> NPs become visible light active material and useful for photo-inactivation bacteria, but the time required

for photo-inactivation is more as compare to UV light exposure. Therefore there is scope to develop a visible light active antibacterial agent with rapid photo-killing of bacteria.

In addition to the host material, it is well known that a few dyes are widely used in the histological stains for bacterial classification like Toluidine blue O (TBO), Methylene blue (MB) and Crystal violet (CV) dyes [24]. Researchers found that, these dyes are also light activated materials and showing photo-inactivation of bacteria in the white light. These dyes are capable of generating singlet oxygen ( $^1\text{O}_2$ ) as well as ROS under light exposure and these species are damaging the bacterial cell wall resulting the inactivating enzymes and DNA leads to cell death. But the generation of these species by these dyes depends on parameter's such as concentration of dye, intensity of light and exposure time [24]. Recently, Parkin et al. studied the various applications of CV, TBO, and MB dyes with polymers to produce antimicrobial surfaces for use in medical devices including tracheal or urinary catheters and tubes for intravenous drips [25]. They have also shown that the incorporation of gold (Au) NPs into a dye impregnated polymer pointedly improved the photo-inactivation of bacteria [26].

Although there are various techniques available for fabrication of antibacterial surface like dip coating, chemical vapor deposition, spin coating, hydrothermal and solvothermal, however these require costly instrumental setup as well high temperature [20, 24]. So, there is a need to develop the antibacterial surface with simple, ease, low cost experimental setup with room or low temperature. In this work, we have used sol-gel method for synthesis Fe-doped  $\text{TiO}_2$ -MWCNTs (Fe- $\text{TiO}_2$ -MWCNTs) nanocomposite (NCs) with CV dye for preparation of visible light activated antibacterial paint (VLAAP). The structural morphological properties of ingredients in VLAAP were studied by XRD analysis and optical properties was also studied by using UV-vis spectrophotometer. The photo-inactivation of bacteria using VLAAP was

tested against Gram-positive *S. aureus* and Gram-negative *E. coli* under visible light irradiation. The photo-inactivation experimental results confirm the synthesized VLAAP is efficient and effective for photo-killing of bacteria rapidly.

### 8.2. Preparation of light activated antibacterial paint (VLAAP)

Fe-TiO<sub>2</sub>-MWCNTs (Fe-TC) NCs powders was synthesized by using earlier reported method [20, 22]. 0.2 g of this synthesized Fe-TC powder was dispersed in 5 mL of alcoholic CV dye solution by ultra-sonication. Then, this whole mixture was stirred with a mixture of 4 mL (10 wt. %) ethyl cellulose and 0.75 g of  $\alpha$ -terpineol for 5 h at room temperature. Thereafter, the content was grinded to remove excess alcohol up to paste formation. The paste was deposited on clean glass surface by using doctor blade technique and then deposited substrate was dried at room temperature for 24 h. After this, the coated glass surface was washed with ethanol and deionized water to remove the unanchored dye moieties. The different antibacterial surfaces were prepared using the similar protocol with varying the concentration of alcoholic dye solution. In present investigation, we have used the various concentrations of CV dye like 250 ppm, 500 ppm, 750 ppm, 1000 ppm and their respective surfaces are denoted as VLAAP 250, VLAAP 500, VLAAP 750 and VLAAP 1000.

### 8.3 Experimental setup for antibacterial testing of VLAAP

To study photo-inactivation activity of VLAAP, the two model bacterial species were selected. These selected bacterial species were cultured on nutrient agar plates at 37 °C for 24 h. The bacterial suspensions were prepared in 5 mL saline solutions to obtain a final concentration of bacteria in 10<sup>6</sup> CFU/mL<sup>-1</sup>. After preparation of final bacterial suspension, 25  $\mu$ L of bacterial suspension was inoculated on to the VLAAP coated glass surface and a sterile



glass cover slip ( $2 \times 2$  cm) was placed on top to ensure good contact between the bacteria and the surface of the sample. The sample were kept in petri dishes containing wet filter paper to maintain humidity, and exposed to visible light with eight fluorescent lamps (Philips TLD, 8 W,  $\lambda > 400$  nm,  $5 \text{ mW cm}^{-2}$ ) and also similar setup run in dark [24]. After 1 h light exposure, samples were placed in 5 ml PBS solution. From this solution  $100 \mu\text{L}$  of solution was spread on Mueller–Hinton agar plates and incubated at  $37^\circ\text{C}$  for 24 h. The standard plate count method was used to determine viable numbers of cells as  $\text{CFU mL}^{-1}$  [20]. The same experiments repeated for three times and average data is presented here.

### 8.4 Characterization

UV–vis absorption spectra of VLAAP coated glass slide were measured from 400 to 800 nm using UV–vis Spectrometer (3092 lab India). To determine structural parameters, X-ray diffraction (XRD) patterns of the samples were recorded on X-ray diffractometer (Bruker D 8-advance) using  $\text{Cu K}\alpha$  ( $1.5406 \text{ \AA}$ ) radiation in the  $2\theta$  range from  $20$ – $80^\circ$ . The equilibrium water contact angle of the VLAAP was measured. A droplet ( $\sim 5 \mu\text{L}$ ) of deionized water was dropped onto the surface of the samples by gravity from a gauge 27 needle, the samples were photographed side on and the images were analyzed using Surf tens 4.5 software

#### 8.4.1 UV-visible spectrophotometer analysis

The different four concentrations of CV dye are chosen for preparation of visible VLAAP surfaces. Fig.8.1 shows the photographs of VLAAP coated on the glass side. The color of Fe-TC NCs thin film is whitish black; while CV incorporated VLAAP surfaces has violet in color. It is observed that the violet color of VLAAP surfaces became more intense with CV concentration.

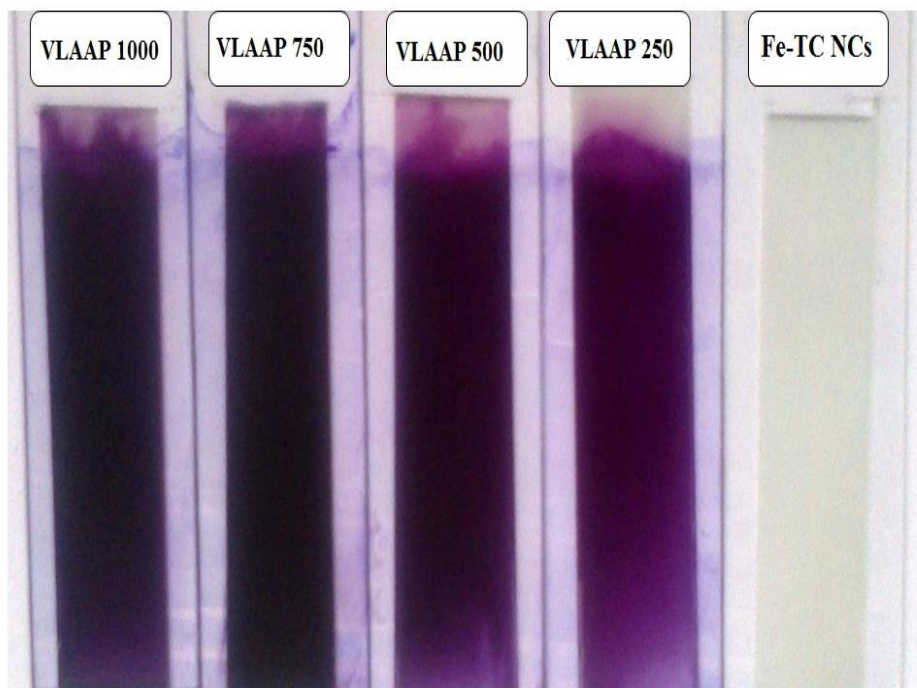


**Fig.8.1 Fe-TC NCs and VLAAP coated on glass slide with different concentration.**

During UV-visible measurement, there was ambiguity in the optical absorption spectra; which is due to intensity detection limit of spectrophotometer beyond 100 ppm dye concentration in VLAAP samples. To overcome this problem, we have prepared the VLAAP surfaces with low dye concentration from 10 to 100 ppm, and thereafter absorbance of VLAAP surfaces was measured using UV-visible spectrophotometer in range of 350 to 800 nm; which is shown in Fig. 8.2. All spectra show the characteristics absorption peak at 584 nm, and its peak intensity was increased with CV concentration [27]. This result revealed that the light absorbance ability of VLAAP surfaces was increased with increasing concentration of dye.

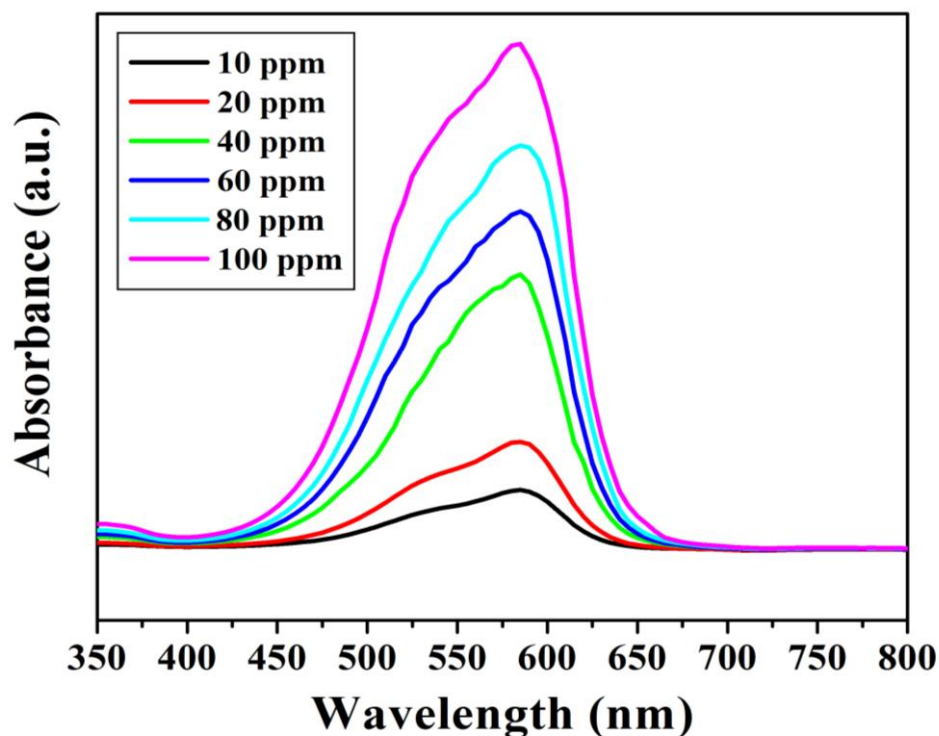


**Fig. 8.2.** UV–vis absorption spectra of VLAAP with various concentrations of 10, 20, 40, 60, 80, and 100 ppm

#### 8.4.2 XRD analysis

Fig. 8.3 shows the XRD patterns of bare Fe-TC and different VLAAP samples. The representative characteristic peaks of Fe-TC are matches with anatase phase of  $\text{TiO}_2$  NPs (JCPDS card-21-1272); therefore it would have higher photocatalytic activity due to presence of anatase phase of  $\text{TiO}_2$  as compared to rutile and brookite phases [28]. XRD patterns of different VLAAP samples have similar nature with respect to FTC; revealing the presence of its characteristics peaks. With CV dye, the intensity of characteristics peaks decreases; which is due to presence of low X-ray scattering power of lighter atoms present in dye. The crystallite size of all samples was calculated by using Scherer's equation [29]. It is found in the range of 8 to 15 nm. Fe-TC and VLAAP showing good crystalline nature up to 750 ppm. The CV dye concentration afterword the crystalline nature of Fe-TC converts to amorphous form

due to excess dye shielding at the surfaces of Fe-TC NCs and hence peak intensity decrease.

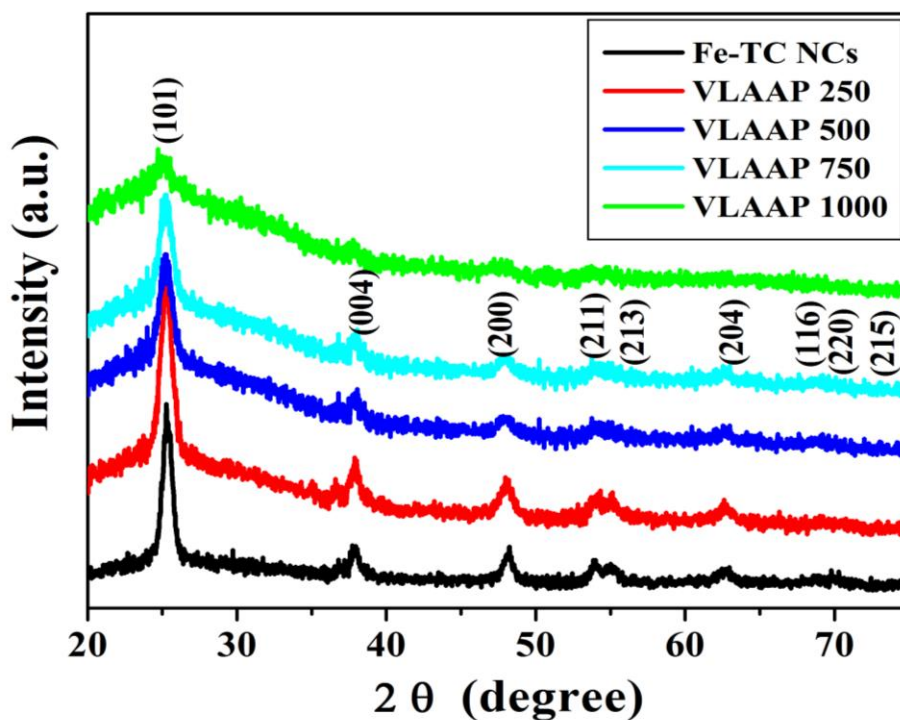


**Fig. 8.3.** XRD patterns of FTC and VLAAP coated on a glass slide with different concentration of CV dye.

#### 8.4. 3 Water contact angles measurement of VLAAP

The VLAAP coated on glass slide was also used to determine contact angle studies. The change in water contact angle of the different VLAAP samples is shown in Fig. 8.4 (a) and also contact angles values are listed in Table 8.1. The images of contact angle measurements for different VLAAP samples are shown in Fig. 8.4 (b). Fe-T NPs coated glass surface is having highly hydrophilic nature therefore the images of Fe-T NPs is not shown here. With increasing concentration of CV dye in VLAAP samples, there is increase in the contact angle; which confirms the increase in hydrophobic nature of samples [26, 30]. The higher hydrophobic nature of samples would be help to reduce HAIs [31].

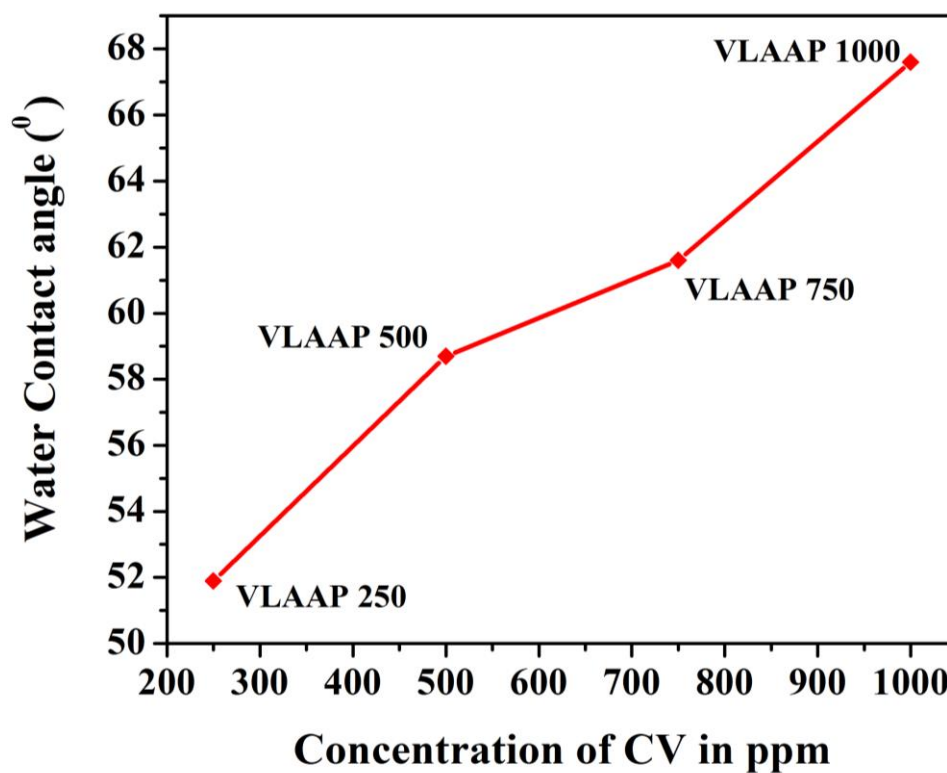


Fig. 8.4 (a). Water contact angles measurement of VLAAP coated on glass slide

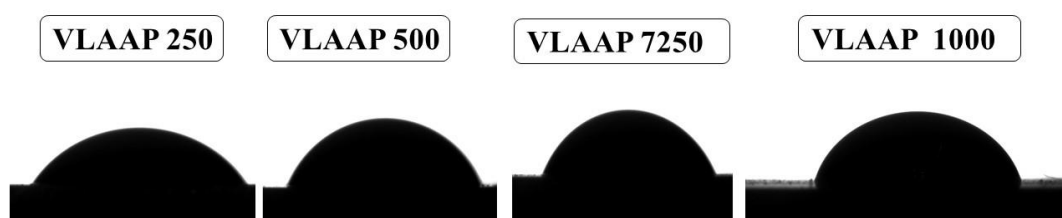


Fig. 8.4 (b). Images of water contact angles measurement

**Table 8.1 Average contact angle measurements (°) of VLAAP**

<b>Samples</b>	<b>Water contact angle (°)</b>
<b>VLAAP 250</b>	<b>51.9</b>
<b>VLAAP 500</b>	<b>59.4</b>
<b>VLAAP 750</b>	<b>61.6</b>
<b>VLAAP 1000</b>	<b>67.2</b>

### **8.5. Leaching Test**

To know the stability of anchored dye, the prepared VLAAP samples was dipped into the solution under leaching test. The piece of 2x2 cm size VLAAP coated on glass slide was immersed in PBS solution and CV dye release from VLAAP was determined by using UV visible spectrophotometer. The LAAP samples were immersed in PBAS solution for 72 h [32]. In VLAAP 1000 sample, the highest amount (20.0 ppm) of dye was released in 12 h. Similarly, VLAAP 750, 500 and 250 samples were releasing CV dye amount of 15.0, 9.0 and 4.0 ppm respectively after 12 h. A plot of CV dye concentration in PBS solution verses Immersion time is shown in Fig. 8.5. The immersion over a period of 60 h the dye release was not observed. The total CV dye released in PBS solution after 72 h. is very low as compared to initial concentration.

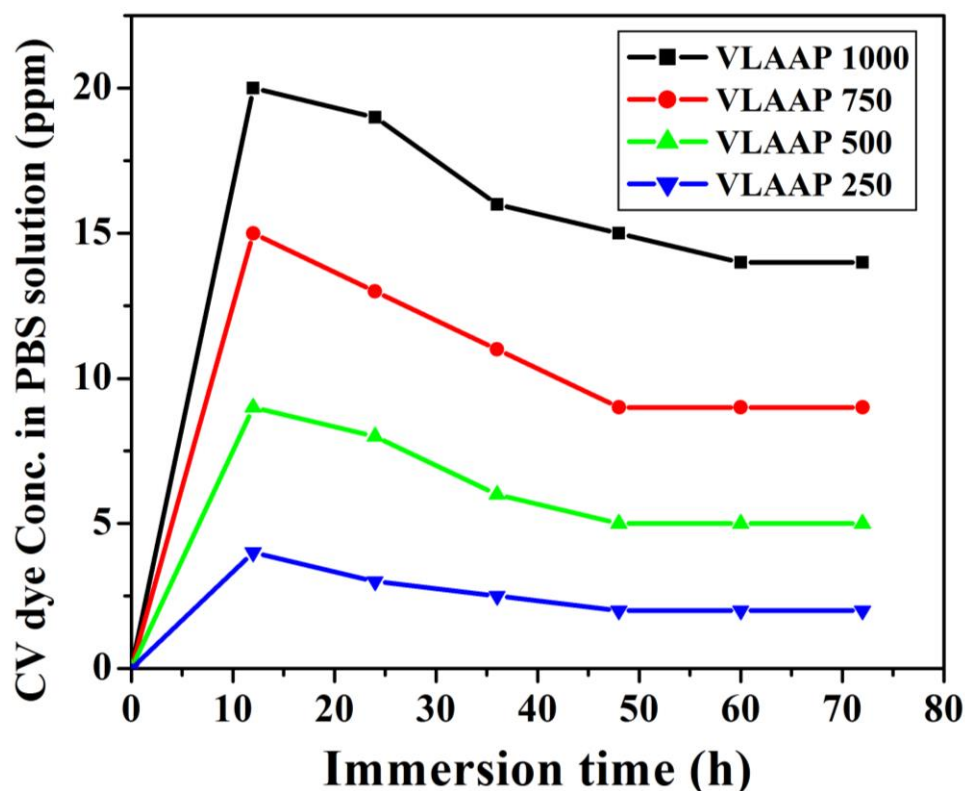


**Fig. 8.5.** Leaching of CV dye from LAAP into PBS solution. The paint coated samples (2 cm × 2 cm) were immersed in 5 mL of PBS for 72 h.

### 8.6. Photo-inactivation of bacteria

To investigate the photo-inactivation capability of VLAAP, two model bacteria were selected gram positive and gram negative bacteria. The whole experiment carried out in sterile condition, to determine the effect of light on photo-inactivation. Fe-TC NCs and VLAAP were treated in dark and visible light irradiation. In the dark condition Fe-TC and VLAAP were not showing any effect on bacterial growth. While after 1h light irradiation on bacterial suspension with Fe-TC NCs and VLAAP showing photo-inactivation of bacteria for both Gram-positive *S. aureus* and Gram-negative *E. coli* bacteria. Control sample without Fe-TC NCs and VLAAP showing heavy growth of bacterial cell this confirms visible light did not show any effect on bacterial cell growth.

Fig. 8.6 shows the percentage survival of *S. aureus* under visible light irradiation on bacterial suspension in the presence of Fe-TC NCs and VLAAP for 1h time. Fe-TC NCs shows about 30% photo-inactivation of bacteria. While VLAAP 750 shows 100% photo-inactivation of *S. aureus* within 1h time. While VLAAP 250, 500 and 1000 shows 50%, 70% and 98% respectively photo-inactivation of bacteria. The increased CV dye concentration in VLAAP increases the photo-inactivation activity up to 750 ppm while VLAAP 1000 showing 90% photo-killing of bacteria. This due to excess concentration of the dye molecule in paint shielding the Fe-TC, which may be directly effect on rate ROS generation. Therefore VLAAP 1000 show less photo-inactivation as compared to VLAAP 750.

Fig. 8.7 shows the photo-inactivation activity of Fe-TC NCs and LAAP against Gram-negative *E.coli* under visible light irradiation on bacterial suspension. Fe-TC NCs showing only 20% of bacteria killing after 1h visible light irradiation while VLAAP showing better photo-inactivation of bacteria VLAAP 750 showing 100% killing of *E. coli* and VLAAP 1000, 500 and 250 showing 90%, 60% and 30% of photo killing of bacteria.



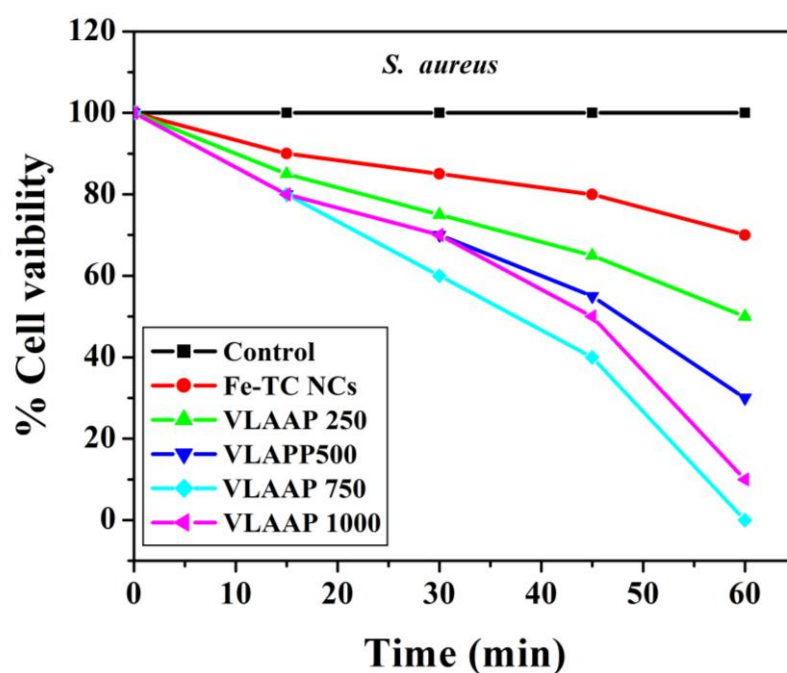


Fig. 8.6. % Survival of *S. aureus* with Fe-TC and LAAP under visible light irradiation

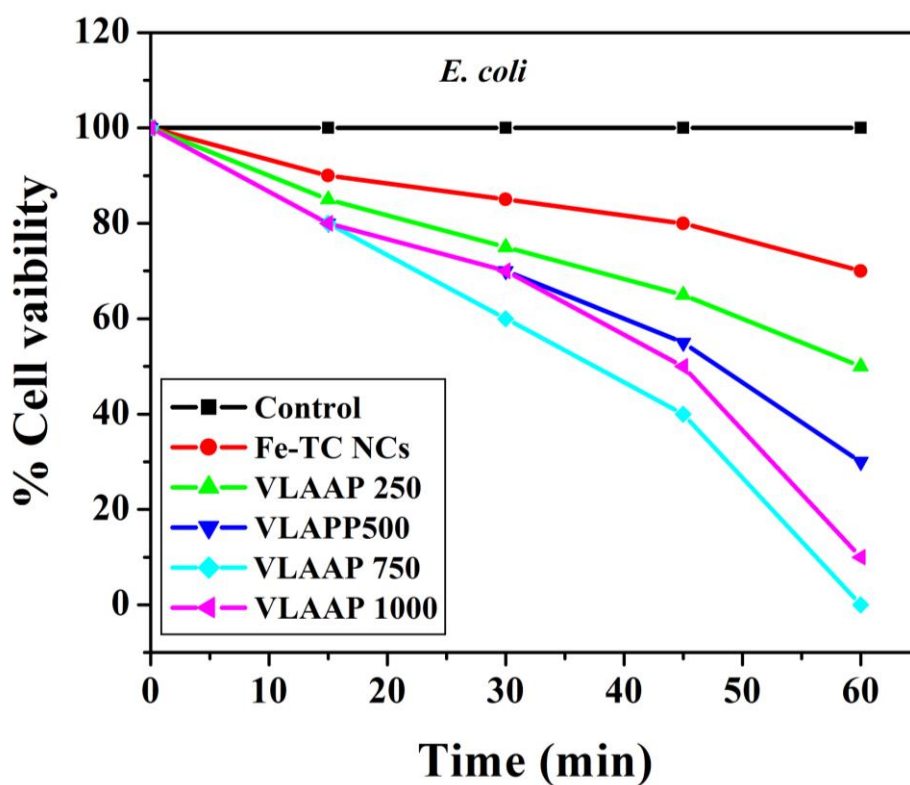


Fig. 8.7 % Survival of *E. coli* with Fe-TC and VLAAP under visible light irradiation

As compared to Gram-positive bacteria, Gram-negative bacteria show more resistance to photo-killing of bacteria this due to the cell wall nature of gram negative bacteria [20]. The photo-inactivation of bacterial experiments confirms the VLAAP is having the capability of rapid photo-killing of bacteria. Therefore, VLAAP can be used to control HAIs by coating the surfaces with VLAAP with advanced disinfection technique. The photo-inactivation mechanism of Fe-TC NCs is well known. In Fe-TC NCs, MWCNTs may act as electron scavengers means it accepts electron from conduction band of  $\text{TiO}_2$  which helps to reduce the recombination rate of electron whole pair which ultimately increase the photocatalytic property of Fe-TC NCs [33]. Another way is MWCNTs act as photosensitizer and itself absorbs the photon energy and thereafter the electrons are transferred to the conduction band of  $\text{TiO}_2$ , this also reduces the recombination rate of electron whole pair and helps to generate high rate of ROS which increase the photocatalytic property [34].

Also the increased in CV dye concentration in VLAAP showing higher photo-inactivation of bacteria due to CV dye present in the paint is excited to a triplet state via an inter system crossing from a slightly higher energy, shorter lived excited singlet state. This formed triplet state dye molecules can undergo one of two photochemical pathways quenching by molecular oxygen including the production of singlet oxygen ( $^1\text{O}_2$ ), or interaction with biomolecules in the area generating radical species [26]. The generated  $^1\text{O}_2$  and radical species can initiate multisite attack on bacteria in the vicinity effecting cell death [32]. In VLAAP paint CV dye molecule acts as photosensitizer and absorb approx.-imately 100% irradiated light, which itself produces oxygen singlet and helps to Fe-TC NCs for generating high rate ROS.

VLAAP developed in this study can be applicable to a wide range of substrate including metal, glass, paper and polymer. However, the preparation of VLAAP is very easy and surface treatment is simple. Therefore possibly VLAAP can be used in nursing homes, clinical care facilities including surgery

centers, dialysis centers, and applied in the home for decoration, and on toilet and kitchen surfaces [24]. To apply in daily life the toxicity effect of CV dye is well studied previously and CV has been widely used in medicine for over 100 years [35]. It is used in diluted form in antiseptics for external wounds from centuries. Leaching test shown only 20 ppm dye was released in PBAS solution from paint contain 250, 500, 750 and 1000 ppm concentration of dye therefore it is very less amount of dye released. The concentration for dye used for preparation is very less compared to the concentration (20000 ppm) causing dermal irritation or sensitization in long-term clinical assessment [36]. Therefore the prepared VLAAP is biocompatible due to very less concentration.

### 8.7 Photocatalytic stability of VLAAP

The photocatalytic stability of VLAAP was investigated by using same experimental procedure for phot-inactivation bacteria under visible light. To carry out this experiment in the Gram-positive species *S. aureus* was selected. After complete inactivation of *S. aureus*, afterword VLAAP coated surface is washed with deionized water for serval time and VLAAP coated surface dried in room temperature for 24 h. The experimental procedure was repeated for seventh times to check VLAAPs photo stability and reusability [44]. Fig. 8.8 shows there are no noticeable changes in percentage photo-inactivation of bacteria up to two cycles. Afterword the rate of photo-inactivation decreases 3<sup>rd</sup> and 4<sup>th</sup> cycle shows 95% and 85% killing of bacteria respectively. While 5<sup>th</sup>, 6<sup>th</sup>, and 7<sup>th</sup> shows 78%, 65% and 60% killing of bacteria. The decrease in rate of photo-inactivation of bacteria may be due to loss of FTC NCs during washing of VLAAP coated surface with deionized water. As well as there is the possibility of CV dye degradation by FTC NCs.

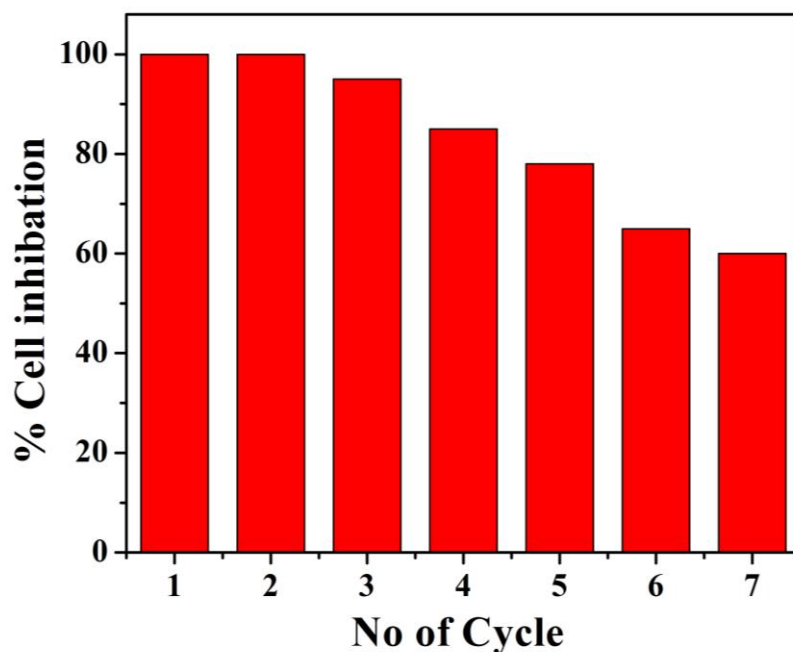


**Fig. 8.8 Photocatalytic stability and reusability of VLAAP**

### 8.7. Conclusion

In this work, we incorporated CV dye in Fe-TC NCs and successfully prepared VLAAP. The structural and optical properties of VLAAP were studied by using XRD and UV-visible spectrophotometer. XRD patterns reveal the crystalline nature of synthesized paint as well as confirm the presence of most photoactive anatase phase of  $\text{TiO}_2$  in VLAAP. UV-visible absorbance study confirms the absorbance of VLAAP increased with increasing concentration CV dye in paint. Leaching test proves the very good stability of VLAAP in PBS solution. Water contact angle measurement confirms the increase in hydrophobic nature of VLAAP. The photo-inactivation study of Gram positive *S aureus* and Gram negative *E.coli* bacteria, confirmed that the 100% photo-killing of bacteria observed in 1h. Therefore, it is a first time for the dye molecule and photoactive nanocomposite used for photo-inactivation of bacteria. Due to this it is expected that this potent VLAAP will be useful in

healthcare applications to reduce surface bacterial contamination and, control the HAIs.

In this study, we did not investigate about the enhancing the photo stability of VLAAP under visible light irradiation. This is an important investigation to maximize the photo-inactivation rate of VLAAP. Thus we are considering experiment regarding enhancing photo-stability of VLAAP in future study.

---

### Reference

- [1] W. G. Kohn, A. S. Collins, J. L. Cleveland, J. A. Harte, K. J. Eklund, and D. M. Malvitz, *MMWR Recomm. Rep.* 52 (2003) 1.
- [2] D. Reed and S. A. Kemmerly, *Ochsner J.* 9 (2009) 27.
- [3] R. E. Gilbert and M. Harden, *Curr. Opin. Infect. Dis.* 21 (2008) 235.
- [4] L. Váradi, J. L. Luo, D. E. Hibbs, J. D. Perry, R. J. Anderson, S. Oreng-ae and P.W. Groundwater. *Chem. Soc. Rev.*, 2017
- [5] S. Magill, J. Edwards, W. Bamberg, W. Hellinger, J. Cohen, T. van der Kooi, J. Mannien, J. Wille, and B. van Benthem, *N. Engl. J. Med.* 2014 (2014) 2542.
- [6] I. Humphery-Smith, *Pharm. Pharmacol.* 5 (2014) 1192.
- [7] R. R. Roberts, B. Hota, I. Ahmad, R. D. Scott, S. D. Foster, F. Abbasi, S. Schabowski, L. M. Kampe, G. G. Ciavarella, and M. Supino, *Clin. Infect. Dis.* 49 (2009) 1175.
- [8] M. A. Dudeck, L. M. Weiner, K. Allen-Bridson, P. J. Malpiedi, K. D. Peterson, D. A. Pollock, D. M. Sievert, and J. R. Edwards, *Am. J. Infect. Control.* 41 (2013) 1148.
- [9] A. Margaret, J. R. Edwards, K. Allen-Bridson, C. Gross, P. J. Malpiedi, K. D. Peterson, D. A. Pollock, L. M. Weiner, and D. M. Sievert, *Am. J. Infect. Control.* 43 (2015) 206.
- [10] V. Hsu, *Am. Fam. Phys.* 90 (2014).
- [11] K. Page, A. Correia, M. Wilson, E. Allan, and I. P. Parkin, *J. Photochem. Photobiol.; A.* 296 (2015) 19.
- [12] S. Noimark, C. W. Dunnill, and I. P. Parkin, *Adv. Drug Delivery Rev.* 65 (2013) 570.
- [13] C. L. Pankhurst and W.A. Coulter, *Basic guide to infection prevention and control in dentistry* (2017).
- [14] S. Bures, J. T. Fishbain, C. F. Uyehara, J. M. Parker, and B. W. Berg, *Am. J. Infect. Control.* 28 (2000) 465.

- 
- [15] K. Page, M. Wilson, N. J. Mordan, W. Chrzanowski, J. Knowles, and I. P. Parkin, *J. Mater. Sci.* 46 (2011) 6355.
- [16] I. A. Hassan, I. P. Parkin, S. P. Nair, and C. J. Carmalt, *J. Mater. Chem.; B.* 2 (2014) 2855.
- [17] R. C. Pangule, S. J. Brooks, C. Z. Dinu, S. S. Bale, S. L. Salmon, G. Zhu, D. W. Metzger, R. S. Kane, and J. S. Dordick, *ACS Nano* 4 (2010) 3993.
- [18] L. Caballero, K. Whitehead, N. Allen, and J. Verran, *J. Photochem. Photobiol.; A.* 202 (2009) 92.
- [19] H. M. Yadav, S. V. Otari, V. B. Koli, S. S. Mali, C. K. Hong, S. H. Pawar, and S. D. Delekar, *J. Photochem. Photobiol.; A.* 280 (2014) 32.
- [20] V. B. Koli, A. G. Dhodamani, A. V. Raut, N. D. Thorat, S. H. Pawar, and S. D. Delekar, *J. Photochem. Photobiol.; A.* 328 (2016) 50.
- [21] R. Barkul, V. Koli, V. Shewale, M. Patil, and S. Delekar, *Mater. Chem. Phys.* 173 (2016) 42.
- [22] H. M. Yadav, T. V. Kolekar, S. H. Pawar, and J. S. Kim, *J. Mater. Sci. Mater. Med.* 27 (2016).
- [23] O. Akhavan, R. Azimirad, S. Safa, and M. Larijani, *J. Mater. Chem.* 20 (2010) 7386.
- [24] G. B. Hwang, E. Allan, and I. P. Parkin, *ACS Appl. Mater. Inter.* 8 (2015) 15033.
- [25] C. W. Dunnill, Z. A. Aiken, J. Pratten, M. Wilson, D. J. Morgan, and I. P. Parkin, *J. Photochem. Photobiol.; A.* 207 (2009) 244.
- [26] S. Noimark, C. W. Dunnill, C. W. Kay, S. Perni, P. Prokopovich, S. Ismail, M. Wilson, and I. P. Parkin, *J. Mater. Chem.* 22 (2012) 15388.
- [27] M. F. H. Al-Kadhemy and W. H. Abaas, *Atti della Fondazione Giorgio Ronchi* 67 (2012) 735.
- [28] H. M. Yadav, J. S. Kim, and S. H. Pawar, *Korean J. Chem. Eng.* 33 (2016) 1989.
-

## Chapter 8

- 
- [29] S. Delekar, H. Yadav, S. Achary, S. Meena, and S. Pawar, *Appl. Surf. Sci.* 263 (2012) 536.
  - [30] E. Ozkan, F. T. Ozkan, E. Allan, and I. P. Parkin, *RSC Adv.* 5 (2015) 8806.
  - [31] B. Gottenbos, D. W. Grijpma, H. C. van der Mei, J. Feijen, and H. J. Busscher, *J. Antimicrob. Chemother.* 48 (2001) 7.
  - [32] E. Ozkan, E. Allan, and I. P. Parkin, *RSC Adv.* 4 (2014) 51711.
  - [33] D. S. Su, S. Perathoner, and G. Centi, *Chem. Rev.* 113 (2013) 5782.
  - [34] K. Rajasekar, S. Thennarasu, R. Rajesh, R. Abirami, K. B. Ameen, and A. Ramasubbu, *Solid State Sci.* 26 (2013) 45.
  - [35] S. N. Moreno, *Mem. Inst. Oswaldo. Cruz.* 83 (1988) 308.
  - [36] M. Saji, S. Taguchi, K. Uchiyama, E. Osono, N. Hayama, and H. Ohkuni, *J. Hosp Infect.* 31 (1995) 225.



## **Chapter 9**

### **Summary and Conclusions**





---

### 9.1 Competent Components of the Thesis

Nanomaterials have been an emerging and promising materials for environmental remediation. Particularly as  $\text{TiO}_2$  NPs is a benchmark photocatalyst for the successful removal of organic pollutants in both liquid and gas phases because of its photocatalytic efficiency photo-stability, reusability, non-toxicity, environmentally benign nature, chemical inertness, strong oxidizing power etc. Recently the photocatalytic bacterial studies of  $\text{TiO}_2$  NPs based NCs received increasing attention. Photocatalytic antibacterial activity is the process in which the photocatalytic inactivation of bacteria is achieved by absorption of light energy by the photocatalyst. Besides its semiconducting nature it also act as a very good catalyst for photo-inactivation of bacteria. In the photocatalytic bactericidal process, the  $\text{TiO}_2$  NPs are absorbs light energy and generate the reactive oxygen species (ROS). These ROS act as redox system have strong oxidant and reductant in nature, which help for the inactivation of bacteria.

The photocatalytic inactivation of bacteria depends on various parameter such as phase purity, band gap energy, surface area, crystallite size, method of preparation, type of bacterial species, light intensity, etc. In  $\text{TiO}_2$  NPs, the anatase phase is widely used phase of  $\text{TiO}_2$  as compare to rutile and brookite phase. Even if  $\text{TiO}_2$  NPs has several advantages, and excellent properties but it has few limitations, such as activity is limited to UV light irradiation based on its band gap, high electron-hole recombination and large-scale technical applications. To overcome these limitations, several approaches have been applied to enhance photocatalytic activity of  $\text{TiO}_2$  NPs by increasing active sites of reaction, retardation of electron-hole recombination and visible light catalysis by modifying optical properties of  $\text{TiO}_2$  NPs. In order to extend its activity in the visible light region, we modified the  $\text{TiO}_2$  NPs with carbon nanostructure. In this work, we prepared the nanocomposite between  $\text{TiO}_2$  NPs and MWCNTs. In photocatalytic inactivation of bacteria, MWCNTs has two roles plausibly in presence of  $\text{TiO}_2$  NPs. As per the literature, MWCNTs may

## Chapter 9

---

acts as electron scavengers in the composites. This is due to its highly conductive nature; which accepts the excited electrons from the conduction band of  $\text{TiO}_2$  resulting in the well separation of charge carriers. Another role of MWCNTs is concerned to the photosensitizer and hence itself absorbs the photon energy and thereafter the electrons are transferred to the conduction band of  $\text{TiO}_2$  NPs. These two possible ways ultimately decrease the probability of the recombination of the electron-hole pairs and hence which may results the absorption of higher wavelength visible light which increases the rate of photocatalytic inactivation of bacteria.

Hence, in the present study, an attempt has been made to synthesis  $\text{TiO}_2$ -MWCNTs NCs for photocatalytic inactivation of pathogenic bacteria in presence of visible light.

The aim of the present work is to determine the effect of MWCNTs content on structural, optical properties of  $\text{TiO}_2$  NPs and its application for photocatalytic inactivation of bacteria. The study also contributed in the development of  $\text{TiO}_2$ -MWCNTs NCs by simple sol-gel method at room temperature. The characterizations of the NCs and photo-inactivation studies were demonstrated in the various chapters and summarized in this chapter.

We have successfully synthesized  $\text{TiO}_2$  NPs by sol-gel method at room temperature. The photocatalytic efficiency of  $\text{TiO}_2$  NPs in presence of UV light irradiation strongly depended on their structural optical parameters of catalyst. . The sol-gel method is very simple and cost effective method for getting desired materials. In  $\text{TiO}_2$  NPs, the crystallite size observed in the range  $\sim 8$  nm with optical band gap energy 3.2 eV. The photocatalytic inactivation activity of pure  $\text{TiO}_2$  NPs carried out under dark and UV light with gram-positive and gram-negative bacteria. Under dark  $\text{TiO}_2$  NPs did not show inhibition of bacteria. While in presence of UV light irradiations the complete inactivation of bacteria occurs in 60 min. but  $\text{TiO}_2$  NPs did not shows bactericidal activity in the

visible light. The XRD and Raman analysis confirmed the pure anatase phase of the TiO<sub>2</sub> NPs.

TiO<sub>2</sub> NCs with varying content of MWCNTs were synthesized by sol-gel method and the effect of MWCNTs content on physiochemical properties as well as photocatalytic properties of TiO<sub>2</sub> NPs was studied. XRD studies confirmed that, the all synthesized NCs are dominant with pure anatase phase of TiO<sub>2</sub> NPs. There are no peaks observed for rutile and brookite phase of TiO<sub>2</sub> NPs. TEM analysis revealed non-spherical TiO<sub>2</sub> NPs uniformly anchored on MWCNTs surface. UV-Vis DRS study demonstrated the optical band gap is reduced from 3.2 eV. to 2.6 eV. due to this NCs absorbing visible light.

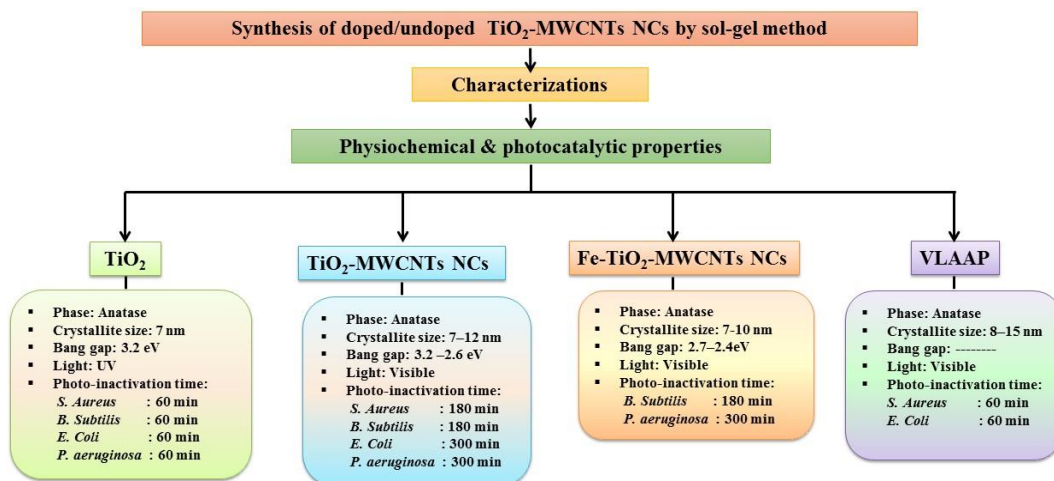
The photocatalytic inactivation of *E. coli*, *P. aeruginosa* and *S. aureus*, *B. subtilis* using TiO<sub>2</sub>-MWCNTs NCs in the presence of visible light ( $\lambda > 420$  nm) has been carried out. These NCs show efficient antibacterial activity under visible light illumination, whereas pure TiO<sub>2</sub> NPs did not show any inhibitory effect on bacteria under visible light exposure. These results suggest that UV light or TiO<sub>2</sub> alone is not effective for photocatalytic disinfection applications. Also, cytotoxicity study reveals that the NCs show better cell viability than pure TiO<sub>2</sub> NPs. Overall, the experimental results suggested that TiO<sub>2</sub>-MWCNTs NPs have been developed as best antibacterial agents against a wide range of microorganisms to prevent and control the persistence and spreading of bacterial infections.

Further to enhance the photocatalytic activity of TiO<sub>2</sub>-MWCNTs NCs, the NCs were prepared between Fe doped TiO<sub>2</sub> and MWCNTs. NCs of Fe-doped TiO<sub>2</sub> with MWCNTs (0.1 to 0.5 wt. %), were prepared by using sol-gel method. The structural and morphological analysis were carried out by using XRD and TEM; which revealed the presence of pure anatase phase and particle sizes in the range of 7-15 nm. XPS was used to determine the surface compositions of the NCs. UV-vis DRS confirming red-shift in the optical absorption edge of NCs with increasing amount of MWCNTs. Photocatalytic

inactivation activity of prepared NCs was studied against Gram-positive *B. subtilis* as well as Gram-negative *P. aeruginosa*. Fe-TiO<sub>2</sub>-MWCNTs (0.5 wt. %) NCs showed higher photo-inactivation efficiency as compared with other NCs. This higher efficiency was supported with photoluminescence (PL) studies which revealed that the Fe-TiO<sub>2</sub>-MWCNTs NCs are capable to generate higher ROS species than that of other NCs. Our experimental result demonstrated that the Fe-TiO<sub>2</sub>-MWCNTs NCs act as efficient antibacterial agents against a wide range of microorganisms.

The synthesized TiO<sub>2</sub>-MWCNTs and Fe-TiO<sub>2</sub>-MWCNTs NCs are efficient NCs for photocatalytic inactivation of bacterial in visible light irradiation. To know their compatibility in applied point of view we have synthesized Visible Light Assisted Antibacterial Paint (VLAAP) by using Fe-TiO<sub>2</sub>-MWCNTs NCs and Crystal violet (CV) dye. The component of VLAAP were characterized by using XRD and UV-visible spectrophotometer. During the preparation of VLAAP various parameter have been optimized for getting better antibacterial. Photo-inactivation experiments revealed that, VLAAP is inactivating both gram- positive as well as gram-negative bacteria within short time. Therefore VLAAP can be used against a wide range of microorganisms to control the hospital acquired infections.

The present work is presented in the following flow diagram



---

### 9.2 Major breakthroughs

- ✓ Designed simple sol–gel method for synthesis of doped/ undoped  $\text{TiO}_2$  NPs as well as its NCs with MWCNTs at room temperature.
- ✓ Pure  $\text{TiO}_2$  NPs show photocatalytic inactivation of bacteria in presence of UV light.
- ✓ Fe doped  $\text{TiO}_2$ -MWCNTs NCs show excellent photocatalytic properties as compared doped/undoped  $\text{TiO}_2$ -MWCNTs NCs.
- ✓ Gram–positive bacteria are more susceptible to photocatalytic activity of photocatalyst than Gram–negative.
- ✓ Tuning of optical band gap of  $\text{TiO}_2$  NPs from UV region to visible region for NCs
- ✓ Preparation of Visible light assisted antibacterial paint successfully using simple method for efficient photo-inactivation of bacteria.

### 9.3 Future scope of the thesis

The present work reveals that the synthesized Fe- $\text{TiO}_2$ -MWCNTs NCs show efficient antibacterial activity towards photocatalytic inactivation of various bacteria species in presence of visible light irradiation. The synthesized NCs and anti-bacterial paint would be optimized so as to obtain prominent candidate for environmental decontaminations. In continuation of present work, different visible light assisted antibacterial paint would be for real time inactivation of microorganisms in hospitals, homes and various public places. These NCs as would be used for surface coating is another option for developing real systems, which is promising for the commercialization of the technology.



# Curriculum Vitae



## **CURRICULUM VITAE**

**Name: Valmiki Balu Koli**

**Ph.D. Student**

**Centre for Interdisciplinary Research**

**D. Y. Patil University, Kolhapur, Maharashtra, India.**

**E-mail:- valmikikoli12@gmail.com**

**Mobile No.: 9623437669**



### **EDUCATIONAL QUALIFICATION**



**Ph.D.: - ( Chemistry); Thesis Submitted (July 2017)**

D. Y. Patil University, Kolhapur.



**M. Sc. :-( Analytical Chemistry); (First Class (72.40%) 2011.)**

Dr.Babasaheb Ambedkar Marathwada University, Sub Campus,  
Osmanabad.



**B.Sc. :-( Second Class (59.40%) 2009.)**

Sawami Vivekanand College, Kolhapur, Shivaji University,  
Kolhapur.



**H.S.C.:-( Second Class (52.00%) 2006.)**

Sambhajirao mane Jr. College Rukadi, Kolhapur Board.



**S.S.C.:-( First Class (68.80%) 2004.)**

Kakasaheb Mane Highschool Rukadi, Kolhapur Board.

### **PERSONAL INFORMATION**

Name : Valmiki Balu Koli

D.O.B : 12 August 1987

Permanent Address : A/P:-Sajani, Tal:-Hatkananagle, Dist:-Kolhapur,  
PIN- 416 115.

Contact Number : Mob.9623437669

Email : [valmikikoli12@gmail.com](mailto:valmikikoli12@gmail.com)

## TITLE OF THESIS

**“Studies on photocatalytic TiO<sub>2</sub>-MWCNTs nanocomposites for antibacterial application”**

## ACADEMIC EXPERIENCE

### Research Experience:

#### **Junior Research Fellow,**

Project:- “Heterojunction nanocomposites of functionalized carbon nanotubes with doped, undoped TiO<sub>2</sub> nanoparticles for solar energy harvesting” Funding

Agency:- Department of Science and Technology New Delhi.

Duration: - **1<sup>st</sup> June 2012 to 31<sup>st</sup> May 2015**

### Teaching Experience:

1. CHB lecturer at Department of chemistry, Dr. B. A. M.U. Sub-Campus, Osmanabad. Duration July 2011 to Nov 2011.
2. Teaching assistant at Department of Medical Physics, D. Y. Patil University, Kolhapur Duration September 2015 to March 2016.

## Awards

1. Worked as **Junior Research Fellow** on DST major research project entitled “Heterojunction nanocomposites of functionalized carbon nanotubes with doped, undoped TiO<sub>2</sub> nanoparticles for solar energy harvesting.” 1<sup>st</sup> June 2012 to 31<sup>st</sup> May 2015.
2. Received International Travel support from SERB under ITS Scheme to attend 19<sup>th</sup> International Conference on “Engineering & Technology,

Computer, and Basic & Applied Sciences” (ECBA- 2017 held from 25-01-2017 to 26-01-2017 in Seoul, South Korea.

3. Received International Travel Fellowship from CICS Chennai to attain 19<sup>th</sup> International Conference on “Engineering & Technology, Computer, and Basic & Applied Sciences” (ECBA- 2017 held from 25-01-2017 to 26-01-2017 in Seoul, South Korea.
4. Best poster presentation award in Emerging Trends in Nanomaterial and Their Application (ETNA-2017) Department of Medical Physics, Center for Interdisciplinary Research, D. Y. Patil University Kolhapur. 2<sup>nd</sup> and 3<sup>rd</sup> June 2017.

#### INTERNATIONAL PUBLICATIONS

1. **VB Koli**, AG Dhodamani, SD Delekar, SH Pawar. In situ sol-gel synthesis of anatase TiO<sub>2</sub>-MWCNTs nanocomposites and their photocatalytic applications. **Journal of Photochemistry and Photobiology A: Chemistry** 333(2017), 40-48. **(Impact Factor = 2.625)**
2. **VB Koli**, SD Delekar, SH Pawar. Photoinactivation of bacteria by using Fe-doped TiO<sub>2</sub>-MWCNTs nanocomposites. **Journal of Materials Science: Materials in Medicine** 27 (2016), (12), 177. **(Impact Factor = 2.325)**
3. **VB Koli**, AG Dhodamani, AV Raut, ND Thorat, SH Pawar, SD Delekar. Visible light photo-induced antibacterial activity of TiO<sub>2</sub>-MWCNTs nanocomposites with varying the contents of MWCNTs. **Journal of Photochemistry and Photobiology A: Chemistry** 328(2016), 50-58. **(Impact Factor = 2.625)**

4. **VB Koli**, AG Dhodamani, KV More, S. F.A. Acquah, DK Panda, SH Pawar, SD Delekar, A simple strategy for the anchoring of anatase titania On multi-walled carbon nanotubes for solar energy harvesting. **Solar Energy** 149(2017) 188-194. **(Impact Factor = 4.018)**
5. RP Barkul, **VB Koli**, VB Shewale, MK Patil, SD Delekar. Visible active nanocrystal-line N-doped anatase TiO<sub>2</sub> particles for photocatalytic mineralization studies, **Materials Chemistry and Physics**, 173, (2016) 42–51. **(Impact Factor = 2.018)**
6. JV Meshram, **VB Koli**, MR. Phadtare, SH Pawar. Anti-microbial surfaces: An approach for deposition of ZnO nanoparticles on PVA-Gelatin composite film by screen printing technique. **Materials Science & Engineering C**, 73, (2017) 257-266. **(Impact Factor = 4.164).**
7. VB Shevale, AG Dhodamani, **VB Koli**, RP Barkul, JP Jadhav, SD Delekar, Efficient degradation of Azorubin S colourant in the commercial jam-jelly food samples using TiO<sub>2</sub>-CoFe<sub>2</sub> O<sub>4</sub> nanocomposites in visible light, **Materials Research Bulletin**. 89 (2017) 79-88. **(Impact Factor = 2.446).**
8. HM Yadav, SV Otari, **VB Koli**, SS Mali, CK Hong, SH Pawar, SD Delekar, Preparation and characterization of copper-doped anatase TiO<sub>2</sub> nanoparticles with visible light photocatalytic antibacterial activity, **Journal of photochemistry and photobiology A: Chemistry**, A: Chemistry 280 (2014) 32–38. **(Impact Factor = 2.625)**
9. ND Thorat, SV Otari, RM Patil, R A Bohara, H M Yadav, **VB Koli**, AK Chaurasia RS Ningthoujam, Synthesis, characterization and bioco-

mpatibility of chitosan functionalized superparamagnetic nanoparticles for heat activated curing of cancer cells **Dalton Transactions** 43 (2014) 17343-17351. **(Impact Factor = 4.177)**

#### SUBMITTED INTERNATIONAL PUBLICATIONS

1. **VB Koli**, SD Delekar, SH Pawar. Engineering the paint with light assisted control of hospital acquired infections.(**manuscript submitted to Photochemical and photo biological science (RSC) 2017**)

#### CONFERENCE/ WORKSHOP PAPER PRESENTED/ ATTENDED

1. Nantional Conference On “Sustanabale Chemistry:Challanges and Opp-ortunity.” At Dr. Babasaheb Ambedkar Marathwada University, Sub-Campus Osmanabad Dated 9<sup>th</sup> & 10<sup>th</sup> Jan 2012 **(Poster Presentation)**.
2. Scince Acadmia Lecture workshop on Instrumental Techniques Chemic-al Scinces, at Dr. Babasaheb Ambedkar Marathwada University, Sub-Campus Osmanabad date:25<sup>th</sup> &26<sup>th</sup> Feb. 2012 **(Poster Presentation)**
3. 7<sup>th</sup> National Symposium and Conference on Solid State Chemistry and Allied Areas. Department of Chemistry Jamia Millia Islamia (Central University) New Delhi 110025, India. November 24<sup>th</sup> and 26<sup>th</sup>, 2011 **(Poster resentation)**

4. International Conference on Emerging Trends in Chemical Sciences at School of Chemical Sciences, Central University of Gujarat, Gandhinagar 14th-15th March 2013 (**Poster Presentation**)
5. International workshop on PhD program for medical innovation (IWP-PMI-2014) February 15<sup>th</sup> and 16<sup>th</sup>, 2014. Center for Interdisciplinary research, D. Y. Patil University Kolhapur.
6. National workshop on Ph.D. program for medical innovations (PPMI-2012), October 18<sup>th</sup> and 19<sup>th</sup>, 2012. D Y Patil University, Kolhapur.
7. National symposium on Current Trends in Chemical and Nano Sciences, (CTCNS-2014), January 17<sup>th</sup> and 18<sup>th</sup>, 2014. Department of Chemistry, Shivaji University, Kolhapur
8. National workshop on Scientific/ Research paper writing, Department of Chemistry, Savitribai Phule Pune University, Pune. 16<sup>th</sup> and 17<sup>th</sup> December 2014
9. National workshop on X-ray crystallography, Department of Chemistry, Faculty of Science The Maharaja Sayajirao University of Baroda Vadodra -390 002, 19<sup>th</sup> -25<sup>th</sup> January 2015.
10. National Conference on “convergence of stem cell and medical nanotechnology” held at D.Y. Patil University Kolhapur dated 2nd and 3rd Sep. 2015 (**Poster presentation**)
11. International Conference on “nanomaterials and Nanotechnology” at K.S. Rangasamy college of Technology, Trihegode, India dated 7<sup>th</sup> to 10<sup>th</sup> Dec. 2015 (**Oral presentation**)



12. DYPU, Anveshan held at D.Y Patil University Kolhapur. Dated 29<sup>th</sup> Dec. 2015 ( Poster presentation )
13. ANVESHAN 2016 Student Research Convention (West Zone) held at Maharaja Ganga Singh University, Bikaner (Rajasthan) India. Dated 12<sup>th</sup> and 13<sup>th</sup> January 2016. **(Oral presentation).**
14. National Seminar on “Application of Chemical Science for Sustainable Development” held at Department of Chemistry, Shivaji University, Kolhapur. Dated 20<sup>th</sup> Feb.2016. **(Poster Presentation)**
15. **International Conference on “Engineering & Technology, Computer, and Basic & Applied Sciences” (ECBA- 2017 to be held from 25-01-2017 to 26-01-2017 in Seoul, South Korea. (Oral Presentation)**
16. National conference on Emerging Trends in Nanomaterial and Their Application (ETNA-2017) Department of Medical Physics, Center for Interdisciplinary Research, D. Y. Patil University Kolhapur. 2<sup>nd</sup> & 3<sup>rd</sup> June 2017. **(Poster presentation)**

## Reference

1. **Prof. (Dr). S. D. Delekar**  
**Professor in Inorganic Chemistry,**  
**Department of Chemistry,**  
**Shivaji University, Kolhapur- 416006**  
**E-mail: [sddelekar7@rediffmail.com](mailto:sddelekar7@rediffmail.com)**  
**Contact No. +91 9890291575**

2. **Prof. (dr.) S. H. Pawar, emeritus scientist (CSIR)**  
**Distinguished Professor and Vice-Chancellor (Emeritus),**  
**D. Y. Patil University, Kolhapur-416 006**  
**Director, CRTD, Sinhgad Institutes, Solapur- 413 225**  
**E-mail: shpawar1946@gmail.com**  
**Contact No. +91 9822878226**
3. **Prof. (Dr). C. D. Lokhande**  
**Research Director And Dean**  
**Center for Interdisciplinary Research**  
**D. Y. Patil University, Kolhapur-416 006**  
**E- mail: [l\\_chandrakant@yahoo.com](mailto:l_chandrakant@yahoo.com)**  
**Contact No: 9922231348**

***Date:***

***Place: Kolhapur***

*Hereby I declare that the information given above is true to the best of my knowledge.*

***Mr. Valmiki B. Koli***